Imaging human sodium iodide symporter (hNIS) gene regulation in breast cancer animal model

By

Madhura Gopal Kelkar

LIFE09201004008

TATA MEMORIAL CENTRE
MUMBAI

A thesis submitted to the Board of Studies in Life Sciences
In partial fulfillment of the requirements for the Degree of

DOCTOR OF PHILOSOPHY
of
HOMI BHABHA NATIONAL INSTITUTE

May, 2017

Homi Bhabha National Institute

Recommendations of the Viva Voce Committee

As members of the Viva Voce Committee, we certify that we have read the dissertation prepared by Ms. Madhura Gopal Kelkar entitled "**Imaging human sodium iodide symporter (hNIS) gene regulation in breast cancer animal model**" and recommend that it may be accepted as fulfilling the thesis requirement for the award of Degree of Doctor of Philosophy.

Chairman – Dr. Neelam Shirsat — Date: 5/5/2017

Guide/Convener – Dr. Abhijit De — Date: 05/05/17

External Examiner– Dr. Kumar Somasundaram — Date: 05/05/17

Member 1 – Dr. Sanjay Gupta — Date:

Member-2– Dr. Sanjeev Waghmare — Date:

Final approval and acceptance of this thesis is contingent upon the candidate's submission of the final copies of the thesis to HBNI.
I hereby certify that I have read this thesis prepared under my direction and recommend that it may be accepted as fulfilling the thesis requirement.

Date: 05.05.2017
Place: Navi Mumbai

05/05/2017.
Dr. Abhijit De
Guide

STATEMENT BY AUTHOR

This dissertation has been submitted in partial fulfillment of requirements for an advanced degree at Homi Bhabha National Institute (HBNI) and is deposited in the Library to be made available to borrowers under rules of the HBNI.

Brief quotations from this dissertation are allowable without special permission, provided that accurate acknowledgement of source is made. Requests for permission for extended quotation from or reproduction of this manuscript in whole or in part may be granted by the Competent Authority of HBNI when in his or her judgment the proposed use of the material is in the interests of scholarship. In all other instances, however, permission must be obtained from the author.

Date: 05/05/2017 **Madhura Kelkar**

Place: Kharghar, Navi Mumbai.

DECLARATION

I, hereby declare that the investigation presented in the thesis has been carried out by me. The work is original and has not been submitted earlier as a whole or in part for a degree / diploma at this or any other Institution / University.

Date: 05/05/2017 **Madhura Kelkar**

Place: Kharghar, Navi Mumbai.

List of Publications arising from thesis

Journal:

1. Enhancement of human sodium iodide symporter gene therapy for breast cancer by HDAC inhibitor mediated transcriptional modulation. **Kelkar M. G.,** Senthilkumar K, Jadhav S, Gupta S, Ahn B C, De A. ***Scientific Reports***. **2016**, 6,19341; doi: 10.1038.
2. p53 exerts negative transcriptional regulation of human sodium iodide symporter (hNIS) gene in breast cancer. **Kelkar M.G.**, Thakur B, Derle A, Chatterjee S, Ray P, De A. **Breast Cancer Research and Treatment** (In press)

Conferences

(Abstracts published)

1. Inverse regulatory role of p53 modulating human sodium iodide symporter gene expression in breast cancer. **Madhura G. Kelkar**, Sushmita Chatterjee, Abhishek Derle and Abhijit De. ***J Cancer Sci Ther*** DOI: 10.4172/1948-5956.S1.047

Presentations

1. Translational Success Of Endogenous Iodine Pump Protein (NIS) Based Targeted Therapy In Breast Cancer May Rely On Its Maneuverability By Transcriptional Modulations. **Madhura Kelkar**, Maitreyi Rathod and Abhijit De. Platinum Jubilee 2016-Tata Memorial Centre, Mumbai.
2. Inverse regulatory role of p53 modulating human sodium iodide symporter gene expression in breast cancer. **Madhura G. Kelkar**, Sushmita Chatterjee, Abhishek Derle and Abhijit De. Global Cancer Summit, 2015, Brisbane, Australia. (Oral presentation)

3. Modulating human sodium iodide symporter - histone deacetylase inhibitors as promising candidates for targeted radio-iodine therapy in breast cancer. **Madhura Kelkar** and Abhijit De. IACR-2014, Indian Association of Cancer Research meeting, Kollam. (Oral presentation)
4. Enhancement of human sodium-iodide symporter gene expression by histone deacetylase inhibitors for effective targeted radio-iodine therapy in breast cancer. **Madhura Kelkar** and Abhijit De. ICRB-2012, Indian Society of Radiation Biology meeting, ACTREC, Navi Mumbai.

Other publications:

1. Surfactant free novel one-minute microwave synthesis, characterization and cell toxicity study of mesoporous strontium hydroxyapatite nanorods. Agrawal S, **Kelkar M**, Kulkarni A R, De A, Gandhi M N. ***RSC Advances*** **2016** 6, 94921-94926
2. An inhibitor of nonhomologous end-joining abrogates double-strand break repair and impedes cancer progression. Srivastava M, Nambiar M, Sharma S, Karki SS, Goldsmith G, Hegde M, Kumar S, Pandey M, Singh RK, Ray P, Natarajan R, **Kelkar M**, De A, Choudhary B, Raghavan SC. ***Cell*** **2012**. 151(7):1474-87.
3. Bioluminescent based *in vivo* screening technologies**. Kelkar M,** De A. ***Current opinion in Pharmacology*** **2012** 12(5):592-600 [Review article]

Madhura Gopal Kelkar

Dedicated to my late grandmother and my beloved family…..

ACKNOWLEDGEMENTS

It feels good to reach the destination, but its journey that matters at the end. I, therefore take the opportunity to thank everyone whose contributions made it a worthwhile and memorable one.

Firstly, I would like to sincerely thank my mentor, Dr. Abhijit De for his constant encouragement, support and critical analysis throughout my tenure. He has introduced me to the intriguing field of Molecular Imaging. He has always been patient towards my shortcomings and kept encouraging me to do better throughout the course of the research project. It would not have been possible to explore the ideas without the freedom and independence he provides at work. I wish to express my gratitude for his contribution in improving my scientific skills.

I sincerely thank Director Dr. S. V. Chiplunkar and Deputy Director Dr. Sudeep Gupta of ACTREC for providing such an excellent infrastructure and facilities at ACTREC. I would also like to give special thanks to my doctoral committee members Dr. Neelam Shirsat, Dr. Sanjay Gupta, Dr. Sanjeev Waghmare for their time to time critical evaluation and suggestions towards progress of the project. I would also like to thank my former chairperson Dr. Rita Mulherkar and DC member (late) Dr. Rajiv Kalraiya for their guidance and assistance. I am grateful to Dr. K.B. Ain (USA) and Dr. Sorab Dalal (ACTREC) for providing plasmid constructs used in the study. A special thanks to Dr. Pritha Ray not only for her valuable suggestions and guidance but also for providing me her lab facilities and material whenever required. I am grateful to our collaborator Prof. B. C. Ahn (Kyungpook National University School of Medicine and Hospital, South Korea) for his assistance with crucial nuclear imaging experiment that helped strengthen the manuscript.

I am grateful to the staff of microscopy, genomics, FACS and radioactive facility for their support. I also thank the staff of animal house, scope cell, steno pool, library, administration, accounts and IT department. I also thank Mr. Dandekar for his prompt help during any problems with the instruments. I am thankful to Dr. M.G.R. Rajan and Dr. Savita Kulkarni from Radiation Medical Center, TMH, Parel for providing the facility to perform radioactivity related experiments.

I am thankful to ACTREC for fellowship during my PhD. I am also thankful to HBNI, ACTREC and Patel Kantilal Trust for providing me financial assistance to present my work in an international platform at Global Cancer Summit, Brisbane, Australia.

This journey is enjoyable because of the wonderful members of the De lab. I thank Renu Malhotra, Dr. Shruti Dutta, Shalini, Maitreyi, Arijit, Gayathri, Prasanna, Shiv, Mahdeih, Mr. Phase for making it a comfortable and absolutely enjoyable experience in lab. I am grateful to Dr. Shruti Dutta for her assistance in manuscript and thesis writing. I thank my juniors Shalini, Maitreyi and Arijit for their support and making the lab atmosphere more lively and healthy. They really made difficult times easier for me with plenty of jokes, funny fights and laughter. I also thank Smita, Tanha and Abhishek who took part in various part of the study and worked sincerely under my guidance. I also acknowledge past members of the lab Sushmita, Amir, Ishan, Frency, Pooja, Akshi, Rohit, Jennifer, Manjari, Nirmal, Akanksha, Dr. Soumya Basu, Namrata, Snehal, Shourya, Deepakji and many others who had always made it a great experience in lab. I am really grateful to Sushmita for all our discussions and always been a constant support in my good and bad times. I am thankful to Amir for his help with many softwares and to improve my presentation and writing skills. I also thank the present and past members of Ray lab for their encouragement and support. I am thankful to my PhD batch mates and ACTREC student community for the help at various times during the course. I express my sincere thanks to my seniors Gaurav, Padma, Monica, Rupa and Ajit Sharma for their suggestions and help at various times.

Finally, I am highly indebted to my parents for their efforts and sacrifices to mould my scientific career. This journey would not have been possible without their unconditional support, faith, love, and encouragement. Thank you Aai, Baba and Aaji for your inspiration and bearing with my absence most of the time.
Above all, I am really grateful to almighty God for the uncountable blessings and mercy on me.

Madhura Kelkar

Synopsis

Homi Bhabha National Institute

Ph. D. PROGRAMME

PROGRESS REVIEW REPORT

1. Name of the Student: Madhura G. Kelkar

2. Name of the Constituent Institution: Tata Memorial Centre-ACTREC

3. Enrolment No.: LIFE09201004008

4. Title of the Thesis: Imaging human sodium iodide symporter (hNIS) gene regulation in breast cancer animal model

5. Board of Studies: Life Sciences

Synopsis

Introduction:

Human Sodium Iodide Symporter (hNIS) is a glycosylated transmembrane protein; primarily present at the basolateral membrane of thyroid follicular cells. It co-transports two Na^+ ions and one I^- ion using energy gradient generated by Na^+/K^+ ATPase. Once iodide is transported

inside the cells, it is used further for the synthesis of thyroid hormones [1]. NIS expression is also observed in several other extra-thyroidal tissues, such as salivary glands, gastric mucosa as well as lactating mammary glands [1]. In breast tissue, NIS is known to be naturally expressed only in lactation phase to support iodide concentration into breast milk for neonatal nutrition [2]. Iodide concentration ability of NIS has been exploited for over 70 years in thyroid function imaging, treatment of hyperthyroidism and targeted radioiodide therapy of differentiated thyroid cancers.

Tazebay et al. for the first time have reported aberrant NIS expression in 80% of the breast cancer (BC) patients in contrast to its absence in healthy, non-lactating breast tissue [3]. Along with the primary tumors, NIS-mediated iodide uptake has been confirmed in breast cancer metastatic nodules by scintigraphy after suppression of thyroidal iodide uptake using T3 and methimazole [4]. In the subsequent years, various groups including ours have reported NIS protein expression in breast tumors of diverse histological and molecular subtypes, implicating potential of NIS gene-targeted radiotherapy in NIS expressing breast tumors [5-8].

Rationale:

Even though moderate NIS expression is encountered in majority of the breast cancer cases, only 15-20% of NIS-positive breast tumors show detectable radionuclide uptake. Further, the amount of NIS protein present in breast cancer cells may not deliver sufficient therapeutic benefit [4, 5]. These discrepancies between NIS expression and its function have encouraged us to focus on the modulation of endogenous NIS expression in breast cancer cell. Achievement of adequate NIS expression is regarded as one promising strategy to enhance the radioiodine therapy efficacy in breast cancer. Thus understanding regulation of NIS expression under the diseased condition of breast cancer cells is important which differs significantly than how it is regulated in the thyroid. In breast cancer cells, all-trans retinoic acid (atRA) alone or in

combination with several glucocorticoids, is reported as a potent inducer of NIS expression and iodide uptake [9-11]. The cardiac homeobox transcription factor Nkx2.5 is involved in lactation induced and atRA-induced NIS expression in MCF-7 cells [12]. Human NIS expression, in both thyroid and non-thyroid cells, is also regulated by epigenetic modifications and the agents targeting these modifications may be used to restore NIS expression and iodide uptake [13, 14]. Although these studies are informative, investigation of other potential regulators and their pertinence to hNIS in breast tumor tissue is of great interest.

Aims and Objectives:

Thus, with the above mentioned rationale, following objectives were framed

1. To establish a cell-based screening platform to identify putative pharmacological/genetic modulators and study their effect on hNIS expression
2. To study the effect of histone acetylation on hNIS expression
3. To characterize p53 mediated modulation of hNIS expression
4. *In vivo* functional assessment of drug effects on hNIS gene function using imaging methods

Results: Out of the four objectives, based on the experimental findings, the results were divided into two parts:

1. **Modulation of human NIS expression by treatment of histone deacetylase inhibitors for improvement of radioiodide therapy efficacy in breast cancer cell and animal model**

1.1: Modulation of NIS expression and function by histone deacetylase inhibitors (HDACi) in breast cancer

We designed and developed a full length (1.34kb) human NIS promoter driven bi-fusion reporter construct (pNIS-Fluc2.TurboFP). MCF-7, Zr-75-1 and MDA-MB-231 cells stably expressing this vector were developed and used as screening platform to test the effect of pharmacological modulators i.e. Histone deacetylase inhibitors (HDACi) or transcriptional regulators (p53) on hNIS expression. Six different drugs i.e. Trichostatin A (TSA), Sodium butyrate (NaB), Valproic acid (VPA), Suberoylanilide hydroxamic acid (SAHA) and Tubastatin A (TBA) representing various chemical classes of HDACi were included in the study. Initially, the minimal drug dose required to promote NIS gene expression was determined by luciferase reporter assays against increasing concentration of each drug using the established MCF-7 clone6 cells which over expresses pNIS-Fluc2.TurboFP. Similarly, cytotoxicity of these HDACi was assessed in both MCF-7 and MDA-MB-231 cell lines to confirm the dose used in gene regulation study is not toxic to the cells. The lowest minimal drug concentration (~IC_{70} equivalent) showing optimum NIS promoter induction was chosen and further used for all successive gene regulation experiments. As a consequence of HDAC inhibition especially by NaB, VPA and CI994, NIS-promoter luciferase reporter activity enhanced significantly by 2-4 fold in MCF-7 and 1.4-2.4 fold in MDA-MB-231 cells ($p<0.05$). Considering the results from the reporter based system, we further verified if the same treatments corroborate in endogenous NIS activation. Thus, quantitative real-time PCR was performed to assess the NIS transcript levels. GAPDH was used as a housekeeping control for this experiment. Overall, we observed variable increment of NIS transcript (2-55 fold, $p\leq0.05$) across all the cell types tested. Particularly, NaB and VPA treatment resulted in highest NIS mRNA induction, while TBA treatment proved to be least effective. Moreover, much higher transcript levels (~3-10 fold) were observed in hormone receptor positive MCF-7 and Zr-75-1 cell lines as compared to receptor negative cells (MDA-MB-231 and MDA-MB-468).

Our observations point out that HDAC inhibition may lead to NIS induction by known mechanism of transcriptional activation and increased DNA binding ability of transcriptional regulators. To gain further insight into the mechanisms leading to NIS up-regulation under HDAC inhibition, we performed transcription factor (TF) activation array for 96 global TF signatures to identify differentially regulated TFs under NaB and VPA drug influence in MCF-7 cells. Our data revealed the activation of 7 TFs i.e. CREB, Stat4, Stat6, Sox9, Smuc, Nkx3.2 and E2F-1, whereas suppression of 5 TFs i.e. XBP, MZF, HNF-1, Hox4C, and PLAG in response to NaB treatment. Alternatively, VPA treatment resulted in activation of 21 different TFs while no significant suppression of any factor was noted. Only Stat4 and E2F-1 were found to be activated in common in response to NaB and VPA treatment in MCF-7 cells. Further, the ability of these TFs binding to the NIS promoter was verified using promoter binding array, where the available TFs compete for binding with the promoter DNA before binding to the well plate. Our results from this array confirmed the binding of CREB, Stat4, Sox9, E2F-1 and Stat6 to NIS promoter upon NaB treatment. In response to VPA treatment, binding potential of 6 out of 21 candidate activated transcription factors was observed. Stat4 was found to be the only common factor after NaB and VPA treatment that binds to the NIS promoter. To further verify our observations, we performed bioinformatics analysis of NIS promoter sequence using the Transfac and Genomatix softwares. The analysis revealed the availability of putative binding sites of the TFs identified by the promoter binding array, demonstrating possible role of TFs like Stat4, CREB, Nkx3.2, AP1 etc. majorly influencing NIS expression in HDACi treated MCF-7 cells.

Next, NIS protein levels were checked by immunofluorescence staining after HDACi treatment in MCF-7 and MDA-MB-231 cells. Quantitation of the immunofluorescence images indicated 2-3 fold increase in NIS protein content in both the cell lines after majority of the HDACi treatment except for TBA. Enhanced protein production was further evidenced

by the western blot analysis of control and drug treated MCF-7 cell lysates. Induction of NIS protein expression after VPA treatment was also validated in Zr-75-1 tumor xenografts by immunohistochemistry using NIS-specific antibody. We then verified the functional significance of NIS modulation by HDACi treatment in cultured cells by iodide uptake assay. As compared to the untreated cells, NaB, VPA, SAHA and CI994 treatment resulted in consistent and significant (1.7-2.8 fold, $p \leq 0.05$) increase in iodide uptake in both MCF-7 and Zr-75-1 cells and around 1.5-2 fold induction ($p \leq 0.05$) was noted with NaB, VPA and CI994 drug treatments in MDA-MB-231 cell line. TSA and TBA treatment displayed marginal increase across all the cell types tested.

1.2: Monitoring therapeutic efficacy of ^{131}I mediated radioablation in breast cancer cells and animal model by molecular imaging techniques

After validating iodide uptake, next we checked therapeutic efficacy of ^{131}I radioablation by clonogenic survival assay. In comparison to ^{131}I exposure alone, HDACi drug pre-treatment resulted in highly significant cell survival reduction (0.45-0.008 fold, $p \leq 0.005$) in all three cell lines. We also confirmed higher DNA damage caused due to radiation in Zr-75-1 cells when they were pre-treated with three HDAC inhibitors than cells treated with radiation alone by staining for γ-H2Ax foci. ^{131}I therapeutic potential *in vivo* was further tested, where we measured ^{131}I radioablative treatment efficacy by non-invasive bioluminescence imaging using Zr-75-1 cells overexpressing luciferase reporter (Fluc2.tdTomato fusion). Thyroid blocking was performed using T4 and methimazole. Non-invasive Cerenkov luminescence imaging (CLI) was performed to check accumulation of radioactive iodine in tumor and thyroid. CLI imaging at 24 and 72 hrs after intra peritoneal injection of 1mCi ^{131}I showed increased accumulation of radioiodine in the tumor bed whereas thyroid uptake was significantly reduced by T4+methimazole blocking. Corresponding bioluminescence imaging data of tumor xenograft showed that in contrast to mice treated with ^{131}I or VPA, there was

75% reduction in luminescence signal at day 3 in combination treatment group (VPA+^{131}I). The reduction in BLI signal continued until day 9 post ^{131}I treatment while mice treated with VPA/^{131}I alone continued to grow. These results indicate the scope of using HDACi treatment to enhance ^{131}I therapeutic efficacy in breast cancer.

2. Transcriptional repression of NIS expression by tumor suppressor p53 in breast cancer

2.1: Regulation of NIS promoter activity by activated p53 in breast cancer cell lines and tumor xenograft model

Genome wide *in silico* analysis of the full length human NIS promoter sequence (-1298 to +32) predicted the availability of ~64 TF binding sites including the presence of two complete and one half binding consensus sequence (RRRCNNGYYY) for p53 on the hNIS promoter [15]. As aberrant NIS expression and p53 mutations both are relevant in the context of breast cancer, we investigated regulatory role of p53 in NIS transcription. To study the regulation of human NIS promoter, MCF-7, Zr-75-1 (wild type for p53) and MDA-MB-453 cells (p53 null, lacking functional protein) were transiently transfected with pNIS-Fluc2-TurboFP plasmid and the reporter activity was measured in response to p53 activation or overexpression in these cell lines. We found significant reduction of normalized NIS promoter activity in MCF-7 (0.7 fold, $p \leq 0.001$) and Zr-75-1 (0.6 fold, $p \leq 0.001$) but not in MDA-MB-453 cells (1.34 fold, $p=0.064$) after doxorubicin (Dox) treatment. Further, in response to wild type p53 overexpression alone or in combination with doxorubicin (drug with known action of p53 activation) treatment, significant promoter attenuation was seen in all cell lines tested (0.2-0.7 fold, $p \leq 0.05$).

Following these indicative results, we performed a series of site directed mutagenesis on the human NIS promoter sequence to abolish the p53 binding sites by either AATT substitution

or deletion mutation. As compared to wild type promoter, the introduction of point mutations disrupting the predicted p53 binding at site 1 and site 3 resulted in significant augmentation of promoter activity in both the cell lines (1.2-1.8 fold, $p \leq 0.05$). However, mutation at site 2 exhibited differential response in the two cell lines (0.82 fold in MCF-7, 1.17 fold in Zr-75-1). Combinatorial AATT substitution at all three sites significantly induced NIS promoter activity in both the cell lines (1.4-1.5 fold, $p \leq 0.05$). Further confirmation of the involvement of p53 in regulating NIS transcriptional activity was provided by treating both the cell lines with doxorubicin. In response to p53 activation, a reduction in luciferase signal was achieved in case of wild type NIS promoter (0.4-0.5 fold, $p \leq 0.05$) but not in either site 3 mutated construct or in combination with other two mutated binding sites (1.4-1.7 fold, $p \leq 0.001$). AATT substitution at site 1 and 2 resulted in reduced suppression of promoter activity (~0.8-0.9 fold) post Dox treatment in both the breast cancer cell lines. On the other hand, deletion of p53 response element at site 3 resulted in dramatic enhancement of gene expression (1.4-2.6 fold, $p \leq 0.0001$). Deletion at site 2 had a minimal effect on transcriptional activity as measured by luciferase signal (~1.2-1.3 fold) while site 1 deletion exhibited heterogeneous response in the cell lines studied. In response to activated p53, site 3 deletion mutant construct exhibited significant increase in luciferase activity (1.4-1.7 fold, $p \leq 0.0001$) while site 1/ 2 deletion promoter constructs exhibited reduced transcriptional repression. Deletion at all three sites in combination displayed a non-significant change in promoter activity that remains unaltered even after doxorubicin treatment. Altogether, these findings indicate that abrogation of p53 binding sites on hNIS promoter enhances NIS transcriptional activity, confirming repressive role of p53.

In order to validate our *in vitro* findings, we developed tumor xenograft model using engineered Zr-75-1 (stably expressing pNIS-Fluc2.Turbo reporter, clone C2) cells. Once the tumor volume reached to a measurable size, mice were randomized into two groups i.e the

control group and the Dox group. Mice in the Dox group received single intraperitoneal injection of 1.5mg/kg doxorubicin to activate p53 *in vivo* while avoiding drug induced toxicity as reported by Briat et al. [16]. The bioluminescence imaging data clearly revealed 0.5 fold attenuation in luciferase activity after 48 hours of treatment in the Dox group, indicating reduced NIS transcription. As expected from the minimal drug dose usage, tumor volumes of mice exhibited no major difference between pre and post Dox treatment.

2.2: Modulation of endogenous NIS expression and function by transcription factor p53 by direct binding to the human NIS promoter in breast cancer cells

Based on the experimental evidences obtained so far, next we attempted to verify the effect of p53 activation on endogenous NIS expression and function. We checked endogenous NIS transcript levels in breast cancer cell lines by real time PCR using NIS-specific TaqMan probe. Following p53 activation, we observed significant attenuation of NIS mRNA levels to 0.4 fold in MCF-7 ($p=0.001$) and 0.5 fold in Zr-75-1 cells ($p=0.046$) but non-significant increase was observed in MDA-MB-453 cells (1.46 fold, $p=0.121$), thus confirming p53-dependent transcriptional repression of NIS. Since endogenous levels of NIS protein are low and p53 decreases the NIS expression, we further validated the effect of p53 on NIS expression and its function in MCF-7 cells overexpressing NIS at the cell membrane. As expected, endogenous p53 activation or exogenous p53 overexpression alone or in combination resulted in 0.4-0.5 fold reduction in NIS protein content further impacting NIS-mediated iodide uptake significantly (0.5-0.7 fold, $p\leq0.05$). Since NIS promoter activity and its endogenous expression and function are dependent on p53 function, we verified if activated p53 directly binds to the human NIS promoter DNA by chromatin immunoprecipitation (ChIP) assay. Our results indicated binding of p53 to the NIS promoter region which enhanced reasonably after Dox treatment (1.31 fold in MCF-7 and 1.56 fold in Zr-75-1 cells). Further to understand which of the site is preferentially occupied by p53, we

checked site specific binding using individual p53-binding site specific primers. The results of real-time PCR revealed that out of the three p53 binding sites, site 1 and site 2 had an overall high occupancy of p53 in both the cell lines studied. Site 3 (a half binding site) displayed very low p53 occupancy in Zr-75-1 cells while p53 binding at site 3 was negligible in MCF-7 cells. In response to doxorubicin mediated p53 activation, the overall binding of p53 to the human NIS promoter at multiple sites was elevated to various extents (0.3-11 fold) for the three sites verified using the two cell lines. Highest binding induction was observed at site 1 which was 11.1 fold in case of MCF-7 and 5.2 fold in case Zr-75-1.

Conclusion:

We have performed a comprehensive investigation to reveal biochemical basis of HDACi mediated modulation of NIS expression and function in breast cancer cell and animal model. Four out of six HDACi tested especially the candidate drugs like NaB, VPA, CI994, and SAHA have shown promising induction in NIS transcript and protein expression. Augmented NIS protein levels are found sufficient for functional improvement in radioiodine uptake and further ^{131}I radioablation in cell culture and animal model. Until now, the regulation of NIS expression and function was studied primarily in receptor positive MCF-7 cells. In our study, we have included 5 different breast cancer cell lines representing both receptor positive as well as receptor negative subtypes of breast cancer cells. The experimental observations indicate possible application of NIS-mediated targeted therapy in receptor negative breast cancer patients who are in great demand of targeted therapy options. The study implicates that epigenetic transcriptional modulation strategy may be extended for clinical trial in near future. The clinical utility of NIS-targeted radiotherapy is undermined largely because of insufficient radioiodide accumulation, short retention time of radioiodine and the intracellular localization of NIS protein in majority of the tumor cases. Even though, treatment with HDACi significantly elicits NIS-mediated iodide uptake, the efflux and the localization of the

protein remain uninfluenced. Future studies leading to identification of potential chemical agents which may improve oragnification of radioiodine in breast cancer cells and NIS protein translocation to the membranemay immensely impact NIS application in clinic.

The findings from the assessment of 96 global transcription factors along with *in silico* analysis also reveals possible role of TFs like Stat4, CREB, Nkx3.2, AP1 etc. in NIS gene regulation in breast cancer. There is no literature available on NIS gene regulation by Stat4, GATA that turned out to be important factors identified in our study. The role of these transcription factors in regulation of functional NIS expression can be explored in future.

On the NIS transcriptional regulation part covered in the thesis, our results reveal novel findings on inverse regulatory role of wild type p53 modulating functional NIS expression in breast cancer. Our experimental evidences indicate direct binding of the activated wild type p53 protein to the human NIS promoter at multiple sites in sequence specific manner. Abrogating p53 response element from the NIS promoter, results in remarkable induction of NIS transcription. The analysis of human NIS promoter sequence has revealed the presence of overlapping binding sites for RXR, Zn finger containing transcription factor and octamer binding protein at site 1 region and Pax4, Smad and GATA binding sites at site 2 and Sp1, Zn finger containing transcription factor at site 3 region of NIS promoter. Disrupting p53 binding sequence might have resulted in interruption of predicted binding of some of these factors. Therefore, co-operative binding of p53 interacting proteins or even additional binding sites formed due to mutational rearrangements require full considerations in future to understand how NIS gene regulation operates through overlapping binding sites. Also, the role of differences in p53 response elements and the mechanism of differential recruitment of p53 at different sites on NIS promoter can be explored in future.

From experimental evidences, inhibition of wild type p53 may allow induction of NIS expression for therapeutic intervention in breast cancer patients. However, since p53 acts as a guardian of the genome protecting normal cells and tissues, use of inhibitors for wild-type 53 is not a practical approach [17, 18]. Instead, determining patient's p53 status may assist in achieving good therapeutic benefit in mutant cases. A group of patients with mutant p53, specifically those affecting the DNA binding activity of p53, would relay to high NIS expression, indicating a scope for extending NIS-based radioiodide therapy.

References:

1. Spitzweg, C., Harrington, K.J., Pinke, L.A., Vile, R.G. & Morris, J.C. Clinical review 132: The sodium iodide symporter and its potential role in cancer therapy. *J Clin Endocrinol Metab* **86**, 3327-35 (2001).
2. Cho, J.Y. et al. Hormonal regulation of radioiodide uptake activity and Na+/I- symporter expression in mammary glands. *J Clin Endocrinol Metab* **85**, 2936-43 (2000).
3. Tazebay, U.H. et al. The mammary gland iodide transporter is expressed during lactation and in breast cancer. *Nat Med* **6**, 871-8 (2000).
4. Wapnir, I.L. et al. The Na+/I- symporter mediates iodide uptake in breast cancer metastases and can be selectively down-regulated in the thyroid. *Clin Cancer Res* **10**, 4294-302 (2004).
5. Moon, D.H. et al. Correlation between 99mTc-pertechnetate uptakes and expressions of human sodium iodide symporter gene in breast tumor tissues. *Nucl Med Biol* **28**, 829-34 (2001).
6. Upadhyay, G. et al. Functional expression of sodium iodide symporter (NIS) in humans breast cancer tissue. *Breast Cancer Res Treat* **77**, 157-65 (2003).
7. Renier, C., Vogel, H., Offor, O., Yao, C. & Wapnir, I. Breast cancer brain metastases express the sodium iodide symporter. *J Neurooncol* **96**, 331-6 (2010).

8. Chatterjee, S. et al. Quantitative immunohistochemical analysis reveals association between sodium iodide symporter and estrogen receptor expression in breast cancer. *PLoS One* **8**, e54055 (2013).

9. Unterholzner, S. et al. Dexamethasone stimulation of retinoic Acid-induced sodium iodide symporter expression and cytotoxicity of 131-I in breast cancer cells. *J Clin Endocrinol Metab* **91**, 69-78 (2006).

10. Kogai, T. & Brent, G.A. The sodium iodide symporter (NIS): regulation and approaches to targeting for cancer therapeutics. *Pharmacol Ther* **135**, 355-70 (2012).

11. Willhauck, M.J., DJ, O.K., Wunderlich, N., Goke, B. & Spitzweg, C. Stimulation of retinoic acid-induced functional sodium iodide symporter (NIS) expression and cytotoxicity of (1)(3)(1)I by carbamazepine in breast cancer cells. *Breast Cancer Res Treat* **125**, 377-86 (2011).

12. Dentice, M. et al. Transcription factor Nkx-2.5 induces sodium/iodide symporter gene expression and participates in retinoic acid- and lactation-induced transcription in mammary cells. *Mol Cell Biol* **24**, 7863-77 (2004).

13. Puppin, C. et al. Cooperative effects of SAHA and VPA on NIS gene expression and proliferation of thyroid cancer cells. *J Mol Endocrinol* **48**, 217-227 (2012).

14. Baldan, F. et al. Histone post-translational modifications induced by histone deacetylase inhibition in transcriptional control units of NIS gene. *Mol Biol Rep* **41**, 5257-65 (2014).

15. Wang, B., Xiao, Z. & Ren, E.C. Redefining the p53 response element. *Proc Natl Acad Sci U S A* **106**, 14373-8 (2009).

16. Briat, A. & Vassaux, G. A new transgenic mouse line to image chemically induced p53 activation in vivo. *Cancer Sci* **99**, 683-8 (2008).

Publications in Refereed Journal:

a. Published:

Kelkar M. G., Senthilkumar K, Jadhav S, Gupta S, Ahn B C, De A. 2016. Enhancement of human sodium iodide symporter gene therapy for breast cancer by HDAC inhibitor mediated transcriptional modulation. *Sci. Rep.* 6, 19341; doi: 10.1038.

b. Accepted: NA

c. Communicated:

Agrawal S, **Kelkar M**, Kulkarni A R, De A, Gandhi M N. Surfactant free novel one-minute microwave synthesis, characterization and cell toxicity study of mesoporous strontium hydroxyapatite nanorods. *RSC Advances* (under review)

d. Other Publications:

Srivastava M, Nambiar M, Sharma S, Karki SS, Goldsmith G, Hegde M, Kumar S, Pandey M, Singh RK, Ray P, Natarajan R, **Kelkar M**, De A, Choudhary B, Raghavan SC. An inhibitor of nonhomologous end-joining abrogates double-strand break repair and impedes cancer progression. *Cell*. 151(7):1474-87.

Kelkar M, De A. Bioluminescent based *in vivo* screening technologies**.** *Current opinion in Pharmacology* 12(5):592-600. [Review article]

Conferences attended:

Translational Success Of Endogenous Iodine Pump Protein (NIS) Based Targeted Therapy In Breast Cancer May Rely On Its Maneuverability By Transcriptional Modulations. **Madhura Kelkar**, Maitreyi Rathod and Abhijit De. Platinum Jubilee 2016-Tata Memorial Centre, Mumbai.

Inverse regulatory role of p53 modulating human sodium iodide symporter gene expression in breast cancer. **Madhura G. Kelkar**, Sushmita Chatterjee, Abhishek Derle and Abhijit De. Global Cancer Summit, 2015, Brisbane, Australia.

Modulating human sodium iodide symporter - histone deacetylase inhibitors as promising candidates for targeted radio-iodine therapy in breast cancer. **Madhura Kelkar** and Abhijit De. IACR-2014, Indian Association of Cancer Research meeting, Kollam.

Enhancement of human sodium-iodide symporter gene expression by histone deacetylase inhibitors for effective targeted radio-iodine therapy in breast cancer. **Madhura Kelkar** and Abhijit De. ICRB-2012, Indian Society of Radiation Biology meeting, ACTREC, Navi Mumbai.

Enhancement of human sodium-iodide symporter gene expression by histone deacetylase inhibitors for effective targeted radio-iodine therapy in breast cancer. **Madhura Kelkar** and Abhijit De. ICRB-2012, Indian Society of Radiation Biology meeting, ACTREC, Navi Mumbai.

Signature of Student: MGKelkar

Date: 19/04/2016

Doctoral Committee:

S. No.	Name	Designation	Signature	Date
1.	Dr. Neelam Shirsat	Chairperson		22-4-16
2.	Dr. Abhijit De	Guide / Convener		22-04-16
3.	Dr. Sanjay Gupta	Member		22/04/16
4.	Dr. Sanjeev Waghmare	Member		22/04/16

Forwarded through:

S.V. Chiplunkar 25/4/16

Dr. S.V. Chiplunkar
Director, ACTREC
Chairperson, Academic & Training Programme
ACTREC

Dr. S. V. Chiplunkar
Director
Advanced Centre for Treatment, Research & Education in Cancer (ACTREC)
Tata Memorial Centre
Kharghar, Navi Mumbai 410210.

Dr. K. Sharma,
Director Academics,
TMC

PROF. K. S. SHARMA
DIRECTOR (ACADEMICS)
TATA MEMORIAL CENTRE,
PAREL, MUMBAI

Table of contents

Abbreviations

3, 3’-diaminobenzidine tetra hydrochloride (DAB)
4, 6’-diamidino-2-phenylindole (DAPI)
Alpha fetoprotein (AFP)
Aromatase inhibitors (AIs)
All-trans retinoic acid (atRA)
Basic-leucine zipper (b-ZIP)
Bioluminescence imaging (BLI)
Bovine serum albumin (BSA)
Breast cancer (BC)
Breast cancer 1 (BRCA1)
Carbamazepine (CBZ)
Cerenkov luminescence imaging (CLI)
Cerenkov radiation (CR)
Charge-coupled device (CCD)
Chicken beta-actin (CAG)
Chromatin immunoprecipitation (ChIP)
cAMP responsive element binding protein (CREB)

Cutaneous T cell Lymphoma (CTCL)

Cytokeratin (CK)
Cytomegalovirus (CMV)
Dexamethasone (Dex)
Doxorubicin (Dox)
Dual Oxidase 2 (DUOX2)
Ductal carcinoma in situ (DCIS)
Epidermal growth factor receptor (EGFR)
ERE (Estrogen Response Element)
Estrogen receptor (ER)
Estrogen receptor alpha (ERα)

Food and Drug Administration (FDA)

Fetal bovine serum (FBS)

Fine needle aspiration (FNA)
Firefly luciferase (Fluc)
Formalin fixed paraffin embedded (FFPE)
Gaussia luciferase (Gluc)
Glucose transporters (GLUTs)
Glyceraldehyde- 3-phosphate dehydrogenase (GAPDH)
Green fluorescent protein (GFP)
Hank’s Balanced Salt Solution (HBSS)
Hepatocellular carcinoma (HCC)
Histone acetyltransferases (HATs)
Histone deacetylases (HDACs)
Histone deacetylase inhibitors (HDACi)
Horse radish peroxidase (HRP)
Human epidermal growth factor receptor (HER2)
Human sodium iodide symporter (hNIS)
Immunohistochemistry (IHC)

Infiltrating ductal carcinoma (IDC)
Inflammatory breast cancer (IBC)
Insulin-like growth factor (IGF)
Interleukin (IL)
Interferon-γ (IFN-γ)
Locally advanced breast cancer (LABC)
Magnetic Resonance Imaging (MRI)
Matrix metalloproteinases (MMPs)
Mean fluorescence intensity (MFI)
Molecular imaging (MI)
Near-infrared (NIR)
NIS upstream enhancer (NUE)
Optical imaging (OI)
Oxytocin antagonist (OTA)
Papillary thyroid carcinoma (PTC)
Peroxisome proliferator-activated receptor-γ (PPARγ)
Phosphate buffered saline (PBS)
Pituitary tumor-transforming gene (PTTG)
PTTG-binding factor (PBF)
Positron emission tomography (PET)
Pregnane X receptor (PXR)
Progesterone receptor (PR)
Prostate specific antigen (PSA)
Protein kinase-A (PKA)
Real time polymerase chain reaction (RT-PCR)
Region of interest (ROI)
Relative light units (RLUs)
Renilla luciferase (Rluc)
Response elements (RE)
Retinoic acid (RA)
Retinoic Acid Receptor (RAR)
Single photon emission computed tomography (SPECT)
Site directed mutagenesis (SDM)
Sodium butyrate (NaB)
Sodium iodide symporter (NIS)
Solute carrier (SLC)
Suberoylanilide hydroxamic acid (SAHA)
Terminal ductal lobular unit (TDLU)
Thymidine kinase (TK)
Thyroglobulin (Tg)
Thyroperoxidase (TPO)
Thyroid transcription factor-1 (TTF-1)
Thyroid stimulating hormone (TSH)
Thyroxine (T4)
Triple negative breast cancer (TNBC)
Transcription factor (TF)
Transforming growth factor-β1 (TGF-β1)
Trichostatin A (TSA)
Triiodothyronine (T3)
Tris borate saline-tween20 (TBST)

TSH receptor (TSHR)
Tubastatin A (TBA)
Tumor necrosis factor α (TNF-α)
Ultraviolet (UV)
Valproic acid (VPA)

List of Figures

List of Tables

1. Introduction and review of literature

1.1: Pathophysiology of mammary gland

Breast tissue is composed of glandular tissues comprising of lobules, ducts and supporting stromal tissues. Lobules are spherical structures composed of polarized cuboidal epithelial cells (physiologically called as luminal epithelial cells) surrounding a lumen and are supported by underlying loosely connected myoepithelial cells. The secretary part of the gland is terminal ductal lobular unit (TDLU), which is connected to an excretory part i.e. the large ductal system (**Figure 1.1**) [19]. In lactating mammary gland, milk is secreted by the lobules into the lumen and transported through the ducts until excreted for nursing [20].

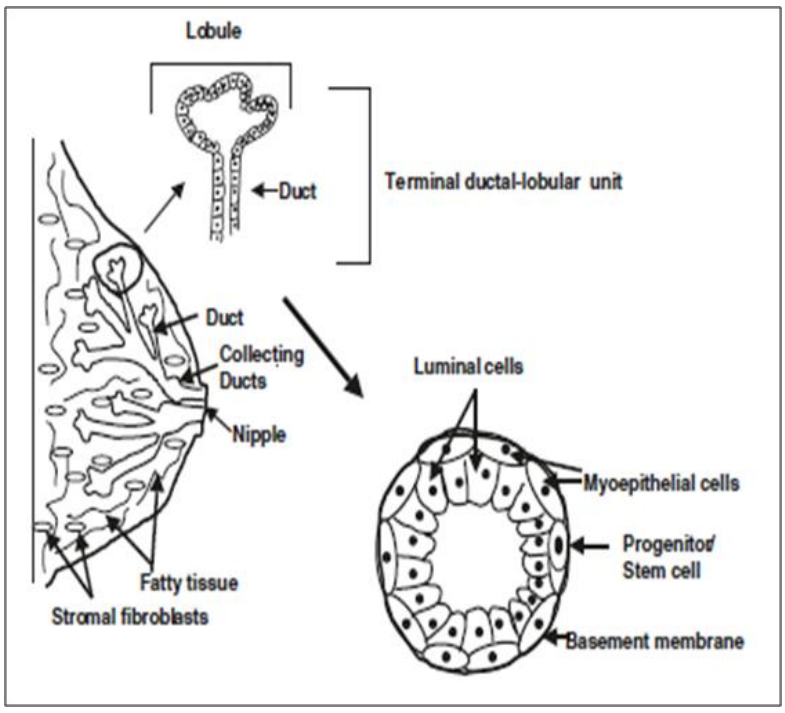

Figure 1.1: Structure of the mammary gland. *Terminal ductal–lobular unit (TDLU), composed of ductal cells, is the unit thought to be the origin of most breast cancers. Lobule is made up of two primary types of cells in normal ducts: outer contractile myoepithelial and inner columnar luminal cells* [19].

A dynamic interplay of hormones regulate cycles of mammary gland morphogenesis in humans. After the release of growth hormone, estrogen, and progesterone during puberty, the

cells of the mammary gland begin to proliferate. Whereas under the influence of prolactin, insulin, cortisol, thyroid hormone, parathyroid hormone and growth hormone during pregnancy and lactation, mammary glands become completely differentiated. Suckling, in turn, results in the release of oxytocin hormone that stimulates contraction of the myoepithelial cells and expels milk for the nursing infant. A combination of milk in the glands and the absence of lactation-associated hormones promote reversible apoptosis of mammary gland epithelial cells during a process called involution. The mammary gland remains in this state until irreversible apoptosis occurs during menopause [20].

1.2: Breast cancer

Breast cancer (BC) is the most frequent cancer among women and 2nd most frequent cancer worldwide, with 1.7 million cases diagnosed in 2012 according to GLOBOCAN 2012. Since the 2008 estimates, BC incidence has increased by more than 20%, while mortality has increased by 14%. BC is also the most common cause of cancer death among women (5,22,000 deaths worldwide in 2012) and the most frequently diagnosed cancer among women in 140 of 184 countries worldwide. At present, it represents one in four of all cancers in women according to the International Agency for Research on Cancer (IARC) report 2013. Global burden of BC will increase to over 2 million new cases / year by 2030 [21].

In India, BC is the most common cancer among females in urban areas [22]. Incidence and mortality rates of BC have now exceeded over cervical cancers among women in India (**Figure 1.2**). The average age of developing a BC has undergone a significant shift over last few decades in the Indian population. The proportion of Indian BC patients under the age of 35 varies between 11% at Tata Memorial Hospital, Mumbai [23] to 26% at SGPGIMS, Lucknow [24]. BC at young age and premenopausal state tends to exhibit larger tumor size, higher number of metastatic lymph nodes, poorer tumor grade, aggressive tumor subtypes,

earlier and more frequent loco-regional recurrences, and poor survival [25, 26]. Hence, early detection of BC and effective measures of BC screening and control are currently needed.

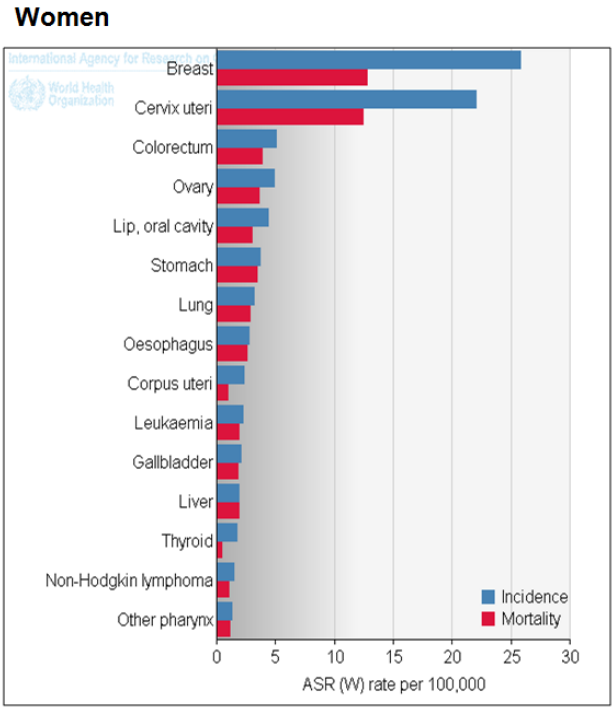

Figure 1.2: Estimated age-standardized incidence and mortality rates in women. *Adapted from GLOBOCAN 2012.*

1.3: Histopathology of breast cancer

BC is a multifaceted disease which comprises of different subtypes that demonstrate heterogeneity in terms of molecular, histopathological or clinical parameters. Currently, breast cancers are typically classified as either ductal or lobular, a histological classification that was originally based on the belief that ductal carcinomas arose from ducts and lobular carcinomas arose from lobules. However, it is now known that both of these arise from the TDLU. While ductal carcinomas often form palpable masses and are detected by mammography, lobular carcinomas rarely form masses that are detected by mammography, and are often diagnosed as a result of a biopsy from another lesion. Histologically, BC is

divided largely into two groups: carcinomas and sarcomas. Carcinomas arise from breast epithelial cells whereas sarcomas arise from stromal cells of the mammary gland. Sarcomas account for less than 1% of all primary breast tumors. Breast carcinomas can be further subclassified into two main groups, carcinoma *in situ* and invasive carcinoma. Ductal carcinoma *in situ* (DCIS) can be described as the earliest form of BC that has not infiltrated through the basement membrane. On the other hand, invasive ductal carcinomas (IDC) infiltrate into the stromal region with a potential to metastasize. Invasive ductal carcinoma accounts for 80% cases and invasive lobular carcinoma accounts for 10-15% cases. Other BC histological types are special types that include colloid (mucinous), medullary, micropapillary and tubular subtypes.

IDCs are further characterized by their tumor grade, tumor stage, and hormone receptor status [27]. Valuable prognostic information can be gained by grading the tumor on a scale of I to III according to the Bloom-Richardson system. Grade I tumors are highly differentiated and more closely resemble normal breast tissue but grade III tumors are poorly differentiated. Histological grading is closely associated with overall survival of patients [28] and plays a vital role for treatment of BC. Tumor prognosis also takes into account TNM staging, which provides information on the tumor size (T), lymph node status (N) and the presence of metastases (M) to locations other than the lymph nodes. Immunohistochemical staining for the estrogen receptor (ER), progesterone receptor (PR) and human epidermal growth factor receptor 2 (HER-2/neu) proteins also provides valuable information regarding tumor prognosis. Generally, ER/PR positive breast tumors tend to be well-differentiated, lymph node-negative, have low proliferation rates and better prognosis, while ER/PR-negative tumors tend to be more aggressive with an increased risk of invasion and metastasis [29].

Recently, molecular classifications from gene expression profiling of breast cancers were done. These systems provided better predictions on tumor outcome than traditional

classifications [30]. Molecular profiling utilizing cDNA microarrays have grouped breast tumors into several major subtypes [31, 32]. Different subclasses include luminal A, luminal B, basal and HER-2/neu-expressing breast tumors. Luminal A breast tumors are mostly ER positive and histologically low grade, whereas luminal B breast tumors are mostly ER-positive, but express low levels of other hormone receptors and are histologically high grade. In contrast, breast tumors in the HER-2/neu classification are ER-negative and show amplification of the HER-2/neu gene. Finally, basal breast tumors are triple negative for ER, PR, and HER-2/neu expression, have high expression of basal cytokeratin 5/6 (CK5/6) and also overexpress many growth factor receptors, such as epidermal growth factor receptor (EGFR) and c-kit, as well as growth factors, including hepatocyte growth factor and insulin growth factor (IGF). Other molecular subtypes such as luminal C and normal breast-like groups have also been identified in some studies, but are less well characterized than the luminal A, luminal B, HER2, and basal-like types [30, 32-35]. A strong link between basal breast tumors and germline mutations in the breast cancer 1 early onset (BRCA1) tumor suppressor gene signature has also been established in literature [36, 37]. BRCA1 mutations are linked with majority of the hereditary BC cases. These BC molecular subtypes differ with regard to their patterns of gene expression, clinical features, prognosis and response to treatment regimens. These differing molecular signatures in BC subtypes could unveil new therapeutic targets for individualized treatment [30].

1.4: Breast cancer screening methods and treatment modalities

In majority of the times, BC is first detected by imaging techniques, such as mammography, magnetic resonance imaging (MRI) or ultrasound. The type of radiographic imaging used depends upon the patient's age and the characteristics of the breast tissue. Currently, mammography is the best diagnostic tool for detecting BC. If an abnormal area is found on

the mammogram, a biopsy is taken to evaluate the presence of malignant tumor. Ultrasound can be used to distinguish between cysts and solid masses as well as benign and malignant tumors. In case of nipple discharge, some of the fluid is collected and is examined under the microscope for presence of cancer cells. However, absence of cancer cells from nipple discharge does not confirm absence of BC. Biopsy is the most common test to determine presence of cancerous tissue and may include fine needle aspiration (FNA), core needle biopsy and excisional biopsy. FNA uses a fine needle to aspirate cells from the lesion. Core needle biopsy consists of a small needle that removes a thin core of tissue out of the mass; it is often performed under radiographic guidance by interventional radiologists. It is commonly used to obtain tissue specimen after initial evaluation of a breast mass or radiographic abnormality. A larger amount of tissue is removed in excisional biopsies and these procedures are performed by surgeons.

Due to the heterogeneity of breast cancers, the major clinical challenge is to decide an optimal treatment regime for BC patients. To determine a suitable treatment for individual patients, many variables need to be considered including pathological factors, like the tumor type, grade, stage, as well as expression of predictive and prognostic biomarkers such as ER, PR, HER2 and Ki67. In addition to these variables, other clinical factors, such as the patient age, personal and family history of breast cancer also have to be considered. The main treatment modalities routinely employed include surgery and radiation therapy.

1.4.1: Surgery

BC patients often undergo surgical removal of the tumor. In lumpectomy/ partial mastectomy/breast conservation surgery, only cancerous tissue plus a rim of normal tissue is removed. In some cases, mastectomy or removal of the entire breast and axial lymph nodes is required. Modified radical mastectomy remained the standard management in early breast

cancer for many years. Several randomized trials have shown the equivalence of breast-conserving therapy and mastectomy in terms of overall survival [38-40] and the former has largely replaced mastectomy in patients with early operable breast cancer [41].

1.4.2: Radiation therapy

These surgical procedures are usually followed by radiation therapy. Radiotherapy plays an essential role in the multimodal treatment of BC. It has a major effect on local control and effective radiotherapy can improve overall survival rates for patients with early stage disease [42, 43]. Most BC patients also receive adjuvant systemic treatment to eliminate cancer cells that have spread to different parts of the body. Common examples of adjuvant therapy in the breast cancer are chemotherapy, hormonal treatment and targeted therapy.

1.4.3: Chemotherapy

Chemotherapy includes treatment of cancer patients using cytotoxic drugs that may be given as intravenous injections or oral pills. Chemotherapy drugs are generally administered in cycles, each period of treatment is followed by a recovery period. The most common drugs used for early BC include the anthracyclines such as doxorubicin (Adriamycin) and epirubicin (Ellence) and the taxanes such as paclitaxel (Taxol) and Docetaxel (Taxotere). These drugs may be used along with certain other drugs, like fluorouracil (5-FU), cyclophosphamide (Cytoxan), methotrexate and carboplatin. Depending on the combination of drugs, adjuvant chemotherapy is usually given for 3 to 6 months. Neoadjuvant chemotherapy is often used to treat cancers that are too big (called locally advanced) to be removed surgically. Chemotherapy is most effective after completion of recommended doses of the drugs in definite cycles in a timely manner.

1.4.4: Hormone treatments

Adjuvant hormonal therapy is commonly used in addition to definitive local therapy to reduce the risk of local and distant recurrence. Estrogen, a hormone produced by the ovaries, promotes the growth of many breast cancers. Women with ER positive breast cancers are often referred to hormone therapy to lower estrogen levels or to block the effects of estrogen on the growth of breast cancer cells. Tamoxifen and toremifene (Fareston) are drugs that prevent binding of estrogen to its receptor present on breast cancer cells and are usually effective in both postmenopausal and premenopausal patients. Fulvestrant (Faslodex) is a newer drug that reduces the number of estrogen receptors on breast tumors. It is often effective in postmenopausal women who are non-responsive to tamoxifen. Adjuvant tamoxifen has been shown to improve the 10-year survival of women with ER-positive and ER-unknown tumors [44]. Some studies have also demonstrated decreased occurrence of contralateral breast cancer with tamoxifen [45]. Adjuvant therapy with tamoxifen is known to reduce disease recurrence and annual death rate by one third [46].

More recently, drugs known as the aromatase inhibitors (AIs) (Anastrozole, Letrozole, and Exemestane) are also used in treatment of both early and advanced hormone receptor positive breast cancer. These are superior to tamoxifen in terms of disease-free survival in postmenopausal women with hormone receptor-positive BC [47, 48]. As a consequence, nowadays, AIs are commonly used in the adjuvant setting in these patients.

1.4.5: Targeted therapies

The approved targeted therapies in BC include trastuzumab, lapatinib and bevacizumab. Approximately 15-30% of breast cancers overproduce the growth-promoting protein HER2/neu. These tumors grow faster and are more likely to recur. Trastuzumab (Herceptin) is a monoclonal antibody that directly targets the HER2 protein of breast tumors and offers a

survival benefit for BC women overexpressing HER2 [49]. Originally used to treat metastatic BC, trastuzumab has also been shown to be effective in early stage breast cancer [50]. Another drug, lapatinib (Tykerb), has been found to be effective in delaying disease progression in women with HER2-positive advanced breast cancers that have developed resistance to trastuzumab [51]. A new generation of anti-HER2 targeted therapies are currently under development [52].

Despite the available therapy options, BC still remains the leading cause of death among women in India, thus warranting the need for novel targeted therapies. One of the target proteins is the sodium iodide symporter that is actively being investigated for BC therapeutic intervention, and also forms the basis of this study.

1.5: Physiological role of the sodium iodide symporter

The sodium iodide symporter (NIS) is a transmembrane N-linked glycoprotein naturally expressed on the basolateral membrane of the thyroid follicular cells and is well known for its role as the mediator of active iodide uptake into the thyroid gland. NIS transports iodide against its concentration gradient from the bloodstream into the thyroid follicular cells by coupling its energy to the transport of two sodium ions along the electrochemical gradient generated by the Na^+/K^+ ATPase. Iodide is then released from the thyroid follicular cells into the lumen through the apical iodide transporter Pendrin, organified further by Thyroid Peroxidase (TPO) to the tyrosine residues of Thyroglobulin (Tg) and used for synthesis of thyroid hormones, Triiodothyronine (T3) or Thyroxine (T4) (**Figure 1.3**).

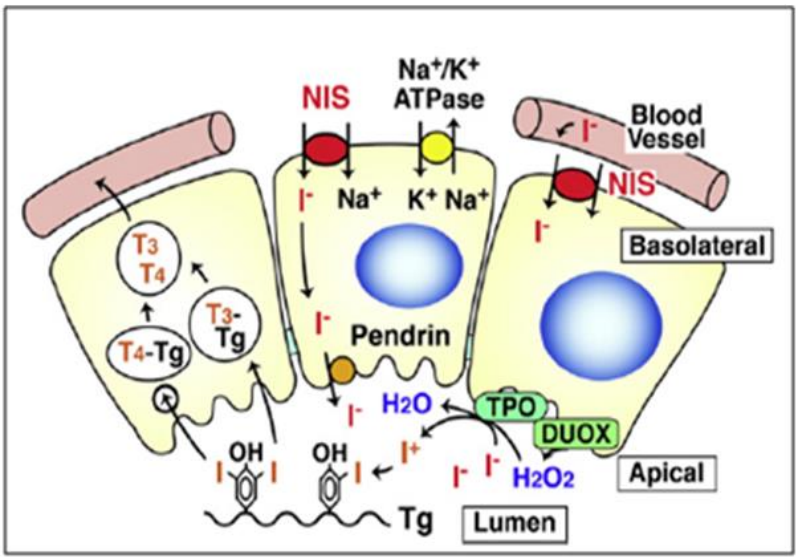

Figure 1.3: Schematic representation of NIS-mediated iodide transport at the basolateral membrane of thyrocytes for biosynthesis of the thyroid hormones. *NIS actively transports I- from the bloodstream against its concentration gradient into the thyroid follicular cells by coupling its energy with the transport of two sodium ions by the electrochemical gradient generated by the Na^+/K^+ ATPase. Iodide trapped in follicular cells is transported into the lumen via apical Pendrin and organified further by Thyroid Peroxidase (TPO) to the tyrosine residues of Thyroglobulin (Tg), in the presence of H_2O_2 produced mainly by Dual Oxidase 2 (DUOX2). The iodinated tyrosine residues are used for synthesis of thyroid hormones, Triiodothyronine (T3) or Thyroxine (T4)* [10].

Functional activity of NIS produces the iodide concentration gradient up to 30-fold from blood as compared to NIS-expressing cells. The successful cloning of NIS has marked the beginning of the molecular characterization of NIS [53, 54]. Eskandari et al. studied the mechanism, stoichiometry, and specificity of NIS by means of electrophysiological, tracer uptake, and electron microscopic methods in NIS expressing *X. laevis* oocytes [55]. Their observation confirmed that NIS activity is electrogenic demonstrating 2:1 Na^+/I^- stoichiometry of the transport. Moreover, from their kinetic studies, these investigators proposed an ordered simultaneous transport mechanism in which Na^+ binds to NIS before I^-, whereas transport of both ions is simultaneous and binding is ordered and sequential. It is

also reported that along with iodide, NIS also transports a wide variety of anions including ClO_3^-, SCN^-, $SeCN^-$, NO_3^-, Br^-, BF_4^-, IO_4^-, and BrO_3^- [55]. Subsequently, along with elucidation of mechanism of transport, NIS protein has been extensively characterized and NIS specific antibodies have been generated [55-57]. NIS belongs to the solute carrier family 5 (SLC5), which transports negatively charged solutes into the cytoplasm using an electrochemical Na^+ gradient [57] and is also known as SLC5A5. Other members of the same family include Na^+/glucose co-transporters, the Na^+/myoinositol transporter and Na^+/monocarboxylate transporter [58]. The human NIS gene has been mapped to chromosome 19 (19p13.2-p12). The entire human NIS transcript spans 3.7 kb and encodes a protein of 643 amino acids [54]. Human NIS protein is anticipated to have a molecular weight of 75-100 kDa depending upon its glycosylation status in different tissues [3, 6, 59].

1.6: Structure of NIS protein

Initially, NIS protein was suggested as an intrinsic membrane protein containing 12 putative transmembrane domains with both intracellular NH_2 and COOH termini [53]. However, the currently accepted secondary model for NIS protein indicates that it has 13 transmembrane domains, with an extracellular NH_2-terminus, an intracellular COOH-terminus, and three extracellular N-linked glycosylation sites (**Figure 1.4**). In fact, Levy et al. confirmed three putative glycosylated asparagine residues within the rat NIS sequence, including N225 on the fourth extracellular domain and N485 and N497 residues on the seventh extracellular domain of the secondary model of rat NIS respectively [60]. Levy et al. also demonstrated that glycosylation is not necessary for NIS activity, as a non-glycosylated rat NIS mutant generated by site-directed mutagenesis had 50% of the radioactive iodide uptake activity exhibited by wild type rat NIS. However, it is uncertain whether this reduction in NIS activity was due to a decrease in iodide turnover rate or inefficient cell surface trafficking of the non-

glycosylated NIS mutant [60]. Three putative glycosylation sites have been proposed to be located at homologous asparagines residues within the human NIS sequence [54].

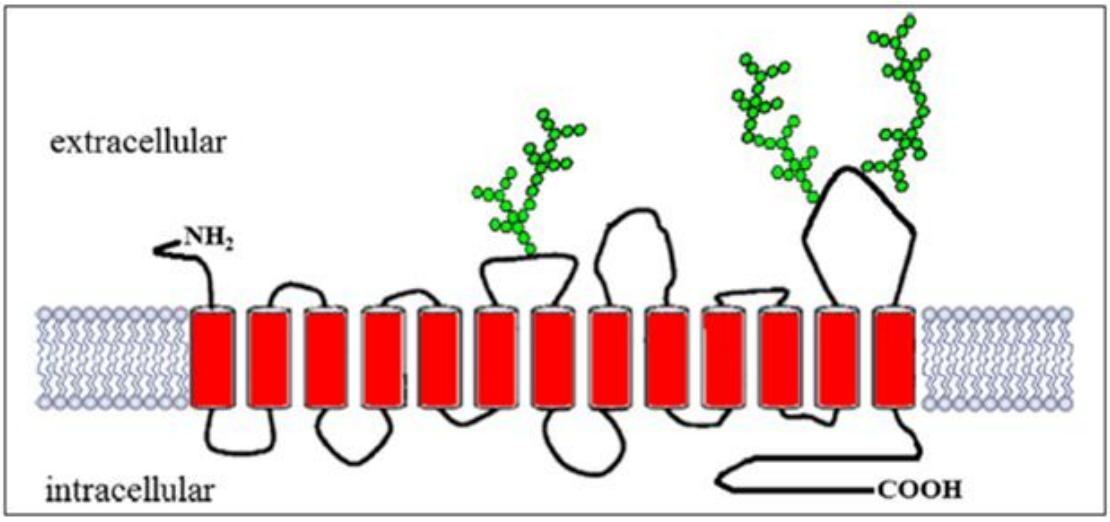

Figure 1.4: Proposed secondary structure of the NIS with thirteen transmembrane domains. *Schematic showing predicted secondary structure of NIS protein indicating presence of thirteen transmembrane domains (in red), an extracellular NH2-terminus, an intracellular COOH-terminus, and three extracellular N-linked glycosylation sites (in green)* [61].

1.7: NIS-mediated radionuclide therapy of thyroid cancer patients

For over seventy years, NIS has been exploited for imaging and targeted radioiodide therapy of residual and metastatic thyroid cancer after total thyroidectomy. In patients suffering from differentiated thyroid cancer, total thyroidectomy is followed by gamma camera imaging with $^{131}I/^{123}I$, as the remaining lesions show efficient iodide absorption due to NIS expression [62]. Since positron emission tomography (PET) imaging provides better resolution than gamma camera imaging, ^{124}I based PET imaging is more sensitive for detection of the residual lesions compared to ^{131}I mediated whole body scintigraphy [63]. Ablation of the thyroid

remnant, following the removal of the primary tumor, may decrease recurrence of differentiated thyroid cancer [64]. If NIS expression is retained in distant metastases, ^{131}I treatment is highly effective and markedly increases the survival rate, especially in younger patients with small metastases [65]. However, expression of endogenous NIS and subsequent radioiodide uptake is often reduced in metastatic thyroid cancer [66]. Therefore, stimulation of NIS expression is often required prior to the ^{131}I administration which is currently achieved by elevating thyroid stimulating hormone (TSH) levels [67, 68]. TSH levels can be elevated by T4 withdrawal or by exogenous administration of recombinant TSH which in turn selectively induces NIS expression and cell surface localization in thyroid follicular cells [69]. Studies have also demonstrated an increase in NIS expression and subsequent enhancement of iodide concentration in thyroid tumor cells, by using inhibitors of oncogenic signaling pathways *in vivo* and *in vitro* [10]. Further, restoration of NIS expression by differentiation inducible agents, by genetic or epigenetic mechanisms [10, 70], or enhancement of iodide uptake by using potential NIS translocation stimulators, have been reported in less differentiated thyroid cancer cells [71]. Altogether, these findings provide a promising basis to expand the radioiodine therapy approach for those thyroid cancer cases which are otherwise nonresponsive.

1.8: NIS expression in extra-thyroidal tissues

NIS expression is also observed in some extra-thyroidal tissues, including salivary gland, gastric mucosa, choroid plexus, lacrimal glands and lactating mammary glands [72]. Modest iodide uptake is usually detected in the salivary gland, stomach, and intestines during whole body imaging with radioiodide [73]. The uptake of iodide in these tissues can be blocked by perchlorate and thiocyanate. As expected, iodide organification is generally not observed in these tissues. Also, TSH exerts no regulatory influence on iodide concentration in extra-thyroidal tissues due to the absence of TSH receptor [74].

1.8.1: NIS expression in mammary tissues

While NIS is not expressed in the normal, non-lactating mammary gland, its expression on the basolateral membrane of the alveolar cells is induced during late pregnancy and lactation phase [2, 3]. Presence of NIS protein accumulates iodide in the milk (20-700 μg/l) (six to fifteen fold higher than the plasma iodine concentration) as a source of nourishment for the newborn to support synthesis of its thyroid hormones important for the developing nervous system, skeletal muscle and lungs [74, 75].

1.9: NIS expression in breast carcinoma samples

Radioactive iodine uptake in malignant breast was detected 40 years ago suggesting possible role of NIS in diagnosis and therapy of BC patients [76]. Following the cloning of human NIS, in a breakthrough study, Tazebay et al. first demonstrated NIS protein expression in 80% BC cases in a cohort of 23 samples compared to only 23% expression in the 13 noncancerous samples adjacent to or in the vicinity of the tumors [3]. In addition, none of the 8 normal samples from reductive mammoplasty displayed NIS expression, indicating its potential in BC management. Moon et al. in 2001 demonstrated ^{99m}Tc pertechnetate uptake in 4 out of 25 BC samples using scintigraphy [5]. In another study, Wapnir et al. reported NIS expression in 76% invasive and 88% of non- invasive breast carcinomas while majority (87%) of normal breast tissues were found to be negative for NIS expression. NIS staining was intense in these cases and localization was predominantly cytoplasmic [77]. To date, NIS expression in BC has been detected by real time polymerase chain reaction (RT-PCR), RNase protection assay, western blot, scintigraphy and IHC. Overall, majority of these studies have established that NIS is expressed in 70-90% of breast cancers with diverse histological and molecular subtypes. All these findings together put forward the scope of NIS-mediated radioiodide imaging and therapy methods as an alternative approach or in combination with other

existing methodologies towards management of the malignant breast disease. But surprisingly, NIS-mediated iodide transport was detectable only in 25% NIS-positive breast cancers [4]. Also, the amount of NIS protein may not be sufficient to elicit therapeutic response. In a recent clinical finding by our group, it has been revealed that out of 70% of the BC cases positive for NIS expression, about 30% of cases (2+ and 3+ score) showed intense staining equivalent to thyroid or salivary gland expression. These BC patients are expected to get benefit of NIS-mediated targeted radiotherapy [8]. But for the rest of the patients with low NIS expression, it may be difficult to achieve therapeutic benefit. These discrepancies between NIS expression and function have led to studies with deeper understanding of NIS gene regulation in breast cancer and to define ways of enhancing the endogenous NIS expression in patients exhibiting moderate or low expression.

1.10: Understanding regulation of NIS expression and function in breast cancer

From previous literature, it is well known that NIS gene regulation is organ specific and its regulation in breast tissue substantially differs from that of the thyroid [10, 78, 79]. In thyroid, it is mainly mediated by TSH, whereas TSH does not exert any modulation of NIS expression and function in mammary tissue. This differential regulation provides an edge in controlling NIS expression in thyroid without affecting its status in breast tissues or vice versa. Therefore, during this study, we focus on understanding the transcriptional regulators in breast cancer cells which are discussed in detail in **Chapter 2** and **Chapter 3**.

1.10.1: Hormonal regulation of human NIS in mammary gland

In healthy individuals, mammary gland NIS is expressed solely during lactation. The functional expression of NIS starts at mid-pregnancy and reaches its peak at end-pregnancy. Interestingly, after birth, NIS expression is suckling-dependent in a reversible manner [2, 3]. As reported in literature, NIS expression in the lactating mammary gland is regulated by levels

of lactogenic hormones. Oxytocin which is released in response to suckling, independently increased NIS protein levels and iodide uptake in the mammary glands of nubile mice [3]. In agreement, Cho et al. reported that an oxytocin antagonist (OTA) inhibited iodide uptake in the lactating rat mammary gland [2]. However, oxytocin-induced NIS expression appears to require prior induction by estrogen. In contrast, Prolactin, another hormone involved in lactation, did not increase NIS protein or iodide uptake but inhibited oxytocin-induced NIS expression in the mammary glands of mice. A combination of estrogen, oxytocin and prolactin, however, produced the highest increment in NIS protein expression in the mammary glands of ovariectomized mice, suggesting that prolactin can further increase NIS expression only in the presence of high levels of estrogen [3]. Estrogen diffuses into cells through membranes and binds to their intranuclear estrogen receptors (ERs) and regulates the expression of many target genes [80]. Estrogen may have a direct effect on mammary gland NIS transcription, as the NIS promoter contains several half-site estrogen-responsive elements [81]. A recent finding by our group also reported a positive association of NIS and ER expression in breast cancer [8].

1.10.2: Regulation by retinoic acids

Retinoids are both naturally occurring or synthetic vitamin A metabolites and analogs. Retinoic acid (RA) is a well-known inducer of differentiation. There are two types of retinoic acid receptors (RAR). These are RAR and RXR receptors which are activated by different ligands and encoded by different genes. While RARs are activated by both 9-cis and all-trans retinoic acid (atRA), RXR is activated only by 9-cis RA. RA receptors dimerize upon ligand binding to activate target genes. Kogai et al. reported that human NIS expression and iodide uptake is stimulated by RA treatment in ER-positive MCF-7 human breast carcinoma cells, whereas there is no effect on NIS expression in ER-negative MDA-MB-231 cells and normal

human breast cells [82]. In another study, Ryan et al. reported upregulation of NIS expression by stimulation of both the retinoic acid and estrogen receptors with their respective ligands (atRA and E2) in epithelial breast cancer cell lines [83]. Other than these few reports, cis- and trans-acting transcriptional regulators of NIS expression in mammary tissue/breast cancer are unknown.

1.11: Theranostic potential of NIS

NIS has distinct advantages as an imaging reporter gene and a therapeutic gene. NIS mediates uptake of a wide variety of radioactive iodide isotopes like ^{125}I, ^{124}I and ^{131}I as well as radiopharmaceuticals like ^{99m}Tc, ^{186}Re, ^{188}Re and ^{211}At. This unique characteristic of NIS protein allows visualization of NIS-expressing cells with planar scintigraphy, or tomographic imaging procedures such as SPECT or PET with respect to the gamma emitting or positron emitting radiotracer administered respectively [84]. The different imaging modalities employed in visualization of NIS function as well as optical imaging techniques are discussed in the following section.

1.11.1: NIS as a reporter gene

In its dual role as a diagnostic reporter as well as a therapeutic gene candidate, NIS allows direct, non-invasive monitoring of its function by ^{123}I-scintigraphy, ^{125}I-SPECT and ^{124}I-PET-imaging. It also allows exact dosimetric calculations before proceeding to therapeutic application of ^{131}I [85]. As a reporter gene, NIS provides an elegant means for non-invasive monitoring of quantitative expression of transgene expression in real time [69, 86-88]. *In vivo* non-invasive imaging of NIS gene was performed for the first time by Shimura et al. by transfection of rat NIS cDNA into malignantly transformed rat thyroid cells (FRTL) [89]. NIS gene based cardiac imaging has also been demonstrated by various groups [90, 91]. Since reporter genes can be used for tracing the localization of transplanted cells, Terrovitis et al.

introduced lentiviral vector expressing NIS in rat cardiac derived stem cells. Transplantation of these cells back to rats enabled ^{125}I mediated SPECT imaging [92]. NIS has also been used as a reporter for studying the recruitment of macrophages at the site of inflammation by ^{124}I micro-PET imaging [93]. NIS has also been used to monitor biodistribution of vectors and trafficking of therapeutic cells [94].

1.11.2: NIS as a therapeutic gene

The therapeutic potential of endogenous NIS in BC has been discussed in detail in the following Chapter. In this section, we have briefly discussed the utility of this therapeutic gene for the treatment of various other cancers including BC.

NIS gene transfer has been successfully performed in a variety of animal models using different vector systems and promoters [95-99]. hNIS-expressing cells were selectively killed *in vitro* and a bystander effect has been suggested in 3-dimensional spheroid cultures [100-102]. Spitzweg et al. demonstrated tissue specific expression of human NIS in androgen sensitive prostate cancer cell line (LnCaP cells) where NIS was expressed under a prostate tissue-specific antigen (PSA) promoter [103]. Further, these stably transfected prostate cancer cells revealed a long biological half life of radioiodine of 45 hours *in vivo* resulting in 84% tumor reduction after a single intraperitoneal application of a very high, 111- MBq, dose of ^{131}I [104, 105]. In another study, Dingli et al. used self inactivating lentiviral vector for NIS gene expression under immunoglobulin promoter, to selectively target multiple myeloma cells and reported efficacious results in mice xenograft model with a tumor free survival in 5 month follow up time [106]. Willhauck et al. used a mouse alpha fetoprotein (AFP) promoter construct to target hepatocellular carcinoma (HCC) cells. The *in vitro* and *in vivo* results showed a sufficient therapeutic effect of ^{131}I for the treatment of liver tumor [107]. Dwyer et al. described possible application of NIS-mediated radiotherapy in ovarian cancer animal model using

engineered NIS-expressing ovarian cancer cells [108]. Ghosh et al. investigated the effect of NIS-mediated ^{131}I radiotherapy in MCF-7 xenograft model overexpressing NIS gene via lentiviral vector system [109]. In a very recent report, Renier et al. investigated the effectiveness of Gemcitabine in NIS-mediated ^{131}I therapy in an experimental breast cancer brain metastasis mouse model and dramatic tumor regression was observed as a result of this combination treatment [110]. Klutz et al. established a systemic nonviral NIS gene delivery approach in a neuroblastoma mouse model (Neuro2A). Tumor-specific iodide accumulation was observed, resulting in a significant therapeutic effect after ^{131}I application even without iodide organification [111]. The same group has further demonstrated that systemic NIS gene transfer using polyplexes coupled to an EGFR-targeting ligand is capable of inducing tumor-specific iodide uptake and significant delay in tumor growth associated with increased survival in humans HCC xenograft; representing scope of systemic NIS gene therapy even in metastatic cancers [112]. Utilizing NIS as a theranostic gene, Knoop et al. demonstrated mesenchymal stem cell-mediated, tumor stroma–targeted radioiodine therapy of metastatic colon cancer [113].

1.12: Molecular imaging

Molecular imaging (MI) depicts the visual representation, characterization and quantification of biological processes at the cellular and subcellular levels in intact living organisms. It is a novel multidisciplinary field that implies the convergence of multiple image-capture techniques, basic cell/molecular biology, chemistry, medicine, pharmacology, medical physics, biomathematics, and bioinformatics into a new imaging paradigm. MI modalities offer simultaneous visualization and quantitation of cellular and molecular processes, pharmacokinetic processes and drug interactions throughout an intact living subject, offering understanding of the genetic basis of diseases and development of new therapies in a more

meaningful manner. Molecular imaging includes both direct imaging with the help of nuclear medicine radiopharmaceuticals and indirect imaging using various reporter systems.

1.12.1: Radionuclide imaging

Nuclear medicine is a discipline focused on the management of patients through the use of injected radiolabelled tracers supporting imaging technologies such as PET and SPECT. PET/SPECT provides 3-dimensional distribution of radiopharmaceuticals and have superior sensitivity and high resolution with excellent tissue penetration depth [114]. These advantages permit these imaging techniques for use in translational research, from cell culture to pre-clinical animal models to clinical applications [115]. NIS protein function can be visualized by planar scintigraphy, SPECT or PET imaging [84]. Both PET and SPECT give quantitative information on NIS gene expression or the number of NIS-expressing cells [84, 115]. There are no issues of labeling processes and stability when using radioiodine pharmaceuticals, which may be a major concern during use of radiolabelled ligands of other radionuclide-based reporter genes such as dopamine D2 receptor or herpes simplex virus thymidine kinase (HSV-tk) genes [116]. Gamma camera imaging with radioiodine (^{131}I or ^{123}I) is utilized to monitor metastatic lesions in differentiated thyroid cancer patients post thyroidectomy as these NIS expressing lesions are capable of iodide trapping [62].

1.12.2: Optical imaging

Optical imaging (OI) has rapidly gained popularity over the other MI techniques. It is a relatively fast imaging technique that can operate through low cost detection devices. OI allows non-invasive *in vivo* imaging by capturing light photons from the subject for extracting relevant biological information in real time. It mainly involves fluorescence and bioluminescence imaging.

In fluorescence imaging, light of one excitation wavelength (in the visible light range of 395–600 nm) illuminates the living subject and a charged-coupled device (CCD) camera collects emitted light of shifted wavelength. Cells tagged with fluorescently labeled antibodies or GFP protein (green fluorescent protein) can be followed by this technique [117, 118]. GFP is a protein from the jellyfish *Aequorea victoria* or other marine animal sources that has been utilized extensively as a reporter in fixed and cultured cells and tissues. Wild-type GFP emits green (509-nm) light after excitation by violet (395-nm) light. The variant EGFP is a 35-fold brighter protein with a shifted excitation spectrum to longer wavelengths [119]. Fluorescence optical imaging can be used for a variety of molecular imaging applications in living subjects. Few examples include study of matrix metalloproteinases (MMPs) activities using activatable imaging agents [120], detection of HER2/neu tumors in animal models using rhodamine green conjugated antibodies [121], monitoring tumor growth and metastasis using GFP-expressing tumors [122].

The two major advantages of fluorescence imaging are that it can be used as a reporter in both live and fixed cells/tissues and no substrate is required for its visualization [123]. However, autofluorescence, limited depth of penetration (<1 cm) and the toxicity of few of the imaging agents (e.g., cadmium based QDots) may limit its use in humans. In contrast to fluorescence imaging in the visible light range, the use of the near-infrared (NIR) spectrum in the 700–900-nm range maximizes tissue penetration and minimizes autofluorescence from non-target tissue [124]. Several NIR fluorochromes have become available [125] that can be coupled to affinity molecules (peptides, antibodies) or that are activatable [126]. Only two fluorescent probes are currently approved (the non-specific indocyanine green and fluorescein) [127, 128] and clinical trials of fluorescent systems continue to progress [129, 130].

Bioluminescence imaging (BLI) is based on the detection of photons emitted from cells or tissues in a living organism resulting from oxidative catalysis of substrates by luciferase

enzymes. Luciferases encompass a broad range of enzymes catalyzing chemical reactions in living organisms with production of light. There are three luciferases that have been studied in detail and are commonly used in biomedical research, these include the *Photinus pyralis* (firefly) luciferase (Fluc); the sea pansy *Renilla reniformis* luciferase (Rluc); and the marine copepod *Gaussia princeps* luciferase (Gluc). Rluc interacts with its substrate coelenterazine (and its analogs) with requirement of oxygen as a cofactor. Gluc is naturally secreted and, similar to Rluc, does not require ATP for activity. The substrate for firefly luciferase is a benzothiazole luciferin. The enzyme needs ATP, Mg^{2+} and oxygen as cofactors and photons are emitted in the range of 560-614 nm light depending on luciferase and the physiological conditions. Since this enzyme requires ATP as well as oxygen, the luciferase expressing cells give maximum signal in a highly metabolic state and aerobic environment. Fluc and Rluc (or Gluc) make use of different substrates and therefore can be utilized as dual reporter system for imaging two different processes simultaneously or sequentially in cultured cells and also from the same living animal, due to distinct kinetics of light production (glow vs flash) [131, 132]. The blue bioluminescence (480 nm peak) of Gluc and Rluc is strongly absorbed by pigmented molecules like hemoglobin and is scattered by tissues, making them less suitable for *in vivo* imaging as compared to Fluc, which emits green light (562 nm). The identification of red-emitting luciferases from *Luciola italica* (Italian firefly) [133] and railroad worm [134], as well as novel chemical reactions leading to red-light output [135-138], will greatly enhance the sensitivity of BLI in deep tissues.

The main advantage of optical bioluminescence imaging is that it can be used to detect very low levels of signal because of the absence of the background signal. It is quick and easy to perform, allowing testing of biological hypotheses in living experimental models. It is also uniquely suited for high-throughput imaging because of its simple operation, short acquisition times (typically 10–60 sec), and simultaneous measurement of upto six anesthetized living

mice [139]. Although optical imaging methods are excellent tools in pre-clinical settings, their use in clinics is limited, as many of these genes and their substrates are immunogenic and tissue depth in human subjects may result in very low signal intensity.

1.12.3: Cerenkov luminescence imaging

Cerenkov luminescence imaging (CLI) is a new emerging hybrid modality which is based on light emission from routinely used medical isotopes. When the charged particles released upon radioactive decay travel through a dielectric medium at a speed faster than speed of light, they polarize water molecules along their path. When these polarized molecules relax, they release a continuous wavelength luminescence mainly in the ultraviolet (UV) and blue end of the visible spectrum, known as the Cerenkov radiation (CR). The Cerenkov radiation is continuous polarized radiation with an intensity distribution that is inversely proportional to the square of the wavelength [140].

Cerenkov luminescence imaging (CLI) utilizes small animal optical imaging equipment for collection of visible light from radiotracers [141]. Various reports indicate good correlation between PET and CLI using multiple radiotracer molecules [140]. Recently, ^{131}I and ^{124}I, which are commonly used for NIS reporter imaging, were reported to have sufficient energy to produce Cerenkov radiation that can be visualized with highly sensitive optical imaging instruments [86, 140]. NIS gene transfected cells were successfully imaged with radioiodine using this modality by an optical imaging instrument in an *in vivo* animal model [86, 93]. In another study, CLI was used to visualize the expression of let-7 in lung adenocarcinoma A549 cells transfected with human sodium/iodine symporter-ras gene (hNIS-RU) [142]. CLI was also used for intraoperative imaging of a radionuclide with the help of HER2/neu monoclonal antibody targeted to cancerous cells [143]. Thus, Cerenkov imaging provides an opportunity to bridge the gap between optical (pre-clinical) and nuclear (clinical) imaging

using approved tracers and therapeutic agents. However, the application of CLI is limited due to its low tissue penetration ability, which restricts the use of CLI to small animal research or in humans with superficial tissue depths. One of the challenges with CLI is the decay of the radioactive material resulting in reduction of active material that can produce Cerenkov radiation. However, this challenge can be overcome by using Cerenkov generating radionuclides with a longer half- life. With further improvements, the technique may enable translation of optical imaging techniques into clinics.

In our study, we have explored two non-invasive optical imaging modalities i.e. Bioluminescence and Cerenkov luminescence imaging to study NIS regulation in breast cancer animal model. We have linked human NIS promoter with an optical imaging compatible bifusion reporter gene, i.e. Fluc2.TurboFP in which Fluc2 represents the firefly luciferase gene and TurboFP represents the red fluorescent reporter gene. This bifusion sensor helps in real time monitoring of the transcriptional activity of promoter driven reporter activity by non-invasive optical imaging method *in vitro* and *in vivo* that can be used to discover potential gene regulators. We have also used CLI to monitor the distribution kinetics of ^{131}I in tumor xenograft and simultaneously performed non-invasive bioluminescence imaging to examine the therapeutic efficacy of ^{131}I treatment *in vivo*.

1.13: Rationale

Currently, majority of breast cancer patients are routinely managed with breast-conserving surgery followed by radiation therapy and adjuvant systemic therapies, including chemotherapy, hormone therapy and trastuzumab. Radiotherapy is also combined with systemic treatment in patients undergoing mastectomy and also in locally advanced disease. There are several side effects of systemic chemotherapy including hair loss, loss of healthy

blood cells, tiredness, loss of appetite, nausea, vomiting, mouth ulcers and diarrhea. Owing to the different therapeutic strategies available, management of breast cancer has become more successful over time [144]. However a few challenges still persist which include the majority of women relapsing and dying of ER-positive breast cancer as a result of dormant micrometastases, which are largely untouched by initial adjuvant systemic therapies and resistance to all systemic therapies. Triple-negative breast cancer (TNBC), dominated by genomic instability, and HER2 overexpressing tumors are associated with a less favorable prognosis and higher risk of mortality [145]. Therefore, search for new targeted therapies which can potentiate effective, affordable treatment with high specificity, while minimizing the side effects to healthy normal tissue, is still on.

NIS protein is one such endogenous transporter protein that offers target specific radioiodide accumulation with lesser side effects to the healthy tissues and is currently the best available systemic radiotherapy option to the clinicians, as evident from years of practice in thyroid cancer. Decades of basic and translational research on NIS-mediated diagnosis and treatment for thyroid cancers has enriched our knowledge of NIS biology. Evidences of aberrant expression of this protein in breast malignancies further imply scope of NIS-mediated targeted radiotherapy for management of breast cancer. However, considerable hurdles exist in its actual clinical application. The field of NIS research in breast cancer is at its nascent state as mammary specific NIS gene regulation is not well understood. Constant research is being pursued to effectively understand NIS regulation in breast cancer.

When this strategy is adopted for the treatment of extrathyroidal tumors, it becomes necessary to prevent radioiodide uptake and concentration in normal thyrocytes. Exploiting the differential mechanism of NIS regulation, Wapnir et al. demonstrated the potential for radioablation of metastatic breast cancer and selective downregulation of NIS expression, as well as inhibition of iodide organification in thyroid using combination of T3 and

methimazole [4]. Organification and retention of iodine in breast tissue is not yet reported. Pharmacologic modulation of cellular radioiodine efflux might offer an alternative approach to increase half-life of radioiodine in breast cancer cells. Lithium has been reported to reduce iodine release from the thyroid and was therefore used to enhance efficacy of radioiodine treatment of differentiated thyroid cancer [146]. Further, the expression of NIS protein is not always sufficient to deliver the therapeutic effect. Thus, efforts are focused on understanding the NIS gene regulation in breast cancer condition to elevate its expression to enable use of radioiodine imaging for treatment of breast cancer. From the earlier studies, all trans retinoic acid (atRA) along with several other glucocorticoids is a known inducer of NIS expression and iodide uptake in MCF-7 cells [147]. The unliganded estrogen receptor alpha (ERα) has also been shown to activate mammary NIS transcription in estrogen receptor positive breast cancer cell lines. This is supported by the presence of an estrogen responsive element on the NIS gene promoter [148]. The cardiac homeobox transcription factor Nkx2.5 is also involved in NIS upregulation in MCF-7 cells [12]. Along with these regulators, human NIS (hNIS) expression is also modulated by epigenetic modifiers such as histone deacetylase inhibitors (HDACi) and these agents are known to restore NIS expression and function in breast cancer cells [14, 149]. Even though all these studies are informative suggesting their potential clinical application, pre-clinical or clinical efficacy has not yet been proven to date. Therefore, investigation of potential regulators and their pertinence to human breast tissue is required.

Based on the above mentioned rationale, following objectives were framed:

1. To establish a cell-based screening platform to identify putative pharmacological/genetic modulators and study their effect on hNIS expression
2. To study the effect of histone acetylation on hNIS expression
3. To characterize p53 mediated modulation of hNIS expression

4. *In vivo* functional assessment of drug effects on hNIS gene function using imaging methods

Objectives 1, 2 and 4 are covered in Chapter 2 while objectives 3 and 4 are covered in Chapter 3 of this thesis.

2. Enhancement of human sodium iodide symporter gene expression by treatment of histone deacetylase inhibitors to improve radioiodide therapeutic efficacy in breast cancer

2.1: Introduction

As mentioned earlier, BC is the most frequent cancer among women all over the world [150]. In recent years, breast cancer has been realized as 'a disease of ten' and metastatic spread as well as resistance development to conventional medicine in practice has raised greater concern in management of BC [151-153]. Therefore the current focus for development of targeted strategies in BC is actively being pursued to identify suitable therapy procedures that can provide treatment with high specificity while minimizing the side effects. In this context, the aberrant overexpression of human sodium iodide symporter (hNIS) protein in breast cancer tissue is gaining great deal of attention. While human NIS is not expressed in normal, non-lactating mammary glands, NIS expression is observed in the lactating mammary glands favoring iodide concentration in the milk for neonatal nutrition [3]. Presence of NIS in breast cancer is first reported by Tazebay et al. showing NIS protein expression in 80% of BC patients, compared to none of the normal breast tissue samples examined from the patients undergoing reductive mammoplasty [3]. It is also reported that, in a transgenic female mice model with active *ras* or *neu* oncogenes under MMTV promoter, NIS mediated ^{99m}TcO4 uptake is seen only in the tumor bearing mammary gland and not in the non-tumor bearing mammary gland [3]. Additionally, study by Moon et al. has confirmed functional NIS expression in humans malignant mammary tissues using ^{99m}TcO4 scintigraphy [5]. Along with NIS expressing primary breast tumors, NIS-mediated iodide uptake has also been confirmed in metastatic nodules by scintigraphy procedure whereas thyroidal iodide uptake was suppressed using T3 and methimazole [4]. Subsequently, reports of NIS protein expression in breast tumors of diverse histological and molecular subtypes, indicate to extend targeted radioiodide therapy in NIS expressing tumors [4, 7, 8, 77]. However, irrespective of moderate NIS expression is encountered in a majority of the BC cases, only 15-20% of NIS-positive breast tumors have detectable radionuclide uptake that may or may not be sufficient for therapeutic

benefit [4, 5]. This discordance between NIS expression and function has encouraged further research studies to focus on modulation approaches of endogenous NIS expression in BC. A recent clinical analysis by our group on subtype specific intensity profiling of NIS expression has revealed that about 30% of NIS positive (2+ and 3+ score) cases have intense NIS staining equivalent to thyroid expression [8]. Therefore, for benefit of patients exhibiting moderate or low protein levels, defining ways to achieve adequate NIS expression can impact NIS based therapy procedure.

NIS gene expression is differentially regulated in thyroid and breast tissue and NIS regulation in breast tissue has not yet well characterized [78, 154]. Several groups have reported that NIS in BC cells can be induced *in vitro* using lactogenic hormones, insulin and even by some nuclear receptor ligands, such as retinoids and peroxisome proliferator-activated receptor-γ (PPARγ) ligands [61, 78, 155, 156]. All-trans retinoic acid (atRA) alone or in combination with other glucocorticoids such as Dexamethasone (Dex) has been demonstrated to induce both NIS gene expression as well as iodide accumulation in MCF-7 cells [9] and *in vivo* mouse model [147] . In another report, Carbamazepine (CBZ), an agonist of pregnane X receptor (PXR), has been described to significantly (~1.8 fold) enhance atRA-induced iodide uptake both in the presence and absence of Dex although a relatively high concentration (100 μM) of CBZ is required for the maximum stimulatory effect [11]. All these findings suggest potential clinical use of atRA. But the NIS induction in BC tissues required a relatively large dose of atRA which is ~17 fold higher than the maximum tolerable dose in humans for solid tumors [157]. The high dose requirement and *in vivo* instability of atRA actually limit its clinical application.

Like most gene functions, NIS expression is also regulated by epigenetic modifications in thyroid and/or breast cancer cells and the agents targeting these modifications can be used to restore NIS expression for therapeutic benefit. Demethylating agents and histone deacetylase

inhibitors (HDACi) are known for exerting epigenetic control by regulating chromatin structure and gene expression [158]. These epigenetic agents are also known to increase NIS expression and function in thyroid cancer cells [159]. The human NIS gene has three CpG-rich regions, located about 100bp upstream of the transcription start site, located in the 5'-untranslated region, and located in the coding region of the first exon. It has been shown that the demethylating agent 5-azacytidine restored NIS mRNA expression in several papillary thyroid cancer cell lines, which was associated with demethylation of NIS DNA in the untranslated region within the first exon [160, 161].

Apart from controlling chromatin architecture and gene expression, HDACi can also modulate a variety of cell functions such as growth, differentiation and survival by affecting non-histone proteins such as transcription factors, molecular chaperones and structural proteins [70, 162]. It has been shown that depsipeptide treatment increases functional NIS expression together with induced expression of TPO, Tg and TTF-1 in several thyroid cancer cell lines [163]. In subsequent years, various studies have reported that NIS expression can be modulated by certain HDACi in thyroid cancer cells [13, 159, 164]. Even though the exact molecular mechanism of NIS induction is poorly understood, the role of thyroid specific transcription factors has been predicted. In this context, effect of HDACi on NIS expression in BC is not studied in detail. Very recently, while this thesis work was ongoing, published reports have shown NIS modulation by HDACi in BC cells as well [14, 149]. Although these studies are informative, the exact mechanism of transcriptional activation of NIS in response to HDACi treatment in BC is still not recognized. Thus, in the present study, we have performed a comprehensive investigation to reveal biochemical basis of HDACi mediated modulation of NIS expression and function in breast cancer cell and animal model. The study implicates that epigenetic transcriptional modulation strategy as a promishing approach and may be attempted for clinical trial in future.

2.2: Materials and methods

2.2.1: Chemicals

HDACi drugs such as TSA [T8852], NaB [B5887], VPA [4543], SAHA [SML0061] and TBA [SML0044] were purchased from Sigma, USA. CI994 (1742-10, 50) was purchased from Biovision, CA, USA. Stock solutions (1M) of TSA, SAHA, CI994 and TBA were prepared in DMSO and for NaB and VPA stocks were prepared by dissolving the drug in sterile MiliQ and stored at -20˚C.

Table 2.1: Various HDAC inhibitors used in this study to check their effect on NIS expression

Group	Compound	HDAC Targets	Potency (in cells)	Type of cancer	Clinical Trial	Reference
Hydroxymate	Trichostatin A (TSA)	Class I, II	Nano Molar	-	-	-
	Suberoylanilide hydroxamic acid (SAHA)	Class I , II	Micro Molar	CTCL	FDA approval for CTCL	[165]
	Tubastatin A (TBA)	HDAC6	-	-	-	-
Aliphatic acid	Valproic acid (VPA)	Class I & IIa	Milli Molar	Prostate cancer	Phase 3	[166]
	Sodium butyrate (NaB)	Class I & IIa	Milli Molar	Lung cancer	Phase 2	[167]
Benzamide	CI994	ND	Micro Molar	Pancreatic cancer	Phase 2	[168]

ND- Not Determined

FDA- Food and Drug Administration

CTCL- Cutaneous T Cell Lymphoma

2.2.2: Plasmid construction and validation

pFluc2.TurboFP vector was cloned earlier in the lab. Fluc2.TurboFP fusion reporter DNA fragment was excised using NheI and BamHI restriction digestion and inserted into the pcDNA3.1+vector (Addgene V790-20) downstream to the CMV (cytomegalovirus) promoter **(Figure 2.1A).** The positive clone was validated by sequencing and restriction digestion analysis **(Figure 2.1B).** pGL3-NIS-luc+ vector containing 1.34kb human NIS promoter was a kind gift from Dr. Kenneth Ain, University of Kentucky, USA. NIS promoter was PCR amplified using primers (5'- GGCACGCGTATGTGCCACCACG and 3'-GGCGCTAGCGGAGGTCGCCTTG) with 5'-MluI and 3'-NheI enzyme sites replacing the CMV promoter from the pcDNA3.1+ Fluc2.TurboFP plasmid DNA (**Figure 2.1C**). Thus, the final clone obtained (pNIS-Fluc2.TurboFP) was confirmed by sequencing and restriction enzyme digestion and used for further experiments (**Figure 2.1D**).

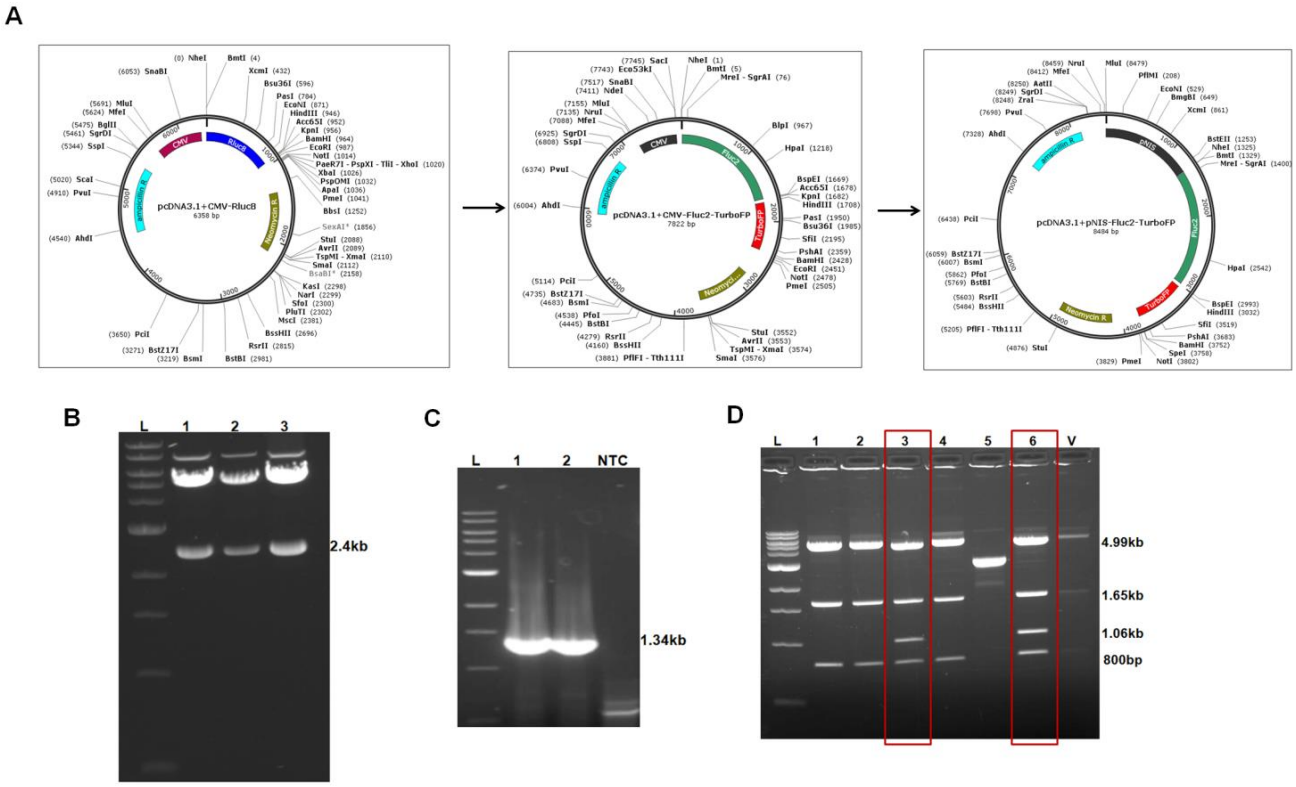

Figure 2.1: Cloning strategy for development of pNIS-Fluc2.TurboFP reporter plasmid. *A. Vector maps of pcDNA3.1+CMV-Rluc8, pcDNA3.1+CMV-Fluc2.TurboFP and pcDNA3.1+pNIS-Fluc2.TurboFP are shown. As a starting material, pcDNA3.1+CMV-Rluc8 was taken, digested with NheI and BamHI and Rluc8 reporter was replaced with Fluc2.TurboFP. In the next step, CMV promoter sequence was replaced by human NIS promoter sequence. B. Confirmation of pcDNA3.1+CMV-Fluc2.TurboFP clone by digestion with NheI and BamHI, showing the release of 2.4kB Fluc2.TurboFP reporter fragment. All the three clones tested were found to be positive. C. PCR amplification of human NIS promoter indicating the amplification of 1.34kb band that was used for the next step of cloning. D. Confirmation of pcDNA3.1+pNIS-Fluc2.TurboFP clones by restriction digestion with ApaI enzyme. As the NIS promoter sequence has one ApaI site, positive clones exhibited four bands of 4.99kb, 1.65kb, 1.06kb and 800bp respectively. The original vector was used as a control to check the insertion of NIS promoter. Out of the 6 clones tested, clone 3 and 6 were identified positive. The final vector constructed was also confirmed by sequencing and used for further experiments.*

2.2.3: Mammalian Cell culture

Several breast cancer cell lines used in the study are listed in the **Table 2.2**

Table 2.2: Details of the breast cancer cell lines used in the study

Name	Origin	Pathology	ER	PR	HER2	p53	Media
MCF-7	Pleural effusion	Invasive ductal carcinoma	+	+	+	wild type	RPMI
Zr-75-1	Ascites	Invasive ductal carcinoma	+	+	+	wild type	RPMI
MDA-MB-231	Pleural effusion	Adenocarcinoma	-	-	-	mutant	L15
MDA-MB-468	Pleural effusion	Adenocarcinoma	-	-	-	mutant	DMEM
MDA-MB-453	Pericardial effusion	Metastatic carcinoma	-	-	-	null (lack functional protein)	L15

Two thyroid cancer cell lines, NPA and ARO (gifted by Dr. Avik Chakraborty, BARC, India), were also included in the study (**Table 2.3)**.

Table 2.3: The different thyroid cancer cell lines used in the study

Name	Subtype	Media
NPA	Papillary thyroid cancer	IMDM
ARO	Anaplastic thyroid cancer	IMDM

Cell culture media were completed 10% fetal bovine serum (FBS) (Gibco, Invitrogen, USA), 1% antibiotic-antimycotic solution (Gibco, Invitrogen, USA). For thyroid cancer cells, media also contained 0.075% gentamycin solution (Sigma, USA). All the cell lines were maintained

at 37°C in a humidified incubator (Thermo Scientific, Rockford, IL, USA) with 5% CO_2 except for MDA-MB-231 and MDA-MB-453.

2.2.4: Stable cell lines

The pNIS-Fluc2.TurboFP plasmid DNA was transfected into MCF-7, MDA-MB-231 and Zr-75-1 cells using lipofectamine 2000 (Life Technologies, USA). Clonal selection was achieved using G418 sulphate (500 μg/ml for all the cell lines) (Sigma, USA). Positive clones were confirmed by luciferase reporter activity.

2.2.5: MTT cell cytotoxicity assay

To evaluate cytotoxicity of various HDACi, MCF-7 and MDA-MB-231 (5×10^3) cells were seeded in 96 well plates (Corning, USA). Cells were exposed to different concentrations of HDACi for 48 hours. Cell viability was assessed using the MTT (3-[4,5-dimethylthiazol-2-ylc-2,5-diphenyltetrazolium bromide) reagent (Sigma, USA).

2.2.6: RNA extraction and quantitative real-time PCR

After the cells were treated with HDACi for 48 hours, RNA was extracted using RNeasy kit (QIAGEN, USA). cDNA was synthesized using the first strand cDNA synthesis kit (Invitrogen, USA). Quantitative real-time PCR was performed using TaqMan probe mix on the 7900HT PCR cycler (Applied Biosystems, USA). The TaqMan probes for human NIS and GAPDH with assay IDs Hs00166567_m1 and Hs02758991_g1 respectively were used (Applied Biosystems, USA). RT-PCR reactions were set in triplicate for each sample. The comparative ΔΔCt method was used to calculate relative gene expression.

2.2.7: Immunoblotting and immunofluorescence procedures

Cells were treated with various HDACi for 48 hours and were lysed using cell lysis buffer (Cell Signaling Technology, USA) containing standard protease inhibitors (Santa Cruz Biotechnology, USA). Equal amount of protein from control and treated cells were resolved in 10% SDS-PAGE gel and transferred onto nitrocellulose membrane (Millipore, USA) by semi-dry method. After blocking with 5% BSA (Bovine Serum Albumin), membranes were probed with respective monoclonal antibodies, such as anti-acetyl-histone H3 antibody (06-598, Upstate, USA) and anti-Fluc antibody (G4751, Promega Corporation, USA), or anti-human NIS antibody (FP5A, Abcam, USA), and anti-α-tubulin antibody (T9026, Sigma, USA) followed by washing and secondary HRP-conjugated antibodies. The blot was developed by chemiluminescence (Invitrogen, USA). To determine even transfer and equal loading, membranes were stripped and re-probed with α-tubulin monoclonal antibody as per standard practice.

For immunofluorescence study, cells were fixed with 4% paraformaldehyde, washed with PBS and blocked with 2% BSA followed by overnight incubation with primary antibody for human NIS and γH2Ax (Pierce Biotechnology, USA) at 4˚ C. An additional permeabilisation step with 0.2% Triton 100 in 4% PFA was carried out for foci staining before BSA blocking step. The cells were then washed with PBS, incubated with anti-mouse (NIS)/ anti rabbit (γH2Ax) Dylight 633 conjugated secondary antibody (Thermo Scientific, Rockford, IL, USA) (1h), washed and counterstained for nucleus using DAPI (Sigma, USA). Fluorescence micrographs were captured using Carl Zeiss LSM 510 Meta confocal microscope.

2.2.8: Luciferase reporter assay

Selected MCF-7 and MDA-MB-231 clonal cell population were seeded at an equal cell density. Lysates were collected using passive lysis buffer (Promega Corporation, USA) and

luciferase activity was counted by measuring photon outputs using a luminescence microplate reader (BMG Labtech, Germany). The data was plotted as relative light unit per second (RLU/sec) normalized with protein concentration estimated by Bradford method (B6916, Sigma, USA).

2.2.9: Transcription factor (TF) activation profiling and NIS promoter binding array

We used a 96 well plate TF activation array (# FA1002, Signosis, USA) as per the manufacturer's guideline. MCF-7 cells were treated with NaB/ VPA for 48 hours and nuclear proteins from both control and treated cells were isolated using standard procedure and used as probe on the array plate. Read-out value of Transcription factor IID (TFIID) was used for normalization for all other readings. TFs were selected by considering the fold-change method (≤1.5 or ≥1.5) of treated over untreated cell samples (**Figure 2.2**).

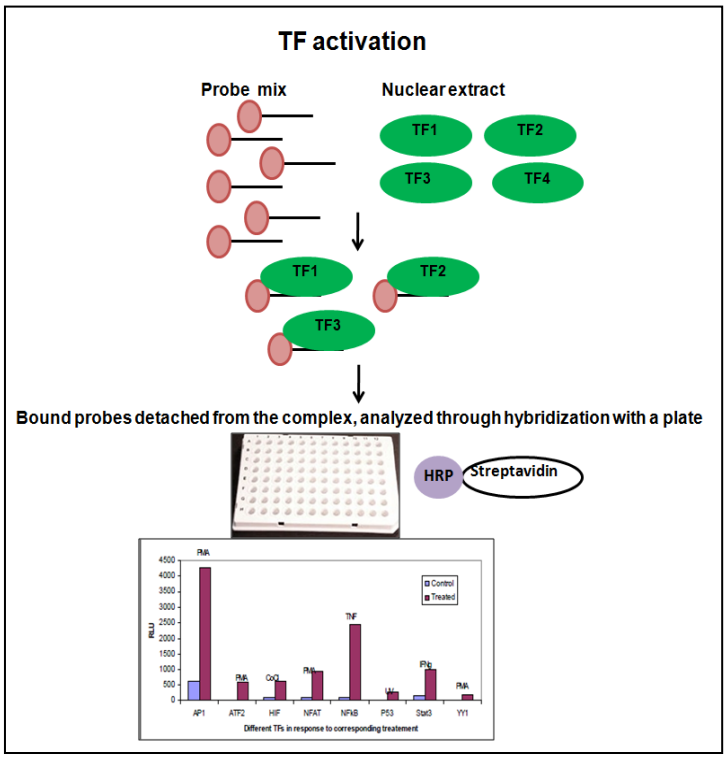

Figure 2.2: Schematic of the work flow of the TF activation assay. *When the probe (biotin labeled) mix is incubated with nuclear extracts, individual probes form TF/probe complexes*

with its corresponding TF, which can be easily separated from free probes through a simple spin column purification method. The bound probes are detached from the complex and analyzed through hybridization with a plate; each well is specifically pre-coated with complementary sequences of the probes. The captured DNA probe is further detected with streptavidin-HRP. Luminescence is reported as relative light units (RLUs) on a microplate luminometer.

To characterize binding of various activated TFs to NIS promoter, promoter binding TF profiling array was performed (FA2002, Signosis, USA) (**Figure 2.3**). Nuclear extracts were prepared from NaB/ VPA treated MCF-7 cells, incubated with oligo-binding mix along with NIS-promoter DNA fragment. Comparing luminescence in presence or absence of competitor human NIS promoter, binding of various TFs to the promoter was predicted. The detailed protocol is provided in the appendix.

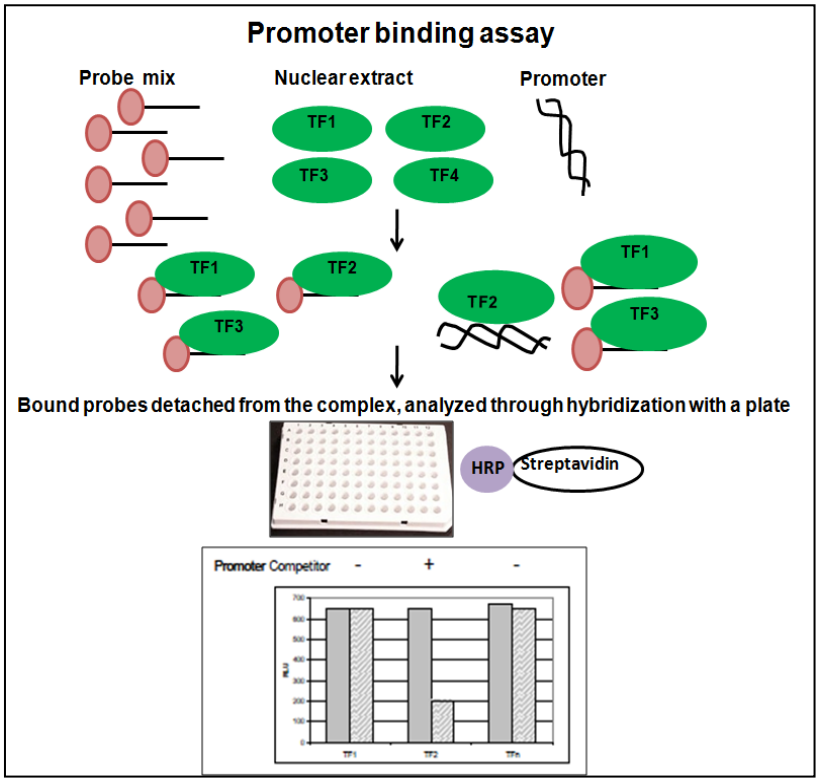

Figure 2.3: Schematic of the work flow of the promoter binding assay. *Promoter-binding TF profiling assay is a competition of TF activation plate assay. In promoter-binding TF*

profiling assay, PCR fragment containing the promoter of interest is mixed with a set of 96 biotin-labeled oligos corresponding to 96 TFs along with the nuclear extract to be assayed. If DNA fragment contains a TF binding sequence, it will complete with the biotin-labeled oligo to bind to the TF in the nuclear extract sample, leading to no or less complex formation and no or lower detection. Comparing luminescence in presence or absence of competitor promoter DNA, binding of various TFs can be predicted.

2.2.10: Iodide uptake and efflux measurement assays

Iodide uptake and efflux study was performed as described previously [102, 169] . After 48 hours of treatment with indicated HDACi, cells were incubated with 10μM NaI in uptake buffer [Hank's Balanced Salt Solution (HBSS) supplemented with 10mM HEPES (pH 7.3)]. To determine NIS-specific iodide uptake, cells were incubated with 30μM KClO4 in uptake buffer for one hour prior to addition of 10μM NaI. After 30 minutes incubation with NaI at 37˚C, cells were washed with ice-cold uptake buffer. Then 10.5mM ammonium cerium (IV) sulphate solution and 24mM sodium arsenite (III) solution were added. The plate was incubated at room temperature (RT) in dark for 30 minutes and the absorbance at 420nm was recorded. Using logarithmic conversion and standard equation of iodide standards, amount of nanomoles (nmoles) of iodide uptake was calculated from absorbance read-outs.

In iodide efflux measurement study, control or drug treated cells were incubated in uptake buffer with 10μM NaI at 37˚C for 30 minutes. Cells were washed with ice cold uptake buffer to stop the reaction and fresh uptake buffer without NaI was added. The medium was replaced after every 10 minutes and 10.5mM ammonium cerium (IV) sulphate solution and 24mM sodium arsenite (III) solution were added. Following incubation at RT in dark for 30 minutes absorbance at 420nm was recorded.

2.2.11: *In vitro* clonogenic assay

Control and NaB/ VPA/ CI994 treated MCF-7/ Zr-75-1/ MDA-MB-231 cells were grown in 25cm^2 flasks and incubated with 50μCi/ml of ^{131}I in case of MCF-7 or MDA-MB-231 and 100μCi/ml in case of Zr-75-1 in HBSS supplemented with 10μM NaI and 10mM HEPES (pH7.3). The *in vitro* clonogenic assay was performed as described by Mandell et al. [102]. The minute experimental details are provided in the appendix section.

2.2.12: *In vivo* optical imaging and immunohistochemistry procedures

The experimental protocol using mice was approved by Institutional Animal Ethics Committee (IAEC) at ACTREC and performed in accordance with the guidelines for the care and use of the laboratory animals. Female BALB/c nude mice (n=9) were used for growing subcutaneous tumor using Zr-75-1 cells labeled with Fluc2.Tdt fusion gene. Mice were divided into three groups: the ^{131}I group (intraperitoneal injection of 1mCi Na-^{131}I on day 0), VPA group (5 doses of 250mg/kg of VPA alone) and the experimental group (5 doses of 250mg/Kg of VPA followed by 1mCi Na-^{131}I on day 0). Mice in all the groups were treated with T4 (2μg) and methimazole (10μg) everyday for 15 days prior to ^{131}I injection, to block the thyroid uptake and the blocking was continued throughout the experiment. Serial Bioluminescence imaging was performed using IVIS-Spectrum (Caliper Life Sciences) after intraperitoneal injecting 30mg/ml of D-luciferin (Biosynth International) and viewed in real time on a computer screen using a color scale expressed as average radiance (photons per second per square centimeter per steradian [photons/sec/cm^2/sr]). Mice were anesthetized with 2% isofluorane throughout the scan time. Data were analyzed using Living Image version 4.4 software.

For immunohistochemistry (IHC), tumors from drug treated (5 daily doses of 250 mg/kg) and control group were harvested and fixed using standard procedures [8]. An additional step of

mouse serum blocking was performed prior to blocking step to reduce the non-specific signal from the mouse tissue sections as the primary antibody is raised in the mouse species. For digital scoring of IHC slides, we used the IHCprofiler plugin for ImageJ (NIH, USA) developed by our group [170] .

2.2.13: Cerenkov luminescence imaging (CLI)

CLI was performed using the same IVIS spectrum system. For *in vivo* Cerenkov imaging, animals in the ^{131}I alone or VPA+^{131}I group were injected with 1mCi of ^{131}I intraperitoneally. Animals were placed in a light-tight chamber under isofluorane anesthesia. Cerenkov imaging was performed after 24 and 72 hours of ^{131}I injection. The detailed procedure is given in the appendix section.

2.2.14: Statistical Analysis

All data are expressed as mean ± SE and are representative of at least two separate experiments. Statistical significance was analyzed by Student t-test using GraphPad Prism 6 (GraphPad Software, La Jolla, CA). P values of ≤ 0.05 were considered statistically significant.

2.3: Results

2.3.1: Development of engineered breast cancer cell lines stably expressing pNIS-Fluc2.TurboFP reporter plasmid

For confirmation of the pNIS-Fluc2.TurboFP reporter plasmid, MCF-7 and MDA-MB-231 cell lines were transiently transfected with the NIS promoter driven bifusion reporter sensor. The expression of the luciferase protein was measured in both the cell lines (**Figure 2.4A-B**). Fluorescent reporter expression of TurboFP was observed using fluorescence microscope

(**Figure 2.4C**). As a positive control for the transfection, CMV-promoter driven bifusion reporter (CMV-Fluc2.TurboFP) was used that exhibited around 10-20 fold higher luciferase activity in both the cell lines established (**Figure 2.4A-B**).

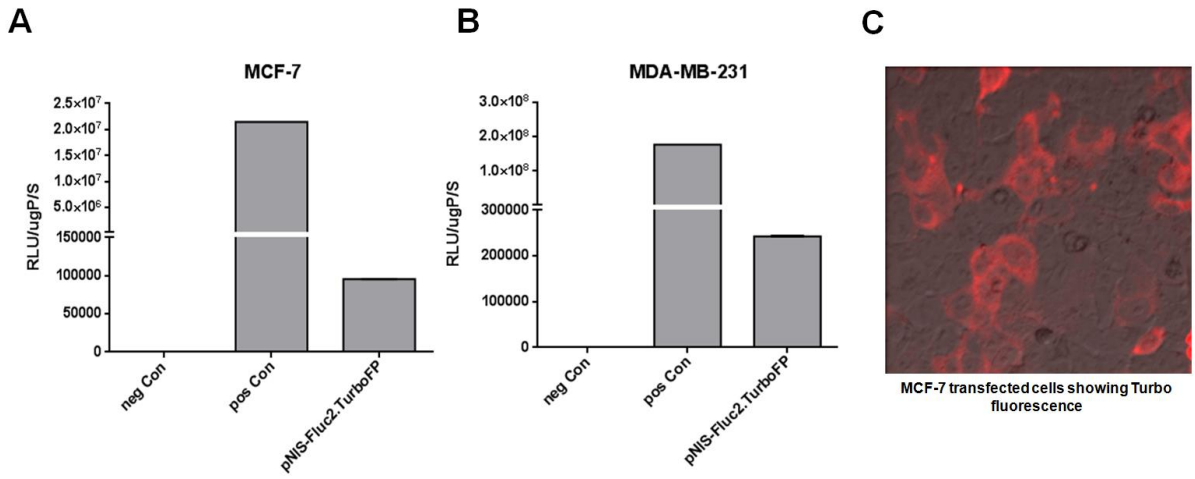

Figure 2.4: Validation of the bifusion reporter plasmid DNA for reporter expression. *A-B. Transient transfection with the bifusion reporter vector showed luciferase activity in two cell lines, i.e. MCF-7 (A) and MDA-MB-231 (B). As a positive control, plasmid containing CMV promoter driving expression of fusion reporter gene (Fluc2.TurboFP) was used. C. Expression of the fluorescent reporter gene (TurboFP) in MCF-7 cells transiently transfected with pNIS-Fluc2.TurboFP reporter.*

After initial validation of reporter gene expression, breast cancer cells stably overexpressing pNIS-Fluc2.TurboFP reporter plasmid were developed. As evident from the **Figure 2.5A-C**, multiple clones having variable levels of luciferase activity were obtained across the multiple cell lines. The clones that were showing response to HDACi treatment were selected and used in further experiments.

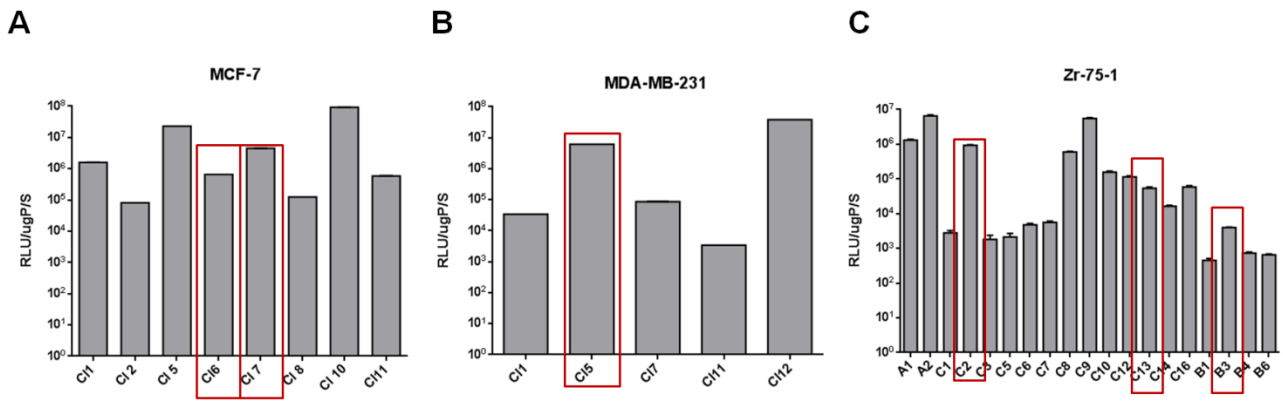

Figure 2.5: Luciferase reporter activity measured from the selected stable clones in breast cancer cell lines expressing the bifusion reporter vector. *Differential luciferase activity in various clones in MCF-7 (A), MDA-MB-231 (B) and Zr-75-1 (C) cells. The clones marked in red were used in further experiments.*

2.3.2: NIS promoter activity significantly induces in response to pan-DAC inhibitors in breast cancer cells

In order to test the effect of HDACi on NIS gene expression, six different drugs representing various chemical classes as shown in **Table 2.1** were included in our study. Initially, the minimal drug dose required to promote NIS gene expression was determined by luciferase reporter assays against increasing concentration of each drug using the established MCF-7 clone6 cells expressing pNIS-Fluc2.TurboFP (**Figure 2.6**). Equal number of the MCF-7 clone6 cells were seeded in 96-black well plates, and exposed to increasing concentrations of HDACi. After 48 hours of drug treatment, NIS promoter activity was monitored using D-luciferin substrate (50µl of 100µg/ml stock per well). Photons emitted from live cells were measured from each well using luminescence microplate reader (BMG Labtech, Germany). The concentration of HDACi showing highest fold increase in NIS promoter activity was chosen as optimal drug concentration for promoter activation and used in subsequent experiments (**Figure 2.6**).

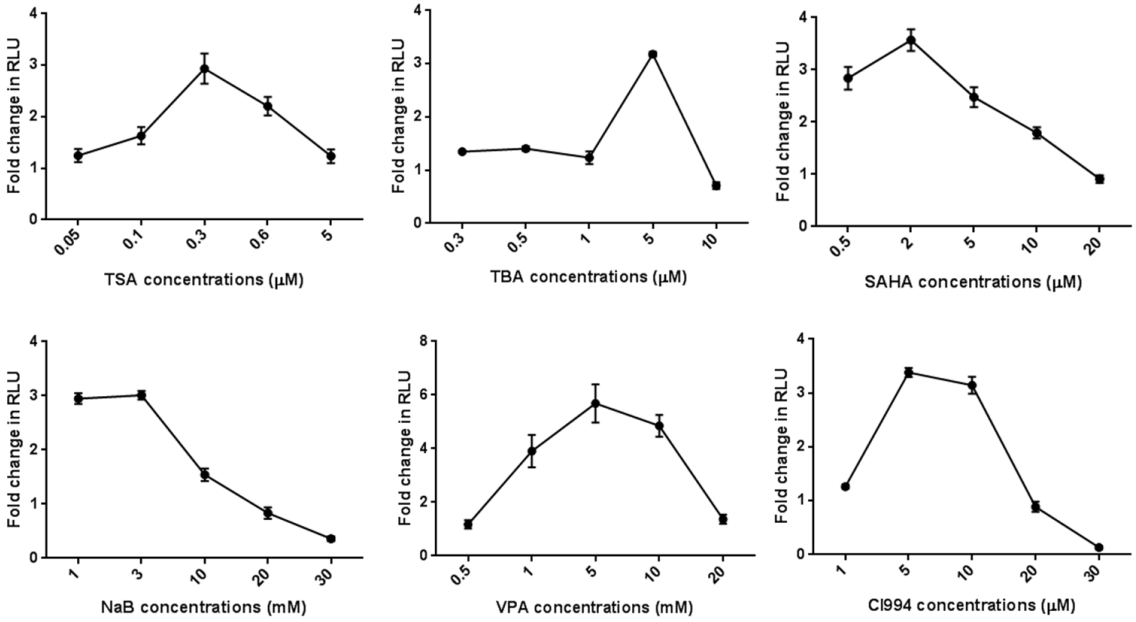

Figure 2.6: Dose dependent effect of various HDACi on NIS promoter in engineered MCF-7 cells stably expressing NIS-promoter driven bifusion reporter. *MCF-7 Cl6 cells were treated with six different HDACi for 48 hours and fold change in luciferase activity as compared to untreated cells were computed. The concentration of HDACi showing highest fold increase in NIS promoter activity was chosen as optimal drug concentration for promoter activation and used for all other experiments.*

Similarly, cytotoxicity of these HDACi was also assessed in both MCF-7 and MDA-MB-231 cell lines to confirm the dose used in gene regulation study is not toxic to the cells (**Figure 2.7**). The lowest minimal drug concentration (~IC_{70} equivalent) showing optimum NIS promoter induction was chosen and further used for all successive gene regulation experiments.

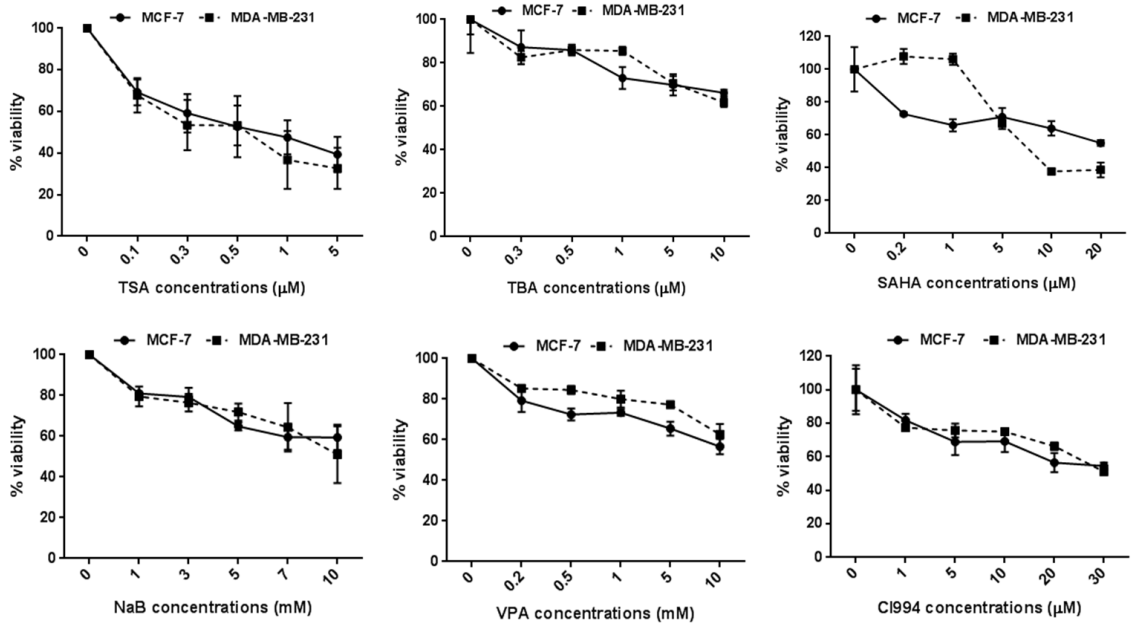

Figure 2.7: Study of cytotoxicity of HDACi treatment in MCF-7 and MDA-MB-231 breast cancer cells. *Cells were incubated with different doses of HDACi for 48 hours and cell viability was measured by the MTT assay. Data represented as percentage viability to untreated controls.*

After deciding the effective dose of the drugs, next modulation of the NIS promoter in response to HDACi drug treatment was tested in engineered MCF-7 and MDA-MB-231 cells. As shown in **Figure 2.8A-B,** NIS-promoter activity enhances 2-4 fold in MCF-7 Cl6 cells and 1.4-2.4 fold in MDA-MB-231 Cl5 cells as a result of HDACi treatment. The effect of HDACi was also tested using the same reporter system in two additional cell lines i.e. Zr-75-1 (hormone receptor positive) and MDA-MB-468 (hormone receptor negative) by transient transfection method. As engineered Zr-75-1 cells were not developed by that time, transient transfection protocol was used. The similar trend of higher fold induction of normalized luciferase activity has been observed in both the cell lines **(Figure 2.8C**). The fold gain in luciferase reporter signal upon drug treatment was further verified by western blot analysis using Fluc antibody in engineered MCF-7 cells (**Figure 2.8D**). The primary molecular effect

of HDACi is to alter the acetylation status of the core histone proteins, facilitating chromatin remodeling and modification in gene expression [158]. So the target effect of these drugs was confirmed in MCF-7 cell line revealing increased histone H3 acetylation except for TBA, which is a known HDAC6 specific inhibitor [171] (**Figure 2.8E**). From the results, of the various HDACi tested, NaB, VPA and CI994 exhibit consistent gain while TSA and SAHA show heterogeneous fold gain in reporter activity across all the cell types tested. Inhibition with TBA, a HDAC6 specific inhibitor, show around 1.5-2 fold gain in reporter activity in breast cancer cell lines.

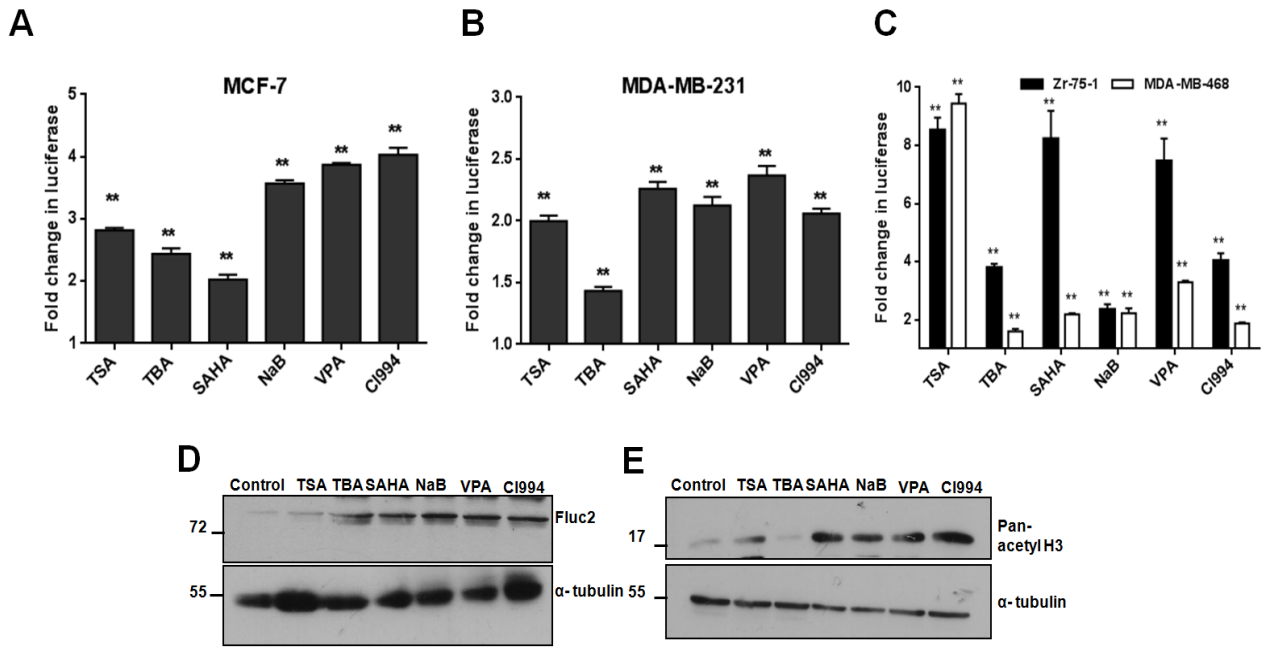

Figure 2.8: Modulation of human NIS promoter activity by HDACi drugs. *A-B. Charts representing reporter signal fold change over untreated control as a measure of NIS promoter activity upon HDACi treatment. Both MCF-7 (Cl6) and MDA-MB-231 (Cl5) engineered cells stably overexpressing pNIS-Fluc2.TurboFP reporter construct were exposed to various HDACi for 48 hours and luciferase activity was measured. C. In addition, Zr-75-1 and MDA-MB-468 cell lines were transiently transfected with pNIS-Fluc2.TurboFP plasmid and normalized by pCMV-TurboFP.Rluc8.6 plasmid. Chart represents fold change in photon values over untreated control cells in these cell lines. ** indicates p≤0.005. D. Western blot analysis of luciferase reporter induction using Fluc antibody in engineered MCF-7 Cl6 cells.*

E. The target effect of HDACi on histone H3 acetylation in MCF-7 cells. Cells exposed to HDACi for 48 hours were assessed by western blotting using pan-acetyl-H3 monoclonal antibody and α-tubulin as loading control.

Additionally, effect of HDACi treatment was tested on two additional ubiquitous promoters like cytomegalovirus (CMV) or chicken beta-actin promoter (CAG) in engineered MCF-7 cells stably expressing Fluc2 reporter protein driven by the individual promoters respectively. As revealed in **Figure 2.9,** no radical change in normalized reporter activity is noted indicating NIS-promoter specific effect of the HDACi used in the study.

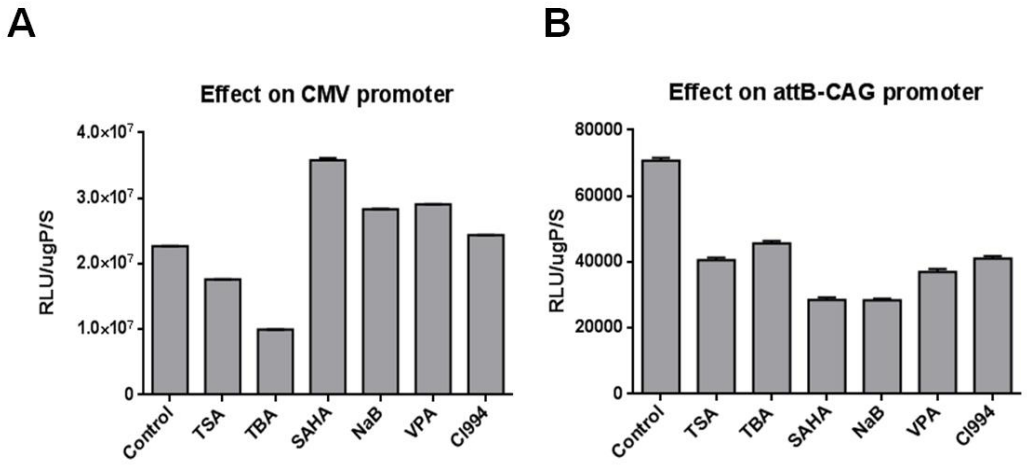

Figure 2.9: Study of promoter specific effect of HDACi treatment. *Effect of six HDACi was tested on two other promoters i.e. cytomegalovirus (CMV) (A) and chicken beta-actin (CAG) (B). MCF-7 cells stably overexpressing mammalian expression plasmids with luciferase reporter cloned under the respective promoter used for measuring drug effect on the promoters.*

2.3.3: HDACi significantly induce endogenous NIS expression in multiple breast cancer cell lines

Based on the results from the reporter based system, we further verified if the same treatments corroborate in endogenous NIS activation. Thus, quantitative real-time PCR was

performed to assess the NIS transcript levels. GAPDH was used as a housekeeping control for normalization in the study. As shown in **Figure 2.10A-B**, each data point represents normalized transcript value relative to their untreated control. Overall, variable increment of NIS transcript (2-55 fold, $p \leq 0.05$) is observed across all the cell types tested. In particular, NaB and VPA treatment results in highest induction of NIS mRNA, while TBA treatment seems to be least effective. Moreover, much higher transcript levels (~3-10 fold) are observed in hormone receptor (ER) positive MCF-7 and Zr-75-1 cell lines as compared to receptor negative cells (MDA-MB-231 and MDA-MB-468).

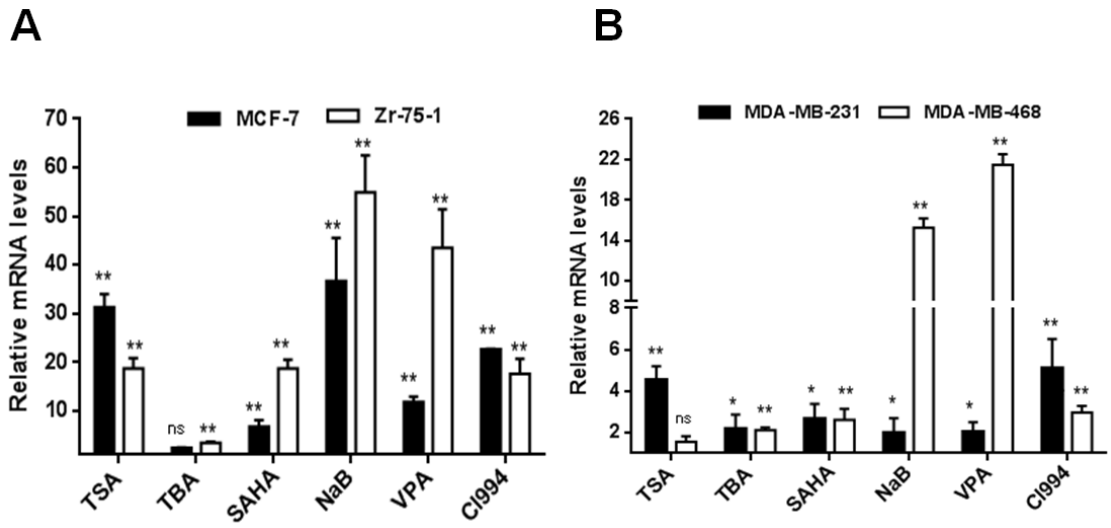

Figure 2.10: Induction of endogenous NIS transcript after HDACi treatment in BC cell lines. *MCF-7 and Zr-75-1 (A); MDA-MB-231 and MDA-MB-468 (B) cells treated with different HDACi for 48 hours were evaluated for NIS mRNA by real-time PCR using ABI probe. Results were normalized for housekeeping gene GAPDH and presented as relative fold differences to untreated control. * indicates p≤0.05, ** indicates p≤0.005, ns indicates non-significant.*

Our observations point out that HDAC inhibition may lead to NIS induction by known mechanism of transcriptional activation and increased DNA binding ability of transcriptional regulators. To gain further insight into the mechanisms leading to NIS up-regulation under

HDAC inhibition, we performed TF activation array for 96 global TF signatures to identify differentially regulated TFs under NaB and VPA drug influence in MCF-7 cells as compared to the untreated cells. **Figure 2.11A-B** indicates the purity and quality of the nuclear extracts isolated from control and drug treated MCF-7 cells used in the assay. Our data reveals the activation of 7 TFs i.e. CREB, Stat4, Stat6, Sox9, Smuc, Nkx3.2 and E2F-1, whereas suppression of 5 TFs like XBP, MZF, HNF-1, Hox4C, and PLAG in response to NaB treatment (**Figure 2.11C**). When checked for VPA treatment, we observe the activation of 21 different transcription factors while no significant suppression of any factor is noted (**Figure 2.11D**). Only Stat4 and E2F-1 are found to be activated in common in response to NaB and VPA treatment in MCF-7 cells. Further, four transcription factors namely AP1, Hox4C, MZF and HNF-1; exhibit differential response to NaB and VPA treatment (**Table 2.4**). Human NIS mRNA induction was also verified in response to NaB and VPA treatment as indicated in **Figure 2.11E-F**.

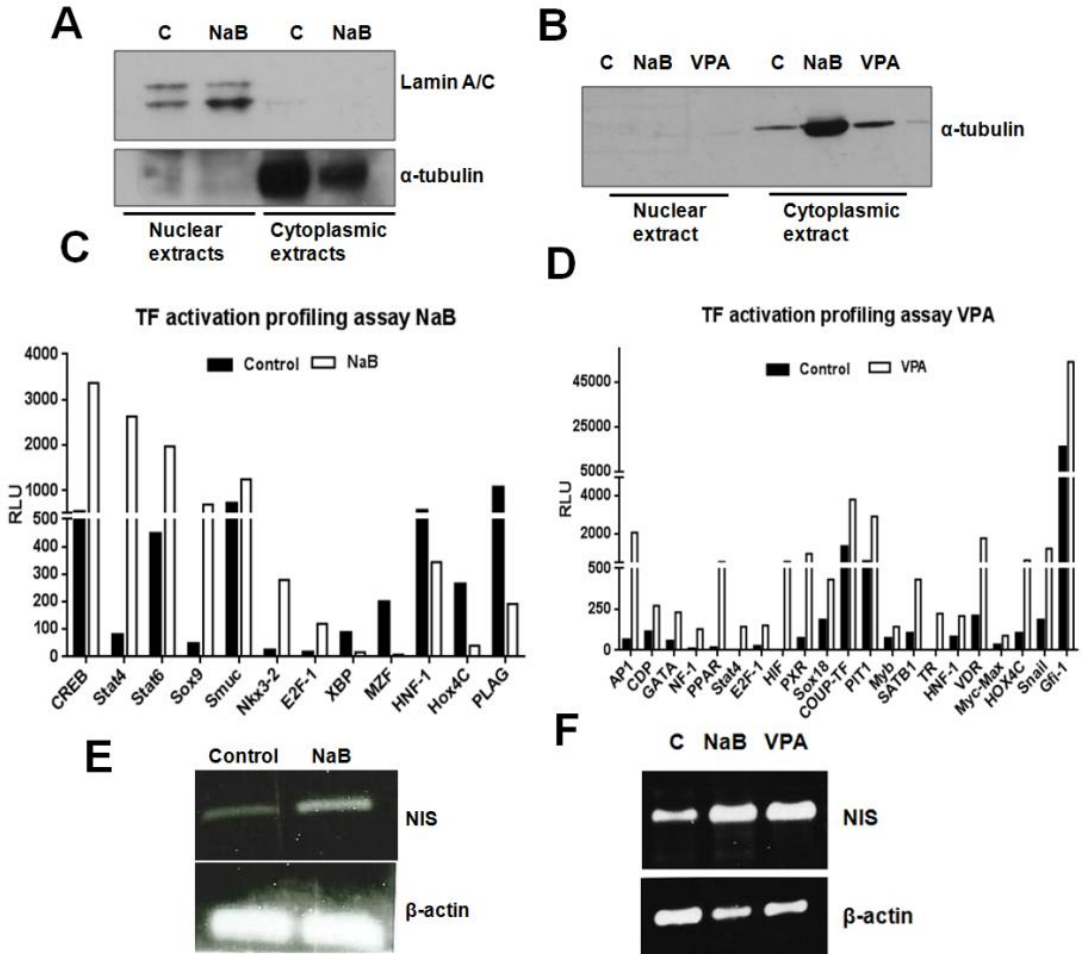

Figure 2.11: Graphs depicting the activation of transcription factors post NaB/VPA treatment in MCF-7 cells. *A-B. Western blots to check the purity of the nuclear and cytoplasmic extracts isolated by using lamin/tubulin as nuclear/cytoplasmic markers respectively. C-D. Graphs showing activation of transcription factors (TFs) post NaB (C) or VPA (D) treatment in MCF-7 cell line. TFIID was used for normalization as per manufacturer's guideline. Candidate TFs showing greater or lesser than 1.5 fold difference in luminescence read-outs after normalization (threshold cut-off) were plotted. E-F. RNA was extracted from the HDACi treated MCF-7 cells to validate the induction of NIS gene expression post NaB and VPA treatment by RT-PCR. β-actin was used as a loading control.*

Table 2.4: Transcription factors exhibiting opposite trend in TF activation assay after NaB/VPA treatment in MCF-7 cells

Transcription factor (TF)	Response to NaB	Response to VPA
AP1	↑	↓
Hox4C	↓	↑
MZF	↓	↑
HNF-1	↓	↑

↑ indicates activation of TF activity

↓ indicates suppression of TF activity

Taking a step further, the ability of these TFs binding to the NIS promoter was verified using promoter binding array where NIS promoter DNA was added in the plate together with the nuclear extract of MCF-7 cells treated or untreated with NaB or VPA. Our results from promoter binding array confirm that 5 of the 7 activated TFs namely CREB, Stat4, Sox9, E2F-1 and Stat6 display binding to NIS promoter under NaB treatment (**Figure 2.12A**). Under the influence of VPA treatment, we observe 6 out of 21 factors bind strongly to the NIS promoter (**Figure 2.12B**). Stat4 is the only factor found in common with both NaB and VPA treatment that binds to the NIS promoter. To further verify our observations, we performed bioinformatics analysis of the NIS promoter sequence using the Transfac and Genomatix softwares. The analysis reveals the availability of TF binding sites for the TFs that exhibited NIS promoter binding in the assay. Together these findings demonstrate possible role of TFs like Stat4, CREB, Nkx3.2, AP1 etc. majorly influence NIS expression in HDACi treated MCF-7 cells (summarized in **Table 2.5**).

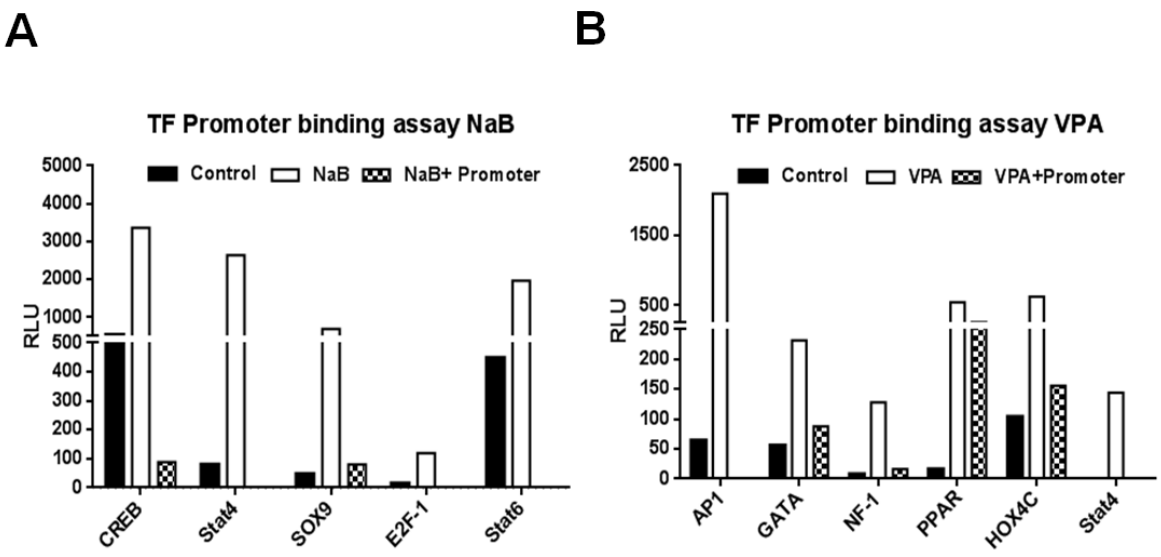

Figure 2.12: Demonstration of the putative transcriptional regulators showing binding to the NIS promoter post NaB/VPA treatment. *A-B. Graphs representing TF binders to human NIS promoter upon NaB (A) and VPA (B) treatment identified by promoter binding array. In comparison to drug treated nuclear extract samples, when NIS promoter is added, the luminescence read-out is lowered due to competitive binding to the promoter.*

Table 2.5: List of transcription factors that are activated and binding to NIS promoter after NaB / VPA treatment

Transcription factor (TF)	Response to HDACi tested	Putative Binding Sequence on NIS promoter as per Transfac/Genomatix analysis	No. of sites	Involved in NIS induction in breast or thyroid cancer	Reference
CREB	NaB	gaagCGTGAcccccc	5	Thyroid	[172]
Sox9	NaB	aggagccAATGaatgaatgaatgaa #	2	ND	
E2F-1	NaB	gctgctcccgtaagccccaaGGCGac ctc	1	ND	
Stat4/Stat6	NaB, VPA	tcgaaTTCTGgga #	1	ND	
AP1	VPA	cggTGACCCggga	1	ND	
GATA	VPA	ggcacTTATCa	6	ND	
NF-1	VPA	ctggcacaggGCCAAct	2	ND	
PPAR	VPA	accagaacctccAGAGgtcaaag	2	Thyroid	[173]
Hox4C	VPA	tggtctcCGCTtattcggg #	6	ND	

# indicates presence of TF binding site belonging to family of TF i.e. Hox, Stat and Sox family of TFs respectively

ND- role in NIS regulation is not determined

From this set of transcription factors, we have chosen Stat4 (novel TF commonly found in response to both the drugs) and CREB (a known NIS inducer in thyroid and showing differential response) for validating our observations from the array. Semi-quantitative PCR was performed from control and NaB/VPA treated samples to check NIS, Stat4 and CREB mRNA levels using gene specific primers in MCF-7 cells. As revealed in **Figure 2.13A-B**,

we observe 1.75 fold and 2.27 fold induction in Stat4 mRNA levels in response to NaB and VPA treatment respectively. Under the influence of same drugs, NIS mRNA expression increases up to 2.2-5.2 fold in MCF-7 cells. These observations corroborate with our assay findings. However, CREB mRNA levels reduce up to 0.65 fold post NaB treatment. CREB is a ubiquitous TF found in the cells associated with the transcriptional activation. Activation of CREB results in its phosphorylation at ser133 residue leading to its nuclear localization [174, 175]. So CREB activation can be verified further by checking phosphorylated CREB protein levels. The comprehensive role of Stat4 and CREB in NIS gene regulation will be elucidated in future.

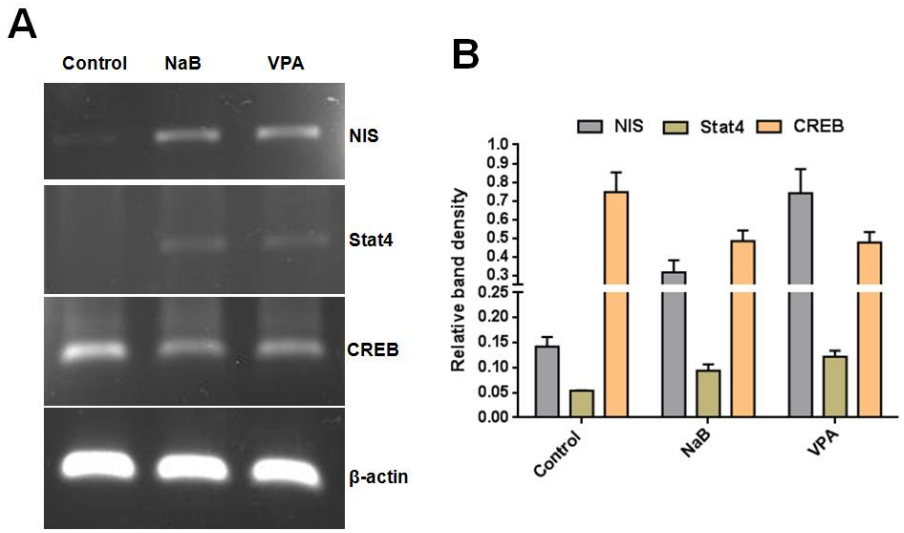

Figure 2.13: Validation of Stat4 and CREB transcript after NaB and VPA treatment in MCF-7 cells. *Representative gel image (A) and densitometric analysis (B) of semi-quantitative PCR to validate human NIS, Stat4 and CREB expression in response to NaB and VPA treatment in MCF-7 cells.*

Further, it was also confirmed that enhanced endogenous NIS transcript under HDACi drug influence successfully translates into enhanced protein production in the cell pool. To prove, immunofluorescence staining after HDACi treatment in MCF-7 and MDA-MB-231 cells was

performed (**Figure 2.14A)**. Quantitation of the immunofluorescence images indicate 2-3 fold increase in NIS protein content in both the cell lines after majority of the HDACi treatment except for TBA (**Figure 2.14B)**. Enhanced protein production is further evidenced by the western blot of the control and drug treated MCF-7 cell lysates using human NIS monoclonal antibody (**Figure 2.14C**). Together, these results suggest that except for HDAC6 specific inhibitor (TBA), other pan-HDAC inhibitors tested here can significantly induce endogenous NIS mRNA and protein expression in breast cancer cell lines.

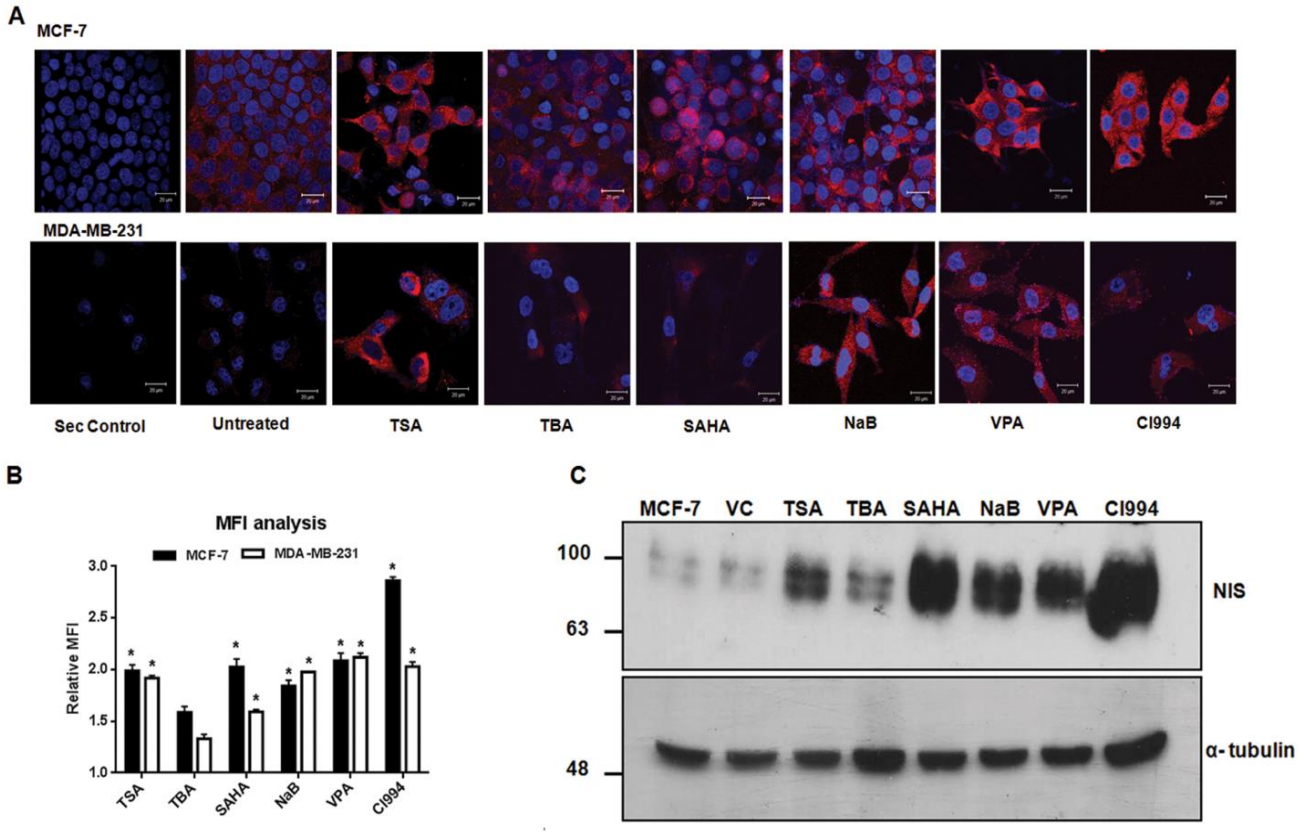

Figure 2.14: Regulation of NIS protein levels by HDACi treatment in breast cancer cells. *A. Immunofluorescence photographs of MCF-7 and MDA-MB-231 cells showing marked increase in NIS protein content when treated with various HDACi. Drug treated and untreated cells were probed with NIS monoclonal antibody and detected with Dylight 633 secondary antibody (red). A secondary antibody control was also included in the study. Cell nuclei were cross stained using DAPI (blue). Scale bar represents 20µm. B. Graph showing fold increase in mean fluorescence intensity (MFI) of NIS staining after HDAC inhibition in MCF-7 and MDA-MB-231 cells. Average MFI was calculated from 30-50 cells using LSM*

*Image browser and fold difference with respect to untreated cells plotted. * indicates p≤0.05. C. Western blot showing NIS protein content in MCF-7 cells after different HDACi treatments. DMSO was used as a vehicle control (VC). Total 60µg of protein was loaded in each lane and alpha-tubulin was used as an endogenous control.*

As NIS is a transporter protein; its localization is very crucial for its function. We have also checked if the treatment with NaB, VPA and CI994 drugs alter the NIS protein localization using MCF-7 clonal cell lines, differentially overexpressing NIS protein either at the membrane or at the cytoplasm [176]. As indicated in **Figure 2.15**, we observe that treatment of HDACi induce NIS protein levels in breast cancer cells without influencing protein localization in the cells.

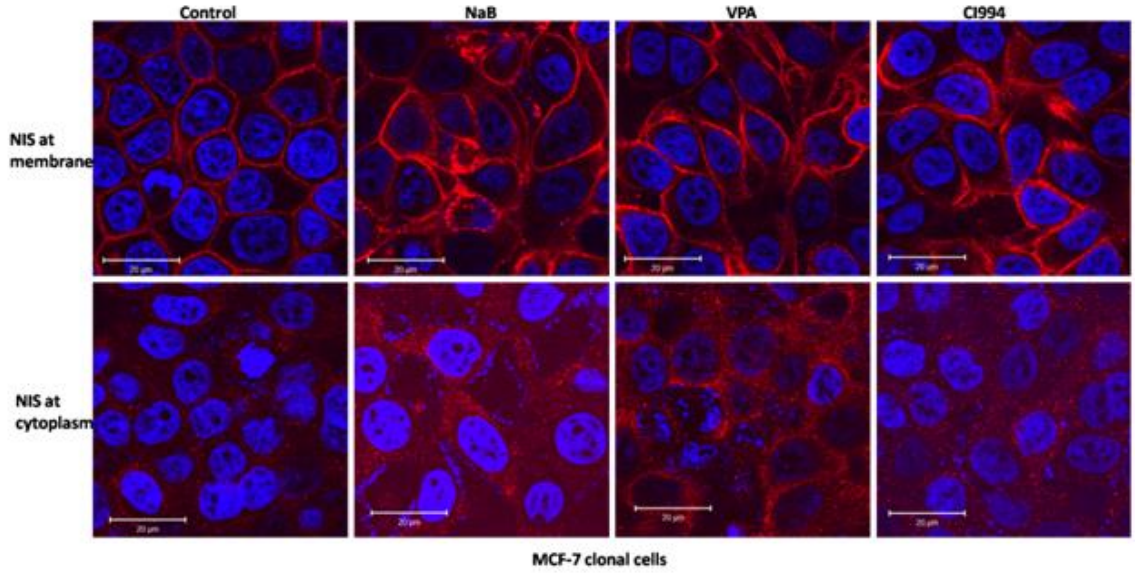

Figure 2.15: Effect of HDACi treatment on NIS localization in MCF-7 cells. *NIS immunofluorescence photographs of MCF-7 clonal cells differentially overexpressing NIS protein either at the membrane (upper panel) or at the cytoplasm (lower panel) treated with NaB, VPA and CI994 drugs.*

2.3.4: HDAC inhibitor treatment significantly influences NIS function impacting ^{131}I mediated radioablation in breast cancer cells

As evidenced from many clinical literatures, high NIS mRNA or protein expression may not necessarily result in higher iodide uptake [56]. Therefore, we next verified the NIS functional modulation by HDACi treatment in cultured cells by iodide uptake assay. As indicated in **Figure 2.16A-B**, the perchlorate sensitive NIS-mediated iodide uptake increases up to 1.7-2.8 fold in MCF-7 and Zr-75-1 cell lines at 48 hours of HDACi treatment. The iodide uptake in MDA-MB-231 cells is found to be much lower (**Figure 2.16C**). As compared to the untreated cells, NaB, VPA, SAHA and CI994 treatment results in consistent and significant (1.7-2.8 fold, $p \leq 0.05$) increase in iodide uptake in both MCF-7 and Zr-75-1 cells (**Figure 2.16A-B**), and around 1.5-2 fold induction ($p \leq 0.05$) is noted with NaB, VPA and CI994 drug treatments in MDA-MB-231 cell line (**Figure 2.16C**). TSA and TBA treatment displays marginal increase across all cell types tested. Iodide retention time in the tumors is another important parameter for achieving good therapeutic efficacy. As the steady-state accumulation is the net outcome of iodide uptake and iodide efflux, we further checked the effect of CI994 on iodide efflux in MCF-7 cells. Compared to the untreated cells, where 88% of accumulated iodide is released during first 10 minutes, CI994 treated cells exhibit similar 84% release in 10 minutes indicating the efflux remaining unaltered (**Figure 2.16D**).

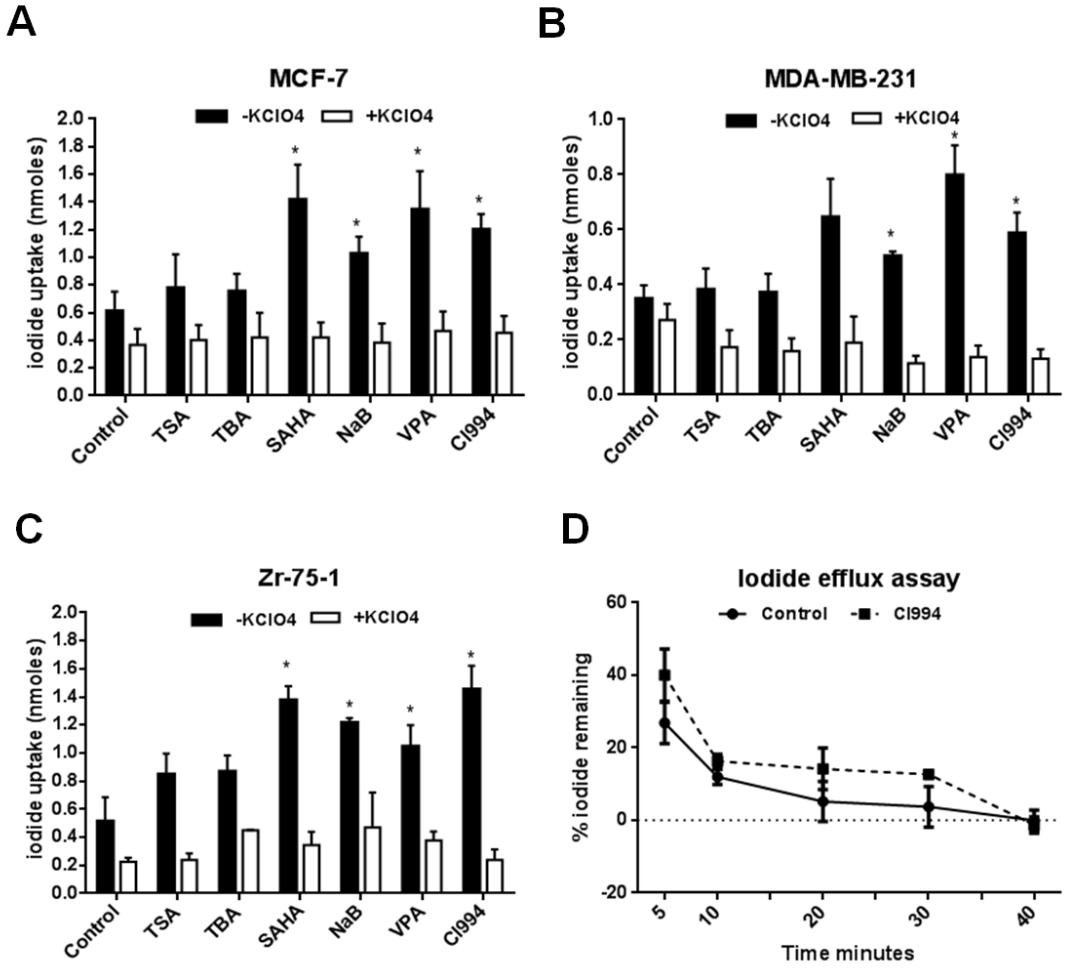

Figure 2.16: Regulation of NIS function by HDACi treatment in breast cancer cells. *A-C. Effect of the HDACi drugs on NIS-mediated iodide accumulation in MCF-7 (A), MDA-MB-231 (B) and Zr-75-1 (C) cells respectively. 30μM potassium perchlorate was used for blocking iodide uptake. The Y axis scale bars represent nanomoles (nmoles) of iodide uptake after 48 hours of HDACi. Error bars indicate standard error of mean. D. Chart showing iodide efflux assessment in MCF-7 cells. CI994 drug was used as a candidate HDACi representative to verify change in efflux upon drug treatment. * indicates p≤0.05.*

After validating iodide uptake, we next checked therapeutic efficacy of ^{131}I radioablation in MCF-7, MDA-MB-231 and Zr-75-1 cell lines with variable endogenous NIS protein levels. The survival fraction was assessed by clonogenic assay using NaB, VPA and CI994 as candidate HDACi drugs. Initially, the dose of ^{131}I required for minimal cell killing was

determined. In contrast to MCF-7 and MDA-MB-231 cells, which required 50μCi/ml ^{131}I dose for ~75% cell survival in culture condition, 100μCi/ml was found to be sufficient for the same efficiency in Zr-75-1 cells. In comparison to ^{131}I exposure alone, HDACi drug pre-treatment results in highly significant cell survival reduction (to 0.008 fold, 0.1 fold and 0.2 fold in MCF-7 and 0.4 fold, 0.45 fold and 0.45 fold in Zr-75-1 cells after NaB, VPA and CI994 pre-treatment respectively, $p \leq 0.005$) (**Figure 2.17A and C**). On the other hand, we observe that NaB pre-treatment results in reduced survival fraction up to 0.5 fold ($p=0.001$) while VPA pre-treatment reduces the survival to 0.2 fold ($p=0.008$) in MDA-MB-231 cell line (**Figure 2.17B**). The reduced survival of cells against minimal ^{131}I radioactivity used further assures that enhanced iodide symporter function by HDACi pre-treatment can be proved to be useful for this NIS gene therapy approach. We have also confirmed specific radiation injury caused in Zr-75-1 cells by staining for γ-H2Ax foci that forms due to DNA double strand break (**Figure 2.17D**). Significant enhancement ($p \leq 0.01$) in the number of γ-H2Ax foci is observed in cells when they are treated with all three HDAC inhibitors than cells treated with radiation alone (**Figure 2.17D-E**), indicating higher DNA damage resulting in higher radioablation.

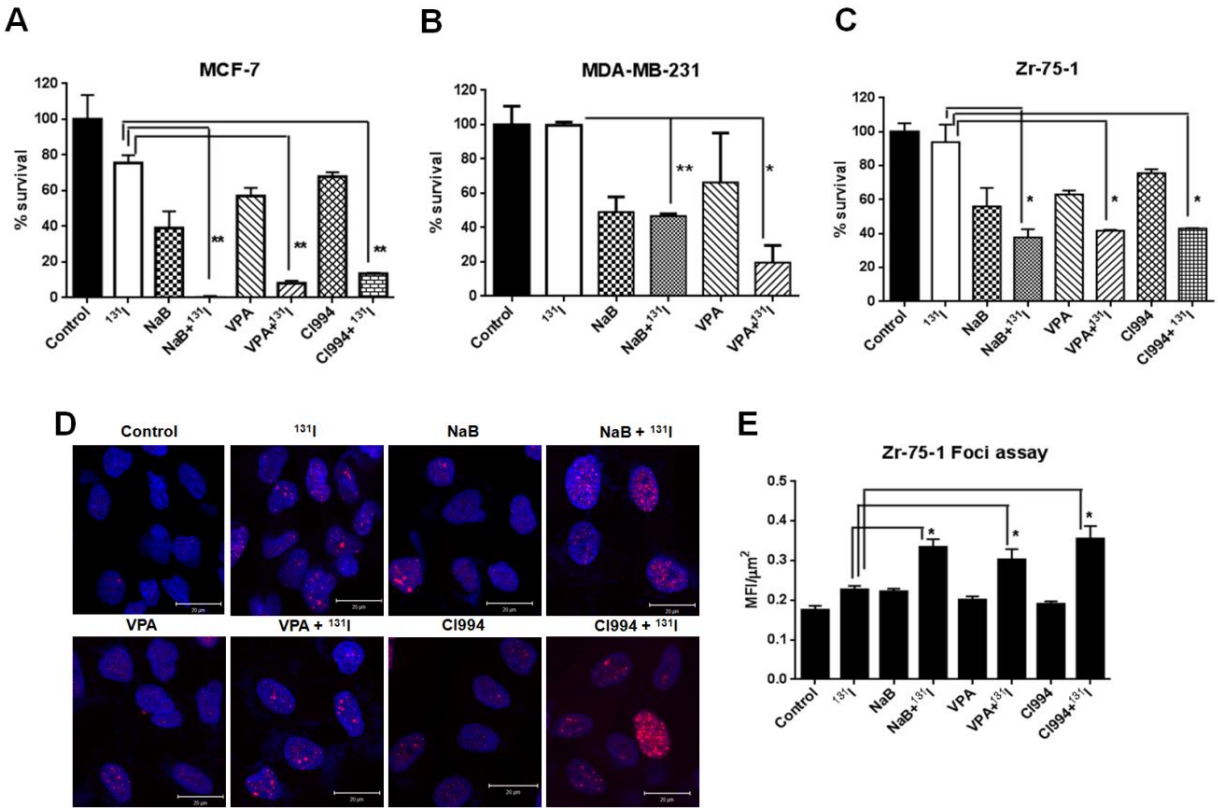

Figure 2.17: ^{131}I cytotoxicity assay after pre-treatment with HDACi in BC cell lines. *A-C. Charts representing the measure of percentage cell survival after selective killing by ^{131}I treatment in the presence or absence of candidate HDACi treatment as marked. MCF-7, MDA-MB-231 cells were exposed to 50μCi/ml of ^{131}I and Zr-75-1 cells were exposed to 100μCi/ml of ^{131}I with or without pre-treatment of NaB/ VPA/ CI994. Cell survival was measured by their colony forming ability. D. Immunofluorescence photographs showing DNA damage response after ^{131}I exposure detected by γ-H2Ax foci formation. Zr-75-1 cells were exposed to 100μCi/ml ^{131}I with or without pre-treatment of NaB/ VPA/ CI994 and probed with γ-H2Ax antibody after fixation. Foci were detected by Dylight 633 secondary antibody (red). Cell nuclei were cross stained using DAPI (blue). Scale bar represents 20μm. E. Graph showing MFI/μm^2 of foci formation after ^{131}I exposure with or without HDACi pre-treatment. Average MFI of 35 cells was calculated using LSM image browser and plotted. * indicates P≤0.05, ** indicates p≤0.005.*

2.3.5: VPA treatment induces NIS protein expression in Zr-75-1 tumor xenografts

Based on *in vitro* cell culture observations, we were encouraged to see if we observe the similar gene regulation *in vivo*. Therefore, to validate our findings, we next checked NIS

protein content in animal model using VPA as the candidate HDACi drug. Zr-75-1 cells were implanted subcutaneously into female nude mice to develop tumor xenografts. Once the tumors were formed, mice were segregated in to two groups; the control group and the VPA treatment group. Mice in the treatment group, received 5 doses of 250mg/kg VPA by intraperitoneal injection. Following the treatment phase, mice were sacrificed; tumors were excised and checked for NIS protein expression by immunohistochemistry (IHC). **Figure 2.18A** shows IHC images of the tumor tissue sections with diffused cytoplasmic NIS staining in the control and VPA treated group while membrane staining is evident in the salivary gland which is used as a positive control. The intensity of NIS staining was calculated using IHCprofiler plugin for ImageJ (NIH, USA) developed by our group [170]. As indicated in **Figure 2.18B,** digital IHC analysis of these samples reveals significant enhancement of NIS-immunopositivity (p=0.014) in 250mg/kg VPA treated tumor. The result indicates that a minimally toxic lower dose of VPA can effectively enhance NIS protein expression *in vivo*.

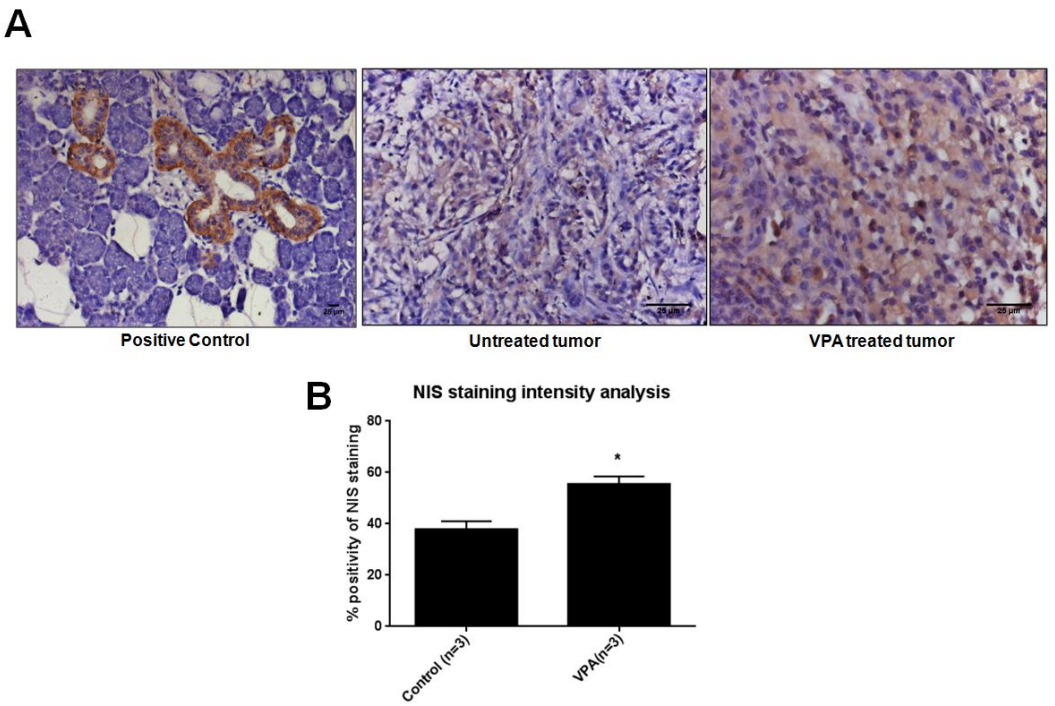

Figure 2.18: Analysis of NIS protein expression after VPA treatment Zr-75-1 tumor xenografts. *A. Representative photomicrographs of NIS antibody stained Zr-75-1 tumor*

xenografts with or without VPA treatment. As positive control, a normal human salivary gland tissue section was used. All images were captured using 20X magnification. B. Chart represents NIS staining intensity comparison of treated and untreated tumor samples with an average of 12 digital sampling collected from multiple xenografts. indicates $p \leq 0.05$.*

2.3.6: Improvement ^{131}I therapy efficacy following VPA pre-treatment *in vivo* in breast cancer tumor xenograft model

Taking lead from *in vitro* and *in vivo* findings, we were encouraged to check ^{131}I therapeutic potential and measure ^{131}I radioablative treatment efficacy *in vivo.* We used Zr-75-1 cells overexpressing luciferase reporter (Fluc2.tdTomato fusion) to generate tumor xenograft so that change in tumor growth can be monitored non-invasively with bioluminescence imaging. Mice in the VPA+^{131}I group received 5 doses of 250mg/kg of VPA followed by 1mCi of ^{131}I injection. The results indicate that in mice treated with ^{131}I (1 mCi/mouse) or 5 doses of VPA (250mg/kg) alone, tumors continued to grow, whereas mice pre-treated with VPA and ^{131}I showed 30% lesser bioluminescence signal 5 days after treatment (**Figure 2.19A-B**).

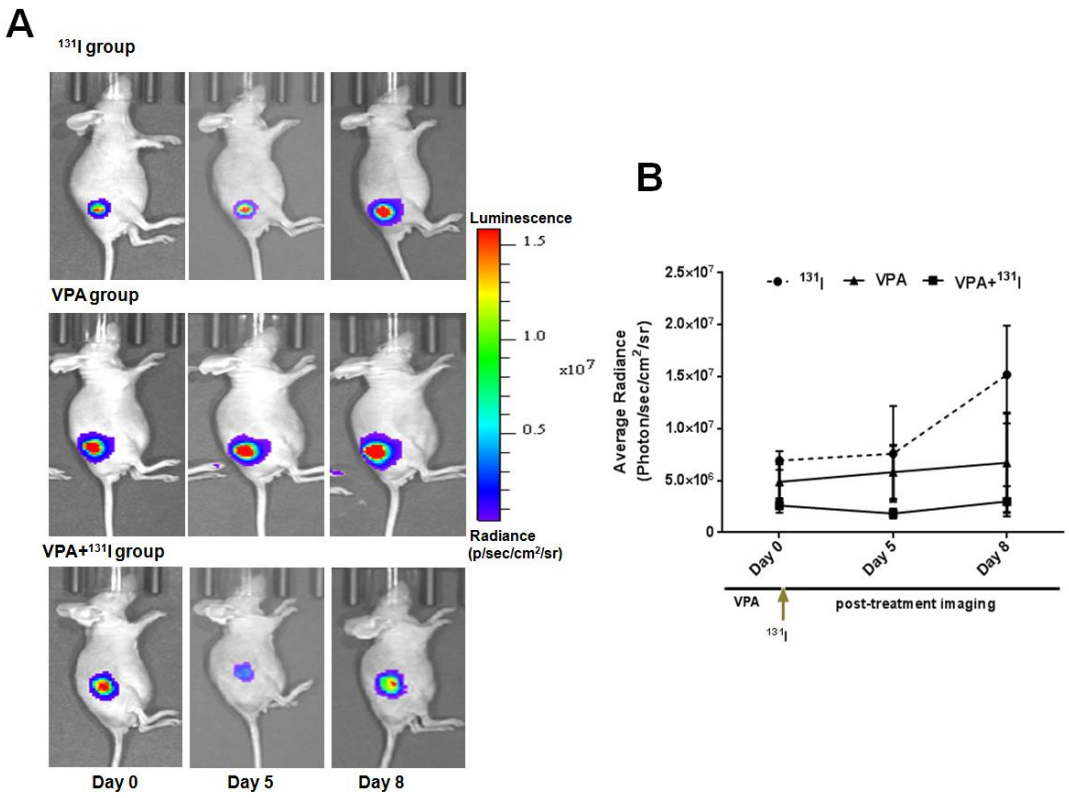

Figure 2.19: Non-invasive bioluminescence monitoring of Zr-75-1 tumor xenograft bearing mice during the treatment phase. *A. Tumor xenografts were established in nude mice using engineered Zr-75-1-CMV-Fluc2.Tdt reporter cells. Mice in ^{131}I group received single intraperitoneal injection of 1mCi of ^{131}I on day 0, and mice in VPA group received 5 doses of 250mg/kg VPA treatment alone while the experimental group undergone pre-treatment with 250mg/kg VPA for 5 days before ^{131}I treatment started. B. Graph illustrates mean bioluminescence signal quantities from sets of mice (n=3) at day 0, day 5 and day 8 when the mice were scanned by injecting D-luciferin.*

The feasibility of ^{131}I radioablation depends on the biological half-life of the isotope in the target breast cancer cells, the dose of radioactivity attained in these tumors and the ability to block accumulation in the thyroid gland. However, in this experiment thyroid blocking was not performed that may be resulting in less availability of ^{131}I to tumor bed. So we repeated the whole experiment using mixture of T4 and methimazole to block the thyroidal uptake of radioactive iodine. Thyroid blocking treatment was started 15 days prior to ^{131}I injection and

was continued throughout the experiment. Non-invasive Cerenkov luminescence imaging was performed to check accumulation of radioactive iodine in tumor and thyroid tissue. CLI imaging post ^{131}I injection shows tumor specific ^{131}I accumulation in the dorsal scan while in the ventral scan; major signal is seen from the partially blocked thyroid. A very faint signal is noted from stomach and bladder (**Figure 2.20A-B**).

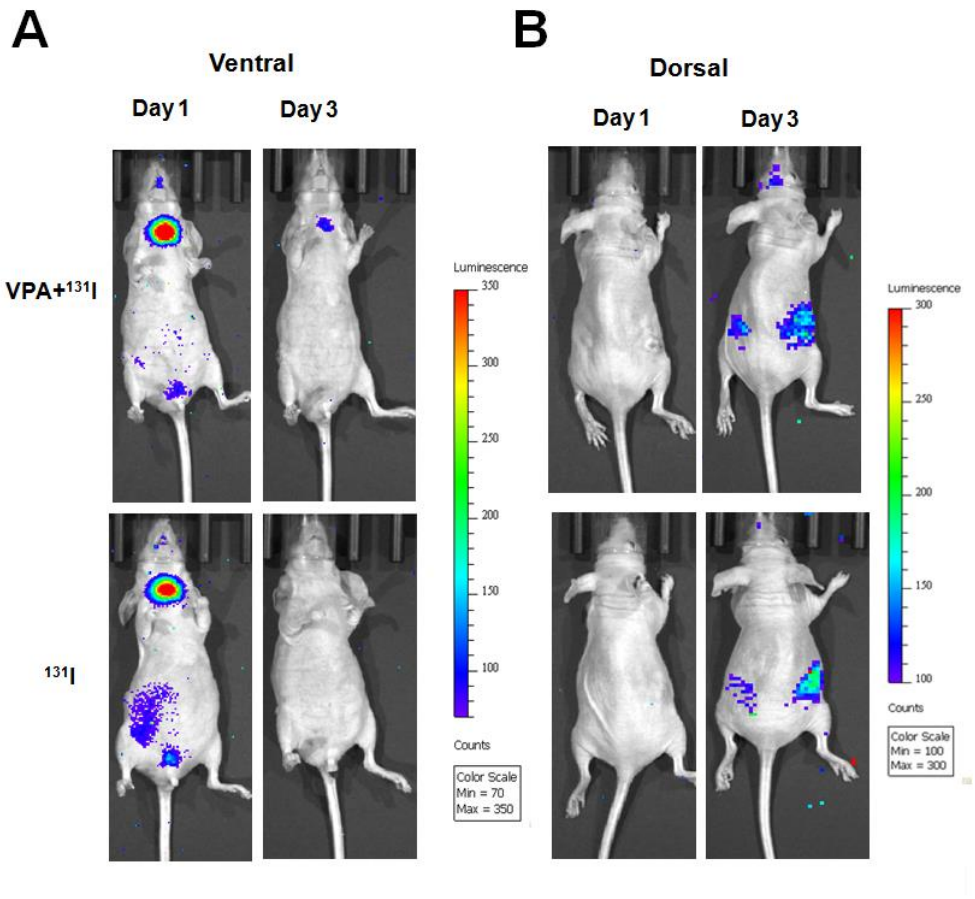

Figure 2.20: *In vivo* Cerenkov luminescence imaging to check ^{131}I distribution in Zr-75-1 tumor xenograft bearing mice. *A-B: Ventral (A) and dorsal (B) scan of non-invasive CLI imaging to check ^{131}I distribution in mice. Mice undergoing methimazole and T4 treatment were non-invasively monitored for ^{131}I uptake at the thyroid (ventral view). Dorsal scan shows accumulation of ^{131}I at tumor site while ventral scan shows major signal from unblocked thyroid. Treatment of Methimazole and T4 started 15 days before ^{131}I injection and continued throughout the experiment. Mice were imaged at various time points as indicated in the figure after single dose of 1mCi ^{131}I.*

Evidenced from bioluminescence imaging data, we observe that in VPA+^{131}I treated group, there is 75% reduction in luminescence signal at day 3 in contrast to mice treated with ^{131}I/VPA alone (**Figure 2.21A**) . The reduction in BLI signal continues until day 9 post ^{131}I treatment while mice treated with VPA/^{131}I alone continued to grow further (**Figure 2.21A-B**). These results are really encouraging indicating the scope of using HDACi treatment to enhance ^{131}I therapeutic efficacy in breast cancer.

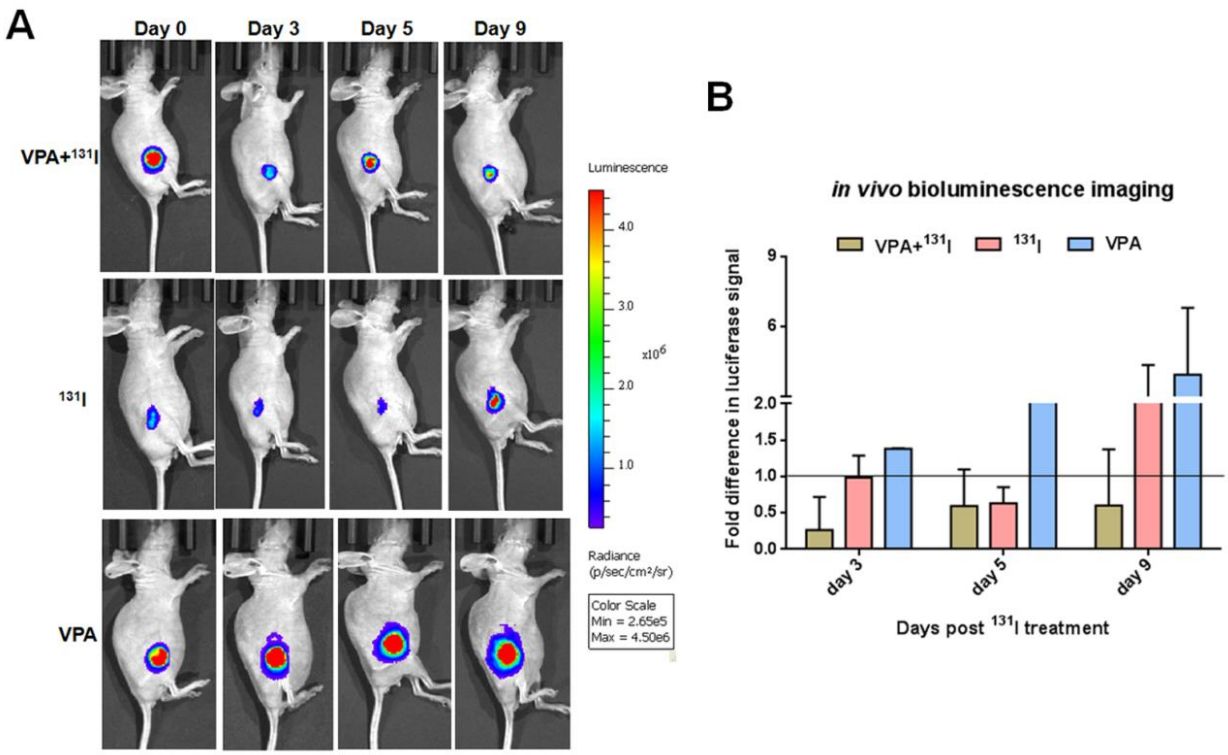

Figure 2.21: Monitoring ^{131}I therapeutic efficacy after pre-treatment with VPA drug *in vivo* in Zr-75-1 tumor xenograft by non-invasive BLI. *A. Representative image of mice in each experimental group i.e VPA+^{131}I, ^{131}I and VPA alone at different time points following treatment phase. B. Graph illustrates fold change in bioluminescence signal in the experimental groups of mice at day 3, day 5 and day 9 when the mice were scanned by injecting D-luciferin.*

2.3.7: Assessment of CI994 influence on breast and thyroid specific NIS expression

As reported in the literature, HDACi like SAHA, VPA are known to induce NIS expression in the thyroid cancer cell lines. So we then tested and compared the effect of benzamide HDACi drug CI994 on NIS induction in breast and thyroid cancer cell lines. As shown in **Figure 2.22A**, elevated NIS mRNA expression (15-25 fold in breast and 4-11 fold in thyroid) is noted more distinctly in breast cancer cells as compared to the thyroid cancer cell lines. Further at the functional level, similar pattern is noticed. CI994 treatment significantly augments NIS-mediated iodide uptake in breast cancer cell lines but no major change is observed in the thyroid cancer cell lines (**Figure 2.22B**). These initial observations imply that CI994 mediated NIS induction may involve modulation of differential tissue-specific transcription factors in the thyroid and breast tissue.

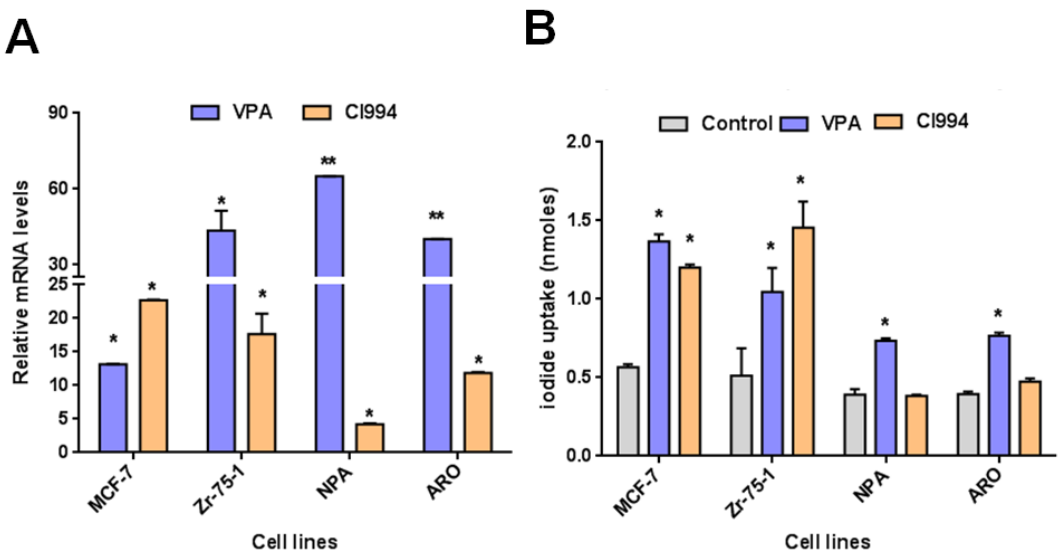

Figure 2.22: Comparison of effect of VPA and CI994 in breast and thyroid NIS expression. *A. MCF-7, Zr-75-1 and two thyroid cancer cell lines i.e. NPA and ARO were tested for the effect of CI994 on NIS expression by real time PCR. VPA is used as positive control that is known to induce thyroid NIS mRNA levels. B. Charts representing the effect of VPA and CI994 on NIS mediated iodide uptake in breast and thyroid cancer cells. * indicates p≤ 0.05, ** indicates p≤0.005.*

2.4: Discussion

After successful cloning of human NIS gene in 1996, research using NIS has progressed at an outstanding pace leading to extensive studies on analyzing structure/function of NIS protein and explicating NIS gene regulation at several levels to novel medical applications. Over the last fifteen years, several studies reporting endogenous and aberrant NIS protein expression in BC have raised the hope of radioiodide therapy in management of this malignancy in women. Endogenous NIS-mediated radioiodide therapy is a gene-targeted, inexpensive and widely available method with relatively lesser side effects as can be revealed by years of practice in thyroid cancer clinic. For realization of this therapy in breast cancer, increased knowledge of mammary NIS regulation is required.

In the present study, we have tested a wide panel of HDAC inhibitors for transcriptional modulation of human NIS in breast cancer cells. As revealed in the schematic diagram (**Figure 2.23**), in addition to histone acetylation activity, distinct HDACi may display different biological responses by acting through various transcriptional factors that in turn can alter human NIS expression. So in the panel of drugs, we have included TSA, TBA, and SAHA which are derivatives of hydroxamic acids, NaB and VPA which are short chain fatty acids and CI994 which is a new benzamide compound. The antifungal antibiotic TSA is a noncompetitive reversible inhibitor of HDAC activity in cultured mammalian cells and is a very potent HDACi at low nanomolar concentrations [177] . SAHA is a known redifferentiating agent and wide-spectrum second generation HDACi. Commercially known as vorinostat, it is the first of the new HDACi to be approved by the Food and Drug Administration (FDA) for clinical use in cancer patients for the treatment of cutaneous T-cell lymphoma [178]. NaB is a low molecular weight non-toxic short chain fatty acid that is produced naturally during the microbial fermentation of dietary fiber in the colon [179]. VPA is a potent anticonvulsant and mood stabilizer and is being used in clinics for the treatment of epilepsy [180]. CI994 is a novel

oral benzamide derivative, has shown antitumor activity in a broad spectrum of mouse, rat and human tumor models [181] and currently in the phase II clinical trials [182]. Importantly, most of these drugs are pan-DAC inhibitors and also in phase 2 or 3 clinical trial (**Table 2.1**), except for TBA which is a HDAC6 specific inhibitor. To our knowledge, this is the first report evaluating such wide scale HDACi class of molecules for altering NIS expression in breast cancer cell and animal model. As the results reveal, four out of six HDACi especially the candidate drugs like NaB, VPA, CI994, and SAHA have shown promising NIS induction also impacting NIS function in breast cancer cells. As anticancer agents, HDACi have serious limitations including cardiac toxicity and very low concentration in solid tumor tissue [183]. However, the whole idea of this study is to use HDACi in a very low quantity to elicit NIS expression for receiving better radioiodine uptake. Thus, future preclinical and clinical trials will actually address the suitability of this strategy in clinic.

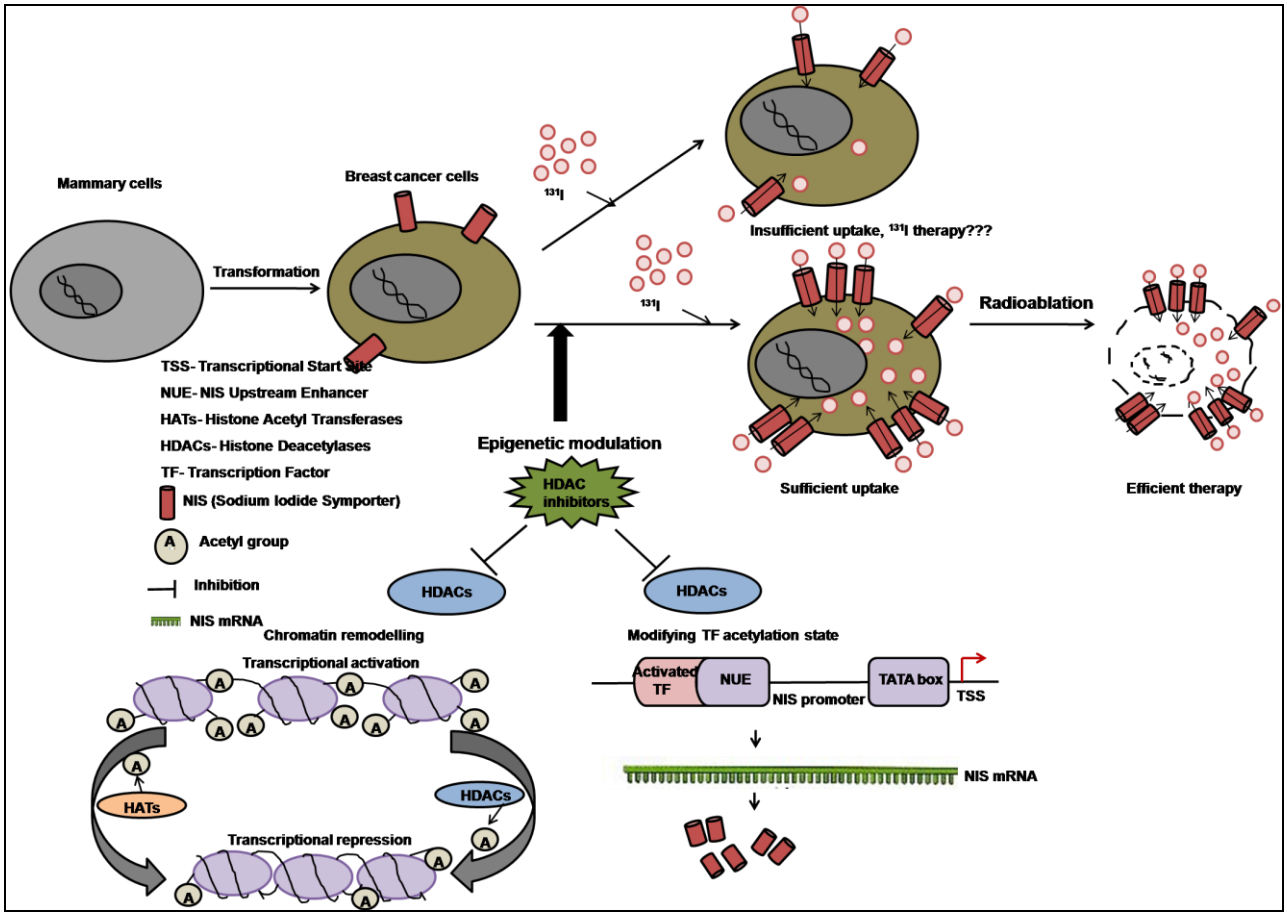

Figure 2.23: Schematic illustration of potential therapeutic applications of HDACi mediated human NIS modulation in breast cancer. *Upregulation of NIS expression during malignant transformation of breast tissue implicated therapeutic application of radioiodine in breast cancer management. To achieve enhanced therapeutic effect, stimulation of functional NIS expression by epigenetic modifiers such as HDACi is a promising strategy.*

An important aspect of our study is the modulation of endogenous NIS expression is observed in both hormone receptor positive and receptor negative cells. Until now enhancement of NIS expression, function and various signaling pathways involved are primarily studied in MCF-7, which is estrogen receptor (ER)-positive cell line [184-186]. Triple negative tumors (ER, PR, HER2 –ve), on the other hand, have worst prognosis and are in high demand of targeted and systemic therapy options [187]. A significant number of TNBC tumor samples showing intense NIS staining [8], can now be modulated further by HDACi, and

thus eventually may improve the scope of applying NIS-based targeted radioiodide therapy for this subgroup of patients. NIS mRNA induction is found more prominently in ER-positive cells than the ER-negative cells. Our recent clinical finding reported a strong association of NIS expression with ER expression among all the BC subtypes [8]. As NIS promoter has several estrogen response elements (revealed by bioinformatics analysis), estrogen is expected to have a direct role in driving NIS transcription. HDACi are also known to act on nuclear receptors including ERα [188]. But surprisingly, in our TF array, ER activation and binding to NIS promoter was not pronounced (i.e. above threshold cutoff margin). Thus, future studies will have to confirm the regulatory mechanism by which HDACi treatment cause enhanced effect in ER positive cells.

Our study also highlights the role of a number of novel transcriptional regulators of NIS expression in breast cancer as evident from the data of TF activation and promoter binding array of 96 global transcription factors. As listed in **Table 2.5**, AP1, CREB, GATA, Stat, PPAR etc. turned out to be important putative NIS regulators in response to HDAC inhibition in breast cancer. Interestingly, it is observed that even though NaB and VPA belong to the same class, transcriptional activation is mediated via differential transcriptional regulators. Further, *in silico* analysis as well as promoter binding array results provide confirmation on the presence of TF binding sites on NIS promoter (as indicated in **Table-2.5**) supporting their potential direct role in modulating cellular NIS expression. There is no literature available regarding NIS regulation by various TFs like AP1, Stat4, GATA etc. in breast cancer. PPAR ligands in combination with other agents were known to induce NIS expression in thyroid tissue [173]. Also, it is a well established fact that TSH stimulation activates cAMP and CREB resulting in activation of NIS expression [172]. But the role of CREB in regulation of NIS in BC is still unknown. All these observations put forward important mechanistic insights on human

NIS promoter induction indicating role of specific TFs in breast tissue which can be explored further in future.

When the benzamide compound CI994 is tested in breast and thyroid cancer cells, NIS induction is found remarkably in breast cancer cells. Benzamide HDACi particularly CI994, are not studied previously with respect to NIS gene regulation. In ^{131}I therapy proposed for non-thyroidal malignancies, ^{131}I accumulation by thyroid glands should be minimized to avoid thyroid damage allowing maximum amount of ^{131}I available to the target tumor. As the NIS gene regulation is organ-specific, the differential regulatory mechanisms could allow stimulation of a selective NIS induction in target tumors with less side effects. Our initial finding illustrates the involvement of tissue-specific transcription factors in NIS induction post CI994 treatment in BC cells. It will be very informative to explore this aspect to discover NIS gene regulation by mammary gland specific transcription factors in future.

The augmented NIS protein levels after NaB, VPA or CI994 treatment are also found to be adequate for ^{131}I radioablation in culture. Together with the data on ^{131}I therapy in cultured cell and mouse studies using non-invasive bioluminescence imaging has clearly indicated HDACi treatment improved therapeutic benefit *in vivo*. Further, thyroid blocking experiment has revealed achievement in improved therapeutic response while protecting the normal thyroid tissue of the subject. Herein, along with BLI, we also monitored the distribution of radioactive iodine by non-invasive CLI. These observations using dual imaging modalities provide insights into the pattern of radiotracer distribution non- invasively and also provide information on time course of radiation effects in humans BC xenograft treated with ^{131}I. For successful implementation of endogenous NIS mediated gene therapy approach, the major obstacles are insufficient radioiodide accumulation in the tumor bed as well as short tracer retention time, putting a question mark on adequate therapeutic value of this approach. In cultured plate, our results indicate that although HDACi treatment significantly improves

NIS-mediated iodide uptake, iodide efflux remains impervious. At this point, organification of iodine in BC cells is not proven [1], and thus whether or not this process can be targeted to enhance efficacy is a matter of research in future. For effective radioiodine therapy, the membrane localization of NIS protein is a critical factor along with its total expression on the cell. From this study, it has been found that treatment of HDACi significantly increases NIS expression but doesn't alter protein localization. Although NIS protein expression has been observed in more than 70% of the breast cancer patients, its clinical utility has been undermined so far due the intracellular localization of the protein in majority of the cases. In our experimental breast cancer cells, even if majority of NIS protein is present at the cytoplasm, VPA pre-treatment elevated NIS expression sufficient enough for radioablation in cell and animal model, implicating its therapeutic potential. Presence of NIS protein at the cell membrane can deliver better therapeutic efficacy. Therefore, discovery of potential agents/signaling pathways targeting NIS protein to the cell the membrane should be pursued in future for improvement of clinical intervention of radioiodine in breast cancer.

In summary, our study provides important mechanistic insights on HDACi mediated NIS induction in breast cancer. This study also demonstrates *in vivo* functional improvement as a step forward towards taking this gene therapy strategy to a success. In breast cancer cases, where NIS protein overexpresses upon cancer onset, use of a brief HDACi pre-treatment can turn NIS mediated radioiodide therapy much more efficacious and thus seems to be a promising strategy for future clinical application. Apart from breast cancer, in thyroid and other non-thyroidal cancer types, where NIS transgene mediated therapy has often been used, may also be impacted further by this transcriptional modulation strategy.

3. Transcriptional regulation of functional NIS expression by tumor suppressor gene p53 in breast cancer

3.1: Introduction

The successful use of NIS-based radioiodide therapy in differentiated thyroid carcinomas and the detection of human NIS protein in extrathyroidal tissues and malignancies, especially in breast cancer, have encouraged a series of studies to extend radioiodide therapy in NIS expressing tumors. However, out of the majority of NIS-positive cases, only 15-20% cases demonstrated detectable radionuclide uptake in tumor. This represents a major obstacle in realization of this gene targeted therapy in breast cancer [4, 5]. Therefore, research efforts are more focused on selective induction of NIS protein expression in breast tissue for improving radioiodide uptake and thus potentiating successful radioablation of cancer cells. To achieve this goal, a better understanding of NIS gene regulation in breast cancer context is realized.

As stated in the previous Chapter, transcriptional regulation of NIS expression is multifaceted area involving the regulatory activities of thyroid-specific, breast-specific and ubiquitous transcription factors. Apparently, set of transcription factors substantially different from that in the thyroid are operational in the breast tissue but their role and the signaling pathways regulating NIS expression in non-lactating, normal breast tissue are largely unknown [78, 154]. After the successful cloning of human NIS promoter, it is discovered that human NIS core promoter region contains a TATA-like motif (AATAAAT) and a GC box (CCCGCCCC) [189, 190]. Binding of Sp-1 and an 'Sp-1-like' protein to the GC box has been previously established, and is essential for full activity of the NIS basal promoter [190]. NIS upstream enhancer (NUE), located between -9470 and -9046 relative to the start site, mediates thyroid specific NIS expression in cAMP dependent manner [10, 81, 191, 192]. These regulatory regions harbor cis-elements for thyroid specific transcription factors, such as Pax8 (a paired domain containing transcription factor) and thyroid transcription factor-1 (TTF-1 or Nkx2.1, a homeo-domain containing transcription factor). Both of these factors are very crucial for thyroid

development and differentiation [193]. The NUE requires Pax8 and c-AMP-responsive element binding protein (CREB) for its full activity [81, 192]. CREB is one of the basic-leucine zipper (b-ZIP) transcription factor containing a leucine zipper domain, that mediates DNA-binding and dimerizations to form homo or heterodimers with other b-ZIP proteins [194]. Recently, it has been shown that miRNA146b-3p acts as a repressor of Pax8, regulating NIS expression in papillary thyroid cancer [195]. In addition to regulation by Pax8, TTF-1/Nkx2.1, role of FoxE1/TTF-2 in NIS gene regulation has been elucidated recently by Fernandez et al. reporting its direct binding to the upstream enhancer region of the NIS promoter [196]. In thyroid cells, TSH is the primary regulator of NIS expression, its function as well as its targeting and retention at the cell membrane [191]. As NIS is an ion transporter, its localization is very crucial for its function. NUE is strongly responsive to TSH stimulation and mediates transcriptional regulation via Pax8, Nkx2.1 and CREB [81, 197]. TSH receptor (TSHR) is a guanine nucleotide-binding protein (G-protein) coupled receptor and activates adenylyl cyclase through stimulatory G protein (Gs protein) to generate cAMP. cAMP production results in activation of both protein kinase-A (PKA)-dependent and PKA-independent pathways in thyroid cells [81, 192, 198] . These pathways include PKA-CREB, APE/Ref-1-Pax8 [197], and the MAPK pathway [10, 199].

Cytokines like transforming growth factor-β1 (TGF-β1), tumor necrosis factor α (TNF-α), TNF-β, interferon-γ (IFN-γ), interleukin-1α (IL-1α), IL-1β, and IL-6 exert an inhibitory effect on TSH-cAMP mediated NIS expression and iodide uptake in humans thyroid cells [200, 201] . In 2003, Costamagna et al. studied NIS gene regulation by TGF-β reporting that TGF-β decreases NIS gene expression in rat thyroid follicular PCCl3 cells by reducing TSH mediated transcriptional activation [202]. In response to TGF-β, activation of Smad 3 and Smad 4 is observed leading to decreased binding of Pax8 to NIS promoter inhibiting its expression. Further in 2009, it is reported that BRAF represses NIS expression by robust induction of

TGF-β secretion resulting in subsequent activation of Smad signaling [203]. The activating mutation $BRAF^{V600E}$ is a frequent mutation occurred in papillary thyroid carcinomas (PTC) that predicts a poor prognosis. BRAF induces secretion of functional TGF-β leading to repression of NIS expression in PTC. Along with TGF-β, NIS expression in thyroid cells is mainly suppressed by PBF [pituitary tumor-transforming gene (PTTG)-binding protein] [204]. PBF binds to NIS and alters its subcellular localization, thereby resulting in reduced iodide uptake. Additionally, NIS-repressor is reported as a trans-acting protein binding to a specific region of the proximal NIS promoter, NIS-repressor binding site (NRBS-P) [205].

In comparison to thyroid, currently, our knowledge of NIS regulatory mechanisms in breast tissue is quite limited. Transcriptional and post translational regulation of NIS by TSH in the thyroid is a well established fact. However, it is clear that the positive control of TSH seen in the thyroid is not involved in NIS regulation in the breast. Disparity in NIS gene regulation in the thyroid and breast tissue leaves a significant gap in our understanding of mammary NIS regulation. In non-neoplastic cells, fetoplacental estrogen and two other pituitary hormones; oxytocin and prolactin, play an important role in NIS induction during the lactation phase of mammary gland [2, 3]. It has also been shown that ERα physically interacts with an estrogen responsive element (ERE) present in human NIS promoter sequence and activates its expression. The ERE sequence is localized only 9 base pairs away from the TATA box element and this position is conserved in rodent and human genomes [206]. In addition to lactating mammary gland, human breast carcinomas and experimental mammary carcinomas in transgenic mice bearing constitutively activated oncogenes are also shown to express NIS protein [3, 207]. These observations indicate that mammary NIS expression can be regulated by the *neu*, *ras* or polyoma T antigen signal pathways. A retinoic acid (RA) response element is also located at position -1375 relative to NIS start codon. Retinoids have a robust effect inducing functional NIS in MCF-7 cells [78, 82, 155]. In contrast to thyroid cells, neither iodide

nor activation of cAMP signaling had a significant effect on NIS expression in MCF-7 cells [208]. atRA as well as several other synthetic ligands of retinoic acid receptor (RAR), significantly induce NIS expression and iodide uptake in MCF-7 cells [9, 11, 208]. NIS regulation by retinoids in BC cells is effected through a downstream intronic enhancer, which binds to RARα and RXR [82, 147, 155, 184, 206]. The activation of the phosphoinositide 3-kinase (PI3K) pathway and the p38MAPK pathway is involved in atRA-mediated NIS induction in MCF-7 cells [184, 209]. Dentice et al. have reported further the role of the cardiac homeobox transcription factor Nkx2.5 in NIS regulation. Upon stimulation, induced Nkx2.5 binds to two cis-acting elements in the NIS promoter located at -446 and -154 relative to ATG, thus elevating NIS expression [12]. Although, these studies are informative, investigation of other potential regulators and their pertinence to NIS in human breast tumor tissue is of great interest. We believe that regulatory factors leading to expression and activation of NIS in lactating mammary tissue are also operational in some breast cancers. Targeting these regulatory mechanisms may help to position NIS based radioiodide therapy sufficiently for breast cancer treatment. To elucidate the role of transcriptional regulators of NIS expression, we first performed *in silico* analysis of human full length NIS promoter sequence using the Transfac and the Genomatix package (cut off score 80%). *In silico* analysis predicted ~64 various transcription factor (TF) binding sites including AP1, CREB, Pax8 etc. (**Figure 3.1A**) (also listed in **Table 3.1**). Sp1, Pax8 and CREB have appeared as regulators of human NIS expression as shown in **Figure 3.1**. As reviewed above, these are the known regulators of thyroidal NIS expression reported in the literature. Interestingly, along with these transcription factor binding sites, it has been observed that human NIS promoter also harbors two full and a half-binding consensus sequence (RRRCNNGYYY) for p53 binding (**Figure 3.1A**) [15]. Additionally, Sp1 which is a known regulator of human NIS expression is also known to interact directly with p53 (**Figure 3.1B**). Nearly one-third of breast cancers have

mutations in the p53 gene that are associated with high histological grade and clinical aggressiveness [210]. Aberrant NIS expression in breast cancer is also a well reported fact at present. This observation encouraged us to look into a direct possible link between NIS and p53, both of which are relevant in the context of breast cancer. Hence, we decided to investigate the role of p53 in NIS gene regulation using our experimental model.

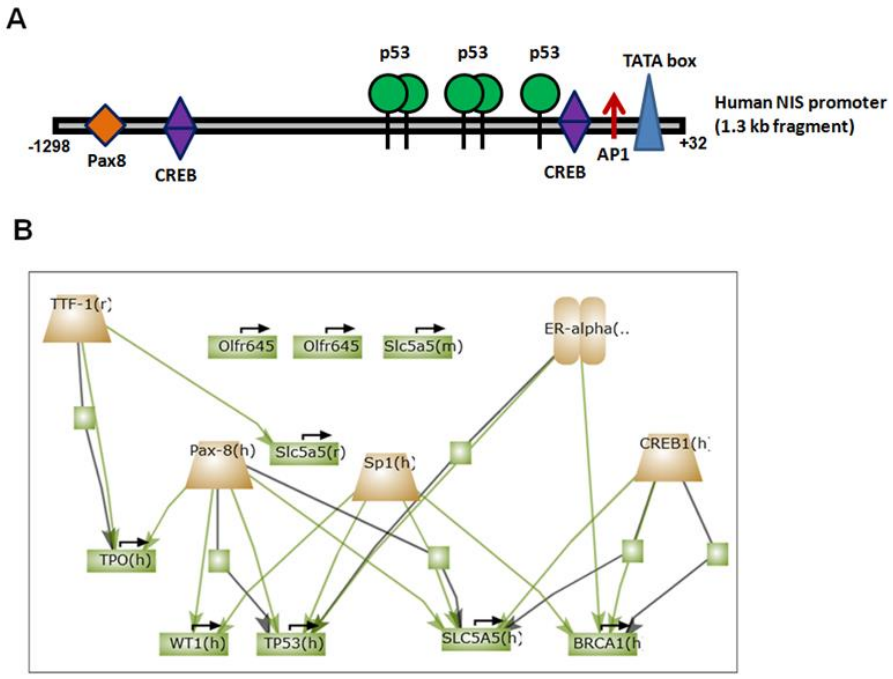

Figure 3.1: Bioinformatics analysis of NIS promoter sequence to identify potential transcriptional NIS regulators. *A. Cartoon representing 1.34kb human NIS promoter fragment harboring various promoter elements (TATA box) along with two complete and one half-binding p53 response elements (RE). It also indicates the presence of different transcription factor binding sites like AP1, CREB, Pax8 etc. on human NIS promoter. B. Potential transcriptional regulatory network of NIS expression derived from BKL Pathfinder, Biobase, Transfac analysis.*

Table 3.1: Bioinformatics analysis with Genomatix software indicates the presence of around 64 putative regulatory transcription factor binding sites on human NIS promoter

No.	Transcription factor	No. of sites	Regulation known
1	AP1	1	-
2	AP2	2	Y
3	CREB	5	Y
4	GATA	6	-
5	Hox4C #	6	-
6	Nuclear factor 1 (NF-1)	2	-
7	Stat #	1	-
8	Sox #	2	-
9	E-box binding factors	2	-
10	Octamer binding protein	6	-
11	Smad family TFs #	3	Y
12	X-box binding factors	5	-
13	MEF-3 binding sites	3	-
14	Heat shock factors	2	-
15	Interferon regulatory factors	4	Y
16	RXR heterodimer binding sites	6	Y

17	Nkx homeo-domain factors [#]	3	Y
18	Estrogen response elements (ERE)	4	Y
19	Sp1 binding sites	5	Y
20	PPAR	2	Y
21	CCAAT binding factor	4	-
22	Pax2	1	-
23	Pax3	2	-
24	Pax5	5	-
25	Pax4/Pax6 paired domain binding site	5	-
26	Pax8	4	Y
27	Microphthalmia TF	1	-
28	AT-rich interactive domain factor	2	-
29	Homeo-domain TF [#]	3	Y
30	Pleomorphic adenoma gene (PLAG)	5	-
31	Ras responsive element binding protein	6	-
32	LEF1/TCF	2	-
33	GLI Zn family TF [#]	6	-
34	Hepatic nuclear factor (HNF)	1	-
35	Nuclear receptor subfamily 2 factors	4	-
36	Serum response element binding factor	3	-
37	C2H2 Zn finger TFs	12	-

38	Krueppel like factors	8	-
39	GT box	2	-
40	Myc associated Zn finger protein	2	-
41	Vertebrate steroidogenic factor	1	-
42	Nuclear factor of activated T-cells (NFAT)	1	-
43	Brn-POU domain factors	7	-
44	PAR/bZIP family[#]	1	-
45	Insulinoma associated factors	5	-
46	Calcium response elements	2	-
47	EVI1 myeloid transforming protein	4	-
48	Farnesoid X-activated receptor response elements	2	-
49	MYT1 C2H2 Zn finger protein	5	-
50	Myoblast determining factors	2	-
51	EGR	3	-
52	Hypoxia inducible factor	1	-
53	Myeloid Zn finger 1 factors	1	-
54	HoxC9	2	-
55	Vitamin D receptor (VDR)	3	-
56	SWI/SNF related nucleophosphoprotein with a ring finger DNA binding motif	4	-
57	Cellular and viral Myb-like transcriptional regulators	2	-

58	SOX/SRY related HMG box factors #	7	-
59	Winged helix binding sites	1	-
60	Y-box binding transcription factors	1	-
61	CLOX and CLOX homology (CDP) factors	2	-
62	Paralog hox genes 1-8 from the four hox clusters A, B, C, D	6	-
63	TFIID	1	-
64	E2-F1	1	-

# indicates presence of TF binding site belonging to family of TF

Y- Role in NIS gene regulation is studied in thyroid/breast tissue

3.2: Materials and methods

3.2.1: Plasmid characterization

Wild type p53 (p53) overexpression plasmid was gifted from Dr. Sorab Dalal, ACTREC, India. The expression of p53 was confirmed by restriction digestion of the plasmid with BamHI that released 1.8 kb fragment of wild type p53 (**Figure 3.2A**). Further, expression analysis was performed by transient transfection in MCF-7 cells and using p53 specific monoclonal antibody (**Figure 3.2B**).

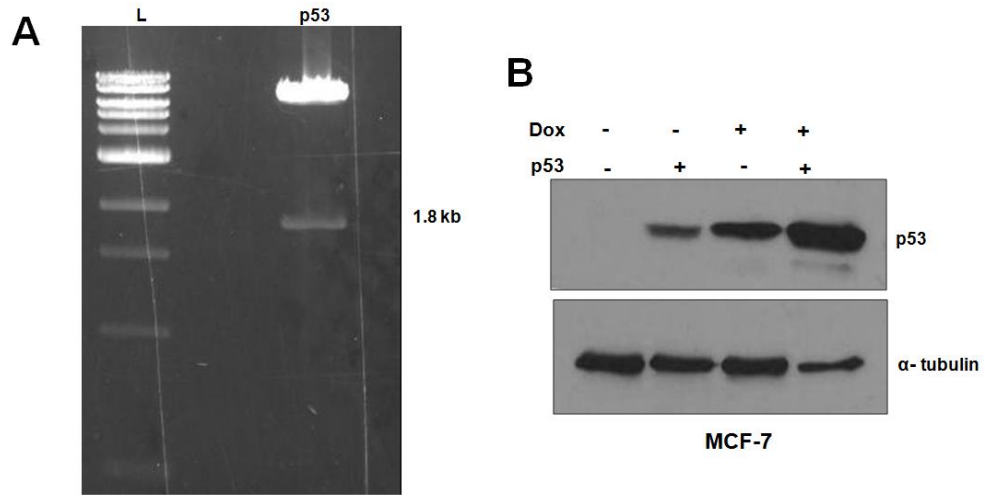

Figure 3.2: Validation of wild type p53 expression plasmid. *A. Restriction enzyme analysis was done with BamHI to confirm release of wild type p53 from the mammalian expression plasmid. B. Western blot analysis validating p53 overexpression and activation in response to doxorubicin treatment in MCF-7 cells.*

3.2.2: Mammalian Cell culture

Several BC cell lines representing various subtypes as well as p53 status were included in the study (Details provided in earlier Chapter, Table 2.2). Engineered cells stably expressing NIS promoter bifusion reporter were used for non-invasive optical imaging experiment *in vitro* and *in vivo*. The experimental details were given in the Chapter 2 and the appendix section.

3.2.3: Luciferase reporter assay

Selected MCF-7 and Zr-75-1clonal cell population were seeded at an equal cell density. For transient transfection experiments, MCF-7 and Zr-75-1 cells were transfected with wild type or mutated pNIS-Fluc2.TurboFP plasmid constructs using Lipofectamine 2000. Thymidine kinase (TK) driven *Renilla luciferase* (RL) reporter was used for transfection normalization. Following 24 hours of Dox treatment, lysates were collected using passive lysis buffer (Promega Corporation, USA) and luciferase activity was measured using luminescence plate

reader (BMG Labtech, Germany). The data was plotted as relative light unit per second (RLU/sec) normalized with protein estimated by Bradford method (Sigma, USA).

3.2.4: Site Directed Mutagenesis

Human NIS promoter having three p53 binding sites was sequentially mutated using the mutagenic primers (as listed in **Table 3.2**) which consist of the substitutions/deletions at the core sequence of p53 binding sites by Dpn-I mediated site directed mutagenesis. The colonies obtained were screened and verified by sequencing for inclusion of the desired mutations. The details are explained in the appendix section.

3.2.5: RNA extraction and quantitative real-time PCR

The detailed procedure of RNA isolation and real time PCR is given in the appendix section. Briefly, after 24 hours of Dox treatment, RNA was extracted using RNeasy kit (QIAGEN, USA). 1.5 μg of RNA was converted to cDNA using the first strand cDNA synthesis kit (Invitrogen, USA). Quantitative real-time PCR was performed using TaqMan probe mix on the Quant Studio 12K Flex (Applied Biosystems, USA). The TaqMan probes for human NIS and GAPDH with assay IDs Hs00166567_m1 and Hs02758991_g1 respectively were used (Applied Biosystems, USA).

3.2.6: Western blotting

Cell lysates were prepared from cells using RIPA buffer (Sigma, USA) containing standard protease inhibitors (Santa Cruz Biotechnology, USA). The proteins were resolved in 10% SDS-PAGE gel and transferred onto nitrocellulose membrane (Millipore, USA) by semi-dry method. After blocking with 5% milk, membranes were probed with anti-human NIS antibody (FP5A, Abcam, USA), anti-p53 antibody (DO-1, Santa Cruz Biotechnology, USA) and anti-α-tubulin antibody (T9026, Sigma, USA) followed by washing and secondary HRP-

conjugated antibodies. The blot was developed by chemiluminescence (Invitrogen, USA). Even transfer and equal loading was determined using α-tubulin levels. The detailed protocol of western blotting is given in the appendix section.

3.2.7: Chromatin Immunoprecipitation (ChIP) assay

Protein complexes were cross-linked to DNA in living nuclei by adding 1% of formaldehyde (Merck, Whitehouse Station, NJ, USA) to the culture medium for 10 minutes at room temperature. Cross-linking was stopped by the addition of 0.125M glycine. Cross-linked cells were scraped, washed with PBS. Cells were pelleted by centrifugation and lysed in FA lysis buffer (1% TritonX, 0.5M EDTA, 0.5M HEPES/KOH, 140mM KCl, 0.1% sodium deoxycholate, 0.1% SDS and protease inhibitors). The resulting chromatin solution was sonicated for 9 pulses of 60 sec at high power (Bioruptor sonicator, Diagenode, Liege, Belgium) to generate 200–1000 bp DNA fragments. After microcentrifugation, the supernatant was precleared with blocked protein G plus (Pierce, Rockford, IL, USA) diluted 1 : 10 with dilution buffer (1% TritonX, 2mM EDTA pH 8, 20mM Tris-HCl pH 8, 150mM NaCl along with protease inhibitors), and divided into aliquots. Five micrograms of antibody was added to each aliquot of chromatin and incubated on a rotating platform for 12–16 h at 4˚C. Antibody–protein–DNA complexes were isolated by immunoprecipitation with blocked protein G beads. Following extensive washings, ChIPed DNA was analyzed by semi-quantitative PCR using specific set of primer pairs as shown in **Table 3.4**.

3.2.8: *In vivo* optical imaging procedures

The experimental protocol was approved by Institutional Animal Ethics Committee (IAEC) and performed in accordance with the guidelines provided for the care and use of the laboratory animals. Female BALB/c nude mice (n=6) were used for growing orthotropic tumor using Zr-75-1 engineered cells stably expressing pNIS-Fluc2.TurboFP fusion reporter.

Mice were divided into two groups: the Dox group (single intraperitoneal injection of 1.5mg/kg of doxorubicin) and the control group. Bioluminescence imaging was performed before and after Doxorubicin treatment using IVIS-Spectrum (Caliper Life Sciences) after intraperitoneal injecting 30mg/ml of D-luciferin (Biosynth International). Mice were anesthetized with 2% isofluorane for the entire duration of the scan time and monitored in real time on a computer screen using a color scale expressed as average radiance (photons per second per square centimeter per steradian [photons/sec/cm^2/sr]). Data were analyzed using Living Image version 4.4 software.

3.2.9: Statistical Analysis

All data are expressed as mean ± SE and are representative of at least two separate experiments. Statistical significance was analyzed by Student t-test using GraphPad Prism 6 (GraphPad Software, La Jolla, CA). P values of ≤ 0.05 were considered statistically significant.

3.3: Results

3.3.1: NIS promoter activity is regulated by activated p53 in breast cancer cell lines and tumor xenograft model

As *in silico* analysis revealed the presence of p53 response elements on human NIS promoter sequence, first we checked NIS promoter mediated reporter modulation in response to activated p53. In the study panel, two breast cancer cell lines i.e. MCF-7 and Zr-75-1 with wild type p53 and MDA-MB-453 cell line (lacking functional p53 protein) were included (**Figure 3.3A**). Various chemotherapeutic drugs including Doxorubicin are known to induce p53 expression [211]. Doxorubicin mediated p53 induction can be clearly observed in **Figure 3.3A**. To study the regulation of human NIS promoter, MCF-7, Zr-75-1 and MDA-MB-453

cells were transiently transfected with pNIS-Fluc2.TurboFP plasmid and the reporter activity was measured in response to p53 activation in these cell lines. Normalized luciferase activity is shown in **Figure 3.3B** and data clearly indicates significant reduction of promoter activity in response to p53 activation in MCF-7 and Zr-75-1 cells but not in MDA-MB-453 cells ($p<0.05$) (**Figure 3.3B**). This observation hints directly at p53 dependent NIS promoter modulation as the effect is observed specifically in p53 wild type cell lines i.e MCF-7 and Zr-75-1 (**Figure 3.3B**). Further, in response to overexpression of wild type p53 as a transgene in the presence or absence of doxorubicin treatment, NIS transcriptional activity drops significantly in all three BC cell lines, confirming p53 mediated transcriptional repression (**Figure 3.3B**). The effect of p53 on NIS transcriptional activity was also confirmed in MCF-7 Cl6 and Zr-75-1 C2 engineered cells by transient transfection of wild type p53 expression plasmid in the presence or absence of doxorubicin treatment (**Figure 3.3C**)**.** Similar pattern of transcriptional repression is observed in these clonal cells (**Figure 3.3C**)**.**

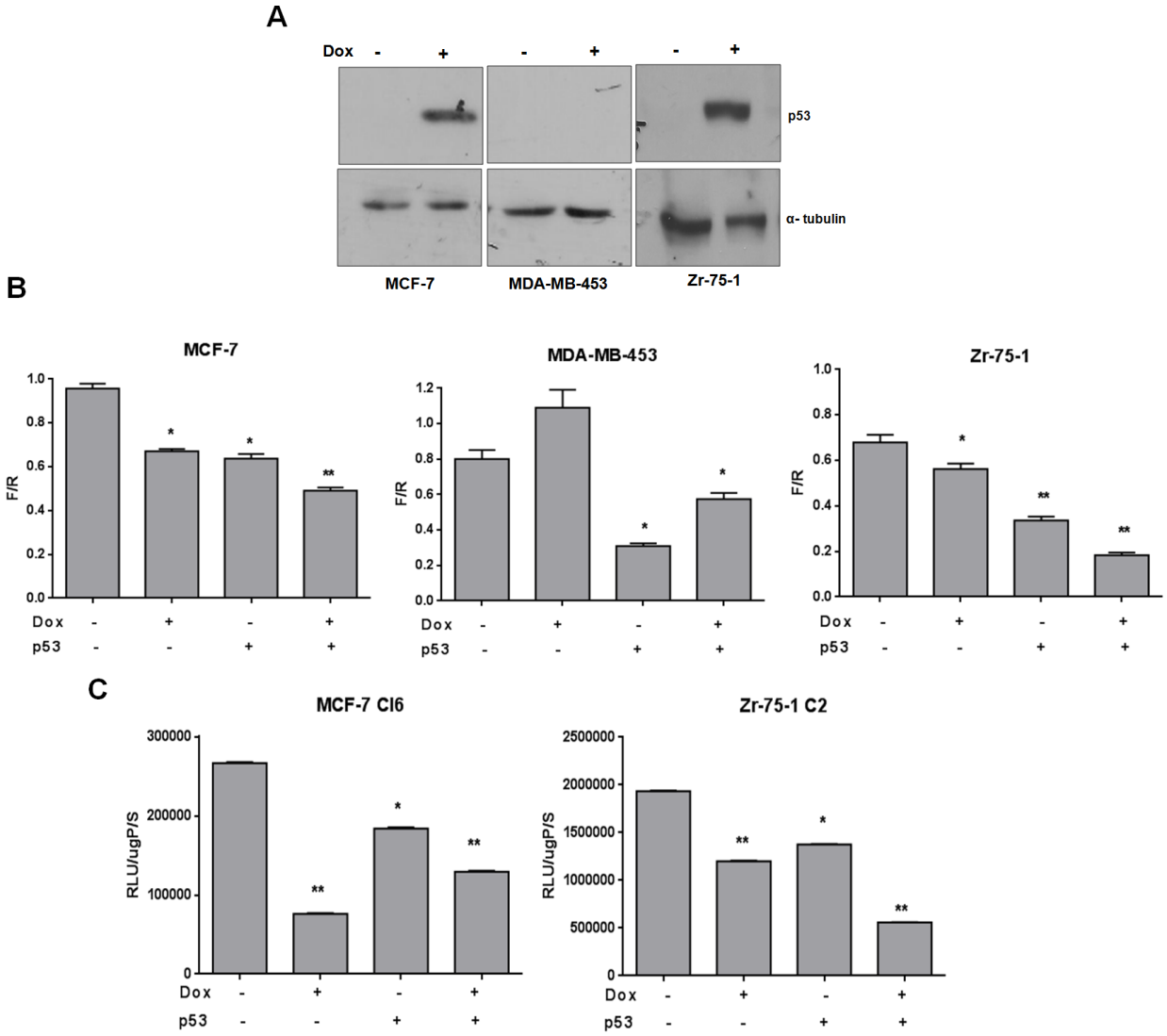

Figure 3.3: NIS is a transcriptional target of p53 in breast cancer. *A. p53 status was verified in MCF-7, MDA-MB-453 and Zr-75-1 cells after doxorubicin treatment by western blotting using p53 specific antibody. α-tubulin was used as loading control. B. Charts showing normalized luciferase activity in response to exogenous wild type p53 overexpression or endogenous p53 activation in breast cancer cells. MCF-7, Zr-75-1 and MDA-MB-453 cells were transiently transfected with pNIS-Fluc2.TurboFP reporter construct. TK-hRL was used for transfection normalization. Doxorubicin (Dox) treatment was given to cells (1μg/ml, for 24 hours) to activate endogenous p53. C. Graphs indicating modulation of NIS promoter activity in engineered breast cancer cell clones in response to p53 activation or wild type p53 overexpression alone or in combination.*

The p53 promoter modulation against increasing Dox concentration was also verified by live cell imaging using IVIS-Spectrum (Caliper Life Sciences). Equal number of the engineered Zr-75-1 clone C2 cells were seeded in 96-black well plates, and exposed to increasing concentrations of doxorubicin (0.5-2µg/ml) for endogenous p53 activation. 24 hours after the drug treatment, NIS promoter activity was monitored using D-luciferin substrate (50µl of 100µg/ml stock per well). Photons emitted from live cells were measured from each well using Living Image software. As indicated in the **Figure 3.4A-B**, NIS promoter activity decreased in a drug dose dependent manner corroborating the observations from cell lysates.

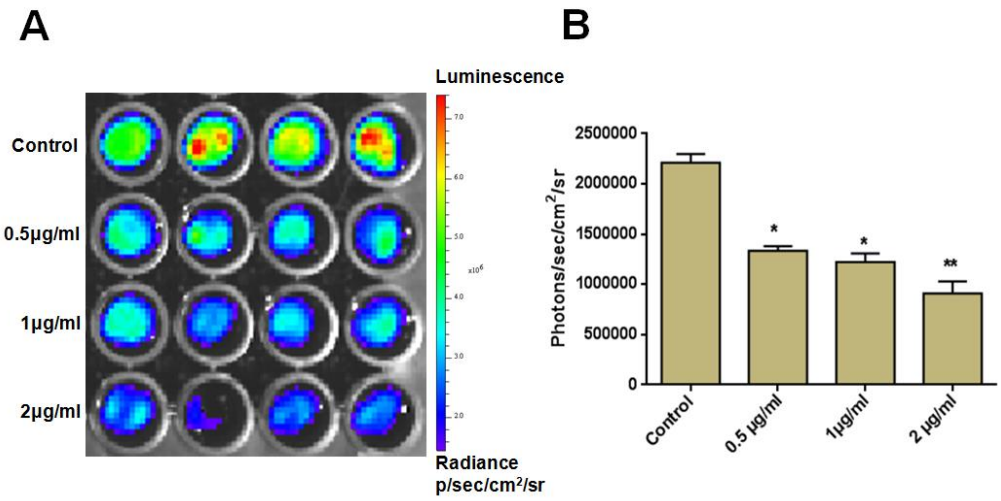

Figure 3.4: Live cell imaging study of NIS promoter modulation by activated p53. *A. A representative image of 96-well black plate loaded with fixed number of engineered Zr-75-1 clone C2 cells used to monitor NIS promoter modulation by bioluminescence imaging in response to increasing concentrations of doxorubicin. Wells on each row represent replicates. B. Graph illustrates mean bioluminescence signal quantities from each row indicating control and doxorubicin treated wells.*

In order to validate *in vitro* findings, tumor xenograft model was established using engineered Zr-75-1 (stably expressing pNIS-Fluc2.TurboFP reporter, clone C2) cells. $6x10^6$ cells were implanted on mammary fat pad of female BALB/c nude mice (n=6) and tumor growth was monitored by bioluminescence imaging. As the tumor volume reached to a measurable size,

mice were randomized into two groups i.e the control group and the Dox group. Mice in the Dox group received single intraperitoneal injection of 1.5mg/kg doxorubicin to activate p53 *in vivo* while avoiding drug induced toxicity as reported by Briat et al. [16]. The representative images of the bioluminescence signal in Zr-75-1 tumor bearing mice pre- and post-treatment are shown in the **Figure 3.5A**. The BLI data clearly reveals 0.5 fold attenuation in luciferase activity after 48 hours of treatment ($1.61\times10^{8} \pm 5.87\times10^{7}$ to $8.07\times10^{7} \pm 2.01\times10^{7}$) in the Dox group. Whereas, in the control group, mice show slight increment in luminescence due to tumor growth within the same 48 hours time period ($1.18\times10^{8} \pm 4.83\times10^{7}$ to $1.48\times10^{8} \pm 7.79\times10^{7}$) (**Figure 3.5B-C**). As expected, tumor volumes of mice exhibit no major difference before and after the Dox treatment as revealed in **Figure 3.5D**.

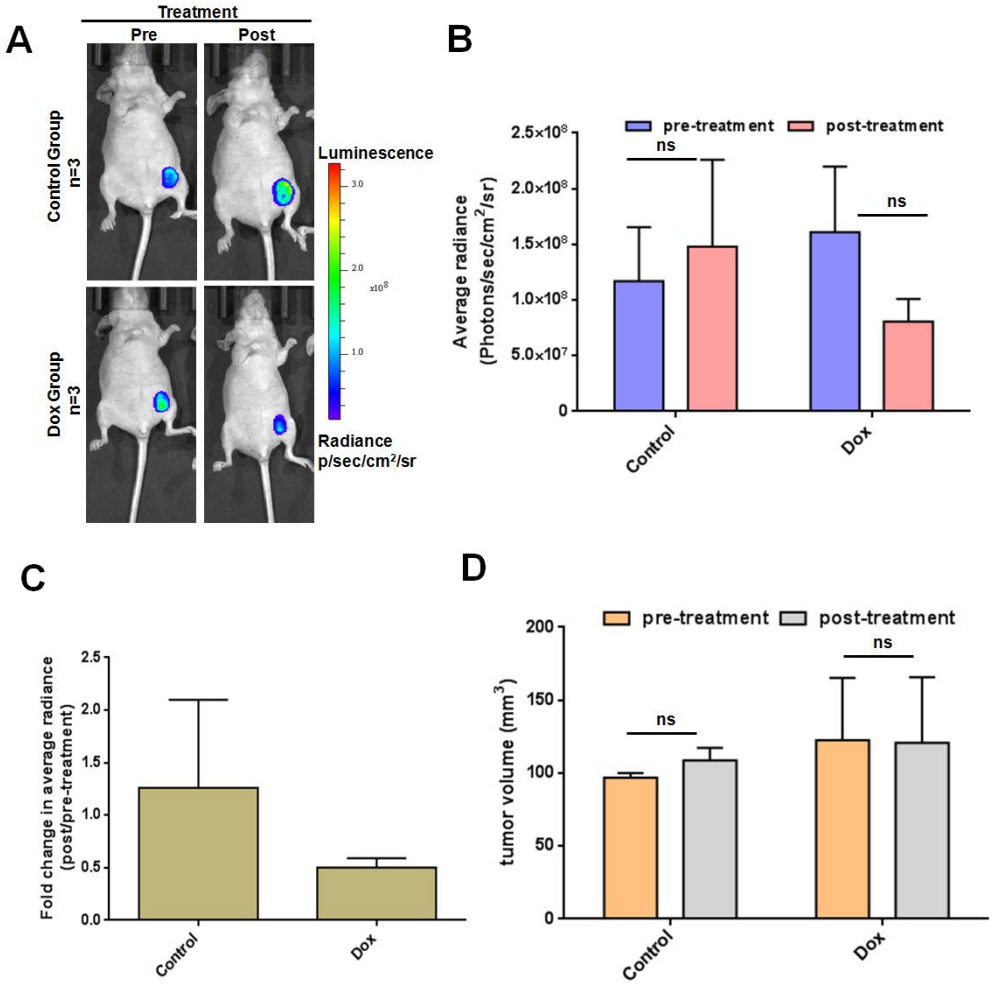

Figure 3.5: Demonstration of NIS gene repression by activated p53 using non-invasive bioluminescence imaging in tumor xenograft model. *A. Orthotropic tumor xenografts were*

established in female nude mice using engineered Zr-75-1-pNIS-Fluc2.TurboFP reporter cells. Representative images of the mice in each group were shown in figure. Mice in the Dox group received single intraperitoneal injection of 1.5mg/kg dose of doxorubicin. B. Graph illustrates mean bioluminescence signal quantities from sets of mice (n=3) pre- and post-doxorubicin treatment when the mice were scanned by injecting D-luciferin substrate. C. Graphical representation of fold-changes in the bioluminescence signals of the control and Dox treated mice. The temporal fold change in bioluminescence signals calculated ratiometrically (post-treatment signal/pre-treatment signal). D. Chart representing the tumor volumes (mm^3) in the control and the Dox group pre- and post-treatment.

3.3.2: Abrogation of p53 binding sites on NIS promoter sequence augments NIS transcriptional activity

Based on the earlier observations, next we performed a series of site directed mutagenesis to abolish p53 binding sites on the human NIS promoter. The core CNNG sequence of p53 response element was either substituted with AATT sequence or the entire p53 response element was deleted in mutagenesis studies (**Figure 3.6A**). Dpn-I-mediated mutagenesis strategy is depicted in **Figure 3.6B.** The complete set of all mutagenic primers is listed in **Table 3.2**. The detailed protocol is given in the appendix section. **Figure 3.6C** demonstrates representative gel image indicating amplification of whole plasmid DNA. PCR condition for SDM is shown in **Table 3.3**. These promoter constructs were thoroughly validated by sequencing for the desired mutations (**Figure 3.6D**) and used further for transfection experiments.

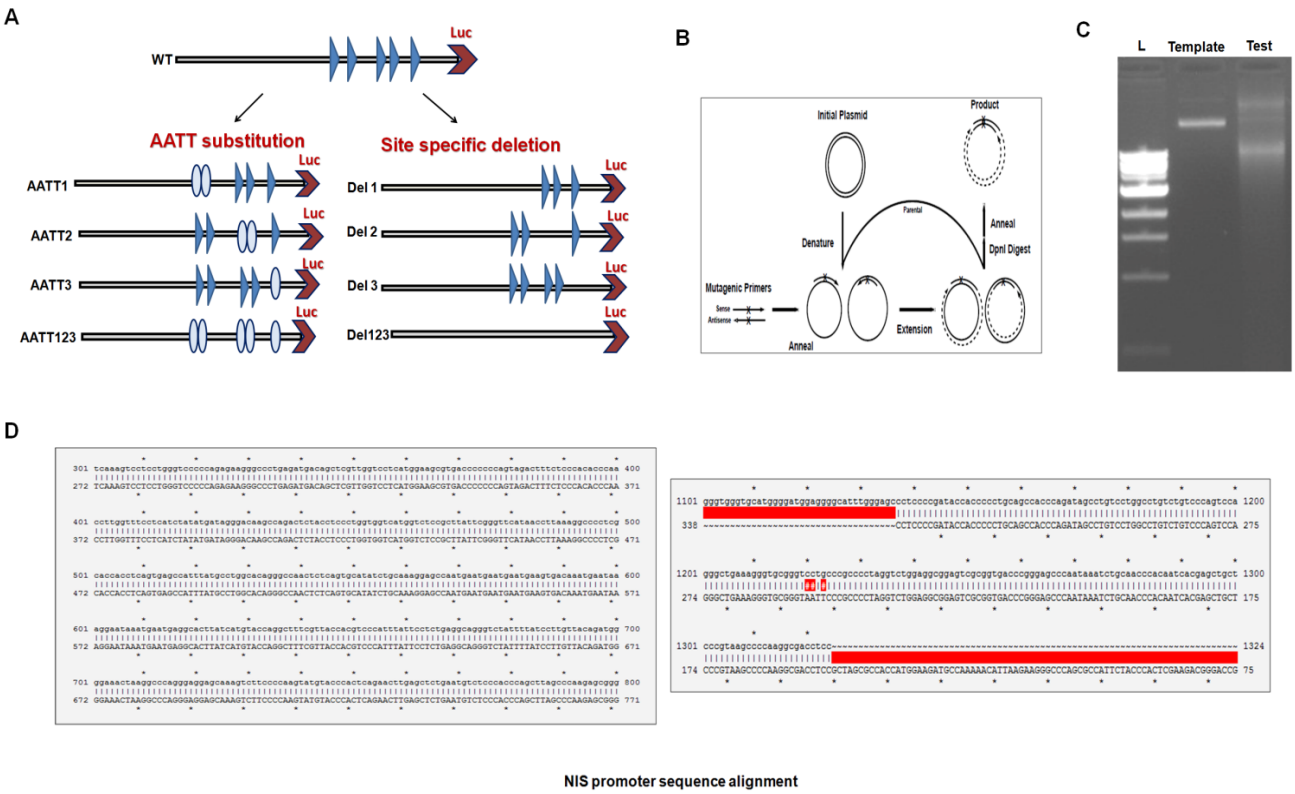

Figure 3.6: Development of mutant NIS promoter plasmid DNA constructs with altered p53 binding sequence. *A. Mutagenesis strategy disrupting the p53 binding site on the human NIS promoter by either AATT substitution of the core CNNG sequence or deletion of entire p53 binding site individually or in combination. B. Cartoon depicting different steps of Dpn-I mediated site directed mutagenesis. C. Representative agarose gel image indicating PCR amplification of SDM product. D. Sequence alignment of site 3 AATT plasmid with wild type NIS promoter plasmid DNA highlighting the desired alteration at site 3 on the NIS promoter.*

Table 3.2: List of primers used in the site directed substitution / deletion mutation of p53 response element on human NIS promoter

Mutagenic primer	Sequence
AATT 1	5'- CTGAAGCAGGCTGTGAATTCTTGGATAGTG-3'Fwd 5'- CACTATCCAAGAATTCACAGCCTGCTTCAG-3' Rev
AATT 2	5'-TAGAATTTCCTGGAATTTCTGTCCCAGTCC-3' Fwd 5'-GGACTGGGACAGAAATTCCAGGAAATTCTA-3' Rev
AATT 3	5'- GGGTGCGGGTAATTCCCGCCCCTAGGTCTG-3' Fwd 5'- CAGACCTAGGGGCGGGAATTACCCGCACCC-3' Rev
Del 1	5'-GTGCTGAAGCAGGCTTCTCTGAGCCTCAAT-3' Fwd 5'-ATTGAGGCTCAGAGAAGCCTGCTTCAGCAC-3' Rev
Del 2	5'- CTGCAGCCACCCAGAGTCCCAGTCCAGGGC-3' Fwd 5'- GCCCTGGACTGGGACTCTGGGTGGCTGCAG-3' Rev
Del 3	5'- GGCTGAAAGGGTGCGGCCCCTAGGTCTGGA-3'Fwd 5'- TCCAGACCTAGGGGCCGCACCCTTTCAGCC-3' Rev

AATT indicates substitution of core "CNNG" sequence from p53 response element by "AATT" sequence disrupting the p53 binding site from the promoter

Del indicates deletion of individual p53 response element from the promoter

Table 3.3: Table demonstrating PCR condition for site directed mutagenesis of plasmid DNA

No. of cycles	Cycle time	Cycle temperature	Comment
1	3 mins	98˚C	Initial Denaturation
30	30 sec 60 sec 8 mins	98˚C 55˚C 72˚C	Denaturation Annealing Extension
1	15 mins	72˚C	Final extension
	forever	4˚C	Hold

In order to better investigate the role of p53 in NIS gene regulation, each of these promoter constructs were transiently transfected into two different breast cancer cell lines i.e MCF-7 and Zr-75-1. The normalized NIS promoter activity was monitored in presence or absence of p53 activation by doxorubicin treatment. As compared to wild type promoter, the introduction of point mutations disrupting the predicted p53 binding at site 1 and site 3 results in significant augmentation of promoter activity in both the cell lines (1.2-1.8 fold, $p \leq 0.05$) (**Figure 3.7A**). However, mutation at site 2 exhibits heterogeneous response in MCF-7 cells (0.82 fold) and Zr-75-1 cells (1.17 fold). AATT substitution at all three sites in combination, significantly induce NIS promoter activity in both the cell lines (1.4-1.5 fold, $p \leq 0.05$) (**Figure 3.7A**), indicating temporary relief from p53-mediated suppression. A further confirmation of the involvement of p53 in regulating NIS transcriptional activity was provided by treating both the cell lines with doxorubicin. In response to p53 activation, a reduction in luciferase signal is achieved in wild type NIS promoter (0.4-0.5 fold, $p \leq 0.05$) but

not in the site 3 mutated construct alone or in combination with other two sites (1.4-1.7 fold, $p \leq 0.001$) suggesting the importance of p53 binding at this region for transcriptional regulation. On the other hand, AATT substitution at site 1 and 2 reduces promoter activity to ~0.8-0.9 fold post Dox treatment in both the breast cancer cell lines (**Figure 3.7A**).

We also investigated the result of deletion of p53 binding site on NIS gene expression. Deletion of p53 response element at site 3 results in dramatic enhancement of gene expression (1.4-2.6 fold, $p \leq 0.0001$) in the two cell lines (**Figure 3.7B**). Deletion at site 2 has a small effect on luciferase signal (~1.2-1.3 fold) while site 1 deletion exhibits heterogeneous response in both the cell lines studied. When gene expression is checked in response to activated p53, site 3 deletion mutant construct exhibits significant increase in luciferase activity (1.4-1.7 fold, $p \leq 0.0001$) in contrast to wild type promoter; indicating failure of p53-mediated repression at this region (**Figure 3.7B**). In site 1 and 2 mutant constructs, transcriptional repression is observed following Dox treatment in both the cell lines. Surprisingly, deletion at all three sites in combination displays a non-significant change in promoter activity that remains unaltered even after doxorubicin treatment especially in MCF-7 cells (**Figure 3.7B**). This observation indicates the presence of other relevant regulatory sites in this region. Altogether, these findings indicate that binding of p53 to the identified putative sites on NIS promoter sequence may be essential for NIS transcriptional regulation.

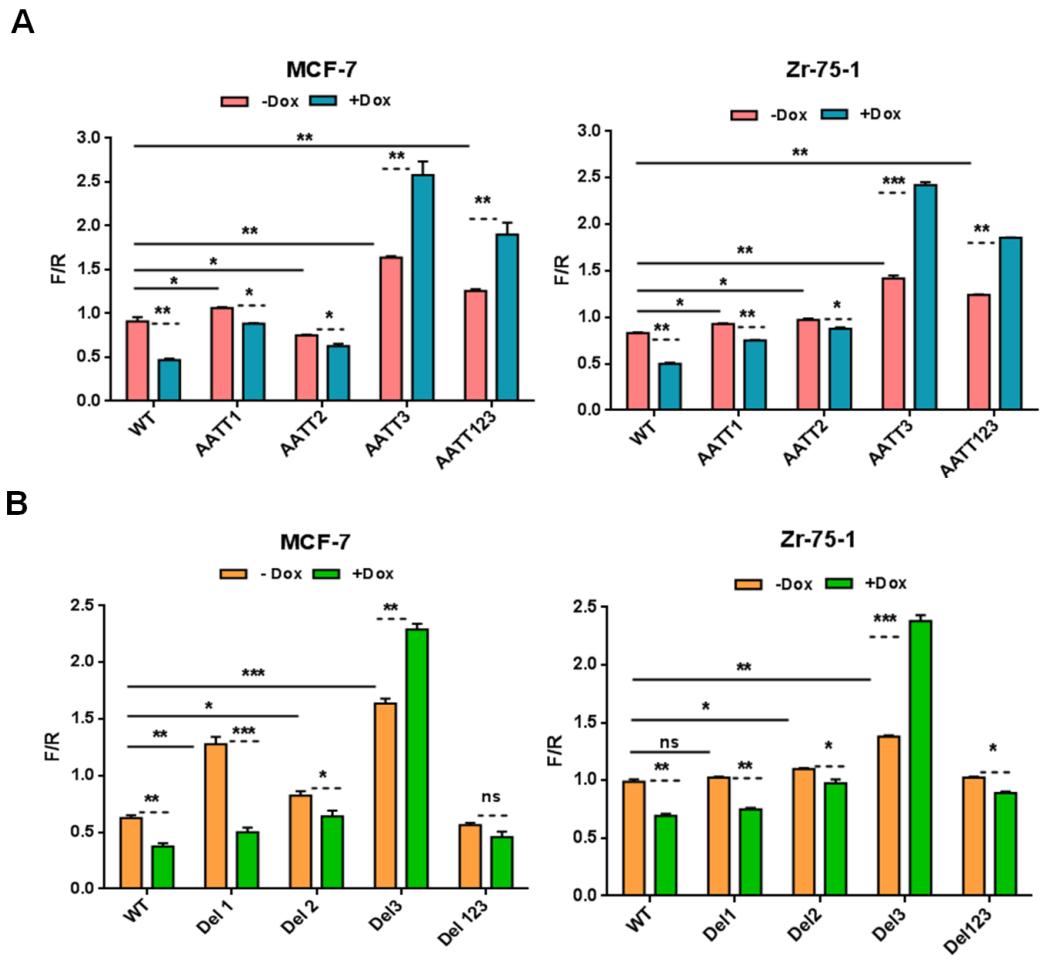

Figure 3.7: Mutations at p53 binding sites result in augmentation of NIS promoter activity. *A. Effect of AATT substitution individually or in combination on NIS promoter activity in MCF-7 and Zr-75-1 cells. The breast cancer cells were transfected with each of these mutant constructs. TK-hRL was used for transfection normalization and luciferase activity was monitored in presence or absence of doxorubicin treatment. B. Effect of deletion of individual or all three p53 binding sites was measured similarly in MCF-7 and Zr-75-1 cells.*

3.3.3: Transcription factor p53 negatively regulates endogenous NIS expression and function in breast cancer cells

Following demonstration of p53 overexpression and activation causing NIS promoter regulation *in vitro* and *in vivo*, next we attempted to check the effect of p53 activation on

endogenous NIS gene expression in various breast cancer cell lines. NIS-specific real-time PCR was performed using TaqMan probe to measure the change in endogenous NIS mRNA content in multiple breast cancer cell lines in response to p53 activation by Dox treatment. We notice that following 24 hours of Dox treatment, NIS mRNA levels lower significantly by 60% in MCF-7 (p=0.001) and 50% in Zr-75-1(p=0.046) cells but non-significant change is observed in MDA-MB-453 cells lacking functional p53 protein (1.46 fold, p=0.121) **(Figure 3.8).** Thus, the results confirm p53-dependent transcriptional repression of NIS in breast cancer cell lines.

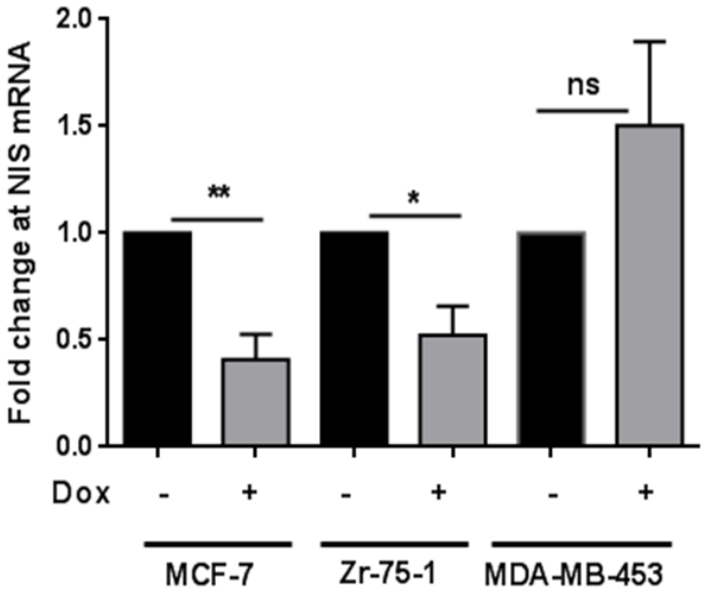

Figure 3.8: Regulation of endogenous NIS expression in BC cell lines. *MCF-7, Zr-75-1 and MDA-MB-453 cells treated with doxorubicin for 24 hours were evaluated for NIS mRNA by real-time PCR using ABI probe. Results were normalized for housekeeping gene GAPDH. * indicates P<0.05, ** indicates P<0.005, ns indicates non-significant.*

Further, to verify whether or not p53 activation alters NIS function, functional analysis was performed as well. Since endogenous levels of NIS protein are low (**Figure 3.9A**) and p53 activation lowers the cellular NIS expression, we tested the effect of p53 on NIS protein

content and its function in MCF-7 cells selected to have NIS overexpression [176] (**Figure 3.9A**). As a result of NIS overexpression at the cell membrane, the difference in NIS protein levels and iodide uptake can be clearly measured by the standard assays as shown in **Figure 3.9A-B**. As anticipated, endogenous p53 activation or exogenous p53 overexpression alone or in combination results in 0.4-0.5 fold reduction in NIS protein content (**Figure 3.9C**) in these cells. The suppression of NIS protein levels does reflect on NIS protein function which was measured by iodide uptake assay. NIS-mediated iodide uptake reduces significantly as a result of p53 overexpression (0.6 fold, p=0.01) or activation (0.7 fold, p=0.02) or combination of both (0.5 fold, p=0.003) in MCF-7 NIS overexpressing cells (**Figure 3.9D**). Together, these findings illustrate that wild type p53 not only exerts transcriptional control but also regulate NIS protein levels and its function in breast cancer cells.

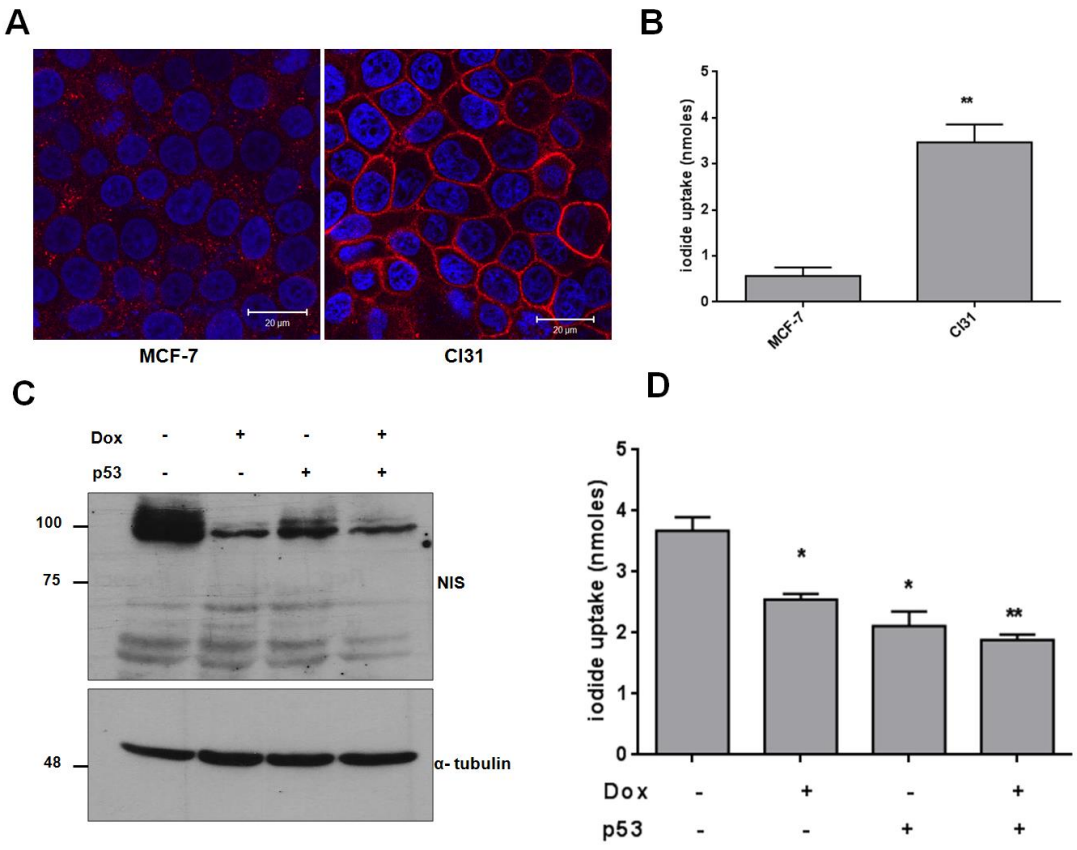

Figure 3.9: Activated p53 modulates NIS expression and function in NIS-overexpressing MCF-7 clonal cells. *A. Immunofluorescence images of MCF-7 and clone 31 showing difference in levels and localization of NIS expression. Scale bar represents 20µm. B. Iodide*

*uptake assay with the MCF-7 plain and membrane clone 31 suggests difference in the amount of iodide uptake according to the level and localization of NIS expression in these clonal cells. C. Western blot showing NIS protein content in MCF-7 clone 31 cells in response to p53 overexpression or activation by doxorubicin treatment. D. Effect of p53 activation on NIS-mediated iodide accumulation in MCF-7 clone 31 cells. The Y axis scale bar represents nanomoles (nmoles) of iodide uptake in cells. Error bars indicate standard error of mean. * indicates P≤0.05, ** indicates P≤0.005.*

3.3.4: Direct recruitment of p53 to NIS promoter to regulate gene expression in breast cancer cell lines

Since NIS promoter activity and its endogenous expression and function are dependent on p53 status, we further verified the possibility of direct binding of p53 to the human NIS promoter DNA. To achieve this, Chromatin immunoprecipitation (ChIP) assay was performed in MCF-7, Zr-75-1 and MDA-MB-453 cells in presence or absence of doxorubicin treatment. **Figure 3.10A-C** shows initial standardization of sonication in MCF-7, Zr-75-1 and MDA-MB-453 cell lines to obtain sheared chromatin fragment of 200-1000 bp size. Further, immunoprecipitation was performed using p53-specific ChIP-grade antibody. Confirmation of immunoprecipitation was done by immunoblotting using p53-specific monoclonal antibody (**Figure 3.10D**).

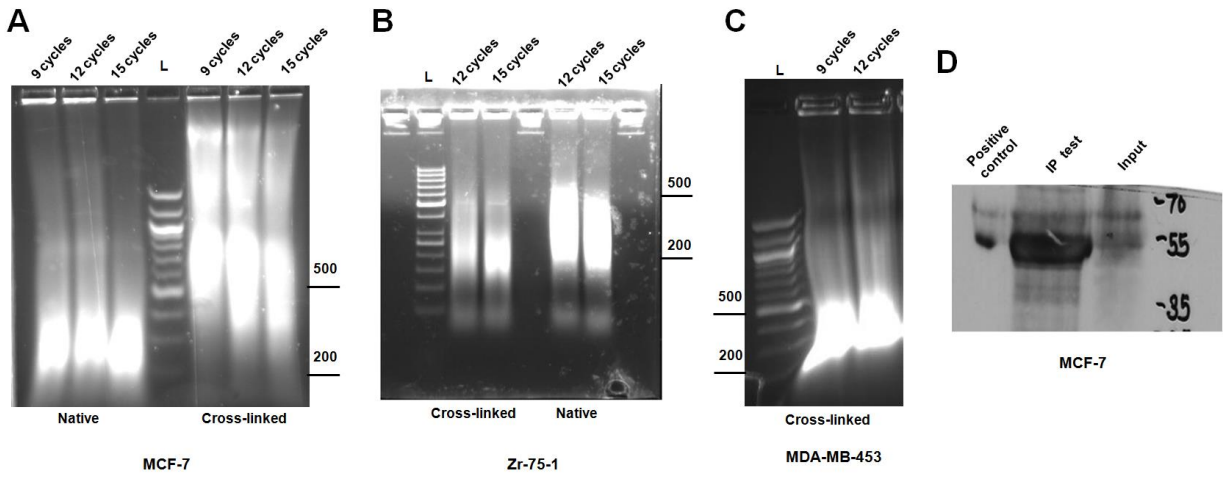

Figure 3.10: Standardization of sonication and immunoprecipitation in MCF-7, Zr-75-1 and MDA-MB-453 cells. *A-C. MCF-7 (A), Zr-75-1 (B) and MDA-MB-453 (C) breast cancer cells cross-linked with 1% formaldehyde were subjected to 9/12/15 cycles of sonication for 60 sec pulses at high power to generate 200–1000 bp DNA fragments. D. Western blot indicating immunoprecipitation by p53-specific monoclonal antibody in MCF-7 cells.*

DNA was isolated from immunoprecipitated DNA-protein complex and used further to check p53 recruitment to NIS promoter by PCR with specific primers. Our results indicate that p53 is bound to 450 bp of NIS promoter region covering all three p53 binding sites (primer set 1, listed in **Table 3.4**) under doxorubicin induced p53 activated state in both MCF-7 and Zr-75-1 cell lines, but not in MDA-MB-453 cells, again establishing functional relevance of active wild type p53 for gene regulation corroborating our earlier findings (**Figure 3.11A-B**). On the other hand, PCR reactions using distant primers (amplifying promoter area devoid of putative p53 DNA binding sites) did not amplify any anti-p53 ChIPed DNA (**Figure 3.11C**), confirming sequence specific binding of p53 to the human NIS promoter. p21 is a known target of p53 and as a validation of immunoprecipitation reaction, binding of p53 to p21 promoter sequence was also verified in Zr-75-1 and MDA-MB-453 cells. As shown in **Figure 3.11D,** p53 binding on p21 promoter is observed which increased further upon Dox

treatment in Zr-75-1 cells. As anticipated, p53 binding to p21 promoter is not observed in MDA-MB-453 cells lacking functional p53 protein.

Table 3.4: Table indicating set of primers used to validate the binding of p53 on the human NIS promoter by PCR

p53 binding specific primers	**Sequence**
Primer I (Spanning all three sites on NIS promoter)	5'-GTGGTAAAGCCAGGTAAGTT-3' Fwd 5'-TTGGGGCTTACGGGAGCAG-3' Rev
Distant primers on NIS promoter	5'-CCTGAGATGACAGCTCGTTGG-3' Fwd 5'-AATGGGACGTGGTAACGAAAGC-3' Rev
p21 promoter binding specific primers	5'-CACCACTGAGCCTTCCTCAC-3' Fwd 5'-CTGACTCCCAGCACACACTC-3' Rev
Site 1 of NIS promoter	5'- GAGTGCTGAAGCAGGCT-3' Fwd 5'- GAAATTGAGGCTCAGAG-3' Rev
Site 2 of NIS promoter	5- CATGGGGATGGAGGGGCATT-3' Fwd 5'- CAGCCCTGGACTGGGA-3' Rev
Site 3 of NIS promoter	5'- GGGCTGAAAGGGTGCG-3' Fwd 5'- GTCGCCTTGGGGCTTACG-3' Rev

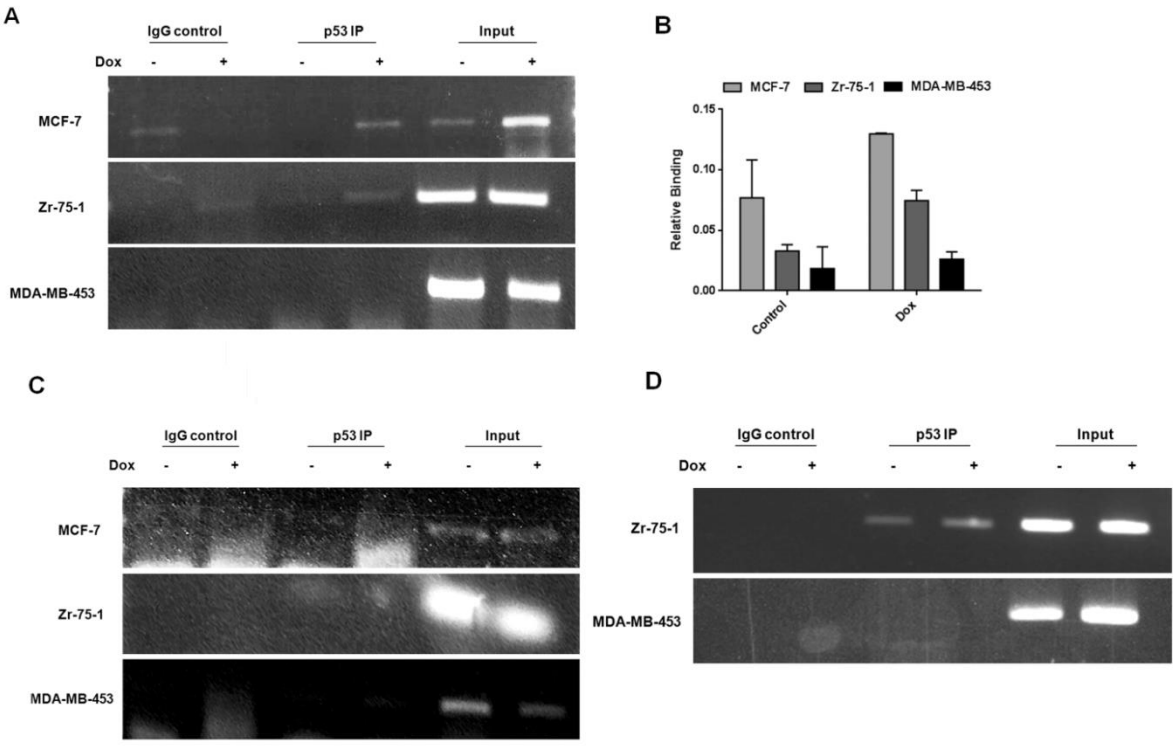

Figure 3.11: NIS transcription is regulated by p53 through its direct recruitment to NIS promoter. *A. Recruitment of p53 onto the 450 bp region (Primer set I) of NIS promoter in MCF-7, Zr-75-1 and MDA-MB-453 cells. Sonicated DNA fragments were pulled with α-p53 antibody and PCR for the 450 bp region was performed in the pulled DNA fragments in the respective panels with and without Doxorubicin treatment. Input represents total sonicated genomic DNA, IP eluate represents the pulled chromatin fraction by p53 antibody and IgG control is the isotype control. B. Chart on right side represents relative binding of p53 to NIS promoter in the presence or absence of doxorubicin in MCF-7, Zr-75-1 and MDA-MB-453 cells. Relative band intensity normalized to input DNA band was calculated and plotted. C. Gel images representing PCR reaction using distant primers in three breast cancer cell lines. D. Gel picture indicating p53 binding to p21 promoter in Zr-75-1 and MDA-MB-453 cells.*

In an attempt to understand which of the site is preferentially occupied by p53, site specific binding was checked using individual p53-binding site specific primers (**Table 3.4**). The **Figure 3.12** represents the real-time PCR quantification of p53 recruitment to site 1, 2 and 3 of the NIS promoter in control and Dox-treated cells. As indicated in **Figure 3.12**, it is observed that out of the three p53 binding sites, site 3 displays low p53 occupancy while site

1 and site 2 have higher occupancy in both the cell lines studied. Overall, the binding of p53 to all three sites increases to various extents (0.3-11 fold) further upon doxorubicin treatment (**Figure 3.12**).

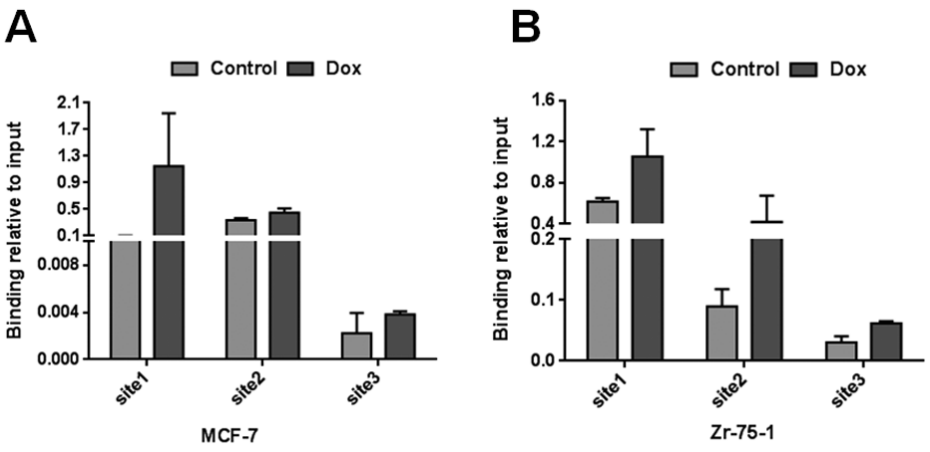

Figure 3.12: Site specific binding of p53 to human NIS promoter. *A-B. Quantitative estimation of p53binding to NIS promoter at individual site was examined using site specific primers and real time PCR in MCF-7(A) and Zr-75-1 (B) cell lines under control and Dox-treated condition.*

3.4: Discussion

In this Chapter, we investigated the role of transcription factor p53 in NIS gene regulation in breast cancer both as *in vitro* assessment and *in vivo* cell and animal model. The results for the first time reveal that p53 acts as a repressor of NIS expression in breast cancer. In a recent report, NIS has been reported as a direct target of p53 family members in liver cancer cells and its expression is augmented in response to DNA damage resulting in differential recruitment of p53 family members including p63 and p73 in liver cancer cells [212]. In contrast, we observed p53 as a repressor of NIS expression. The observed differences in NIS gene regulation by p53 in liver or breast cancer cells may be due to the complexity of the p53 family, that includes a large number of isoforms like p63, p73 etc. that can exert opposite

transcriptional effects in different cells of different origin or states [213]. NIS gene regulation also differs significantly in different cells based on their tissue origin [78, 154]. Further, the overall p53 functional outcome depends upon its extensive post-translational modifications [214, 215], binding partners and co-operativity [215, 216], basal transcription machinery [217] and genomic binding sites [15, 218, 219]. Adding to this complexity, the family members such as p63 and p73 [220] and the isoforms expression patterns in the family [221, 222] have a major impact on the p53 properties. In our study, we could not consider the role of other p53 isoforms and breast cancer relevant p53 mutational status. Thus, how NIS is regulated in normal and cancer cells other than liver or breast tissue and the role of p53 isoforms or its mutational status affecting the gene regulation remains to be explored in future. It will be also be interesting to study the role of p53 family members (like p63 and p73) and know their role in relation to human NIS expression in BC patients representing different subtypes.

Bioinformatics analysis of full length human NIS promoter has listed around 64 different potential transcriptional regulators (summarized in **Table 3.1**). These include TTF-1/Nkx2.1, Pax8 etc. that are known to have regulatory role in thyroid, while TFs such as CREB, AP1, Sp1, RXR, Stat family proteins are present ubiquitously in various tissues. Importantly, multiple p53 response elements are also found present on NIS promoter sequence indicating p53 may have a major role in regulating NIS gene expression. p53 mutations are frequently present (25%) in BC [210] and about 80% of the TNBC cases with mutant p53 have poor prognosis [187]. Inflammatory breast cancer (IBC) is a distinct clinical subtype of locally advanced breast cancer (LABC), with a particularly aggressive behaviour and poor prognosis [223] and frequent p53 mutations (50%) [224, 225]. On the other hand, as discussed earlier, aberrant NIS expression is also found in more than 70% of the BC patients. With this perspective, we hypothesized that p53 status in breast cancer cell may have profound impact on observed NIS expression and subsequently it's function in terms of its iodine pumping ability in the cells.

Our results show that wild type p53 acts as a transcriptional repressor of NIS promoter in breast cancer cells (summarized in **Figure 3.13**). We have evaluated NIS promoter modulation by activated p53 in response to chemotherapeutic drug doxorubicin in breast cancer cells and tumor xenograft model. We have further evidenced these observations by disrupting the DNA binding sites of p53 on the NIS promoter sequence by mutagenesis. Abolishment of p53 binding sequence by sequential or combinatorial substitution or deletion; particularly at site 3, results in remarkable induction in the NIS transcription (measured by promoter activity) that shows further increment upon Dox treatment; in contrast to wild type promoter, indicating temporary release from p53-mediated repression. Whereas, mutation at site 1/2 also exhibits elevated gene expression but why Dox mediated p53 activation still displays gene repression remains to be studied further. This observation implies the presence of other relevant regulatory sites at this region of NIS promoter. It is to be remembered that p53 binding site 3 is still intact in site1/2 mutant construct, partially explaining for the observed gene repression. Further, careful analysis NIS promoter sequence displays overlapping transcription factor binding sites for RXR, Zn finger TF and octamer binding protein at site 1 while Pax4, Smad family and GATA binding sites at site 2 along with p53 binding site. Disruption of p53 binding sequence at site 1/2 also results in interruption of putative binding of these TFs to the NIS promoter. So altogether, role of p53 interacting proteins, the co-operative binding of set of transcription factors on NIS promoter or exogenous transcription factor binding sites created during the mutagenesis need to be considered to explain the experimental results.

In our study, changes in the NIS transcript has also reflected on cellular content of the protein and further at the functional level as NIS-mediated iodide uptake substantially dropped following p53 activation in BC cells. However, the exact mechanism of this gene regulation is not entirely known. There are mainly following possible mechanisms to explain p53-

mediated repression [226]. Transcriptional repression can occur through steric interference with the functions of transcriptional activators by the binding of p53 protein to the transcription factor itself or by the direct binding of p53 protein to the target gene promoter DNA. Alternatively, repression can be brought about by p53-mediated recruitment of transcriptional repressors like histone deacetylases (HDACs) [226]. Earlier results of mutagenesis experiment imply the probability of p53 binding to the NIS-promoter. Further, ChIP analysis indicates direct basal binding of p53 to human NIS promoter at sequence specific region and binding increases further upon doxorubicin treatment specifically in p53 wild type cells, confirming the importance of wild type p53 for gene regulation. This observation provides us the mechanistic evidence of NIS gene regulation by p53 in breast cancer cell lines. It is generally assumed that p53 binds co-operatively along with set of cis-interacting proteins/cofactors in a master regulatory network to exert gene regulation. In future, synergistic interaction of p53 with additional members of the NIS-regulating transcriptional complex can be studied in detail. Data of site-specific p53 binding indicates highest recruitment of p53 to site 2 in MCF-7 cells and to site 1 in Zr-75-1 cells. The occupancy of p53 is lowest at site 3 in both the cell lines. This may be partially explained due to differences in p53-response elements (RE), the affinity of p53 to individual binding site etc [15, 227]. If the p53 response elements of these sites are compared, site 1 and 2 are present as a complete p53 binding site, while site 3 is a half-p53 binding site. The presence of CATG sequence in p53 RE, indicates higher binding affinity of p53 [15]. This sequence is present at the second half site of site 1 of NIS promoter. So higher p53 binding at site 1 can be expected. In response to p53 activation, its binding to site 3 increases to around 2 fold in both the cells while differential induction in binding at site 1 and 2 is observed in MCF-7 and Zr-75-1 cells. The reason for differential recruitment of p53 in two cell lines is not clear and can be studied further. The assembly of p53 with other

transcriptional activators or co-repressors may also affect its differential recruitment to individual sites that needs to be understood in future.

Another aspect of our study is that NIS promoter modulation has been demonstrated by non-invasive bioluminescence imaging in live cells and tumor xenograft model (**Figure 3.13**). Non-invasive molecular imaging of living animals with reporter genes has opened up new avenues to understand fundamental molecular pathways in modern biomedicine [126]. A variety of reporter genes have been developed for Optical, Magnetic Resonance and Radionuclide imaging techniques to study specific biological processes and monitor disease progression and therapy [228-231]. Modality specific reporter genes when used in combination add extra advantage of generating superior information with higher sensitivity, resolution and tomography. Multimodality imaging vectors generated by 'fusion gene' approach are most suitable for visualizing molecular events from both live cells and living organisms. Using Fluc2 as a reporter gene in our study, the modulation of NIS promoter is monitored in breast cancer cells. The findings are in accordance with the data obtained from cell lysates. Also, from *in vivo* mice imaging experiment, 50% reduction in luminescence is observed as a measure of NIS promoter activity following doxorubicin treatment validating our *in vitro* findings. Earlier, it has been shown that optical imaging with the multimodality fusion reporter genes can be used to monitor gene expression changes *in vivo* [232]. Engineered pNIS-Fluc2.TurboFP bimodal fusion reporter sensor used in the study can be used further to extend the screen of the various novel transcriptional regulators of NIS expression in relevant cancer model.

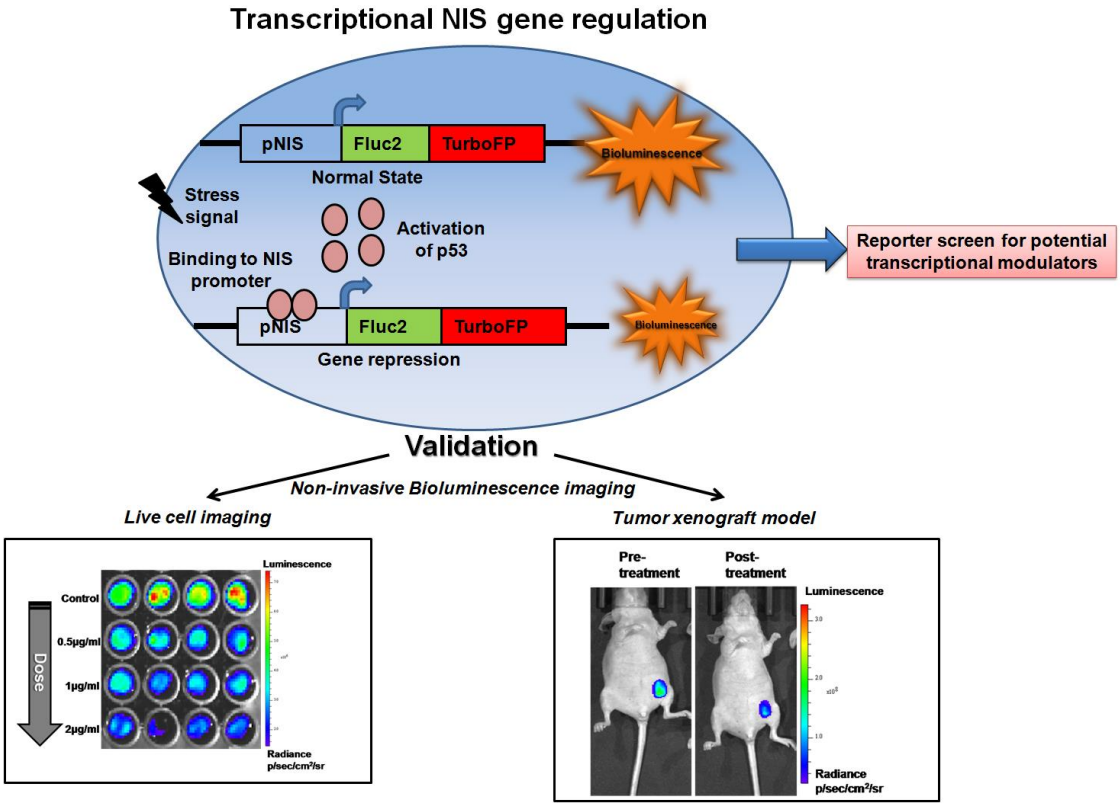

Figure 3.13: Schematic illustrating NIS gene regulation by transcription factor p53 in breast cancer model. *In the experimental model developed, NIS promoter driving bifusion reporter was used to monitor NIS transcription in vitro and in vivo, in response to doxorubicin induced activated p53 using non-invasive optical imaging techniques. The same sensor can be used further to screen for potential transcriptional regulators of NIS gene expression.*

p53 protein is a critical tumor suppressor protein in cancer biology and mutation or changes in expression is an almost universal feature of human cancer cells leading to the altered regulation of hundreds of genes that are directly influenced by this sequence-specific transcription factor [233]. Many functions have been attributed to p53, including direct roles in repair and recombination, association with proteins involved in genome stability and chromatin modification [234]. However, beyond the indisputable importance of p53 as a tumor suppressor, its broadest cellular effect is that of a transcription factor (TF) [218]. In its role as a master regulator of thousands of genes, diverse biological activities like cell cycle regulation,

apoptosis, senescence, energy metabolism, angiogenesis [235, 236], immune response [237], cell differentiation, motility and migration [238-240] and cell–cell communication [241] are precisely controlled. Interestingly, we are discovering NIS which is a membrane transporter, as a direct target of p53 in breast cancer in our study. NIS, also known as SLC5A5, is expressed exclusively in gestation and lactation in breast tissue in contrast to its constitutive expression in the thyroid. However, its aberrant expression is observed in fibroadenoma and breast malignancies [83, 242, 243]. In the process of normal to benign to malignant carcinoma transition, NIS deregulation (mainly by negative regulators) may be leading to unusual NIS expression that remains to be elucidated. Further, in majority of the breast malignancies, NIS expression is found pre-dominantly cytoplasmic. In the intracellular compartment, NIS may be having a biological function other than ion transport which is not known at present. According to a report by Lacoste et al., NIS expression leads to enhanced cell migration and invasion without involving ion transport. It is also observed that these functions are mediated by binding of NIS to the leukemia associated RhoA guanine exchange factor that activates small GTPase RhoA [244]. A number of solute carrier (SLC) proteins are subject to changes in expression and activity during carcinogenesis. The members of solute-linked carrier family 5 (SLC5) mediate the secondary active transport of nutrients and ions. Modifications to their transport activities have been associated with carcinogenesis [245]. Whether these changes play a role in carcinogenesis is unclear, except for some nutrients and ion carriers whose deregulation ensures the necessary reprogramming of energy metabolism in cancer cells. It is reported that p53 is a master regulator for several metabolic genes, including glucose transporters 1 and 4 (GLUT1 and GLUT4) [246]. Tumorigenesis is characterized by an increase in glucose metabolism and consequently glucose uptake. Thus, the GLUTs that mediate glucose uptake in eukaryotic cells are potential candidates for regulation by tumor suppressors like p53. In a report by Wei et al., SLC4A10 which is a member of solute carrier

family; is shown as a direct target of p53 implicating novel aspects of p53 functions although the exact functional regulation was unidentified [247]. In view of this information, the functional relevance of NIS gene regulation by tumor suppressor p53 is still undisclosed and can be explored in future.

Since its discovery in 1979, p53 has become the focus of intensive cancer-based research around the world. Despite the intensive p53-based therapeutic research, reality dictates the significant challenges and unresolved issues needed to be addressed before p53-targeted therapies find clinical application. As mentioned earlier, triple negative breast cancer (TNBC or hormone and Her2 receptor negative tumor subtype) patients display more aggressive tumors with frequent p53 gene mutations, leading to worst prognosis and are in high demand of targeted and systemic therapy options [187]. In our study, we found that wild type p53 acts as a negative transcriptional regulator of NIS gene and thus may reduce the NIS protein content in such cases diminishing the chance of applying radioiodine therapy in them. Once such relativity is established by analyzing clinical cases, inhibiting wild type p53 may allow induction of NIS expression for therapeutic intervention in BC patients. However, from a clinical point of view, p53 is a challenging target for drug discovery. p53 does not offer the accessibility of a receptor-ligand interaction or an enzyme active site. Rather, it involves complicated protein-protein interactions of this tetrameric transcription factor regulating numerous downstream effectors. Since p53 acts as a guardian of the genome and protects normal cells and tissues, use of wild type 53 inhibitors is not a practical approach [17, 18]. Instead, the development of tumor p53 biomarker profile could provide the most appropriate application of this targeted gene therapy in breast cancer patients. A group of patients with mutant p53 status, specifically those mutations which prevents DNA binding activity of p53, would relay to high NIS expression. Hopefully, higher NIS content in p53 mutant cancer cell may provide higher chance of successful radioiodide therapy.

In summary, to best of our knowledge, this is the first study reporting human NIS as a direct target of the transcription factor p53 in breast cancer. By combining luciferase reporter assays, SDM data, endogenous NIS expression, functional analysis and chromatin immunoprecipitation, we prove that human NIS expression and function is inhibited by activated p53 in breast cancer. Our study opens up a scope for extending NIS-based radioiodide therapy in breast cancer patients exhibiting mutant p53 and aberrant NIS expression in clinic.

Summary and Future directions

The global burden of BC is continuously rising and currently, it is the 2nd most frequent cancer worldwide [150]. Although the disease is managed effectively with the advent of targeted therapies especially for ER and HER2 positive tumors, a few challenges still persist. Recurrence of the disease primarily due to dormant micrometastases and development of resistance to all systemic therapies pose serious challenges to overall therapeutic success [151, 152]. Therefore, development of effective targeted therapies eradicating BC cells specifically with lower off target effect, for better management of the disease is highly desired. In this regard, human sodium iodide symporter has drawn significant attention in recent years. NIS is an iodide transporter protein, primarily operating at the basolateral membrane of thyrocytes for thyroid hormone synthesis. NIS-mediated targeted radioablation of well differentiated thyroid cancers is being practiced in the clinic for several decades. Evidences of aberrant expression of NIS protein in breast malignancies in contrast to normal breast tissue raise the hope of possible utilization of NIS-mediated targeted radioiodide therapy for this disease management [8, 77]. However, the major hurdle in adapting this protocol for breast disease is the lack of iodide organification in non-lactating breast cancer cells. Further, clinical analysis has shown that of majority of NIS-positive breast tumors, only 15-20% cases have shown detectable radionuclide uptake by imaging, representing a major obstacle in realization of this targeted therapy in BC [4, 5]. Thereafter, major efforts are focused on modulating NIS expression to improve radioiodide uptake in BC cells.

During this study, we focused on understanding NIS gene regulatory mechanisms to find better prospects on impacting NIS-mediated radioiodine therapy in breast cancer. Specifically, two different approaches were used to achieve this goal-

1. Effect of pharmacological modulators on NIS expression
2. Role of genetic regulators in transcriptional modulation of NIS gene

To investigate the effect of pharmacological modulators, six different HDACi of varying specificity were tested in four different BC cell lines representing two major BC subtypes. Of the HDACi tested, candidate drugs like NaB, VPA, CI994, and SAHA exhibited promising induction in promoter transcription resulting in marked increment of NIS transcript and protein content. Augmented NIS protein levels further resulted into significant improvement of radioiodine uptake and radioablation verified in three different BC cell lines, signifying functional relevance. HDACi drug treatment significantly increased NIS protein levels without altering its localization. In majority of BC cells, the NIS protein is localized at the cytoplasm (similar to clinical observations made [77]) and HDACi pre-treatment elevated the protein pool of cellular NIS, improving radioablation effect of cells. Presence of NIS protein at the cell membrane can of course deliver better therapeutic efficacy. In future, identification of potential agents/signaling pathways targeting NIS protein from cytoplasm to the cell membrane can improve the functional outcome. Further, to explore biochemical basis of HDACi mediated NIS regulation, TF activation array and promoter binding TF array were performed for 96 candidates. The analysis revealed activation and binding of TFs like Stat4, CREB, Nkx3.2, AP1 etc. to NIS promoter in response to HDAC inhibition, implying the possible roles of these TFs in NIS transcriptional regulation. Remarkably, based on TF array findings and *in silico* analysis of the NIS promoter sequence, the data obtained first time indicated that Stat4, Sox9 and GATA tend to have potential role in NIS regulation in BC. The exact comprehensive role of these TFs can be studied further. When few of these HDACi drugs were tested in thyroid cancer lines, it was found that CI994, a benzamide HDACi compound, brings about differential NIS induction in breast and thyroid cancer cell lines. The involvement of tissue specific transcription factors/signaling mechanism can be speculated for differential NIS regulation observed between breast and thyroid cancer cells.

Further, to replicate *in vitro* findings in intact physiological context, tumor xenograft was generated in nude mice using Zr-75-1 cells. IHC analysis demonstrated increased NIS protein expression after VPA treatment in tumor xenografts. ^{131}I therapeutic potential *in vivo* was further tested, where ^{131}I radioablative treatment efficacy was monitored by non-invasive bioluminescence imaging using Zr-75-1 cells overexpressing luciferase reporter (Fluc2.tdTomato fusion). The accumulation of radioactive iodine (^{131}I) in tumor and thyroid was analyzed by non-invasive Cerenkov luminescence imaging. A significant reduction in thyroidal iodine uptake was seen after blocking thyroid with T4 and methimazole. This suggests prevention of damage to the healthy tissues by increasing radioiodine accumulation specifically in the tumor bed. As an effect, reduced bioluminescence signal was observed in VPA pre-treated tumor tissue indicating higher radioablative effect when compared to VPA or ^{131}I treatment groups alone. These results confirm that, HDACi pretreatment strategy to enhance NIS expression and ^{131}I therapeutic efficacy as a promising approach and may be attempted for clinical trial in near future.

Regarding transcriptional control of the NIS protein, our results revealed novel findings presenting experimental evidences of activated wild type p53 protein acting as a transcriptional repressor of functional NIS expression in breast cancer. Three p53 response elements were identified on human NIS promoter by *in silico* analysis. NIS promoter activity was found significantly compromised in response to activation of endogenous p53 by doxorubicin treatment or exogenous overexpression of wild type p53 in BC cells expressing NIS promoter driven reporter sensor. Further, when p53 response elements on NIS promoter were mutated, significant increase in NIS transcriptional activity was observed, confirming repressive role of p53. NIS gene repression by activated p53 was also checked *in vivo* in mouse model. Marked attenuation of NIS promoter by activated p53 was evident from decreased bioluminescence signal from the Dox treated group as compared to the control

group, corroborating our *in vitro* results. Similarly, endogenous NIS protein content also reduced greatly, impacting NIS-mediated iodide uptake significantly in response to p53 activation or overexpression in BC cell. Direct binding of p53 to the human NIS promoter was observed by chromatin immunoprecipitation analysis in multiple BC cell lines and binding increased further in response to p53 activation, confirming its role in gene regulation. It is generally known that p53 binds co-operatively along with set of cis-interacting cofactors in a master regulatory network to exert gene regulation. Synergistic interaction of p53 with additional members of the NIS-regulating transcriptional complex can be tested in future. The p53 isoforms such as p63 and p73 can influence p53-mediated transactivation of target genes [248]. So the role of p53 family members i.e. p63 and p73 can be tested further in NIS gene regulation in BC. It will be very interesting to study the association between human NIS and p53 protein in breast cancer patients representing multiple subtypes. Especially, TNBC patients lacking ER, PR and HER2 receptor expression, display more aggressive forms of the disease with frequent p53 mutations and are in high demand of a targeted and systemic therapy options [187]. These patients with mutant p53 may actually present higher NIS protein expression and thus may help in achieving better therapy response from this target protein.

Bibliography

1. Spitzweg, C., Harrington, K.J., Pinke, L.A., Vile, R.G. & Morris, J.C. Clinical review 132: The sodium iodide symporter and its potential role in cancer therapy. *J Clin Endocrinol Metab* **86**, 3327-35 (2001).
2. Cho, J.Y. et al. Hormonal regulation of radioiodide uptake activity and Na+/I- symporter expression in mammary glands. *J Clin Endocrinol Metab* **85**, 2936-43 (2000).
3. Tazebay, U.H. et al. The mammary gland iodide transporter is expressed during lactation and in breast cancer. *Nat Med* **6**, 871-8 (2000).
4. Wapnir, I.L. et al. The Na+/I- symporter mediates iodide uptake in breast cancer metastases and can be selectively down-regulated in the thyroid. *Clin Cancer Res* **10**, 4294-302 (2004).
5. Moon, D.H. et al. Correlation between 99mTc-pertechnetate uptakes and expressions of human sodium iodide symporter gene in breast tumor tissues. *Nucl Med Biol* **28**, 829-34 (2001).
6. Upadhyay, G. et al. Functional expression of sodium iodide symporter (NIS) in human breast cancer tissue. *Breast Cancer Res Treat* **77**, 157-65 (2003).
7. Renier, C., Vogel, H., Offor, O., Yao, C. & Wapnir, I. Breast cancer brain metastases express the sodium iodide symporter. *J Neurooncol* **96**, 331-6 (2010).
8. Chatterjee, S. et al. Quantitative immunohistochemical analysis reveals association between sodium iodide symporter and estrogen receptor expression in breast cancer. *PLoS One* **8**, e54055 (2013).
9. Unterholzner, S. et al. Dexamethasone stimulation of retinoic Acid-induced sodium iodide symporter expression and cytotoxicity of 131-I in breast cancer cells. *J Clin Endocrinol Metab* **91**, 69-78 (2006).
10. Kogai, T. & Brent, G.A. The sodium iodide symporter (NIS): regulation and approaches to targeting for cancer therapeutics. *Pharmacol Ther* **135**, 355-70 (2012).
11. Willhauck, M.J., DJ, O.K., Wunderlich, N., Goke, B. & Spitzweg, C. Stimulation of retinoic acid-induced functional sodium iodide symporter (NIS) expression and cytotoxicity of (1)(3)(1)I by carbamazepine in breast cancer cells. *Breast Cancer Res Treat* **125**, 377-86 (2011).
12. Dentice, M. et al. Transcription factor Nkx-2.5 induces sodium/iodide symporter gene expression and participates in retinoic acid- and lactation-induced transcription in mammary cells. *Mol Cell Biol* **24**, 7863-77 (2004).
13. Puppin, C. et al. Cooperative effects of SAHA and VPA on NIS gene expression and proliferation of thyroid cancer cells. *J Mol Endocrinol* **48**, 217-227 (2012).
14. Baldan, F. et al. Histone post-translational modifications induced by histone deacetylase inhibition in transcriptional control units of NIS gene. *Mol Biol Rep* **41**, 5257-65 (2014).
15. Wang, B., Xiao, Z. & Ren, E.C. Redefining the p53 response element. *Proc Natl Acad Sci U S A* **106**, 14373-8 (2009).
16. Briat, A. & Vassaux, G. A new transgenic mouse line to image chemically induced p53 activation in vivo. *Cancer Sci* **99**, 683-8 (2008).
17. Bouchet, B.P., Caron de Fromentel, C., Puisieux, A. & Galmarini, C.M. p53 as a target for anti-cancer drug development. *Crit Rev Oncol Hematol* **58**, 190-207 (2006).
18. Fuster, J.J., Sanz-Gonzalez, S.M., Moll, U.M. & Andres, V. Classic and novel roles of p53: prospects for anticancer therapy. *Trends Mol Med* **13**, 192-9 (2007).
19. Dimri, G., Band, H. & Band, V. Mammary epithelial cell transformation: insights from cell culture and mouse models. *Breast Cancer Res* **7**, 171-9 (2005).
20. Lithgow, D. & Covington, C. Chronic inflammation and breast pathology: a theoretical model. *Biol Res Nurs* **7**, 118-29 (2005).
21. Ferlay, J. et al. Estimates of worldwide burden of cancer in 2008: GLOBOCAN 2008. *Int J Cancer* **127**, 2893-917 (2010).
22. Murthy, N.S., Chaudhry, K., Nadayil, D., Agarwal, U.K. & Saxena, S. Changing trends in incidence of breast cancer: Indian scenario. *Indian J Cancer* **46**, 73-4 (2009).

23. Dinshaw, K.A. et al. Safety and feasibility of breast conserving therapy in Indian women: two decades of experience at Tata Memorial Hospital. *J Surg Oncol* **94**, 105-13 (2006).
24. Agarwal, G., Pradeep, P.V., Aggarwal, V., Yip, C.H. & Cheung, P.S. Spectrum of breast cancer in Asian women. *World J Surg* **31**, 1031-40 (2007).
25. Mathew, A., Pandey, M. & Rajan, B. Do younger women with non-metastatic and non-inflammatory breast carcinoma have poor prognosis? *World J Surg Oncol* **2**, 2 (2004).
26. Shavers, V.L., Harlan, L.C. & Stevens, J.L. Racial/ethnic variation in clinical presentation, treatment, and survival among breast cancer patients under age 35. *Cancer* **97**, 134-47 (2003).
27. Sainsbury, J.R., Anderson, T.J. & Morgan, D.A. ABC of breast diseases: breast cancer. *BMJ* **321**, 745-50 (2000).
28. Henson, D.E., Ries, L., Freedman, L.S. & Carriaga, M. Relationship among outcome, stage of disease, and histologic grade for 22,616 cases of breast cancer. The basis for a prognostic index. *Cancer* **68**, 2142-9 (1991).
29. Ross, J.S. et al. Breast cancer biomarkers and molecular medicine. *Expert Rev Mol Diagn* **3**, 573-85 (2003).
30. Sotiriou, C. & Pusztai, L. Gene-expression signatures in breast cancer. *N Engl J Med* **360**, 790-800 (2009).
31. Perou, C.M. et al. Molecular portraits of human breast tumours. *Nature* **406**, 747-52 (2000).
32. Sorlie, T. et al. Gene expression patterns of breast carcinomas distinguish tumor subclasses with clinical implications. *Proc Natl Acad Sci U S A* **98**, 10869-74 (2001).
33. Sorlie, T. et al. Repeated observation of breast tumor subtypes in independent gene expression data sets. *Proc Natl Acad Sci U S A* **100**, 8418-23 (2003).
34. Rakha, E.A., El-Sayed, M.E., Reis-Filho, J.S. & Ellis, I.O. Expression profiling technology: its contribution to our understanding of breast cancer. *Histopathology* **52**, 67-81 (2008).
35. Parker, J.S. et al. Supervised risk predictor of breast cancer based on intrinsic subtypes. *J Clin Oncol* **27**, 1160-7 (2009).
36. Foulkes, W.D. et al. Germline BRCA1 mutations and a basal epithelial phenotype in breast cancer. *J Natl Cancer Inst* **95**, 1482-5 (2003).
37. Atchley, D.P. et al. Clinical and pathologic characteristics of patients with BRCA-positive and BRCA-negative breast cancer. *J Clin Oncol* **26**, 4282-8 (2008).
38. Veronesi, U. et al. Twenty-year follow-up of a randomized study comparing breast-conserving surgery with radical mastectomy for early breast cancer. *N Engl J Med* **347**, 1227-32 (2002).
39. Fisher, B. et al. Twenty-year follow-up of a randomized trial comparing total mastectomy, lumpectomy, and lumpectomy plus irradiation for the treatment of invasive breast cancer. *N Engl J Med* **347**, 1233-41 (2002).
40. van Dongen, J.A. et al. Long-term results of a randomized trial comparing breast-conserving therapy with mastectomy: European Organization for Research and Treatment of Cancer 10801 trial. *J Natl Cancer Inst* **92**, 1143-50 (2000).
41. Clarke, M. et al. Effects of radiotherapy and of differences in the extent of surgery for early breast cancer on local recurrence and 15-year survival: an overview of the randomised trials. *Lancet* **366**, 2087-106 (2005).
42. Nielsen, H.M., Overgaard, M., Grau, C., Jensen, A.R. & Overgaard, J. Study of failure pattern among high-risk breast cancer patients with or without postmastectomy radiotherapy in addition to adjuvant systemic therapy: long-term results from the Danish Breast Cancer Cooperative Group DBCG 82 b and c randomized studies. *J Clin Oncol* **24**, 2268-75 (2006).
43. Ragaz, J. et al. Locoregional radiation therapy in patients with high-risk breast cancer receiving adjuvant chemotherapy: 20-year results of the British Columbia randomized trial. *J Natl Cancer Inst* **97**, 116-26 (2005).

44. Tamoxifen for early breast cancer: an overview of the randomised trials. Early Breast Cancer Trialists' Collaborative Group. *Lancet* **351**, 1451-67 (1998).
45. Narod, S.A. et al. Tamoxifen and risk of contralateral breast cancer in BRCA1 and BRCA2 mutation carriers: a case-control study. Hereditary Breast Cancer Clinical Study Group. *Lancet* **356**, 1876-81 (2000).
46. Effects of chemotherapy and hormonal therapy for early breast cancer on recurrence and 15-year survival: an overview of the randomised trials. *Lancet* **365**, 1687-717 (2005).
47. Goss, P.E. et al. A randomized trial of letrozole in postmenopausal women after five years of tamoxifen therapy for early-stage breast cancer. *N Engl J Med* **349**, 1793-802 (2003).
48. Coombes, R.C. et al. A randomized trial of exemestane after two to three years of tamoxifen therapy in postmenopausal women with primary breast cancer. *N Engl J Med* **350**, 1081-92 (2004).
49. Slamon, D.J. et al. Use of chemotherapy plus a monoclonal antibody against HER2 for metastatic breast cancer that overexpresses HER2. *N Engl J Med* **344**, 783-92 (2001).
50. Bryant, J. & Geyer, C.E. Trastuzumab for early breast cancer. *Lancet* **367**, 728 (2006).
51. Geyer, C.E. et al. Lapatinib plus capecitabine for HER2-positive advanced breast cancer. *N Engl J Med* **355**, 2733-43 (2006).
52. Alvarez, R.H., Valero, V. & Hortobagyi, G.N. Emerging targeted therapies for breast cancer. *J Clin Oncol* **28**, 3366-79 (2010).
53. Dai, G., Levy, O. & Carrasco, N. Cloning and characterization of the thyroid iodide transporter. *Nature* **379**, 458-60 (1996).
54. Smanik, P.A. et al. Cloning of the human sodium lodide symporter. *Biochem Biophys Res Commun* **226**, 339-45 (1996).
55. Eskandari, S. et al. Thyroid Na+/I- symporter. Mechanism, stoichiometry, and specificity. *J Biol Chem* **272**, 27230-8 (1997).
56. Dohan, O., Baloch, Z., Banrevi, Z., Livolsi, V. & Carrasco, N. Rapid communication: predominant intracellular overexpression of the Na(+)/I(-) symporter (NIS) in a large sampling of thyroid cancer cases. *J Clin Endocrinol Metab* **86**, 2697-700 (2001).
57. Dohan, O. & Carrasco, N. Advances in Na(+)/I(-) symporter (NIS) research in the thyroid and beyond. *Mol Cell Endocrinol* **213**, 59-70 (2003).
58. Wright, E.M. & Turk, E. The sodium/glucose cotransport family SLC5. *Pflugers Arch* **447**, 510-8 (2004).
59. Beyer, S.J., Jimenez, R.E., Shapiro, C.L., Cho, J.Y. & Jhiang, S.M. Do cell surface trafficking impairments account for variable cell surface sodium iodide symporter levels in breast cancer? *Breast Cancer Res Treat* **115**, 205-12 (2009).
60. Levy, O., De la Vieja, A. & Carrasco, N. The Na+/I- symporter (NIS): recent advances. *J Bioenerg Biomembr* **30**, 195-206 (1998).
61. Micali, S. et al. Sodium iodide symporter (NIS) in extrathyroidal malignancies: focus on breast and urological cancer. *BMC Cancer* **14**, 303 (2014).
62. Ahn, B.C., Lee, S.W., Lee, J. & Kim, C. Pulmonary aspergilloma mimicking metastasis from papillary thyroid cancer. *Thyroid* **21**, 555-8 (2011).
63. Capoccetti, F., Biggi, E. & Brianzoni, E. Differentiated thyroid carcinoma: diagnosis and dosimetry using 124I PET/CT. *Clin Transl Imaging*, 185-193 (2013).
64. Sawka, A.M. et al. Clinical review 170: A systematic review and metaanalysis of the effectiveness of radioactive iodine remnant ablation for well-differentiated thyroid cancer. *J Clin Endocrinol Metab* **89**, 3668-76 (2004).
65. Durante, C. et al. Long-term outcome of 444 patients with distant metastases from papillary and follicular thyroid carcinoma: benefits and limits of radioiodine therapy. *J Clin Endocrinol Metab* **91**, 2892-9 (2006).

66. Arturi, F., Russo, D., Giuffrida, D., Schlumberger, M. & Filetti, S. Sodium-iodide symporter (NIS) gene expression in lymph-node metastases of papillary thyroid carcinomas. *Eur J Endocrinol* **143**, 623-7 (2000).
67. Schlumberger, M., Lacroix, L., Russo, D., Filetti, S. & Bidart, J.M. Defects in iodide metabolism in thyroid cancer and implications for the follow-up and treatment of patients. *Nat Clin Pract Endocrinol Metab* **3**, 260-9 (2007).
68. Wartofsky, L. & Van Nostrand, D. Radioiodine treatment of well-differentiated thyroid cancer. *Endocrine* **42**, 506-13 (2012).
69. Mazzaferri, E.L. & Kloos, R.T. Clinical review 128: Current approaches to primary therapy for papillary and follicular thyroid cancer. *J Clin Endocrinol Metab* **86**, 1447-63 (2001).
70. Russo, D., Damante, G., Puxeddu, E., Durante, C. & Filetti, S. Epigenetics of thyroid cancer and novel therapeutic targets. *J Mol Endocrinol* **46**, R73-81 (2011).
71. Smith, V.E. et al. Manipulation of PBF/PTTG1IP phosphorylation status; a potential new therapeutic strategy for improving radioiodine uptake in thyroid and other tumors. *J Clin Endocrinol Metab* **98**, 2876-86 (2013).
72. Dohan, O. et al. The sodium/iodide Symporter (NIS): characterization, regulation, and medical significance. *Endocr Rev* **24**, 48-77 (2003).
73. Bruno, R. et al. Sodium iodide symporter expression and radioiodine distribution in extrathyroidal tissues. *J Endocrinol Invest* **27**, 1010-4 (2004).
74. Carrasco, N. Iodide transport in the thyroid gland. *Biochim Biophys Acta* **1154**, 65-82 (1993).
75. Nurnberger, C.E. & Lipscomb, A. Transmission of radioiodine (I131) to infants through human maternal milk. *J Am Med Assoc* **150**, 1398-1400 (1952).
76. Eskin, B.A., Parker, J.A., Bassett, J.G. & George, D.L. Human breast uptake of radioactive iodine. *Obstet Gynecol* **44**, 398-402 (1974).
77. Wapnir, I.L. et al. Immunohistochemical profile of the sodium/iodide symporter in thyroid, breast, and other carcinomas using high density tissue microarrays and conventional sections. *J Clin Endocrinol Metab* **88**, 1880-8 (2003).
78. Kogai, T. et al. Differential regulation of sodium/iodide symporter gene expression by nuclear receptor ligands in MCF-7 breast cancer cells. *Endocrinology* **146**, 3059-69 (2005).
79. Beyer, S. et al. KT5823 differentially modulates sodium iodide symporter expression, activity, and glycosylation between thyroid and breast cancer cells. *Endocrinology* **152**, 782-92 (2011).
80. Gronemeyer, H. & Laudet, V. Transcription factors 3: nuclear receptors. *Protein Profile* **2**, 1173-308 (1995).
81. Ohno, M., Zannini, M., Levy, O., Carrasco, N. & di Lauro, R. The paired-domain transcription factor Pax8 binds to the upstream enhancer of the rat sodium/iodide symporter gene and participates in both thyroid-specific and cyclic-AMP-dependent transcription. *Mol Cell Biol* **19**, 2051-60 (1999).
82. Kogai, T., Schultz, J.J., Johnson, L.S., Huang, M. & Brent, G.A. Retinoic acid induces sodium/iodide symporter gene expression and radioiodide uptake in the MCF-7 breast cancer cell line. *Proc Natl Acad Sci U S A* **97**, 8519-24 (2000).
83. Ryan, J. et al. The sodium iodide symporter (NIS) and potential regulators in normal, benign and malignant human breast tissue. *PLoS One* **6**, e16023 (2011).
84. Baril, P., Martin-Duque, P. & Vassaux, G. Visualization of gene expression in the live subject using the Na/I symporter as a reporter gene: applications in biotherapy. *Br J Pharmacol* **159**, 761-71 (2010).
85. Spitzweg, C. & Morris, J.C. The sodium iodide symporter: its pathophysiological and therapeutic implications. *Clin Endocrinol (Oxf)* **57**, 559-74 (2002).
86. Jeong, S.Y. et al. Combined Cerenkov luminescence and nuclear imaging of radioiodine in the thyroid gland and thyroid cancer cells expressing sodium iodide symporter: initial feasibility study. *Endocr J* **58**, 575-83 (2011).

87. Johnson, N.A., LeBeau, S.O. & Tublin, M.E. Imaging surveillance of differentiated thyroid cancer. *Radiol Clin North Am* **49**, 473-87, vi (2011).
88. Seidlin, S.M., Marinelli, L.D. & Oshry, E. Radioactive iodine therapy; effect on functioning metastases of adenocarcinoma of the thyroid. *J Am Med Assoc* **132**, 838-47 (1946).
89. Shimura, H., Haraguchi, K., Miyazaki, A., Endo, T. & Onaya, T. Iodide uptake and experimental 131I therapy in transplanted undifferentiated thyroid cancer cells expressing the Na+/I- symporter gene. *Endocrinology* **138**, 4493-6 (1997).
90. Miyagawa, M. et al. Non-invasive imaging of cardiac transgene expression with PET: comparison of the human sodium/iodide symporter gene and HSV1-tk as the reporter gene. *Eur J Nucl Med Mol Imaging* **32**, 1108-14 (2005).
91. Miyagawa, M. et al. Cardiac reporter gene imaging using the human sodium/iodide symporter gene. *Cardiovasc Res* **65**, 195-202 (2005).
92. Terrovitis, J. et al. Ectopic expression of the sodium-iodide symporter enables imaging of transplanted cardiac stem cells in vivo by single-photon emission computed tomography or positron emission tomography. *J Am Coll Cardiol* **52**, 1652-60 (2008).
93. Seo, J.H. et al. Trafficking macrophage migration using reporter gene imaging with human sodium iodide symporter in animal models of inflammation. *J Nucl Med* **51**, 1637-43 (2010).
94. Barton, K.N. et al. Phase I study of noninvasive imaging of adenovirus-mediated gene expression in the human prostate. *Mol Ther* **16**, 1761-9 (2008).
95. Boland, A. et al. Adenovirus-mediated transfer of the thyroid sodium/iodide symporter gene into tumors for a targeted radiotherapy. *Cancer Res* **60**, 3484-92 (2000).
96. Smit, J.W. et al. Reestablishment of in vitro and in vivo iodide uptake by transfection of the human sodium iodide symporter (hNIS) in a hNIS defective human thyroid carcinoma cell line. *Thyroid* **10**, 939-43 (2000).
97. Cho, J.Y. et al. In vivo imaging and radioiodine therapy following sodium iodide symporter gene transfer in animal model of intracerebral gliomas. *Gene Ther* **9**, 1139-45 (2002).
98. Dwyer, R.M. et al. A preclinical large animal model of adenovirus-mediated expression of the sodium-iodide symporter for radioiodide imaging and therapy of locally recurrent prostate cancer. *Mol Ther* **12**, 835-41 (2005).
99. Dutta, S. & De, A. Cancer gene therapy: Prospects of using human sodium iodide symporter gene in non-thyroidal cancer. *Biomedical Research Journal* **2**, 198-219 (2015).
100. Carlin, S., Cunningham, S.H., Boyd, M., McCluskey, A.G. & Mairs, R.J. Experimental targeted radioiodide therapy following transfection of the sodium iodide symporter gene: effect on clonogenicity in both two-and three-dimensional models. *Cancer Gene Ther* **7**, 1529-36 (2000).
101. Schipper, M.L. et al. Radioiodide treatment after sodium iodide symporter gene transfer is a highly effective therapy in neuroendocrine tumor cells. *Cancer Res* **63**, 1333-8 (2003).
102. Mandell, R.B., Mandell, L.Z. & Link, C.J., Jr. Radioisotope concentrator gene therapy using the sodium/iodide symporter gene. *Cancer Res* **59**, 661-8 (1999).
103. Spitzweg, C. et al. Prostate-specific antigen (PSA) promoter-driven androgen-inducible expression of sodium iodide symporter in prostate cancer cell lines. *Cancer Res* **59**, 2136-41 (1999).
104. Spitzweg, C. et al. Treatment of prostate cancer by radioiodine therapy after tissue-specific expression of the sodium iodide symporter. *Cancer Res* **60**, 6526-30 (2000).
105. Spitzweg, C. et al. In vivo sodium iodide symporter gene therapy of prostate cancer. *Gene Ther* **8**, 1524-31 (2001).
106. Dingli, D. et al. Genetically targeted radiotherapy for multiple myeloma. *Blood* **102**, 489-96 (2003).
107. Willhauck, M.J. et al. Alpha-fetoprotein promoter-targeted sodium iodide symporter gene therapy of hepatocellular carcinoma. *Gene Ther* **15**, 214-23 (2008).

108. Dwyer, R.M., Bergert, E.R., O'Connor, M.K., Gendler, S.J. & Morris, J.C. Sodium iodide symporter-mediated radioiodide imaging and therapy of ovarian tumor xenografts in mice. *Gene Ther* **13**, 60-6 (2006).
109. Ghosh, M. et al. Bioluminescent monitoring of NIS-mediated (131)I ablative effects in MCF-7 xenografts. *Mol Imaging* **5**, 76-84 (2006).
110. Renier, C. et al. Regression of experimental NIS-expressing breast cancer brain metastases in response to radioiodide/gemcitabine dual therapy. *Oncotarget* (2016).
111. Klutz, K. et al. Targeted radioiodine therapy of neuroblastoma tumors following systemic nonviral delivery of the sodium iodide symporter gene. *Clin Cancer Res* **15**, 6079-86 (2009).
112. Klutz, K. et al. Epidermal growth factor receptor-targeted (131)I-therapy of liver cancer following systemic delivery of the sodium iodide symporter gene. *Mol Ther* **19**, 676-85 (2011).
113. Knoop, K. et al. Mesenchymal stem cell-mediated, tumor stroma-targeted radioiodine therapy of metastatic colon cancer using the sodium iodide symporter as theranostic gene. *J Nucl Med* **56**, 600-6 (2015).
114. Pichler, B.J., Wehrl, H.F. & Judenhofer, M.S. Latest advances in molecular imaging instrumentation. *J Nucl Med* **49 Suppl 2**, 5S-23S (2008).
115. Ahn, B.C. Applications of molecular imaging in drug discovery and development process. *Curr Pharm Biotechnol* **12**, 459-68 (2011).
116. Chung, J.K. Sodium iodide symporter: its role in nuclear medicine. *J Nucl Med* **43**, 1188-200 (2002).
117. Lippincott-Schwartz, J., Snapp, E. & Kenworthy, A. Studying protein dynamics in living cells. *Nat Rev Mol Cell Biol* **2**, 444-56 (2001).
118. Remington, S.J. Negotiating the speed bumps to fluorescence. *Nat Biotechnol* **20**, 28-9 (2002).
119. Kaneko, K. et al. Detection of peritoneal micrometastases of gastric carcinoma with green fluorescent protein and carcinoembryonic antigen promoter. *Cancer Res* **61**, 5570-4 (2001).
120. Bremer, C., Bredow, S., Mahmood, U., Weissleder, R. & Tung, C.H. Optical imaging of matrix metalloproteinase-2 activity in tumors: feasibility study in a mouse model. *Radiology* **221**, 523-9 (2001).
121. Koyama, Y. et al. Spectral fluorescence molecular imaging of lung metastases targeting HER2/neu. *Clin Cancer Res* **13**, 2936-45 (2007).
122. Hoffman, R.M. Visualization of GFP-expressing tumors and metastasis in vivo. *Biotechniques* **30**, 1016-22, 1024-6 (2001).
123. Spergel, D.J., Kruth, U., Shimshek, D.R., Sprengel, R. & Seeburg, P.H. Using reporter genes to label selected neuronal populations in transgenic mice for gene promoter, anatomical, and physiological studies. *Prog Neurobiol* **63**, 673-86 (2001).
124. Weissleder, R. Scaling down imaging: molecular mapping of cancer in mice. *Nat Rev Cancer* **2**, 11-8 (2002).
125. Lin, Y., Weissleder, R. & Tung, C.H. Novel near-infrared cyanine fluorochromes: synthesis, properties, and bioconjugation. *Bioconjug Chem* **13**, 605-10 (2002).
126. Massoud, T.F. & Gambhir, S.S. Molecular imaging in living subjects: seeing fundamental biological processes in a new light. *Genes Dev* **17**, 545-80 (2003).
127. Alford, R. et al. Toxicity of organic fluorophores used in molecular imaging: literature review. *Mol Imaging* **8**, 341-54 (2009).
128. Nguyen, Q.T. & Tsien, R.Y. Fluorescence-guided surgery with live molecular navigation--a new cutting edge. *Nat Rev Cancer* **13**, 653-62 (2013).
129. Bremer, C., Ntziachristos, V. & Weissleder, R. Optical-based molecular imaging: contrast agents and potential medical applications. *Eur Radiol* **13**, 231-43 (2003).

130. Choy, G., Choyke, P. & Libutti, S.K. Current advances in molecular imaging: noninvasive in vivo bioluminescent and fluorescent optical imaging in cancer research. *Mol Imaging* **2**, 303-12 (2003).
131. Bhaumik, S. & Gambhir, S.S. Optical imaging of Renilla luciferase reporter gene expression in living mice. *Proc Natl Acad Sci U S A* **99**, 377-82 (2002).
132. Shah, K., Tang, Y., Breakefield, X. & Weissleder, R. Real-time imaging of TRAIL-induced apoptosis of glioma tumors in vivo. *Oncogene* **22**, 6865-72 (2003).
133. Branchini, B.R., Southworth, T.L., DeAngelis, J.P., Roda, A. & Michelini, E. Luciferase from the Italian firefly Luciola italica: molecular cloning and expression. *Comp Biochem Physiol B Biochem Mol Biol* **145**, 159-67 (2006).
134. Viviani, V.R. et al. Active-site properties of Phrixotrix railroad worm green and red bioluminescence-eliciting luciferases. *J Biochem* **140**, 467-74 (2006).
135. Caysa, H. et al. A redshifted codon-optimized firefly luciferase is a sensitive reporter for bioluminescence imaging. *Photochem Photobiol Sci* **8**, 52-6 (2009).
136. Branchini, B.R. et al. Thermostable red and green light-producing firefly luciferase mutants for bioluminescent reporter applications. *Anal Biochem* **361**, 253-62 (2007).
137. Ma, N., Marshall, A.F. & Rao, J. Near-infrared light emitting luciferase via biomineralization. *J Am Chem Soc* **132**, 6884-5 (2010).
138. Wu, C. et al. In vivo far-red luminescence imaging of a biomarker based on BRET from Cypridina bioluminescence to an organic dye. *Proc Natl Acad Sci U S A* **106**, 15599-603 (2009).
139. Vooijs, M., Jonkers, J., Lyons, S. & Berns, A. Noninvasive imaging of spontaneous retinoblastoma pathway-dependent tumors in mice. *Cancer Res* **62**, 1862-7 (2002).
140. Thorek, D. et al. Cerenkov imaging - a new modality for molecular imaging. *Am J Nucl Med Mol Imaging* **2**, 163-73 (2012).
141. Robertson, R. et al. Optical imaging of Cerenkov light generation from positron-emitting radiotracers. *Phys Med Biol* **54**, N355-65 (2009).
142. Yang, W. et al. Comparison of Cerenkov luminescence imaging (CLI) and gamma camera imaging for visualization of let-7 expression in lung adenocarcinoma A549 Cells. *Nucl Med Biol* **39**, 948-53 (2012).
143. Holland, J.P., Normand, G., Ruggiero, A., Lewis, J.S. & Grimm, J. Intraoperative imaging of positron emission tomographic radiotracers using Cerenkov luminescence emissions. *Mol Imaging* **10**, 177-86, 1-3 (2011).
144. Berry, D.A. et al. Effect of screening and adjuvant therapy on mortality from breast cancer. *N Engl J Med* **353**, 1784-92 (2005).
145. Onitilo, A.A., Engel, J.M., Greenlee, R.T. & Mukesh, B.N. Breast cancer subtypes based on ER/PR and Her2 expression: comparison of clinicopathologic features and survival. *Clin Med Res* **7**, 4-13 (2009).
146. Koong, S.S. et al. Lithium as a potential adjuvant to 131I therapy of metastatic, well differentiated thyroid carcinoma. *J Clin Endocrinol Metab* **84**, 912-6 (1999).
147. Kogai, T. et al. Systemic retinoic acid treatment induces sodium/iodide symporter expression and radioiodide uptake in mouse breast cancer models. *Cancer Res* **64**, 415-22 (2004).
148. Alotaibi, H., Yaman, E.C., Demirpence, E. & Tazebay, U.H. Unliganded estrogen receptor-alpha activates transcription of the mammary gland Na+/I- symporter gene. *Biochem Biophys Res Commun* **345**, 1487-96 (2006).
149. Fortunati, N. et al. The pan-DAC inhibitor LBH589 is a multi-functional agent in breast cancer cells: cytotoxic drug and inducer of sodium-iodide symporter (NIS). *Breast Cancer Res Treat* **124**, 667-75 (2010).
150. DeSantis, C., Siegel, R., Bandi, P. & Jemal, A. Breast cancer statistics, 2011. *CA Cancer J Clin* **61**, 409-18 (2011).

151. Gonzalez-Angulo, A.M., Morales-Vasquez, F. & Hortobagyi, G.N. Overview of resistance to systemic therapy in patients with breast cancer. *Adv Exp Med Biol* **608**, 1-22 (2007).
152. Cardoso, F. et al. International guidelines for management of metastatic breast cancer: combination vs sequential single-agent chemotherapy. *J Natl Cancer Inst* **101**, 1174-81 (2009).
153. Curtis, C. et al. The genomic and transcriptomic architecture of 2,000 breast tumours reveals novel subgroups. *Nature* **486**, 346-52 (2012).
154. Spitzweg, C. [The sodium-iodide symporter. Pathophysiologic, diagnostic and therapeutic significance]. *Internist (Berl)* **44**, 396-402, 404-8, 410-1 (2003).
155. Tanosaki, S. et al. Effect of ligands of nuclear hormone receptors on sodium/iodide symporter expression and activity in breast cancer cells. *Breast Cancer Res Treat* **79**, 335-45 (2003).
156. Arturi, F. et al. Regulation of iodide uptake and sodium/iodide symporter expression in the mcf-7 human breast cancer cell line. *J Clin Endocrinol Metab* **90**, 2321-6 (2005).
157. Conley, B.A. et al. Phase I clinical trial of all-trans-retinoic acid with correlation of its pharmacokinetics and pharmacodynamics. *Cancer Chemother Pharmacol* **39**, 291-9 (1997).
158. Zhang, X. & Ho, S.M. Epigenetics meets endocrinology. *J Mol Endocrinol* **46**, R11-32 (2011).
159. Puppin, C. et al. Effects of histone acetylation on sodium iodide symporter promoter and expression of thyroid-specific transcription factors. *Endocrinology* **146**, 3967-74 (2005).
160. Venkataraman, G.M., Yatin, M., Marcinek, R. & Ain, K.B. Restoration of iodide uptake in dedifferentiated thyroid carcinoma: relationship to human Na+/I-symporter gene methylation status. *J Clin Endocrinol Metab* **84**, 2449-57 (1999).
161. Provenzano, M.J., Fitzgerald, M.P., Krager, K. & Domann, F.E. Increased iodine uptake in thyroid carcinoma after treatment with sodium butyrate and decitabine (5-Aza-dC). *Otolaryngol Head Neck Surg* **137**, 722-8 (2007).
162. Xu, W.S., Parmigiani, R.B. & Marks, P.A. Histone deacetylase inhibitors: molecular mechanisms of action. *Oncogene* **26**, 5541-52 (2007).
163. Kitazono, M. et al. Low concentrations of the histone deacetylase inhibitor, depsipeptide (FR901228), increase expression of the Na(+)/I(-) symporter and iodine accumulation in poorly differentiated thyroid carcinoma cells. *J Clin Endocrinol Metab* **86**, 3430-5 (2001).
164. Fortunati, N. et al. Valproic acid induces the expression of the Na+/I- symporter and iodine uptake in poorly differentiated thyroid cancer cells. *J Clin Endocrinol Metab* **89**, 1006-9 (2004).
165. Mann, B.S., Johnson, J.R., Cohen, M.H., Justice, R. & Pazdur, R. FDA approval summary: vorinostat for treatment of advanced primary cutaneous T-cell lymphoma. *Oncologist* **12**, 1247-52 (2007).
166. Sharma, S. et al. A Phase II Clinical Trial of Oral Valproic Acid in Patients with Castration-Resistant Prostate Cancers Using an Intensive Biomarker Sampling Strategy. *Transl Oncol* **1**, 141-7 (2008).
167. Yang, J.J. et al. A randomized phase II clinical trial of nab-paclitaxel and carboplatin compared with gemcitabine and carboplatin as first-line therapy in locally advanced or metastatic squamous cell carcinoma of lung. *BMC Cancer* **14**, 684 (2014).
168. Richards, D.A. et al. Gemcitabine plus CI-994 offers no advantage over gemcitabine alone in the treatment of patients with advanced pancreatic cancer: results of a phase II randomized, double-blind, placebo-controlled, multicenter study. *Ann Oncol* **17**, 1096-102 (2006).
169. Waltz, F., Pillette, L. & Ambroise, Y. A nonradioactive iodide uptake assay for sodium iodide symporter function. *Anal Biochem* **396**, 91-5 (2010).
170. Varghese, F., Bukhari, A.B., Malhotra, R. & De, A. IHC Profiler: an open source plugin for the quantitative evaluation and automated scoring of immunohistochemistry images of human tissue samples. *PLoS One* **9**, e96801 (2014).

171. Haggarty, S.J., Koeller, K.M., Wong, J.C., Grozinger, C.M. & Schreiber, S.L. Domain-selective small-molecule inhibitor of histone deacetylase 6 (HDAC6)-mediated tubulin deacetylation. *Proc Natl Acad Sci U S A* **100**, 4389-94 (2003).
172. Kogai, T., Taki, K. & Brent, G.A. Enhancement of sodium/iodide symporter expression in thyroid and breast cancer. *Endocr Relat Cancer* **13**, 797-826 (2006).
173. Park, J.W. et al. Troglitazone, the peroxisome proliferator-activated receptor-gamma agonist, induces antiproliferation and redifferentiation in human thyroid cancer cell lines. *Thyroid* **15**, 222-31 (2005).
174. Mayr, B. & Montminy, M. Transcriptional regulation by the phosphorylation-dependent factor CREB. *Nat Rev Mol Cell Biol* **2**, 599-609 (2001).
175. Delghandi, M.P., Johannessen, M. & Moens, U. The cAMP signalling pathway activates CREB through PKA, p38 and MSK1 in NIH 3T3 cells. *Cell Signal* **17**, 1343-51 (2005).
176. Chatterjee, S., Thaker, N. & De, A. Combined 2-deoxy glucose and metformin improves therapeutic efficacy of sodium-iodide symporter-mediated targeted radioiodine therapy in breast cancer cells. *Breast Cancer (Dove Med Press)* **7**, 251-65 (2015).
177. Suzuki, T. et al. Effect of trichostatin A on cell growth and expression of cell cycle- and apoptosis-related molecules in human gastric and oral carcinoma cell lines. *Int J Cancer* **88**, 992-7 (2000).
178. Mann, B.S. et al. Vorinostat for treatment of cutaneous manifestations of advanced primary cutaneous T-cell lymphoma. *Clin Cancer Res* **13**, 2318-22 (2007).
179. Cummings, J.H., Pomare, E.W., Branch, W.J., Naylor, C.P. & Macfarlane, G.T. Short chain fatty acids in human large intestine, portal, hepatic and venous blood. *Gut* **28**, 1221-7 (1987).
180. Phiel, C.J. et al. Histone deacetylase is a direct target of valproic acid, a potent anticonvulsant, mood stabilizer, and teratogen. *J Biol Chem* **276**, 36734-41 (2001).
181. LoRusso, P.M. et al. Preclinical antitumor activity of CI-994. *Invest New Drugs* **14**, 349-56 (1996).
182. Kraker, A.J. et al. Modulation of histone acetylation by [4-(acetylamino)-N-(2-amino-phenyl) benzamide] in HCT-8 colon carcinoma. *Mol Cancer Ther* **2**, 401-8 (2003).
183. Gryder, B.E., Sodji, Q.H. & Oyelere, A.K. Targeted cancer therapy: giving histone deacetylase inhibitors all they need to succeed. *Future Med Chem* **4**, 505-24 (2012).
184. Ohashi, E., Kogai, T., Kagechika, H. & Brent, G.A. Activation of the PI3 kinase pathway by retinoic acid mediates sodium/iodide symporter induction and iodide transport in MCF-7 breast cancer cells. *Cancer Res* **69**, 3443-50 (2009).
185. Jung, K.H., Paik, J.Y., Ko, B.H. & Lee, K.H. Mitogen-activated protein kinase signaling enhances sodium iodide symporter function and efficacy of radioiodide therapy in nonthyroidal cancer cells. *J Nucl Med* **49**, 1966-72 (2008).
186. Vadysirisack, D.D., Venkateswaran, A., Zhang, Z. & Jhiang, S.M. MEK signaling modulates sodium iodide symporter at multiple levels and in a paradoxical manner. *Endocr Relat Cancer* **14**, 421-32 (2007).
187. Shapira, I., Lee, A., Vora, R. & Budman, D.R. P53 mutations in triple negative breast cancer upregulate endosomal recycling of epidermal growth factor receptor (EGFR) increasing its oncogenic potency. *Crit Rev Oncol Hematol* **88**, 284-92 (2013).
188. Nebbioso, A. et al. HDACs class II-selective inhibition alters nuclear receptor-dependent differentiation. *J Mol Endocrinol* **45**, 219-28 (2010).
189. Behr, M., Schmitt, T.L., Espinoza, C.R. & Loos, U. Cloning of a functional promoter of the human sodium/iodide-symporter gene. *Biochem J* **331 (Pt 2)**, 359-63 (1998).
190. Xu, J., Kogai, T., Brent, G.A. & Hershman, J.M. A GC box in the human sodium iodide symporter gene promoter is essential for full activity. *Thyroid* **12**, 107-14 (2002).
191. Riedel, C., Dohan, O., De la Vieja, A., Ginter, C.S. & Carrasco, N. Journey of the iodide transporter NIS: from its molecular identification to its clinical role in cancer. *Trends Biochem Sci* **26**, 490-6 (2001).

192. Taki, K., Kogai, T., Kanamoto, Y., Hershman, J.M. & Brent, G.A. A thyroid-specific far-upstream enhancer in the human sodium/iodide symporter gene requires Pax-8 binding and cyclic adenosine 3',5'-monophosphate response element-like sequence binding proteins for full activity and is differentially regulated in normal and thyroid cancer cells. *Mol Endocrinol* **16**, 2266-82 (2002).
193. De Felice, M. & Di Lauro, R. Thyroid development and its disorders: genetics and molecular mechanisms. *Endocr Rev* **25**, 722-46 (2004).
194. Vinson, C. et al. Classification of human B-ZIP proteins based on dimerization properties. *Mol Cell Biol* **22**, 6321-35 (2002).
195. Riesco-Eizaguirre, G. et al. The miR-146b-3p/PAX8/NIS Regulatory Circuit Modulates the Differentiation Phenotype and Function of Thyroid Cells during Carcinogenesis. *Cancer Res* **75**, 4119-30 (2015).
196. Fernandez, L.P., Lopez-Marquez, A., Martinez, A.M., Gomez-Lopez, G. & Santisteban, P. New insights into FoxE1 functions: identification of direct FoxE1 targets in thyroid cells. *PLoS One* **8**, e62849 (2013).
197. Puppin, C. et al. Transcriptional regulation of human sodium/iodide symporter gene: a role for redox factor-1. *Endocrinology* **145**, 1290-3 (2004).
198. Chun, J.T., Di Dato, V., D'Andrea, B., Zannini, M. & Di Lauro, R. The CRE-like element inside the 5'-upstream region of the rat sodium/iodide symporter gene interacts with diverse classes of b-Zip molecules that regulate transcriptional activities through strong synergy with Pax-8. *Mol Endocrinol* **18**, 2817-29 (2004).
199. Pomerance, M., Abdullah, H.B., Kamerji, S., Correze, C. & Blondeau, J.P. Thyroid-stimulating hormone and cyclic AMP activate p38 mitogen-activated protein kinase cascade. Involvement of protein kinase A, rac1, and reactive oxygen species. *J Biol Chem* **275**, 40539-46 (2000).
200. Ajjan, R.A. et al. The sodium iodide symporter gene and its regulation by cytokines found in autoimmunity. *J Endocrinol* **158**, 351-8 (1998).
201. Ajjan, R.A. et al. Regulation and tissue distribution of the human sodium iodide symporter gene. *Clin Endocrinol (Oxf)* **49**, 517-23 (1998).
202. Costamagna, E., Garcia, B. & Santisteban, P. The functional interaction between the paired domain transcription factor Pax8 and Smad3 is involved in transforming growth factor-beta repression of the sodium/iodide symporter gene. *J Biol Chem* **279**, 3439-46 (2004).
203. Riesco-Eizaguirre, G. et al. The BRAFV600E oncogene induces transforming growth factor beta secretion leading to sodium iodide symporter repression and increased malignancy in thyroid cancer. *Cancer Res* **69**, 8317-25 (2009).
204. Smith, V.E. et al. A novel mechanism of sodium iodide symporter repression in differentiated thyroid cancer. *J Cell Sci* **122**, 3393-402 (2009).
205. Li, W. & Ain, K.B. Human sodium-iodide symporter (hNIS) gene expression is inhibited by a trans-active transcriptional repressor, NIS-repressor, containing PARP-1 in thyroid cancer cells. *Endocr Relat Cancer* **17**, 383-98 (2010).
206. Alotaibi, H. et al. Intronic elements in the Na+/I- symporter gene (NIS) interact with retinoic acid receptors and mediate initiation of transcription. *Nucleic Acids Res* **38**, 3172-85 (2006).
207. Knostman, K.A. et al. Signaling through 3',5'-cyclic adenosine monophosphate and phosphoinositide-3 kinase induces sodium/iodide symporter expression in breast cancer. *J Clin Endocrinol Metab* **89**, 5196-203 (2004).
208. Dohan, O., De la Vieja, A. & Carrasco, N. Hydrocortisone and purinergic signaling stimulate sodium/iodide symporter (NIS)-mediated iodide transport in breast cancer cells. *Mol Endocrinol* **20**, 1121-37 (2006).
209. Kogai, T., Liu, Y.Y., Mody, K., Shamsian, D.V. & Brent, G.A. Regulation of sodium iodide symporter gene expression by Rac1/p38beta mitogen-activated protein kinase signaling pathway in MCF-7 breast cancer cells. *J Biol Chem* **287**, 3292-300 (2012).

210. Alsner, J., Yilmaz, M., Guldberg, P., Hansen, L.L. & Overgaard, J. Heterogeneity in the clinical phenotype of TP53 mutations in breast cancer patients. *Clin Cancer Res* **6**, 3923-31 (2000).
211. Meek, D.W. The p53 response to DNA damage. *DNA Repair (Amst)* **3**, 1049-56 (2004).
212. Guerrieri, F. et al. The sodium/iodide symporter NIS is a transcriptional target of the p53-family members in liver cancer cells. *Cell Death Dis* **4**, e807 (2013).
213. Marcel, V. et al. Biological functions of p53 isoforms through evolution: lessons from animal and cellular models. *Cell Death Differ* **18**, 1815-24 (2011).
214. Meek, D.W. & Anderson, C.W. Posttranslational modification of p53: cooperative integrators of function. *Cold Spring Harb Perspect Biol* **1**, a000950 (2009).
215. Braithwaite, A.W., Del Sal, G. & Lu, X. Some p53-binding proteins that can function as arbiters of life and death. *Cell Death Differ* **13**, 984-93 (2006).
216. Brandt, T., Townsley, F.M., Teufel, D.P., Freund, S.M. & Veprintsev, D.B. Molecular basis for modulation of the p53 target selectivity by KLF4. *PLoS One* **7**, e48252 (2012).
217. Espinosa, J.M. & Emerson, B.M. Transcriptional regulation by p53 through intrinsic DNA/chromatin binding and site-directed cofactor recruitment. *Mol Cell* **8**, 57-69 (2001).
218. Riley, T., Sontag, E., Chen, P. & Levine, A. Transcriptional control of human p53-regulated genes. *Nat Rev Mol Cell Biol* **9**, 402-12 (2008).
219. Horvath, M.M., Wang, X., Resnick, M.A. & Bell, D.A. Divergent evolution of human p53 binding sites: cell cycle versus apoptosis. *PLoS Genet* **3**, e127 (2007).
220. Belyi, V.A. et al. The origins and evolution of the p53 family of genes. *Cold Spring Harb Perspect Biol* **2**, a001198 (2010).
221. Marcel, V., Fernandes, K., Terrier, O., Lane, D.P. & Bourdon, J.C. Modulation of p53beta and p53gamma expression by regulating the alternative splicing of TP53 gene modifies cellular response. *Cell Death Differ* **21**, 1377-87 (2014).
222. Bourdon, J.C. et al. p53 isoforms can regulate p53 transcriptional activity. *Genes Dev* **19**, 2122-37 (2005).
223. Van Laere, S. et al. Distinct molecular phenotype of inflammatory breast cancer compared to non-inflammatory breast cancer using Affymetrix-based genome-wide gene-expression analysis. *Br J Cancer* **97**, 1165-74 (2007).
224. Turpin, E. et al. Increased incidence of ERBB2 overexpression and TP53 mutation in inflammatory breast cancer. *Oncogene* **21**, 7593-7 (2002).
225. Sawaki, M. et al. High prevalence of HER-2/neu and p53 overexpression in inflammatory breast cancer. *Breast Cancer* **13**, 172-8 (2006).
226. Ho, J. & Benchimol, S. Transcriptional repression mediated by the p53 tumour suppressor. *Cell Death Differ* **10**, 404-8 (2003).
227. Inga, A., Storici, F., Darden, T.A. & Resnick, M.A. Differential transactivation by the p53 transcription factor is highly dependent on p53 level and promoter target sequence. *Mol Cell Biol* **22**, 8612-25 (2002).
228. Ray, P. et al. Monitoring gene therapy with reporter gene imaging. *Semin Nucl Med* **31**, 312-20 (2001).
229. Doubrovin, M., Serganova, I., Mayer-Kuckuk, P., Ponomarev, V. & Blasberg, R.G. Multimodality in vivo molecular-genetic imaging. *Bioconjug Chem* **15**, 1376-88 (2004).
230. Mayer-Kuckuk, P., Menon, L.G., Blasberg, R.G., Bertino, J.R. & Banerjee, D. Role of reporter gene imaging in molecular and cellular biology. *Biol Chem* **385**, 353-61 (2004).
231. De, A., Lewis, X.Z. & Gambhir, S.S. Noninvasive imaging of lentiviral-mediated reporter gene expression in living mice. *Mol Ther* **7**, 681-91 (2003).
232. Ray, P., De, A., Min, J.J., Tsien, R.Y. & Gambhir, S.S. Imaging tri-fusion multimodality reporter gene expression in living subjects. *Cancer Res* **64**, 1323-30 (2004).
233. Menendez, D., Inga, A. & Resnick, M.A. The expanding universe of p53 targets. *Nat Rev Cancer* **9**, 724-37 (2009).

234. Helton, E.S. & Chen, X. p53 modulation of the DNA damage response. *J Cell Biochem* **100**, 883-96 (2007).
235. Teodoro, J.G., Parker, A.E., Zhu, X. & Green, M.R. p53-mediated inhibition of angiogenesis through up-regulation of a collagen prolyl hydroxylase. *Science* **313**, 968-71 (2006).
236. Pal, S., Datta, K. & Mukhopadhyay, D. Central role of p53 on regulation of vascular permeability factor/vascular endothelial growth factor (VPF/VEGF) expression in mammary carcinoma. *Cancer Res* **61**, 6952-7 (2001).
237. Taura, M. et al. p53 regulates Toll-like receptor 3 expression and function in human epithelial cell lines. *Mol Cell Biol* **28**, 6557-67 (2008).
238. Singh, K. et al. p53 target gene SMAR1 is dysregulated in breast cancer: its role in cancer cell migration and invasion. *PLoS One* **2**, e660 (2007).
239. Qin, Q. et al. A novel function for p53: regulation of growth cone motility through interaction with Rho kinase. *J Neurosci* **29**, 5183-92 (2009).
240. Roger, L., Gadea, G. & Roux, P. Control of cell migration: a tumour suppressor function for p53? *Biol Cell* **98**, 141-52 (2006).
241. Yu, X., Harris, S.L. & Levine, A.J. The regulation of exosome secretion: a novel function of the p53 protein. *Cancer Res* **66**, 4795-801 (2006).
242. Berger, F. et al. Mammary radioiodine accumulation due to functional sodium iodide symporter expression in a benign fibroadenoma. *Biochem Biophys Res Commun* **349**, 1258-63 (2006).
243. Rai, R. et al. Human sodium iodide symporter (hNIS) in fibroadenoma breast--a immunohistochemical study. *Indian J Exp Biol* **49**, 113-7 (2011).
244. Lacoste, C. et al. Iodide transporter NIS regulates cancer cell motility and invasiveness by interacting with the Rho guanine nucleotide exchange factor LARG. *Cancer Res* **72**, 5505-15 (2012).
245. Ganapathy, V., Thangaraju, M. & Prasad, P.D. Nutrient transporters in cancer: relevance to Warburg hypothesis and beyond. *Pharmacol Ther* **121**, 29-40 (2009).
246. Schwartzenberg-Bar-Yoseph, F., Armoni, M. & Karnieli, E. The tumor suppressor p53 down-regulates glucose transporters GLUT1 and GLUT4 gene expression. *Cancer Res* **64**, 2627-33 (2004).
247. Wei, C.L. et al. A global map of p53 transcription-factor binding sites in the human genome. *Cell* **124**, 207-19 (2006).
248. Marcel, V., Olivier, M., Mollereau, B., Hainaut, P. & Bourdon, J.C. First International p53 Isoforms Meeting: 'p53 isoforms through evolution: from identification to biological function'. *Cell Death Differ* **18**, 563-4 (2011).

Appendix

Materials and Methods:

Materials:

HDACi drugs such as TSA (T8852), NaB (B5887), VPA (4543), SAHA (SML0061) and TBA (SML0044) were purchased from **Sigma, USA**. CI994 (1742-10, 50) was purchased from **Biovision, CA, USA**.

List of antibodies used in the study:

NIS (FP5A, Abcam, USA), Pan-acetyl-histone H3 antibody (06-598, Upstate, USA), Fluc antibody (G4751, Promega Corporation, USA), α-tubulin antibody (T9026, Sigma, USA), p53 antibody (DO-1, Santa Cruz Biotechnology, USA), γH2Ax ((MA5-15130, Pierce Biotechnology, USA). Rabbit polyclonal secondary antibody to mouse IgG (HRP) (ab6728), secondary antibody to rabbit IgG (HRP), anti rabbit secondary antibody labeled with Dylight633 (35562) and anti-mouse secondary antibody labeled with Dylight633 (35512) from Thermo Scientific, USA.

The following materials were obtained from **Applied Biosystems, Invitrogen:**

Agarose powder (15510-027), DNA loading dye (Blue juice, 10816-015), 2X TaqMan master mix (Part No. 4384266), primer probe mix for human NIS (Hs00166567_m1), GAPDH (Hs02758991_g1), MicroAmp optical 384-well reaction plate with Barcode (4309849) and MicroAmp optical adhesive film kit (4313663), MTT (M6494), Superscript first strand cDNA synthesis kit (18080-051), RPMI (31800-02), IMDM (12200-028), DMEM (12800-017), Heat inactivated FBS (10082-147), Antibiotic-Antimycotic (15240-062), 0.25%

Trypsin-EDTA (25200-072), Lipofectamine (11668-027), HBSS (24020-117), plasmid mini-prep isolation kit (K210011), Novex Chemiluminescence detection system (WP20005).

The following materials were obtained from **Sigma Chemicals:**

L15 (M6395), Poly L-Lysine (P8920), TRIS (T1378), Tween-20 (P9416), BSA (A7030), DAPI (D8417), β -mercaptoethanol (M3148), PIPES (P2949), CaCl2 (C7902), MnCl2 (M8054), MgCl2 (M4880), NaCl (71736), Ampicillin salt (A9518), G418 (A1720), DEPC (D5758), DMSO (D8418), EDTA, Ethidium bromide (E8751), L-15 (L4386), Para formaldehyde (P6148), Triton X-100 (T8787), HEPES (H4034), Ponceau stain (P7170), Bradford reagent (B6916), Potassium perchlorate (241830), Formamide (F9037), DAB enhanced liquid substrate system (D3939), L-Thyroxine (T2376), Methimazole (M8506), Ammonium Cerium (31173), Arsenic oxide (A1010), Sodium citrate (W302600), Doxorubicin hydrochloride (D1515), RIPA buffer (R0278)

RNA extraction kit (74106) and Gel extraction kit (28706) were obtained from **Qiagen**.

The following chemicals were obtained from **Thermo Fisher Scientific:**

Hydrogen peroxide (18755), Xylene (32297), Pfu Fusion polymerase (F-530S), dNTPs (R0191).

The following chemicals were obtained from **Merck, SRL or SD fine chemicals:**

Methanol (Merck 106009), Glacial Acetic Acid (Merck 100063), Sodium borohydrate (SRL 1948108), Ethanol (SD fine chemical 58051), Boric acid (Merck 194810), Formaldehyde (CB4F640180), Protease inhibitor cocktail (Merck 535140)

Prism ultra protein ladder (ab116028) was obtained from **Abcam:**

Gel cast tray, run unit and power pack for western blotting was from **Biorad**.

Luciferase assay system (E4030) and Passive lysis buffer (E1941) were obtained from **Promega Incorporations, USA.**

Vecta shield (H1000) was obtained from **Vector laboratories.**

Luria broth and agar was obtained from **HiMedia** (M557 & M575), restriction enzymes, T4 DNA ligase, molecular biology buffers and DNA gel ladder were obtained from **NEB**, Taq DNA polymerase (M0273L) was obtained from **NEB**. MOPS was obtained from **Amresco**, Cell lysis buffer (#9803) was obtained from **Cell signaling.**

TF activation array (FA-1002) and Promoter binding TF array Kit (FA-2002) were purchased from **Signosis, USA.**

D-luciferin (L8220) for *in vivo* imaging was obtained from **Biosynth International, Switzerland.**

The water used for the preparation of all solutions and reagents was Ultrapure water (Resistivity = 18 MΩ cm) obtained from a Milli-Q water plant (**Millipore,** Billerica, MA, USA). Disposable plastic ware (certified DNase, RNase, and protease-free) was obtained from **Axygen**. Disposable sterile plastic ware for tissue culture was obtained from **Nunc**.

Methods:

Bacterial culture

Luria-Bertani (LB) medium: A minimal growth medium is used for culture and maintenance of different *E. coli* strain DH5α. This strain is further used for harboring desired plasmids. Powdered Luria broth (20 g) was dissolved in 800 ml deionized miliQ processed water (D/W) and the volume was adjusted to 1 liter (L) with D/W and sterilized by autoclaving. For making LB-agar plates, 35 g Luria agar powder was dissolved/ L, sterilized by autoclaving and poured in 90 mm sterile plates. Specific antibiotic (ampicillin) was added in the medium according to the plasmid antibiotic marker.

1. Preparation of ultra-competent cells

Composition of transformation buffer (TB): The following components were added to 100 ml of distilled water; 10mM PIPES, 15mM CaCl2, 250 mM KCl, adjusted pH to 6.7 with 5N KOH, 55 mM $MnCl_2$, filter sterilized through 0.2 μ membrane filter.

Composition of super optimal broth (SOB): Following components were mixed in the required volume of D/W; 2% Bactotryptone, 0.5%Yeast extract, 10 mM NaCl, 2.5 mM KCl, 10 mM $MgCl_2$, and 10 mM $MgSO_4$.

Protocol:

1. *E. coli* DH5α strain glycerol stock was streaked on a fresh LB agar plates without antibiotics and incubated overnight at 37˚C.

2. Single colony was inoculated in 250 ml SOB broth and incubated at 18˚C /250 rpm till O.D.600 reached ~0.4 (Approximately 3-4 days of incubation are required).

3. The cells were harvested by pelleting down at 4˚C and resuspended in 80 ml of TB followed by incubation on ice for 10 minutes and centrifugation.

4. The cell pellet was resuspended in 18.6 ml TB. 1.4 ml (7%) DMSO was added to the cells and mixed completely.

5. 100µl aliquots of the cells were made in sterile microfuge tubes and snap frozen in liquid nitrogen followed by storage at -80˚C.

2. Bacterial transformation

1. Competent cells (100 µl) were thawed on ice and mixed with 1-5ng of plasmid DNA or 20 µl of ligation mixture and incubated on ice for 30 minutes.

2. Heat shock was given to the mixture at 42˚C for 60 seconds and the sample was snap chilled on ice.

3. LB medium was added to the cells and incubated at 37˚C for 60 minutes at 170 rpm.

4. The cells were then plated on an LB agar plate with the appropriate antibiotic.

3. The required 1X TBE buffer is then poured into the tank over the gel. Before loading the PCR product into the wells, the PCR product is mixed with the loading dye containing glycerol and bromophenol blue which indicate the DNA migration front.

4. Standard DNA markers of known fragment sizes were run in parallel to the samples in order to have standard reference. The gel was run at a constant voltage.

5. EtBr stained DNA bands were visualized and documented on a gel documentation system.

3. PCR

The NIS promoter was PCR amplified using following conditions:

Components	**Volume**
5X HF buffer	5 µl
10mM dNTP	1µl
10 µM Fwd primer	1µl
10 µM Fwd primer	1µl
Pfu enzyme	0.5 µl
Template DNA	0.5 µl
miliQ water	16 µl

The cycling conditions are given below:

PCR step	**Temperature**	**Time**
Initial denaturation	95°C	10 min
Denaturation	95°C	30 sec
Primer annealing	44°C	30 sec
Primer Extension	72°C	60 sec
Final extension	72°C	10 min
Hold	4°C	forever

4. Restriction digestion

Both PCR amplified insert and vector were digested with two RE enzymes simultaneously. NEB buffer that results in maximum activity of both the enzymes was chosen using the enzyme activity chart. Before beginning with digestion the recommended buffer was thawed completely on ice and the water bath was set at 37°C. The reaction mixture for digestion was incubated at 37°C water bath, overnight.

5. Gel extraction

The digested product was gel extracted and purified by using Qiagen gel extraction kit. Briefly, the following procedure was followed:

1. The DNA fragment from the agarose gel was excised with a clean, sharp scalpel.

2. The gel slice was weighed in a micro centrifuge tube. 3 volumes Buffer QG was added to 1 volume gel (100 mg ~ 100 µl).

3. Reaction was incubated at 50°C for 10 minutes (or until the gel slice has completely dissolved). The tube was vortexed every 2–3 minutes to help dissolve gel.

4. 1 gel volume of isopropanol was added to the sample and mixed. Thereafter, a Qiaquick spin column were placed on a 2 ml collection tube and the above reaction mix was added in the column.

5. The tube was incubated for 1-2 minutes and centrifuged for 1 minute at 13,000 rpm.

6. The flow-through was discarded and further washed with 0.5ml of buffer QG by centrifugation for 1minute at 13,000 rpm.

7. Buffer PE (0.75 ml) was added to QIAquick column and was incubated for 5 minutes before centrifuging for 1 minute at 13,000 rpm. The flow-through was discarded and was given another wash with buffer PE.

8. An additional dry spin was given to the column and the column was placed in a clean 1.5 ml micro centrifuge tube.

9. To elute DNA, 50 µl Buffer EB (10 mM Tris-HCl, pH 8.5) or water was added to the centre of the QIAquick membrane and centrifuged at 13,000 rpm for 1 minute.

6. Ligation

The ligation reaction was set depending upon the concentration of the insert. Ideally the vector to insert ratio is (1:3) which is essential for carrying out successful ligation reaction.

1. The ligation reaction was carried out at 4°C for overnight using T4 DNA ligase and transformed next day in the DH5α competent cells.

2. After transformation ampicillin containing LB agar plates were placed in the incubator for overnight. After 16-18 hours of incubation, the plates were checked for colonies.

3. Colonies were cultured in LB broth and plasmid was isolated. Screening for the positive clone was performed by restriction digestion. Positive clone obtained by cloning was further verified by DNA sequencing. Sequencing was performed using the ABI automated DNA sequencer present in the genomics facility of ACTREC.

7. Plasmid DNA mini-preparation

The plasmid isolation was performed following the procedure described in the Invitrogen mini prep kit. Briefly following steps were performed.

1. Overnight grown, 5 ml of bacterial cultures transformed with plasmids were spun in a micro-centrifuge tube at 3500 rpm for 15-20 minutes at 4°C.

2. Bacterial pellet was resuspended in 250µl of Buffer R3 (Re-suspension buffer containing RNase (10mg/ml)).

3. The cells were incubated at room temperature (RT) for 5 minutes and 250µl Buffer L7 (lysis solution) was added followed by invert mixing.

4. The cells were incubated at RT for 5 minutes and 350 µl of Precipitation Buffer N4 (neutralizing solution) was added and incubated at RT for 5 minutes after complete invert mixing.

5. The above mixture was then centrifuged at 12,000 g for 10 minutes.

6. The supernatant was loaded onto Spin Column and incubated for 1 minute.

7. The column was centrifuged for 1 minute and the flow-through was discarded.

8. Spin Column was washed by adding 700 µl of buffer W9 and centrifuged at 12,000 g for 1 minute.

9. Discarding the flow through, the column was centrifuged again at 12,000 g for 1 minute.

10. The Spin Column was placed in a clean 1.5 ml micro centrifuge tube. DNA was eluted by addition of 40 µl buffer EB (10 mM Tris-HCl, pH 8.5) or pre-warmed miliQ water and incubated for 15-20 minutes at room temperature.

11. The column was centrifuged at 12,000 g for 2 minutes. The eluate contains pure DNA which is measured by nanodrop spectrophotometer.

8. Site Directed mutagenesis (SDM)

SDM is a molecular technique that deliberately changes sequences in gene or DNA locus with specific intensions. It is used to create point mutation, deletion, insertion or substitution of one or more than one base pair. The technique is widely used study of amino acid changes of protein structure and function, promoter sequence changes to understand the binding of transcriptional regulators in control of gene expression.

Guidelines for primer design:

Mutagenic primers introduce specific experimental mutations. The mutagenic oligonucleotide

primers for use in this protocol must be designed individually according to the desired mutation. The following considerations should be made for designing mutagenic site and selection primers:

1. Both the mutagenic primers must contain the desired mutation and anneal to the same sequence on opposite strands of the plasmid.

2. Primers should be between 25 and 45 bases in length, and the melting temperature (*T*m) of the primers should be greater than or equal to 78°C. The following formula is commonly used for estimating the *T*m of primers:

$T_m = 81.5 + 0.41(\%GC) - 675 / N - \%\ mismatch$

where *N* is the primer length in base pairs.

3. The desired mutation (deletion or insertion) should be in the middle of the primer with ~10–15 bases of correct sequence on both sides.

4. The primers optimally should have a minimum GC content of 40% and should terminate in one or more C or G bases.

5. It is important to keep primer concentration in excess.

Using this technique, site specific mutations can be generated in virtually any double-stranded plasmid with a four-step procedure:

I. Plasmid preparation

Preparation of template DNA for SDM was done using miniprep plasmid isolation kit. DNA was isolated from the *E. coli* strains that produce methylated DNA susceptible to Dpn I digestion.

II. PCR amplification

Temperature recycling involves three main steps-

1. Denaturation of the plasmid
2. Annealing of the mutagenic primers

3. *Pfu turbo* DNA polymerase , that does not displace the newly synthesized strand and stops the extension, is used to extend and incorporate mutagenic primers resulting in the nicked circular DNA strands

III. Dpn I digestion

The methylated and non-mutated template DNA is digested with Dpn I restriction enzyme (overnight at 37°C). Dpn I endonuclease (target sequence- 5'-Gm6ATC-3') is specific for methylated and hemi-methylated DNA and is used to digest the parental DNA template to specifically select newly synthesized DNA harboring desired mutations.

IV. Transformation

The circular nicked double stranded DNA is transformed in DH5α *E.coli* competent cells. After transformation, the competent cells repair the nicks in the mutated plasmids.

Colonies obtained after transformation were grown further, plasmid DNA was isolated and confirmed for desired mutation by sequencing analysis.

Cell culture:

Composition of Phosphate Buffered Saline (PBS) (pH 7.4) 10X / 1L: 80g NaCl, 2g KCl, 14.4g Na2HPO4, 2.4g KH2PO4, Dissolve in 800ml autoclaved water. Adjust the pH 7.4. Make up the volume to 1L.

Cell lines & sub-culturing: Standard aseptic practice was followed for performing cell culture. All the adherent cell lines were maintained and sub-cultured in their respective media supplemented with 10% FBS, 100U/ml penicillin and 100 µg/ml streptomycin solutions.

9. Procedure of sub-culturing

1. Spent medium was aspirated off from the culture flask using a 10 ml glass pipette.

2. The cells were given two gentle washes with sterile phosphate buffered saline (PBS) (1X)

3. The cells were treated with 1 ml trypsin (for a 10 cm^2 culture plate) and incubated in a 5% CO2 incubator for 2- 3 minutes.

4. The trypsin was neutralized by addition of complete RMPI medium (1 part Trypsin: 2 parts complete RPMI).

5. The cells were flushed in and out thoroughly using a micropipette in order to ensure most of the cells had detached from the surface of the culture plate and to obtain a homogenous cell suspension.

6**.** A suitable cell density was transferred to a new culture plate and provided with fresh complete RPMI for their optimal growth and survival.

10. Cryopreservation

1. Adherent cells in culture were trypsinized and a homogenous cell suspension was obtained.

2. The cell suspension was centrifuged at a speed of 1500 rpm at $4^{\circ}C$ for 3-5 minutes in order to obtain a cell pellet.

3. Freezing medium was prepared by adding 90% FBS, 0-5% incomplete medium and 5-10% DMSO.

4. 1-2x10^6 cells were suspended in 1 ml of freezing medium, mixed thoroughly and immediately transferred to the cryopreservation vial.

5. The cryovial was then placed in an isopropanol containing freezing container which allows temperature decrease at the rate of -1°/ hour in a $-80^{\circ}C$ refrigerator. Finally cells were transferred to liquid nitrogen container maintained at $-196^{\circ}C$.

11. Revival of cryopreserved cells

1. Cryopreserved cells were thawed in a water bath preset at 37°C.

2. The thawed cells were suspended in 1 ml of complete RPMI medium.

3. The contents of the tube were centrifuged at a speed of 1200 rpm at 4°C for 2- 3 minutes to obtain the cell pellet.

4. The cell pellet was resuspended with 1ml of PBS and centrifuged at 1200 rpm at 4°C for 2-3 minutes.

5. The cell pellet was resuspended in a suitable volume of complete RPMI medium and transferred to a new culture flask and supplied with fresh complete medium.

6. The culture flask was incubated in a 5% CO_2 incubator for maintenance of the revived culture.

12. Transfection

Transfection was done using Lipofectamine transfection reagent as per manufacturer's instructions. In brief, the following procedure was followed for transient/stable transfection of cell lines.

Protocol for lipofectamine based transfection:

1. Prior to the day of transfection cells were seeded in culture vessel at a confluency of 70-90%.

2. Four amounts of lipofectamine were diluted in opti MEM or incomplete media. The complex was incubated for 5 minutes.

3. In a separate tube required amount of DNA is diluted in opti MEM media. Volume of lipofectamine, DNA and opti MEM media are decided by the culture vessel chosen for transfection. The complex was incubated for 5 minutes.

4. Diluted DNA was added to diluted lipofectamine in a 1:1 ratio and the complex was incubated for 25 minutes.

5. In the meantime the medium from the culture vessel was aspirated and fresh complete media was added to the cells.

6. After 25 minutes of incubation, definite amount of complete media was added to the transfection mixture and this was added in the culture vessel. The plate was swirled gently to uniformly distribute the complex and incubated at 37°C, 5% CO_2 incubator.

7. After 6 hours, the transfection media was aspirated, the cells were washed with 1X PBS and complete media was added to the cells. For stable transfection, after 48 hours of transfection, the cells were trypsinized and are sub cultured in the selection media containing G418.

13. MTT Assay

1. The cells were seeded in 96 well plate in triplicates at a density of 3000 cells per well.

2. Next day, cells were treated with various drug concentration of six different HDACi.

3. After 48 hours of treatment 20µl of 5mg/ml MTT was added into each well and incubated for 5 hours.

4. The spent media from each well was removed completely. 200µl DMSO per well was added to solubilize the formazan crystals.

6. It was then kept in shaker for 15-20 minutes until the crystal get solubilized and then proceeded for measuring the absorbance at wavelength 560nm and 670nm.

Note- The absorbance at 560nm is subtracted from the absorbance at 670nm to remove the background caused by the presence of DMSO and % viability is calculated with respect to untreated cells.

14. Immunofluorescence assay

1. $1x10^6$ cells were seeded on a sterile cover slip in a 35 mm culture plate and incubated in a 5% CO_2 incubator overnight.

2. Next day cells were washed with 1X PBS thrice, each for 5 minutes at 37°C.

3. The cells were fixed using 4% paraformaldehyde (4% PFA prepared in 1X PBS) and incubated for 10 minutes at 37°C.

4. For staining of nuclear proteins, an additional step of permeabilisation was performed by treating cells with 0.2% TritonX 100 in 4% PFA for 7-10 minutes at room temperature.

5. The fixed cells were given three washes with 1X PBS for 5 minutes each at room temperature.

6. Non- specificity was reduced by incubating the cells in BSA (2% BSA prepared in 1X PBS) for 30 to 45 minutes at room temperature.

7. The cells were then incubated overnight at 4°C with antibody diluted in PBS (1X).

8. Cells were again washed with 1X PBS thrice, for 5 minutes each at room temperature.

9. From this point onwards, all steps of the experiment were performed in dark.

10. Cells on the cover slip were incubated for 30 to 45 minutes at room temperature with secondary antibody diluted in 1X PBS.

11. Cells were given three washes of 1X PBS each for 10 minutes at room temperature for the removal of unbound secondary antibody from cells.

12. Nucleus of the cells was stained with DAPI for 1 minute and cells were again washed with 1X PBS for 5 minutes.

13. The coverslips were mounted onto glass slides using Vecta Shield and images were taken using a Confocal Microscope (Zeiss).

15. Iodide uptake assay

Non radioactive colorimetric method

The standard assay for NIS function is based on the measurement of radioiodide uptake (^{125}I) in NIS expressing cells. However its applications are limited due to cost and safety issues. Thus we used a simple spectrophotometric assay for the determination of iodide accumulation in NIS expressing cells based on the catalytic effect of iodide on the reduction of yellow cerium (IV) to colorless cerium (III) in the presence of arsenious acid (Sandell-Kolthoff reaction). Assay reliability is tested by using known inhibitors of iodide uptake like $ClO4^-$ anions.

Composition of ammonium cerium sulfate (42mM): Ammonium cerium (IV) sulfate hydrate (12.53 gm) was dissolved in water (200 ml). Concentrated H_2SO_4 (50 ml) was then added to the solution, which was cooled with an ice bath. After cooling, the solution was diluted to 500 ml with water. This solution was diluted fourfold with water prior to use.

Composition of sodium arsenite solution (96mM): Arsenic (III) oxide (4.75 gm) and NaCl (24 g) were dissolved in 2 M NaOH (50 ml). The mixture was then diluted to 500 ml with water and centrifuged to remove insoluble material. This solution was diluted fourfold with water prior to use.

Protocol:

1. 30,000 cells were seeded in triplicate in a 96-well plate and incubated overnight in a 5% CO_2 incubator.

2. Media was first decanted only from wells seeded with cells that were to be blocked with $KClO_4$, an inhibitor to iodide uptake by NIS. Upto 90 µl of Uptake Buffer (10mM HEPES in HBSS) was added to each of these wells.

3. These cells were then treated with $KClO_4$ (30µM) and incubated in a 5% CO_2 Incubator for 30 minutes.

4. Media was decanted from the remaining wells of the 96-well plate and was replaced by 90 µl of uptake buffer per well.

5. Next, NaI (100 µM) was added to all the wells and the plate was incubated for 60 minutes in a 5% CO_2 Incubator.

6. The wells were washed with an appropriate volume of chilled uptake buffer following the incubation. This was done to terminate any further uptake of iodide by the cells.

7. Remaining uptake buffer was removed from the wells by inverting over a tissue paper.

8. 100 µl Ammonium Cerium Sulphate (42 mM), followed by 100 µl Sodium Arsenite (96 mM) were added to each well and incubated for 30 minutes in dark at room temperature.

9**.** The absorbance at 420 nm was recorded in a spectrophotometer.

16. Iodide efflux assay

Efflux assay is performed to evaluate the time for which iodide retains inside NIS expressing cells in absence of any organification system.

1. Control or drug treated cells were incubated in uptake buffer with 10µM NaI at 37°C for 30 minutes.

2. Cells were washed with ice cold uptake buffer to stop the reaction and fresh uptake buffer without NaI was added.

3. The medium was replaced after every 10 minutes and 10.5mM ammonium cerium (IV) sulphate solution and 24mM sodium arsenite (III) solution were added.

4. Following incubation at RT in dark for 30 minutes absorbance at 420nm was recorded.

17. RNA Extraction from cells

RNeasy mini kit (Qiagen) was used for the extraction of total RNA from cells. Protocol:

1. A 70-80% confluent monolayer of cells in culture was trypsinized and cells were pelleted down by centrifugation at a speed of 1200 rpm for 5 minutes at 4°C.

2. The cells were given two gentle washes with sterile PBS (1X) and taken in a 1.5 ml eppendorf tube.

3. The cells were completely resuspended in 350 µl buffer RLT by pipetting to mix.

4. The cell suspension was then homogenized using a hand held homogenizer for 30 seconds.

5. 350µl of 70% Ethanol, prepared in Diethylpyrocarbonate (DEPC) treated water was added to the homogenized lysate and mixed well by pipetting.

6. Upto 700µl of the sample was transferred to an RNeasy spin column placed in a 2 ml-collection tube. The lid was closed gently and centrifuged for 30 seconds at 14,000 rpm. The flow- through was discarded.

7. 500µl buffer RPE was added to the RNeasy spin column. The lid was closed gently, and centrifuged for 30 seconds at 14,000 rpm to wash the spin column membrane. The flow-through was discarded.

8. 500µl buffer RPE was added to the RNeasy spin column. The lid was closed gently, and centrifuged for 2 minutes at 14,000 rpm to wash the spin column membrane.

9. The RNeasy spin column was placed in a new 2 ml- collection tube, the lid was closed gently and centrifuged at full speed for 1 minute. This step ensured that any residual buffer RPE or ethanol was eliminated from the column.

10. The RNeasy spin column was placed in a new 1.5 ml- collection tube. 30- 50µl RNase-free water was added directly to the spin column membrane and centrifuged for 1 minute at 14,000 rpm to elute the RNA.

11. The total RNA extracted was quantified by NanoDrop.

18. Quality check of RNA

Before preparation of cDNA from the RNA obtained, quality of RNA was checked in a denaturing agarose gel. The RNA sample was thus run on a denaturing agarose gel electrophoresis. RNA bands were visualized by ethidium bromide (EtBr) staining.

Composition of 1% denaturing agarose gel: Agarose (1.08g) was added to 76.5 ml RNase free water and boiled to melt agarose completely. 10X MOPS buffer (9ml) and formaldehyde (4.5ml) and EtBr were added. The gel was poured in the gel casting tray with a comb and allowed to solidify.

Protocol:

1. The denaturing agarose gel was cast and 1µg RNA was loaded onto the gel along with the RNA loading dye. The composition of the mixture is as follows:

Component	**Amount**
RNA	2 µg
10X MOPS buffer	1 µl
Formamide	3 µl
Formaldehyde	1 µl
Blue juice loading dye (10X)	1 µl
RNase free water	To 10µl

2. After loading the RNA sample gel was run at 80 V.

3. EtBr staining for visualization of bands was carried out by placing the gel in a chamber immersed in 100 ml DEPC treated water containing 5µl EtBr dye for 30-40 minutes.

4. Destaining was performed by immersing the gel in 100 ml DEPC treated water and kept on slow rocking for 15 – 20 minutes. This step was repeated once more.

5. Visualization of bands was carried out using a UV transilluminator.

6. RNA was considered as of good quality when 2 bands were visualized on gel and the density of upper band was twice the density of the lower band.

19. cDNA synthesis for real time PCR

cDNA from RNA is prepared by superscript III first strand synthesis system (Invitrogen). This kit allows cDNA synthesis from 0.5µg to 5µg RNA.

Protocol:

1. All the contents of the kit are thawed and briefly centrifuged before use.

2. Following components are added in a 0.6 ml tube.

Components	**Volume**
RNA 1.5 µg	N µl
50 µM oligo dT	1µl
50ng/µl Random hexamers	0.5µl
10mM dNTP	1µl
DEPC treated water	To 10µl

3. The mix of the above components were incubated in a dry bath at 65°C for 5 minute and then placed on ice for at least 1 minute.

4. For cDNA syntheses following components were mixed in the same order as indicated.

Component	Volume
10X RT buffer	2µl
25mM $MgCl_2$	4µl
0.1mM DTT	2µl
RNase OUT (40 units/µl)	1µl
Superscript III RT	1µl

5. 10µl of cDNA synthesis mix was added to 10 µl of RNA and primer mix made previously. Both the mixtures are mixed gently and briefly centrifuged.

6. The mixture was placed in a PCR tube and following cycle was run in a thermal cycler

Temperature	Time
25°C	10 min
50°C	50 min
85°C	5 min

7. Reaction was chilled on ice and collected by brief centrifugation.

8. 1µl RNase H was added in each tube and the reaction is incubated at 37°C for 20 minutes.

9. cDNA made was either used immediately for PCR or stored at -20°C.

20. Real-time PCR

Real- time PCR based on TaqMan chemistry was performed to check the effect of various treatments NIS mRNA expression in multiple cancer cell lines. The housekeeping gene Glyceraldehyde 3-phosphate dehydrogenase (GAPDH) was used for normalization of results. The PCR plate was run on a real time cycler (Quant Studio 12K Flex, Applied Biosystems)

Protocol:

1. cDNA obtained from reverse transcription reaction was diluted to 10 ng/µl with DEPC-treated miliQ water for use in the PCR reaction.

2. In a separate tube TaqMan master mix and TaqMan primer and probe mix for the gene of interest were added in the following concentration:

Component	**Volume**
2X TaqMan master mix	2.5 µl
TaqMan Primer-probe	0.25 µl
RNase free water	To 4 µl

3. 1µl of diluted cDNA (10ng/µl) was added to the TaqMan master mix and primer + probe mix and this whole mixture was added to a well of 396 well real time PCR plate.

4. In 1 of the sample TaqMan master mix and primer + probe is mixed with RNase free water instead of cDNA. Ct value from this well was used as non template control to detect any contamination or non specificity in the reaction.

5. GAPDH gene was used as an endogenous control.

6. For each sample and gene, reaction was carried out in triplicate and average Ct value was used to determine fold change.

7. After addition of reaction in different wells, PCR plate is sealed.

8. The plate was centrifuged briefly to remove any air bubble and to bring the mixture at the bottom of the well.

9. The real time PCR was performed using following PCR protocol:

PCR step	Temperature	Time
Initial denaturation	95°C	5 min
Denaturation	95°C	45 sec
Primer annealing	60°C	45sec
Primer Extension	72°C	45sec
Final extension	72°C	5 min
Hold	72°C	5 min

21. Western blot analysis

Preparation of sample

1. Cells were washed with cold 1X PBS (2x) in 6-well plate.

2. 50µl of RIPA buffer was added to cells and plate was incubated on ice for 5 minutes.

3. Cells were gently scraped using cell scraper and collected in an ice cold eppendorf tube.

4. Cells were vortexed vigorously for 30 seconds.

5. Cells were incubated on ice for 2 hours on ice with intermediate vortexing.

6. The lysed cells were then sonicated at 10% amplitude for 10 seconds for 3 cycles.

7. Lysed cells were centrifuged at 14,000 rpm 4°C for 45 minutes.

8. The supernatant was collected and stored at 4°C.

9. Protein estimation was done using the above lysate.

Protein estimation by Bradford assay: Bradford is a colorimetric protein assay based on the absorbance shift of the dye Coomassie Brilliant Blue G-250 in which under acidic conditions the red/brown form of the dye is converted into its bluer form to bind to the

protein being assayed. This color change is estimated by using the formula obtained by plotting the absorbance of standards (1-5 µg/ml) in a linear regression analysis.

Protocol:

1. BSA standards were made by serially diluting 1mg/ml stock in transparent 96 well flat bottom plates.

Concentration	**Volume of BSA**	**Volume of miliQ water**
Blank	0 µl	5 µl
1µg	1 µl	4 µl
2µg	2 µl	3 µl
3µg	3 µl	2 µl
4µg	4 µl	1 µl
5µg	5 µl	0 µl

2. Absorbance was measured at 595nm, values were subtracted against the blank and a standard curve was plotted by using the linear regression analysis. The formula derived from the standard curve was used for estimating protein concentration of the cell lysates.

3. Lysates were diluted 5X using 1X PBS.

4. 250µl of Bradford reagent was added in each well of a 96 well plate.

5. 5µl of protein lysate was added per well and mixed thoroughly.

6. Absorbance was measured at 595nm in a spectrophotometer.

7. Protein concentration was calculated using the formula derived from the standard curve. Appropriate volume of protein lysate for the desired concentration was taken and mixed with gel loading dye. The reaction mix was heated at 37°C for 30 minutes in water bath and a short spin was given. The samples were kept on ice until they were loaded on the gel.

Protocol:

1. Glass plates were cleaned thoroughly and were set up carefully in the casting stand.

2. According to the protein of interest, the required percentage of resolving gel was prepared.

3. Immediately the resolving gel solution was loaded between the glass plates using the pipette and the gel was overlaid with 1ml of miliQ.

4. The gel was allowed to polymerize for 35-40 minutes.

5. After the resolving gel was solidified completely, the miliQ layer was washed thoroughly and the stacking gel was prepared.

6. The wells for loading the samples were formed by placing the 10-well comb. The gel was allowed to polymerize for 15-25 minutes.

7. The solidified gel was placed in the cassette and fitted with electrodes in the tank.

8. The tank was filled with 1X running buffer till $(1/4)^{th}$ of its volume. The comb was then gently removed and the wells were washed with the buffer to remove the traces of any acryl/bisacrylamide deposits.

9. The sample prepared was then loaded into respective wells and 4 µl of pre-stained ladder was also loaded in one of the wells.

10. The gel electrophoresis was performed at 60V, 400mA. After the sample entered the resolving gel the voltage was increased to 80V. The run was stopped as soon as the dye reached the bottom of the gel.

11. The gel, blotting paper and nitrocellulose membrane were then soaked in 1X transfer buffer and incubated for 10 minutes.

12. Onto the base of the Trans blot system the two soaked blotting papers were placed one after another, the transfer buffer was poured on top of the membrane and the air bubbles were removed carefully. Then, the nitrocellulose membrane was placed and the gel was placed over it properly.

13. The remaining two blotting papers were placed on the top of the gel and same as before the transfer buffer was poured, ensuring that the bubbles were removed. Then, the system was started and the transfer was set to 13V, 400mA for 1 hour.

14. After complete transfer the membrane was removed carefully and then incubated in 10ml of 5% non-fat milk for 1 hour on a shaker.

15. After blocking, the membrane was probed with NIS primary antibody and incubated overnight at 4 °C with gentle shaking.

16. Next day, the membrane was washed thrice with the wash buffer (1X TBST) and then incubated with the secondary antibody for 1 hour.

17. After the secondary antibody incubation the membrane was again washed thrice with the wash buffer.

18. The proteins present on the membrane could be visualized by using the advance chemiluminescence detection system.

Stripping and reprobing of the membrane:

1. In order to reprobe the membrane with another primary antibody, stripping protocol was used.

2. For stripping, the membrane was incubated with the stripping buffer for 10 minutes at RT.

3. The membrane was then washed thrice with 1X TBST, blocked with the blocking buffer for 1 hour, then incubated with primary antibody overnight at 4 °C with gentle shaking.

4. The next day, the membrane was again washed with 1X TBST, incubated with secondary antibody for 1-2 hours at RT with continuous shaking and then washed with wash buffer and developed in dark with the ECL detection system.

Component	10% Resolving gel (10ml)	4% Stacking gel (3ml)
miliQ	4.1 ml	1.82 ml
30% acrylamide solution	3.3 ml	0.4 ml
1.5M Tris pH8.8	2.5 ml	-
0.5M Tris pH6.8	-	0.75 ml
10% SDS	0.1 ml	0.03 ml
10 % APS	50 µl	15 µl
TEMED	5 µl	2 µl

10 X Running buffer pH 8.3

Component	
Tris base	15.15 g
Glycine	72 g
SDS	5 g
Dissolve the components and bring the final volume to 500 ml. Store at 4 °C.	

10 X Transfer buffer

Component	
Tris base	36.3 g
Glycine	144 g
SDS	3.7 g
Dissolve the components and bring the final volume to 1000 ml. Store at 4 °C. 20% methanol is added freshly in 1X transfer buffer before use.	

22. Chromatin immunoprecipitation assay:

Chromatin Immunoprecipitation (ChIP) assays are used to evaluate the association of proteins with specific DNA regions. The technique involves cross-linking of proteins with

DNA, fragmentation and preparation of soluble chromatin followed by immunoprecipitation with an antibody recognizing the protein of interest. The segment of the genome associated with the protein is then identified by PCR amplification of the DNA in the immunoprecipitated.

A- Cross-linking and cell harvesting

1. In control and Dox treated breast cancer cell lines ($1x10^7$- $5x10^7$ cells per $10cm^2$ dish), cross-linking of proteins to DNA was performed by adding formaldehyde to the media to a final concentration of 0.75% v/v (203 µl of 37% formaldehyde for 10 ml media). The plates were rotated gently at room temperature for 10 minutes.
2. Glycine was to a final concentration of 125 mM to the media and the plates were incubated with shaking for 5 minutes at RT.
3. Cells were rinsed 2 X with 10 ml cold PBS.
4. Cells were scraped into 5 ml cold PBS and transferred into 15 ml tubes.
5. 3-5 ml PBS was added to dishes and the remainder of the cells was transferred to the 15 ml tubes.
6. The cell suspension was centrifuged for 5 minutes, 1,000 g at $4^{\circ}C$.
7. Supernatant was carefully aspirated off and pellet was resuspended in ChIP Lysis Buffer (750 µl per $1x10^7$ cells).

Composition of ChIP lysis buffer (FA lysis buffer):

Component	**Volume**
0.1M HEPES-KOH	2.5 ml
4M NaCl	1750 µl
0.5M EDTA pH8	10 µl
0.1% Na-deoxycholate	50 µl
0.1% SDS	50 µl
Protease inhibitors	50 µl (to be added freshly)
miliQ	640 µl

B- Sonication

1. Cells were incubated on ice for 10-15 minutes.
2. Lysates were sonicated to shear DNA to an average fragment size of 200-1000 bp. The sonication conditions were standardized to 9 cycles of 60 sec ON/60 sec OFF using Bioruptor sonicator.
3. After sonication, cells were pelleted by centrifugation for 1 minute, 4˚C, 8,000 g. supernatant was transferred to a new tube. This chromatin preparation was used further for the immunoprecipitation (IP).
4. 50 µl of each sonicated sample was removed. This sample is the INPUT and is used to quantify the DNA concentration as a control in the PCR step.

In order to check the fragmentation, cross-links were reversed by Heating the samples at 65˚C for 4-5 hours. After a short spin, samples were loaded on 1.5% agarose gel to confirm the size of sheared DNA. The sonicated chromatin can be snap frozen in liquid nitrogen and stored at -80˚C for up to 2 months. Avoid multiple cycles of freeze thaw.

C- Immunoprecipitation

1. Chromatin containing approximately 25 µg of DNA was used for immunoprecipitation (IP) reaction.
2. Each sample was diluted 1:10 with IP Dilution Buffer.
3. 5 µg of p53 primary antibody was added to all samples except the beads only control incubated on a rotating platform for 12–16 hours at 4˚C.

Preparation of protein G beads with single-stranded herring sperm DNA. Protein G beads were washed 3X in IP Dilution Buffer. IP Dilution Buffer was removed and single stranded herring sperm DNA was added to a final concentration of 75 ng/µl beads and BSA was added to a final concentration of 0.1 µg/µl beads. IP Dilution Buffer was added to twice the bead volume and incubated for 30 minutes with rotation at RT. Beads were washed once with IP Dilution Buffer and IP Dilution buffer was added to twice the bead volume.

IP dilution buffer (10ml):

Component	**Volume**
4M NaCl	1250 µl
1M Tris pH7.5	200 µl
10M NaB	20 µl
0.5M Na_2-EDTA	500 µl
miliQ	9155 µl

4. The protein G beads were centrifuged for 1 minute, 2,000 g and the supernatant was removed.

5. The beads were washed 3X with 1 ml Wash Buffer and centrifuged for 1 minute, 2,000 g at 4˚C.
6. The beads were washed 1X with 1 ml Final Wash Buffer and centrifuge for 1 minute, 2,000 g at 4˚C.

	Wash buffer (10 ml)	**Final Wash buffer (10ml)**
10%SDS	100 µl	100 µl
Triton X	100 µl	100 µl
0.5M EDTA pH8	40 µl	40 µl
4M NaCl	375 µl	1250 µl
1M Tris pH8	200 µl	200 µl
miliQ	8285 µl	7410 µl

D- Elution and reverse cross links

1. DNA was eluted by adding 120 µl of Elution Buffer to the protein G beads and rotated for 15 min, 30˚C.

2. The samples were centrifuged for 1 min 2,000 g, and the supernatant was transferred into a fresh tube. The samples can be stored at -20˚C.

3. 80 µl of Elution Buffer was added to each sample. 2 µl of RNaseA was added to a final concentration of (0.5mg/ml). The samples were heated at 65˚C overnight or 4-5 hours.

4. The DNA can be purified using a PCR purification kit (ABI, Invitrogen Miniprep Kit).

5. 500 µl of wash buffer W10 with ethanol was added to each tube and sample was transferred to column and the column was centrifuged at 14,000 rpm for 1 minute.

6. Flow-through was discarded. 500 µl of wash buffer W9 with ethanol was added to each tube. The columns were centrifuged at 14,000 rpm for 1 minute.

7. The same step was repeated to give one more dry spin to the sample.

8. The columns were placed in the new tubes and DNA was eluted with 40 µl of pre-heated miliQ. After 10 minutes of incubation, columns were centrifuged at 14,000 rpm for 2 minutes.

9. DNA levels were quantitatively measured by semi-quantitative PCR using primers listed in **Table 3.4**.

Composition of Elution buffer (1ml):

Component	**Volume**
10% SDS	10 µl
1M $NaHCO_3$	100 µl
miliQ	890 µl

23. Transcription factor profiling array

Principle:

Signosis' TF activation profiling plate array is used for monitoring the activation of multiple TFs simultaneously. In this technology, a series of biotin-labeled probes are made based on the consensus sequences of TF DNA-binding sites. When the probe mix incubates with nuclear extracts, individual probes will find its corresponding TF and form TF/probe complexes, which can be easily separated from free probes through a simple spin column purification method. The bound probes are detached from the complex and analyzed through hybridization with a plate; each well is specifically pre-coated with complementary sequences of the probes. The captured DNA probe is further detected with streptavidin-HRP. Luminescence is reported as relative light units (RLUs) on a microplate luminometer.

Alternatively, Promoter-binding TF profiling assay is a competition of Signosis' TF activation profiling plate array. In this assay, PCR fragment containing promoter of interest is

mixed with a set of biotin-labelled oligos corresponding to 96 TFs along with an assayed sample. If the DNA fragment contains a TF binding sequence, it will compete with the biotin-labeled oligo to bind to the TF in the sample, leading to no or less complex formation and no or lower detection. Through comparison in the presence or absence of the competitor plasmid or DNA fragment, promoter TFs can be identified.

Nuclear extracts were isolated for the assay using following protocol:

1. Control and HDACi treated cells were collected, washed with PBS and centrifuged at 2000 rpm for 5 minutes.
2. 5X PCV (5 times packed cell volume) of Cytoplasmic extraction (CE) buffer was added to the cell pellet (max volume upto 300 µl) containing protease inhibitors and mixed by vortexing.
3. The cells were incubated on ice for 10 minutes with intermediate vortexing. After 10 minutes, 0.3% NP40 was added and cells were vortexed continuously for 10-20 seconds.
4. The cells were centrifuged at 3000 rpm at 4˚C for 20 minutes. The supernatant obtained is the cytoplasmic fraction.
5. The cell pellet was washed with 1ml of CE buffer without protease inhibitors for 3-4 times. Cells were centrifuged at 3000 rpm at 4˚C for 5 minutes each time.
6. To the nuclei pellet, 1X PCV of Nuclear Extraction (NE) buffer with protease inhibitors was added and incubated on ice for 10 minutes with intermediate vortexing.
7. The mixture was centrifuged at 14,000 rpm for 20 minutes at 4˚C. The supernatant collected is the nuclear extract.

The nuclear extracts were checked for their quality and used further for the TF assay.

	CE buffer	**NE buffer**
1M HEPES pH 7.9	50 µl (10mM)	100 µl (20mM)
2M KCl	25 µl (10mM)	-
5M NaCl	-	400 µl (0.4M)
0.5 M EDTA	1 µl (0.1mM)	10 µl (1mM)
Glycerol	-	1.25 ml (25%)
Distilled water	Upto 5 ml	Upto 5 ml

A.TF-DNA complex formation

1. The following were mixed in a PCR tube:

Component	**Volume**
TF binding buffer mix	15 µl
TF probe mix II	5 µl
Nuclear extract (5-15µg)	X µl
ddH2O	To 30 µl

in case of promoter binding assay, 0.1-0.5 µM PCR amplified promoter DNA was added in the reaction mix.

2. The mix was incubated at RT for 30 minutes.

B. Separation of TF-DNA complexes from free probes

1. Isolation column was equilibrated by adding 200 µl cold filter binding buffer. It was centrifuged at 6000 rpm for 1 min at RT.

2. The reaction mix was loaded onto equilibrated column and incubated on ice for 30 minutes.

3. 500 µl of cold filter wash buffer was added to the column and incubated for 2-3 minutes on ice. The column was centrifuged at 6000 rpm for 1 minute at 4˚C. Flow through was discarded.

4. The column was washed similarly for four times more in a similar way.

C. Elution of the bound probe

1. 100 µl of elution buffer was added to the center of the column and incubated at RT for 5 minutes.

2. The column was put in fresh 1.5ml tube and centrifuged at 10,000 rpm for 2 minutes at RT.

3. In another 1.5ml tube, 500 µl of ddH_2O was chilled by keeping the tube on ice at least for 10 minutes.

4. The eluted probes were transferred to a PCR tube and denatured at 98 ˚C for 5 minutes.

5. The denatured probes were immediately transferred to the chilled ddH_2O and placed on ice. The samples can be used for hybridization.

D- Hybridization of the eluted probe with hybridization plate

1. The sealing film of the hybridization plate was removed.
2. 10 ml of pre-warmed hybridization buffer was added to a dispensing reservoir (DNase free) and 600 µl of denatured probes were mixed by gentle shaking.
3. 100 µl of the mixture was dispensed immediately into the corresponding wells with multi-channel pipette. (For a blank well, 1X hybridization buffer was added without eluted probe)
4. The wells of the plate were sealed securely with foil film and the plate was hybridized at 42 ˚C for overnight.

E- Detection of the bound probe

1. The plate was inverted over an appropriate container and the contents were expelled forcibly. The plate was washed thrice by adding 200 µl of pre-warmed 1X plate hybridization buffer to each well.
2. The liquid was removed completely at each wash by firmly tapping the plate against clean paper towels.
3. 200 µl of blocking buffer was added and the plate was incubated for 15 minutes at RT with gentle shaking.
4. The plate was inverted to remove the blocking buffer. 20 µl of streptavidin-HRP conjugate was added in 10 ml blocking buffer (1:500 dilution), enough for two plates. 95 µl of diluted streptavidin-HRP conjugate was added to each well and incubated for 45 minutes at RT with gentle shaking.
5. The plate was washed with 200 µl of 1X detection wash buffer for 5 minutes. Two additional washes were given similarly. The liquid was removed completely at each wash by firmly tapping the plate against clean paper towels.
6. The substrate solution was freshly prepared by adding 1 ml substrate A, 1 ml substrate B and 8 ml substrate dilution buffer. 95 µl of substrate solution was added to each well and the plate was incubated for 1-5 minutes. The reading was taken in the luminometer within 5-20 minutes (integration time 1 second, no filter position).

24. Clonogenic assay

1. After HDACi/ ^{131}I therapy, cells were trypsinized, washed with 1X PBS and counted in a cell counter.

2. 1000 cells/well were seeded in 6 well plate in duplicates.

3. Cells were then incubated in 5% CO_2 at 37°C for 14 days.

4. Cells were fed with fresh media at duration of 3 days.

5. After 14 days, cells were washed thrice with PBS for 5 minutes and fixed in 1ml chilled formalin i.e. 10% formaldehyde in PBS for 20 minutes at 4°C.

6. Formalin was removed after 20 minutes and cells were washed with 1XPBS (X3).

7. After washing cells were stained with 1ml of 0.5% crystal violet in 25% methanol for 5 minutes at room temperature.

8. After 5 minutes, crystal violet was removed and excess stain was washed with fresh water.

9. Number of colonies were counted under microscope. Colonies consisting of at least 50 cells were counted.

10. Survival fraction was calculated using the formula mentioned in previous literature.

25. Luciferase assay

The luciferase reporter assay is commonly used as a tool to study gene expression at the transcriptional level. Luciferases make up a class of oxidative enzymes found in several species that enable the organisms that express them to "bioluminescence" or emit light. The light emitted is a by-product of the oxidative reaction catalyzed by the luciferase enzyme. The protocol is as follows:

1. Transfected cells were collected and lysate was made by passive lysis buffer.

2. 10µl of lysate was added in each well. Lysate from untransfected cells was used as negative control.

3. 50µl of LAR2 was added to each well and photons generated were measured in a Berthold luminometer in open filter for 1 second.

4. The relative light unit per second (RLU/sec) obtained was normalised with protein estimated by Bradford method.

Preparation of lysates

1. 1-2×10^6 cells were harvested after trypsinization by centrifugation at 1200 rpm for 5minutes at 4˚C.

2. The cell pellet was washed with 1X PBS by centrifugation at 1200 rpm for 5 minutes.

3. Supernatant was discarded and approximately 50µl of 1X passive lysis buffer/1×10^6 cells was added.

4. Thereafter, 1µl of 10X protease inhibitor per 100µl of 1X passive lysis buffer was added in the cell lysate.

5. The reaction was thoroughly mixed by vortexing and incubated at RT for 10-15 minutes.

6. After incubation the reaction mixture was centrifuged at 13,000 rpm for 25 minutes at 4˚C.

7. The supernatant was collected and protein estimation was performed using Bradford reagent.

26. Immunohistochemistry of mouse tissue tumor sections

Composition of TBS: 500mM Tris base, 1500mM NaCl. Dissolve in 800ml autoclaved water. Adjust the pH 7.5 with HCl. Make up the volume to 1L. (10X buffer stock was made and diluted to 1X for use) (10X buffer stock was made and diluted to 1X for use)

Protocol :

1. 5µm sized tissue sections were obtained in poly L-lysine coated slides.

2. Slides containing tissue sections were incubated at 60˚C for overnight.

3. Next day tissue sections were deparaffinized by 3 washes of xylene for 10 minutes each at room temperature.

4. Tissue sections were air dried to remove remaining xylene and rehydrated with subsequent washes of alcohol from 100% to 90% and then to 75%.

5. Slides were washed under tap water for 15 minutes.

6. Next, endogenous peroxidase activity was quenched with 3% H_2O_2 in methanol for 30 minutes in dark at room temperature.

7. Tissues were then subjected to antigen retrieval using 10 mM sodium citrate. For antigen retrieval sections were heated in sodium citrate solution serially at 850, 650 and 340 mega watts, each for 3 minutes. Tissues were kept for cooling till they come to room temperature.

8. After the antigen retrieval, sections were washed with TBST (0.01% Tween 20) twice each for 5 minutes at room temperature.

9. Tissues were then blocked with 5% BSA for one hour at room temperature.

10. As the tumor tissues were of mouse origin and primary antibody is also raised in mice, an additional step of blocking with mouse serum was performed before staining with the primary antibody.

11. Slides were then incubated at 4°C overnight with the mouse monoclonal antibody against NIS diluted with TBS in 1:50 ratio.

* For secondary control a tissue section was incubated with TBS instead of NIS antibody.

12. Slides were then washed for 5 minutes in TBST, 3 times and incubated for 1 hour with HRP conjugated anti mouse antibody diluted with TBS in 1:200 ratio.

13. Tissue sections were washed with TBST for 3 times, 5 minutes each.

14. After washing, tissues were incubated with DAB (1:30) (3, 3'-diaminobenzidine tetra hydrochloride) till the appearance of brown staining

15. Tissues were immediately washed under tap water.

16. Sections were further dehydrated with graded alcohol and xylene. For each batch of sample staining, a papillary thyroid carcinoma case was kept as positive control for NIS expression.

17. All the slides were counter stained with hematoxylin.

18. Slides were DPX mounted and observed under light microscope (Carl Zeiss).

27. *In vivo* bioluminescence imaging in living mice

BLI allows a non-invasive and real time analysis of biological processes at the molecular level in living organisms. We measured *in vivo* bioluminescence by Cooled charge-coupled device (CCD)-based Xenogen IVIS 200 biophotonic imager from Caliper (Alameda, CA.). The system excels at imaging light emitted from small animals such as mice or rats but can also be used to image light emitted directly from cells in 96-well plates. The system is capable of measuring the intensities of BL signals produced by luciferases and other bioluminescent reporters, as well as fluorescence signals produced by fluorescent proteins (GFP, RFP, etc.) and other fluorescent molecules. The output is generally a superimposed image of photographic and luminescence/fluorescence image captured sequentially.

Cell preparation:

The cells were cultured in standard growth conditions and amplified in amount required for implantation in specific number of mice. While amplification, cells were always maintained in log phase, which means they were never more than 70-80% confluent. An *in vitro* validation of the bioluminescence activity was performed earlier by *in vitro* luciferase assay.

Animal injection:

1. From a 70-80% confluent flask cells were harvested by trypsinisation and counted using trypan blue.

2. 6×10^6 cells per mouse were used for implantation. Accordingly total number of live cells required were counted and pelleted down. The pelleted cells were then resuspended in PBS in a concentration of 6×10^6 cells/50-100 µl PBS.

3. Usually, in order to facilitate optimal formation of tumor athymic immunocompromised mice were preferred for implantation. Animal care and euthanasia were performed with the approval from Institutional Animal Ethics Committee of ACTREC. Cells were implanted subcutaneously in the right flank of the mice.

Animal anesthesia:

1. The mice were placed into a clear plexiglass anesthesia box that allows visual monitoring of mice to realize the effect of anesthesia. The release of isofluorane can be adjusted from 1-5% according to the weight and number of mice.

2. The tube that supplies the anesthesia to the box is split so that the same concentration of anesthesia is pumped to the anesthesia manifold located inside the imaging chamber.

3. After the mice were fully anesthetized, they were transferred to the imaging chamber with their snout placed to the nose cones attached inside and close the door.

Preparation and injection of D-luciferin:

1. A fresh stock solution of D-luciferin 30 mg/ml in PBS was prepared.

2. Each mouse was injected with 100 µl of 30 mg/ml of D-luciferin (to deliver 3 mg).

3. D-luciferin solution was injected via an intraperitoneal (i.p.) route and substrate was allowed to distribute in animals for about 5–15 minutes.

Image acquisition and data analysis:

1. As per manufacture's recommendation, the IVIS system was initialized before starting image acquisition.

2. Animals were placed inside the black box imaging chamber and postured with the imaging surface facing the camera. This is important to minimize the path length of the luminescent light through different tissues/organs.

3. Now, on the IVIS software, different parameters were set, such as integration time, bin, FOV, and emission filter. Integration time can range from 10 seconds to 5 minutes depending

upon the cellular luciferase expression. Bin is generally set medium, which balances between sensitivity and resolution of the CCD camera. Depending upon number of mice scanned at a time, the FOV can be set at higher or lower range.

4. Images were acquired by clicking the "acquire image" button on the displayed screen. After the acquisition is over, a superimposed image of the photographic view and the pseudo color luminescence image will appear on the screen.

5. Images were acquired in sequence till increase in the luciferase activity is observed. For data analysis image with the maximum luciferase activity was used to quantitate activity.

6. For data analysis, ROI was drawn by clicking on the "create ROI" button and by clicking on the measure button photon values were measured.

28. *In vivo* Cerenkov imaging in living mice

CLI is an emerging hybrid modality in which light emitted from commonly used medical isotopes is used for generation of signal. Cerenkov radiation has been described before 100 years but its application for biomedical imaging purpose is known since past few years only. The modality is of great interest as it allows use of commonly used BLI equipments for visualization of clinical diagnostic (all PET radioisotopes) and many therapeutic radionuclides. The disadvantage is that the signal intensity generated is significantly lower than that in other optical imaging techniques such as bioluminescence and fluorescence. However, significant advantages include the use of approved radiotracers and lack of an incident light source, resulting in high signal to background ratios.

^{131}I injection:

1. 10 days prior to ^{131}I therapy thyroid blocking was initiated by daily dose of T4 and methimazole by intra peritoneal injection.

2. On the day of treatment ^{131}I present in the vial was measured by gamma counter and volume required for 1mCi ^{131}I was calculated.

3. 1mCi ^{131}I was removed from the vial to the syringe. Each animal in the treated group was injected with 1mCi ^{131}I.

4. The radioactivity in the syringe was further measured to ensure the amount of radioactivity injected in mice.

5. Before removing the mice from cage the working area of the hood was covered with spread sheet. This was done to reduce the risk of contamination with radioactivity.

6. All the mice in the treated group were administered with intra peritoneal injection of 1mCi of ^{131}I.

* Note: All the radioactivity experiments were performed with extreme care to avoid any spillage or contamination through radioactivity. While handling radioactivity body was covered with full sleeves apron, mask and double gloves. TLD batch was constantly worn during the radioactivity experiments and to check contamination all the area was inspected with dosimeter after the experiments.

Animal anesthesia:

Animal anesthesia was given in the same way as mentioned in the section except that a sheet was spread to the floor of the anesthesia chamber to avoid contamination.

Cerenkov image acquisition:

1. Cerenkov imaging was performed after 24 and 72 hours of ^{131}I administration.

2. Imaging was performed in the same way as the BLI. For Cerenkov imaging images were acquired by keeping dorsal as well ventral surface facing the camera to understand the distribution of ^{131}I.

*Note: To avoid radioactivity contamination a black paper is placed at the base of the IVIS chamber to keep the mice and the paper is thrown into the radioactive discard after the experiment.

Publications

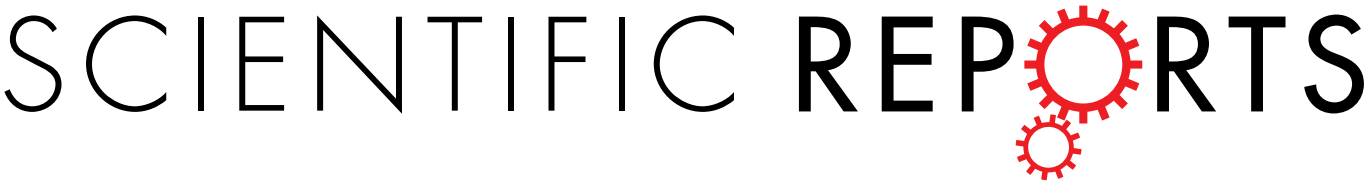

OPEN

Received: 23 June 2015
Accepted: 02 December 2015
Published: 18 January 2016

Enhancement of human sodium iodide symporter gene therapy for breast cancer by HDAC inhibitor mediated transcriptional modulation

Madhura G. Kelkar[1], Kalimuthu Senthilkumar[2], Smita Jadhav[1], Sudeep Gupta[3], Beyong-Cheol Ahn[2] & Abhijit De[1]

The aberrant expression of human sodium iodide symporter (NIS) in breast cancer (BC) has raised the possibility of using targeted radioiodide therapy. Here we investigate modulation of endogenous, functional NIS expression by histone deacetylase inhibitors (HDACi) *in vitro* and *in vivo*. Luciferase reporter based initial screening of six different HDACi shows 2–10 fold enhancement of NIS promoter activity in majority of the cell types tested. As a result of drug treatment, endogenous NIS transcript and protein shows profound induction in BC cells. To get an insight on the mechanism of such transcriptional activation, role of Stat4, CREB and other transcription factors are revealed by transcription factor profiling array. Further, NIS-mediated intracellular iodide uptake also enhances substantially ($p < 0.05$) signifying functional relevance of the transcriptional modulation strategy. Gamma camera imaging confirms 30% higher uptake in VPA or NaB treated BC tumor xenograft. Corroborating with such functional impact of NIS, significant reduction in cell survival ($p < 0.005$) is observed in VPA, NaB or CI994 drug and ^{131}I combination treatment *in vivo* indicating effective radioablation. Thus, for the first time this study reveals the mechanistic basis and demonstrates functional relevance of HDACi pre-treatment strategy in elevating NIS gene therapy approach for BC management in clinic.

The current focus for development of targeted strategies in breast cancer (BC) is actively being researched to identify suitable therapy procedures that can eliminate BC cells with high specificity while minimizing the side effects. In this context, the aberrant over-expression of human sodium iodide symporter (NIS) protein in breast cancer tissue is gaining great deal of attention. Being a member of the solute carrier transporter (SLC5A5), NIS is an intrinsic plasma membrane glycoprotein that mediates active iodide transport in thyroid follicular cells. NIS mediated iodide transport is also seen in extra-thyroidal tissues such as salivary gland, gastric mucosa and lactating mammary tissue where NIS is differentially regulated or subjected to distinct post-translational modifications that are not entirely understood[1,2]. As an endogenous protein, NIS function can be visualized using gamma or positron emitting isotopes such as ^{99m}Tc, ^{125}I or ^{124}I respectively. The same protein can also be applied for therapy purposes using beta- or alpha-emitting isotopes like ^{131}I, ^{186}Re, ^{188}Re and ^{211}At[3,4]. Thus endogenous NIS-mediated radioiodide therapy is a gene-targeted, inexpensive method with relatively lesser side effects as can be revealed by years of practice in thyroid cancer clinic.

The pioneering study by Tazebay *et al.* showed aberrant over-expression of NIS in breast malignancies over normal breast tissue indicating its potential role for BC management[5]. Further study using ^{99m}TcO4 has confirmed functional NIS expression in human malignant mammary tissues[6]. NIS-mediated iodide uptake in BC metastatic nodules has also been confirmed by scintigraphic procedure while suppressing thyroidal iodide uptake using T3

[1]Molecular Functional Imaging Lab, ACTREC, Tata Memorial Centre, Kharghar, Navi Mumbai, India. [2]Department of Nuclear Medicine, Kyungpook National University, Republic of Korea. [3]Department of Medical Oncology, Tata Memorial Hospital, Parel, Mumbai, India. Correspondence and requests for materials should be addressed to A.D. (email: ade@actrec.gov.in)

Group	Compound	HDAC Targets	Potency (in cells)	Type of cancer	Clinical Trial	Reference
Hydroxymate	Trichostatin A (TSA)	Class I, II	Nano Molar	—	—	—
	Suberoylanilide hydroxamic acid (SAHA)	Class I, II	Micro Molar	CTCL	FDA approval for CTCL	32
	Tubastatin A (TBA)	HDAC6	—	—	—	—
Aliphatic acid	Valproic acid (VPA)	Class I & IIa	Milli Molar	Prostate cancer	Phase 2	33
	Sodium butyrate (NaB)	Class I & IIa	Milli Molar	Lung cancer	Phase 2	34
Benzamide	CI994	NA	Micro Molar	Pancreatic cancer	Phase 2	35

Table 1. Various HDAC inhibitors used in this study to check their effect on NIS expression. NA- Not Available. FDA- Food and Drug Administration. CTCL- Cutaneous T Cell Lymphoma.

and methimazole[7]. Culminating data from all these literatures indicate that NIS-mediated radioiodide imaging and therapy methods could potentially be used as an alternative approach or in combination with other existing methodologies towards management of the malignant breast disease. Recently our group has also reported analysis on BC subtype specific intensity profiling of NIS expression in a relatively large dataset[8]. The results revealed that while ~70% of the BC cases are positive for NIS expression, about 30% of NIS positive (2+ and 3+ score) cases showed intense staining equivalent to thyroid or salivary gland expression. Therefore, to use this gene-targeted radioiodide therapy in patients exhibiting moderate or low scores (i.e. lesser than 2+ score), defining ways to elevate this endogenous target expression can impact NIS based therapy procedure.

Various groups around the world have initiated research looking for ways to modulate endogenous target expression of NIS in thyroid, mammary or other tissue targets. NIS gene expression is differentially regulated in thyroid and breast tissue and potential regulators of NIS expression in breast tissue are not well characterized. Several groups have reported that NIS in BC cells can be induced *in vitro* using lactogenic hormones, insulin and even by some nuclear receptor ligands, such as retinoids and peroxisome proliferator-activated receptor-γ (PPARγ) ligands[2,9–11]. All-trans retinoic acid (atRA) alone or in combination with other glucocorticoids has been demonstrated to induce both NIS gene expression as well as iodide accumulation in MCF-7 cells and *in vivo* mouse model[12,13]. Even though these findings suggest their potential clinical use, to date preclinical or clinical efficacy is not yet proven.

Histone deacetylase inhibitors (HDACi) are known for exerting epigenetic control by regulating chromatin structure and gene expression. Additionally, HDACi can also modulate variety of cell functions such as growth, differentiation and survival by affecting non-histone proteins such as transcription factors, molecular chaperones and structural components[14,15]. Similarly, it is also repoted that NIS expression can be modulated by certain HDACi in thyroid cells even though their exact molecular mechanisms are not understood[16,17]. Very recently, reports have shown the effect of HDACi on BC cells as well[18,19]. Since NIS gene regulation in thyroid and breast tissue is differentially regulated, studying HDACi mediated modulation of NIS expression and function *in vivo* are of great interest. Thus, in the present study, we have performed a comprehensive investigation to reveal biochemical basis of HDACi mediated modulation of NIS expression and function in BC cell and animal model. The study implicates that epigenetic transcriptional modulation strategy as a promishing approach, which may be extended for clinical trial in near future.

Results

Pan-HDAC inhibitors representing various chemical classes enhance NIS promoter activity in breast cancer cells. Six different HDACi i.e. Trichostatin A (TSA), Sodium butyrate (NaB), Valproic acid (VPA), Suberoylanilide hydroxamic acid (SAHA) and Tubastatin A (TBA) representing various chemical classes (Table 1) were tested for NIS promoter transcription modulation in multiple BC cell lines. We have included receptor positive MCF-7 as well as receptor negative MDA-MB-231 cells over-expressing NIS promoter-reporter (pNIS-Fluc2.TurboFP) plasmid. The target effect of HDACi drugs was tested in MCF-7 cell line revealing increased histone H3 acetylation except for TBA, which is a known HDAC6 specific inhibitor[20] (Fig. 1A). Further the minimal drug dose requirement to promote NIS gene expression was determined by luciferase reporter assays against increasing concentration of each drug using the established MCF-7 cell line expressing pNIS-Fluc2.TurboFP (Supplementary Fig. 1). Cytotoxicity assessment was also done using a concentration dependent cell survival analysis of both MCF-7 and MDA-MB-231 cell lines (Supplementary Fig. 2). The same minimal drug concentration (~IC_{70} equivalent) was further used for all successive promoter regulation experiments. Candidate drug effects on engineered MCF-7 cells showed significantly higher Fluc2 expression as reveled by western blot analysis (Fig. 1B). Further, luciferase reporter activity also confirmed a 2–4 fold enhanced photon output in MCF-7 and a 1.4–2.4 fold increment in MDA-MB-231 cells (Fig. 1C,D). The fold gain in reporter activity upon drug treatment was found to be significantly higher ($p \leq 0.005$) when compared to the untreated control in these cells. The same reporter system was also tested by transient transfection method in two additional cell lines i.e. Zr-75-1 (hormone receptor positive) and MDA-MB-468 (hormone receptor negative) and similar trend of higher fold induction of normalized luciferase activity have been observed (Supplement Fig. 3A). The point to note here is that, of the various drugs tested, NaB, VPA and CI994 showed consistent gain in reporter activity across the cell lines. Inhibition with TBA, a HDAC6 specific inhibitor, showed around 1.5–2 fold gain in reporter activity in hormone receptor negative cell lines, while TSA and SAHA showed heterogeneous fold gain in reporter activity across all the cell types tested. Additionally, the NIS promoter specific effect of HDACi treatment was proven by

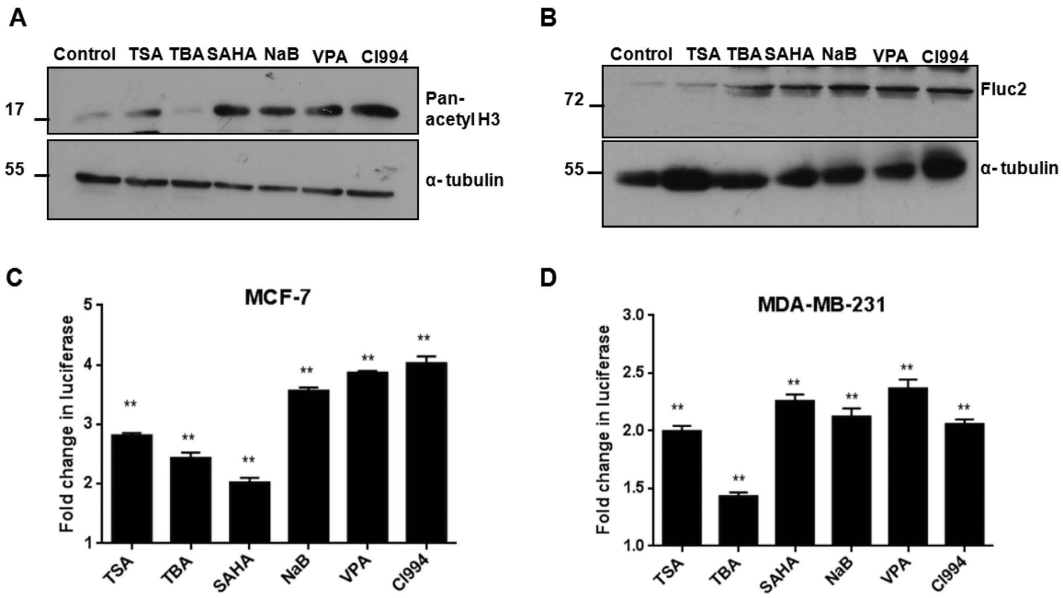

Figure 1. HDACi drugs significantly enhance human NIS promoter activity. (**A**) The target effect of HDACi on histone H3 acetylation in MCF-7 cells. Cells exposed to HDACi for 48 hours were assessed by western blotting using pan-acetyl-H3 monoclonal antibody and α-tubulin as loading control. (**B**) Western blot analysis of luciferase reporter induction using Fluc antibody in engineered MCF-7 pNIS-Fluc2.TurboFP cells. Full length western blots for the acetyl-H3 and Fluc2 were shown in supplementary Fig. 8A,B respectively. (**C,D**) Charts representing reporter signal fold change over untreated control (**indicates high significance $p < 0.005$, ns indicates non-significant) as a measure of NIS promoter activity upon HDACi treatment. Both MCF-7 and MDA-MB-231 engineered cells stably over-expressing pNIS-Fluc2.TurboFP reporter construct were exposed to various HDACi for 48 hours and luciferase activity was measured.

testing other ubiquitous promoters like CMV or chicken beta-actin promoter (CAG), where no radical change in reporter activity noted (Supplementary Fig. 4). Considering HDACi mediated up-regulation of NIS gene can have broader scope in thyroid and other cancer types, the possibility was tested by using several additional human cancer cell lines such as NPA and ARO (thyroid cancer), A2780 (ovarian cancer) and HT1080 (fibrosarcoma) over-expressing the pNIS-Fluc2.TurboFP plasmid. Candidate HDACi drug effects of SAHA, VPA and CI994 at 48 hours revealed that except for the CI994 in thyroid cancer cell lines, all other non-breast cancer cell lines showed significant increase in NIS promoter activity (Supplementary Fig. 3B). Together, these results suggest that the effect of HDAC inhibition may lead to NIS promoter activation by known mechanism of increased DNA binding ability, but for certain HDACi candidate the NIS promoter activation in breast cancer cells may happen through independent (or tissue-specific) activation of factors than their thyroid counterparts.

HDAC inhibition enhances endogenous NIS gene expression through Stat4, CREB and other transcription factors (TF) in breast cancer cells. Based on the results obtained from the reporter based system, we were encouraged to see if the same treatments corroborate in endogenous NIS activation. Therefore, we isolated cDNA from drug treated and untreated MCF-7, Zr-75-1, MDA-MB-231 and MDA-MB-468 cells and assessed NIS transcript using Taqman real-time PCR probe for human NIS and GAPDH as housekeeping control. As shown in Fig. 2A,B, each data point represents normalized transcript value relative to their untreated control. Overall, variable increment of NIS transcript (2–55 folds) was observed across all cell types tested ($p \leq 0.005$). In particular, NaB and VPA treatment showed highest fold change of NIS mRNA expression, while TBA treatment proved to be least effective. Point to be indicated here is that hormone receptor positive MCF-7 and Zr-75-1 cell lines showed much higher transcript levels (~3–10 fold) than the receptor negative cells (MDA-MB-231 and MDA-MB-468). Further, fold induction in NIS transcript expression under drug influence was also observed in the non-breast cancer cell lines NPA and ARO, HT1080 and A2780 (data not shown).

To gain further insight into the mechanisms leading to NIS up-regulation, bioinformatics analysis of the NIS promoter sequence using the Transfac and Genomatix softwares revealed the availability of ~64 putative transcription factor (TF) binding sites. Following this analysis, we performed TF activation array for 96 global TF signatures to identify differentially regulated TFs under NaB and VPA drug influence in MCF-7 cells and compared to the untreated cells. Of these 96 common TF candidates present in the array, ~56 candidates were found in common where at least one putative DNA binding site available on human NIS promoter. As revealed from the array data, HDAC inhibition by NaB markedly increased (>1.5 fold) expression of 7 TFs i.e. CREB, Stat4, Stat6, Sox9, Smuc, Nkx3.2 and E2F-1, whereas 5 others like XBP, MZF, HNF-1, Hox4C, and PLAG exhibited suppression (< -1.5 fold) (Fig. 2C). The same cell line when checked for VPA induced TF activation, 21 factors showed higher than 1.5 fold activation (Fig. 2D), but no significant suppression of any factor. Only Stat4 and E2F-1 were found to be activated in common with those under NaB influence.

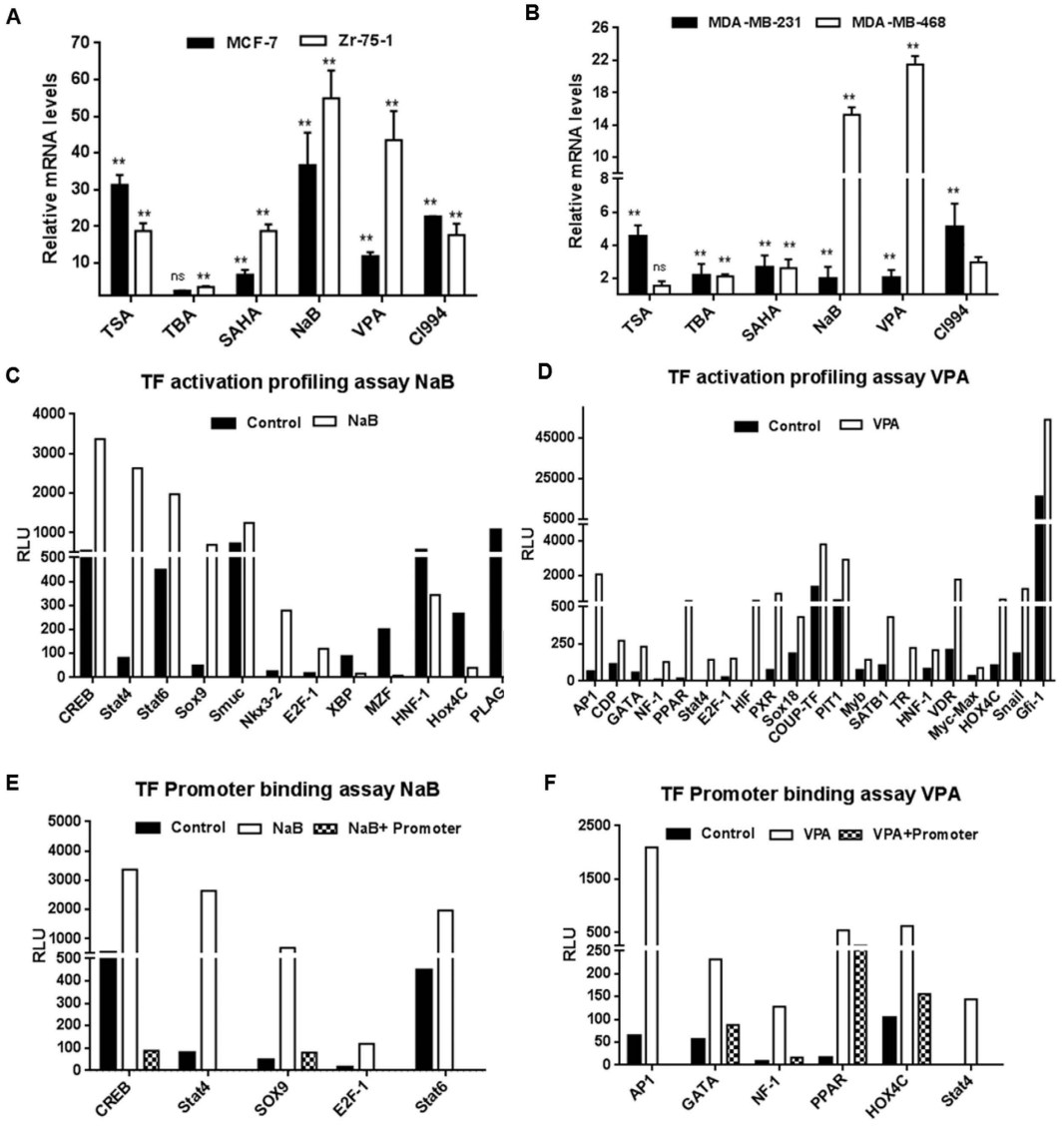

Figure 2. Induction of endogenous NIS transcript after HDACi treatment in BC cell lines. (**A,B**) MCF-7, MDA-MB-231, Zr-75-1 and MDA-MB-468 cells treated with different HDACi for 48 hours were evaluated for NIS mRNA by real-time PCR using ABI probe. Results were normalized for housekeeping gene GAPDH and presented as relative fold differences to untreated control (**indicates high significance $p < 0.005$, ns indicates non-significant). (**C,D**) Graphs showing activation of transcription factors (TFs) post NaB (**C**) or VPA (**D**) treatment in MCF-7 cell line. TFIID was used for normalization as per manufacturer's guideline. Candidate TFs showing greater or lesser than 1.5 folds difference in luminescence read-outs after normalization (threshold cut-off) were plotted. (**E**) Graph represents TF binders to human NIS promoter upon NaB treatment identified by promoter binding array. In comparison to drug treated nuclear extract samples, when NIS promoter is added, the luminescence read-out is lowered due to competitive binding to the promoter. Candidates like CREB, Stat4, Stat6, Sox9 and E2F-1 showed significant binding efficiency to the promoter. (**F**) TF binders identified such as AP1, GATA, NF-1, PPAR, Hox4C and Stat4 upon VPA treatment using the same array.

Further, the ability of TF binding to the NIS promoter was verified using promoter binding array where NIS promoter DNA was added in the plate together with the nuclear extract of MCF-7 cells treated or untreated with NaB (Fig. 2E) or VPA (Fig. 2F). Promoter binding array results confirmed that 5 of the 7 TFs bind under NaB treatment and for VPA treatment 6 out of 21 factors bind significantly to the NIS promoter. Stat4 was the only factor found in common that binds to the NIS promoter. Together these findings demonstrate possible role of TFs like Stat4, CREB, Nkx3.2, AP1 etc. majorly influence NIS expression in HDACi treated MCF-7 cells (summarized in Table 2).

HDAC inhibitor treatment significantly impacts NIS function in breast cancer cells. Taking the study more towards functional validation, first we have verified if enhanced endogenous NIS transcript under HDACi drug influence successfully translates into enhanced protein expression. A 2–3 folds increase in NIS

Transcription factor (TF)	Response to HDACi tested	Putative Binding Sequence on NIS promoter as per Transfac/Genomatix analysis	No. of sites	Involved in NIS induction in breast or thyroid cancer	Reference
CREB	NaB	gaagCGTGAccccc	5	Thyroid	27
AP1	VPA	cggTGACCCggga	1	ND	
GATA	VPA	ggcacTTATCa	6	ND	
NF-1	VPA	ctggcacaggGCCAAct	2	ND	
PPAR	VPA	accagaacctccAGAGgtcaaag	2	Thyroid	28
Hox4C	VPA	tggtctcCGCTtattcggg #	6	ND	
Stat4/Stat6	NaB, VPA	tcgaaTTCTGgga #	1	ND	
Sox9	NaB	aggagccAATGaatgaatgaatgaa #	2	ND	
E2F-1	NaB	gctgctcccgtaagccccaaGGCGacctc	1	ND	

Table 2. List of transcription factors that are activated and binding to NIS promoter after NaB/VPA treatment. #indicates presence of TF binding site belonging to family of TF i.e. Hox, Stat and Sox family of TFs respectively. ND- role in NIS regulation is not determined.

protein content was recorded in both MCF-7 and MDA-MB-231 cells after majority of the HDACi treatment except for TBA (Fig. 3A,B). Enhanced protein production was further evidenced by performing western blotting using human NIS monoclonal antibody (Fig. 3C). Using MCF-7 clonal cell lines, differentially over-expressing NIS protein either at the membrane or at the cytoplasm[21], we have also checked if the effect of NaB, VPA and CI994 drugs alter the NIS protein localization in cells (Fig. 3D). Together, these results suggest that except for HDAC6 specific inhibitor (TBA), other pan-HDAC inhibitors tested here can significantly induce endogenous NIS protein expression without influencing the protein localization in the cells.

As evidenced from many clinical literatures, high NIS mRNA or protein expression may not necessarily result in higher iodide uptake[22]. Therefore, we then verified the NIS functional modulation by HDACi treatment in cultured cells. BC cells treated with the same set of six HDACi were tested for their functional significance by iodide uptake assay. The all trans retinoic acid (atRA) was used as a known inducer of NIS function in breast cancer cell lines. In line of previous reports, we have recorded significant higher iodide uptake in MCF-7 and Zr-75-1 cells, but only a marginal increase in MDA-MB-231 cells after 24 hours of treatment with 1 μM atRA (Suppl. Fig. 5). Interestingly, the uptake in response to atRA reduces significantly at 48 hours. On the other hand, the perchlorate sensitive NIS-mediated iodide uptake increased up to 1.7–2.8 folds in MCF-7 and Zr-75-1 cell lines at 48 hours and it remain nearly unchanged at 24 hours of HDACi drug treatment. The iodide uptake in MDA-MB-231 cells was found to be much lower (Fig. 4A,C). When compared to the untreated cells, NaB, VPA, SAHA and CI994 treatment showed consistent and significant ($p < 0.05$) increase in iodide uptake in both MCF-7 and Zr-75-1 cells, and around 1.5–2 fold induction in uptake was noted with NaB, VPA and CI994 drug treatments in MDA-MB-231 cell line. TSA and TBA treatment resulted in marginal increase across all cell types tested. Further, as the steady-state accumulation is the net outcome of iodide uptake and iodide efflux, iodide retention time being another important parameter for achieving good therapeutic efficacy. Therefore, we performed iodide efflux assay using untreated and CI994 treated MCF-7 cells. Compared to the untreated cells, where 88% of accumulated iodide was released during first 10 minutes, CI994 treated cells showed similar 84% release in 10 minutes (Fig. 4D).

NaB/VPA/CI994 treatment augments ^{131}I mediated radioablation in breast cancer cells. Therapeutic efficacy of ^{131}I radioablation was verified in MCF-7, MDA-MB-231 and Zr-75-1 cell lines with variable endogenous NIS protein content and survival assessment was done by clonogenic assay (Fig. 4E–G). Since the judgment to make here is whether HDACi treatment affects survival fraction, first the minimal amount of ^{131}I required was determined. In case of MCF-7 and MDA-MB-231 50 μCi/ml and for Zr-75-1 100 μCi/ml was found to be sufficient for more than 75% cell survival. In comparison, drug treated cells when exposed to the same amount of ^{131}I, highly significant reduction in the cell survival ($p \leq 0.005$) was observed in all three cell lines. In the presence of perchlorate, HDACi and ^{131}I treated MCF-7 cells survived to a greater extent indicating NIS specific radioablation (Suppl. Fig. 6). The reduced survival percentage of cells against minimal ^{131}I radioactivity used further assures that enhanced iodide symporter function by HDACi pre-treatment can be proved to be useful for this gene therapy approach. We have also confirmed specific radiation injury caused in Zr-75-1 cells by staining for γ-H2Ax foci that forms due to DNA double strand break (Fig. 4H,I). Significant enhancement ($p \leq 0.01$) in the number of γ-H2Ax foci was observed in cells when they are treated with all three HDAC inhibitors than cells treated with radiation alone.

Low dose HDACi pre-treatment *in vivo* improves radiotracer uptake and ^{131}I therapy efficacy in breast cancer tumor xenograft. In order to validate our *in vitro* and cell culture findings, we performed noninvasive gamma camera imaging to first study the effect of NaB or VPA on NIS-mediated ^{99m}Tc-pertechnetate uptake in MDA-MB-231 xenograft model. The results reveal 30% higher accumulation of radiotracer in tumor in VPA treated cases than in vehicle control. These results indicate that a minimally toxic lower dose of NaB or VPA can effectively enhance NIS expression *in vivo* resulting in increased uptake value. Besides tumor uptake, high radiotracer uptake was also seen in tissues such as stomach and thyroid where NIS protein is naturally present for physiological reasons (Fig. 5A). Interestingly, treatment with NaB (500 mg/kg and 1000 mg/kg tested) shows higher ^{99m}Tc-pertechnetate accumulation in tumor but not in the thyroid of the mice (Fig. 5B,C). Similarly, by

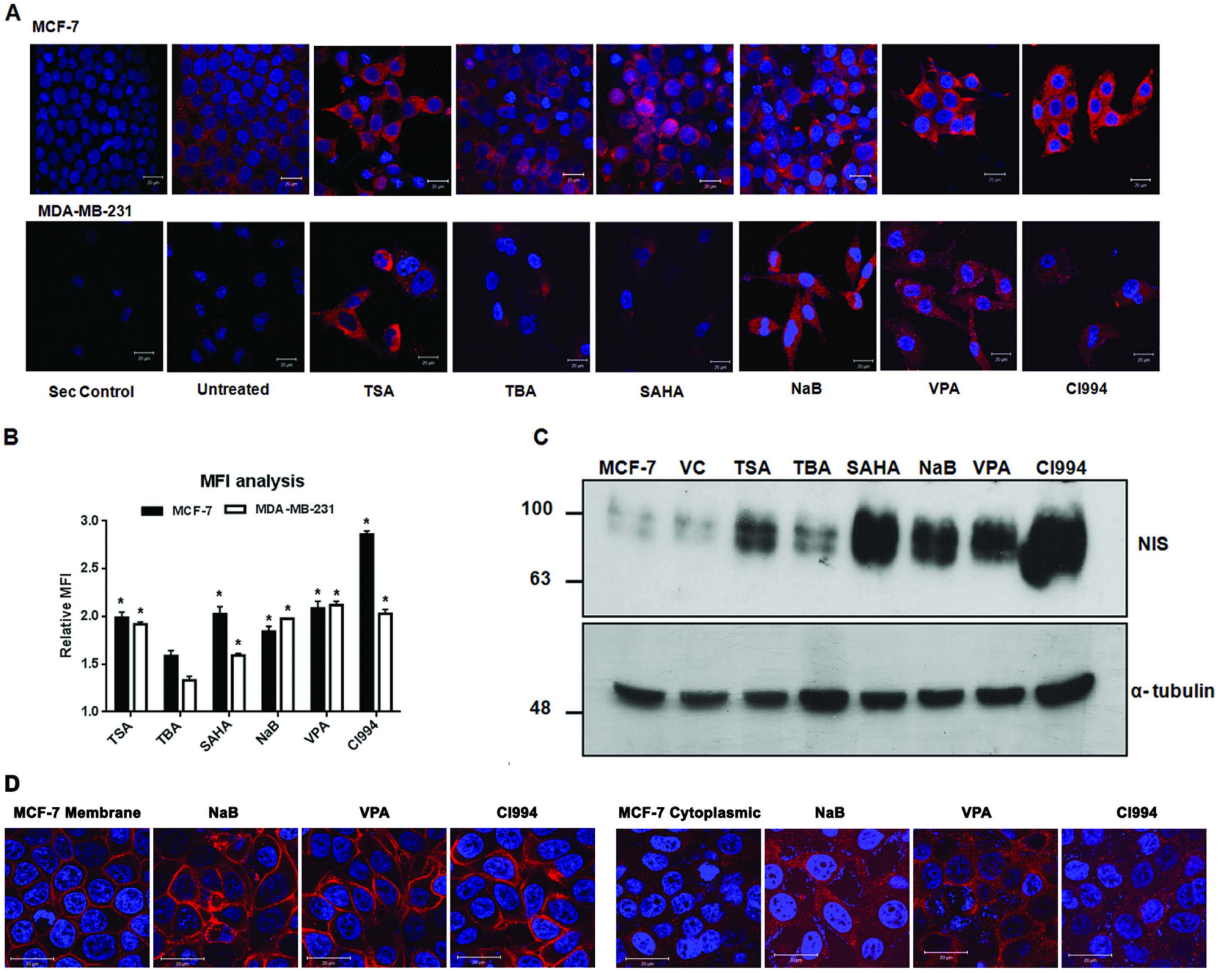

Figure 3. Enhancement of NIS protein by HDACi treatment in breast cancer cells. (A) Immunofluorescence photographs of MCF-7 and MDA-MB-231 cells showing marked increase in NIS protein content when treated with various HDACi. Drug treated and untreated cells were probed with NIS monoclonal antibody and detected with Dylight 633 secondary antibody (red). A secondary antibody control was also included in the study. Cell nuclei were cross stained using DAPI (blue). Scale bar represents 20 μm. **(B)** Graph showing fold increase in mean fluorescence intensity (MFI) of NIS staining after HDAC inhibition in MCF-7 and MDA-MB-231 cells. Average MFI was calculated from 30–50 cells using LSM Image browser and fold difference with respect to untreated cells plotted. **(C)** Western blot showing NIS protein content in MCF-7 cells after different HDACi treatments. DMSO was used as a vehicle control (VC). Total 60 μg of protein was loaded in each lane and alpha-tubulin was used as an endogenous control. Full length western blot for NIS protein was shown in supplementary Fig. 8C. **(D)** NIS immunofluorescence photographs of MCF-7 clonal cells differentially over-expressing NIS protein either at the membrane (left panel) or at the cytoplasm (right panel) treated with NaB, VPA and CI994 drugs.

computing normalized tumor and thyroid uptake in mice, significant increase in tumor uptake was observed after 250 mg/kg VPA treatment but not 500 mg/kg dose (Fig. 5D,E). Since these drugs at the delivered dose are expected to show some anti-proliferative effect on the tumor cells, expected reduction of tumor size may have complicated the net radiotracer uptake at the tumor site. Autoradiography of NIS mediated radio-iodine uptake in MDA-MB-231 tumor xenograft clearly displayed much higher accumulation of ^{125}I in treated group of mice (Fig. 5F,G). The ROI analysis of autoradiograph image has confirmed significantly higher uptake in VPA (250 mg/kg) and NaB (500 mg/kg) treated mice than in untreated control group. To further support *in vivo* uptake studies, we checked NIS protein content in untreated and VPA treated Zr-75-1 tumor xenograft tissue by immunohistochemistry (IHC). As shown in Supplementary Fig. 7, digital IHC analysis of these samples revealed significant enhancement of NIS-immunopositivity ($p = 0.014$) in 250 mg/kg VPA treated tumor.

Further, ^{131}I therapeutic potential *in vivo* was also tested, where ^{131}I radioablative treatment efficacy was measured by noninvasive bioluminescence imaging. Here we used Zr-75-1 cells over-expressing luciferase reporter (Fluc2.tdTomato fusion) so that change in tumor growth can be monitored non-invasively. The results reveal that in mice treated with ^{131}I (1 mCi/mouse) or 5 doses of VPA (250 mg/kg) alone, tumors continue to grow, whereas mice pre-treated with VPA and ^{131}I showed 30% lesser bioluminescence signal 5 days after treatment (Fig. 6A,B).

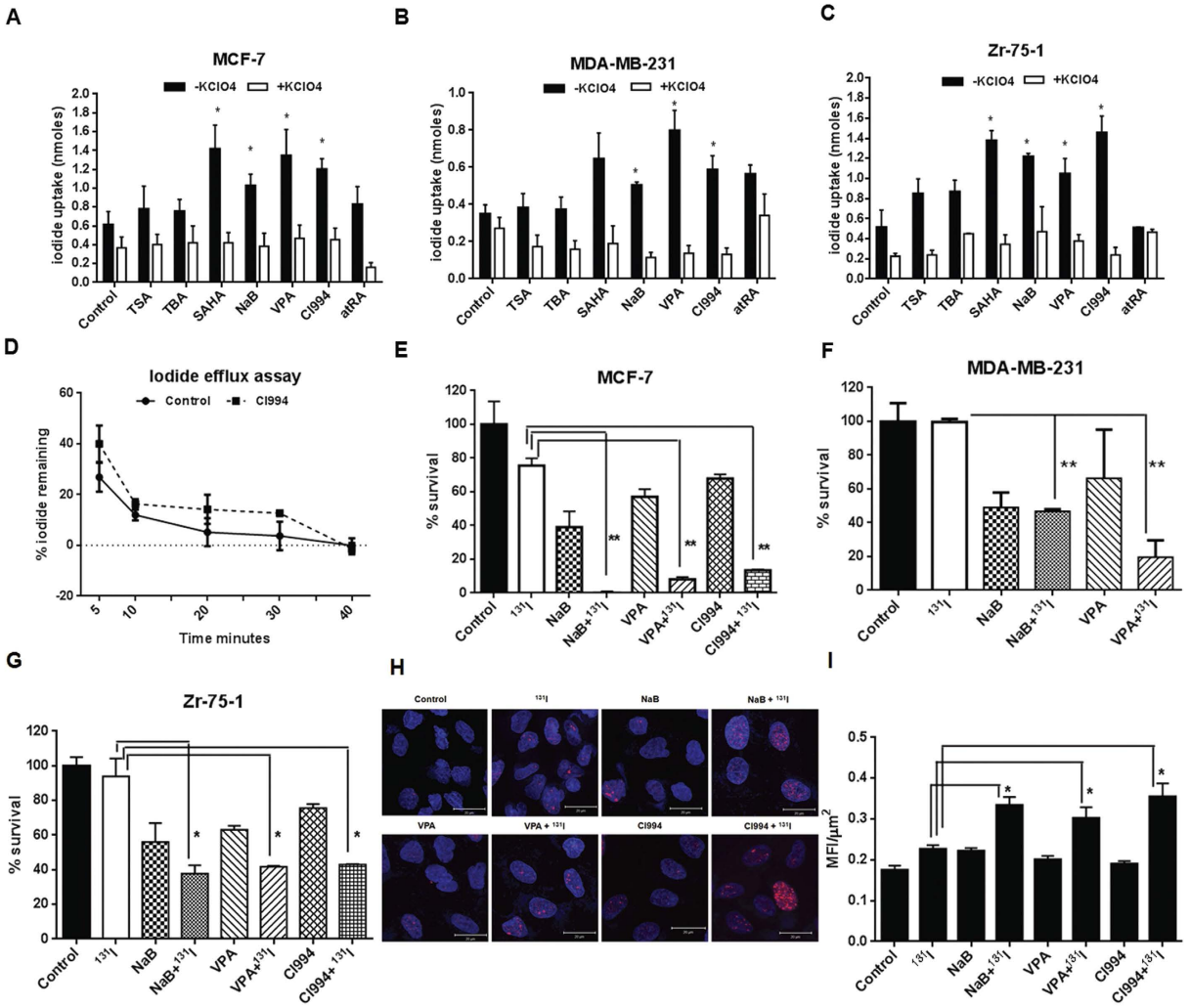

Figure 4. Modulation of NIS function by HDACi in BC cells. (**A**–**C**) Effect of the HDACi drugs and atRA on NIS-mediated iodide accumulation in MCF-7, MDA-MB-231 and Zr-75-1 cells respectively. 30 μM potassium perchlorate was used for blocking iodide uptake. The Y axis scale bars represent nanomoles (nmoles) of iodide uptake after 48 hours of HDACi and atRA treatment of cells. Error bars indicate standard error of mean. (**D**) Chart showing iodide efflux assessment done using MCF-7 cells. CI994 drug was used as a candidate HDACi representative to verify change in efflux upon drug treatment. (**E**–**G**) Charts represent measure of percentage cell survival after selective killing by ^{131}I treatment in the presence or absence of candidate HDACi treatment as marked. MCF-7, MDA-MB-231 were exposed to 50 μCi/ml of ^{131}I and Zr-75-1 cells were exposed to 100 μCi/ml of ^{131}I with or without pre-treatment of NaB/ VPA/ CI994. Cell survival was measured by their colony forming ability (**indicates high significance $p < 0.005$). (**H**) Immunofluorescence photographs showing DNA damage response after ^{131}I exposure detected by γ-H2Ax foci formation. Zr-75-1 cells were exposed to 100 μCi/ml ^{131}I with or without pre-treatment of NaB/ VPA/ CI994 and probed with γ-H2Ax antibody after fixation. Foci were detected by Dylight 633 secondary antibody (red). Cell nuclei were cross stained using DAPI (blue). Scale bar represents 20 μm. (**I**) Graph showing MFI/μm^2 of foci formation after ^{131}I exposure with or without HDACi pre-treatment. Average MFI of 35 cells was calculated using LSM image browser and plotted.

As lowered luciferase signal is a direct measure of tumor burden, these first hand results seem encouraging indicating the scope of using HDACi treatment to enhance ^{131}I therapeutic efficacy in breast cancer.

Discussion

Over the last fifteen years, several studies have reported NIS expression in BC raising the possibility of NIS gene-targeted radionuclide imaging and therapy. Although moderate NIS expression is encountered in majority of BC cases, sufficient radioiodide accumulation has been found in a very small fraction of cases. Therefore, selective induction of NIS protein expression in breast tissue has appeared to be an important strategy towards achieving this goal. In the present study, we have tested a wide panel of HDAC inhibitors for transcriptional modulation of human NIS in breast cancer cells. As revealed in the schematic diagram (Fig. 7), in addition to histone acetylation activity, distinct HDACi may display different biological responses by acting through various

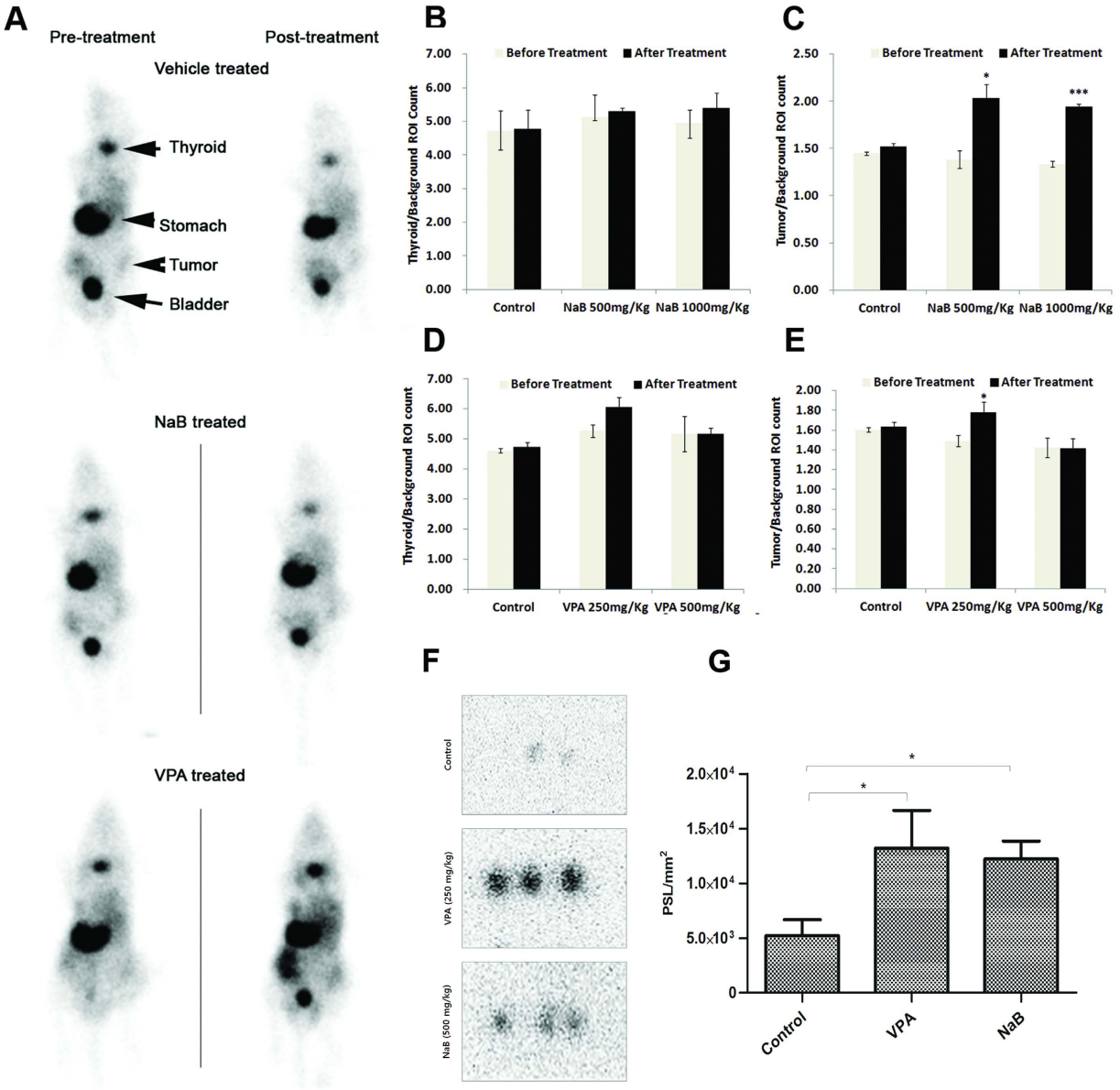

Figure 5. Preclinical validation of NIS functional augmentation by NaB and VPA treatment. (**A**) Accumulation of ^{99m}Tc-pertechnetate in NIS-expressing tissues like thyroid, gastric mucosa (stomach) and MDA-MB-231 tumor xenografts pre- and post-NaB and VPA treatment was recorded by gamma camera imaging 20 minutes after radiotracer injection. Mice untreated or treated with lower dose of the candidate drugs i.e. 250 mg/kg for VPA and 500 mg/kg of NaB tested are represented. (**B,C**) Charts representing normalized ^{99m}Tc-pertechnetate uptake (count) measured from thyroid (**B**) and tumor (**C**) tissue of mice images untreated or treated with two different concentration of NaB. (**D,E**) Chart representing similar uptake values upon VPA treatment. **F**. Digital autoradiography images showing intra-tumor uptake of ^{125}I at 4 hours after tracer injection. Images represent MDA-MB-231 tumor tissue sections which were grown on nude mice treated as vehicle control, VPA (250 mg/kg) and NaB (500 mg/kg) as marked. (**G**) ROI analysis from autoradiograph images above. The quantitative results are expressed as PSL/mm2 (mean ± SD) and *indicate $p < 0.05$.

transcriptional factors that in turn can alter human NIS expression. So in the panel of drugs, we have included TSA, TBA, and SAHA which are derivatives of hydroxamic acids, NaB and VPA which are short chain fatty acids and CI994 which is a new benzamide compound. Importantly, most of these drugs are pan-DAC inhibitors and also in phase 2 or 3 clinical trial (Table 1), except for TBA which was included in our study as a HDAC6 specific inhibitor. To our knowledge, this is the first report evaluating such wide scale HDACi class of molecules for altering NIS expression in breast cancer as well as several other non-thyroid and thyroid cancer cell types. As the results reflect, four out of six HDACi especially the candidate drugs like NaB, VPA, CI994, and SAHA have shown promising induction in NIS transcript and protein expression.

Focusing on breast cancer, one key aspect of our study is the differential modulation observed in endogenous NIS expression of hormone receptor positive cells than receptor negative cells. Until now enhancement of NIS

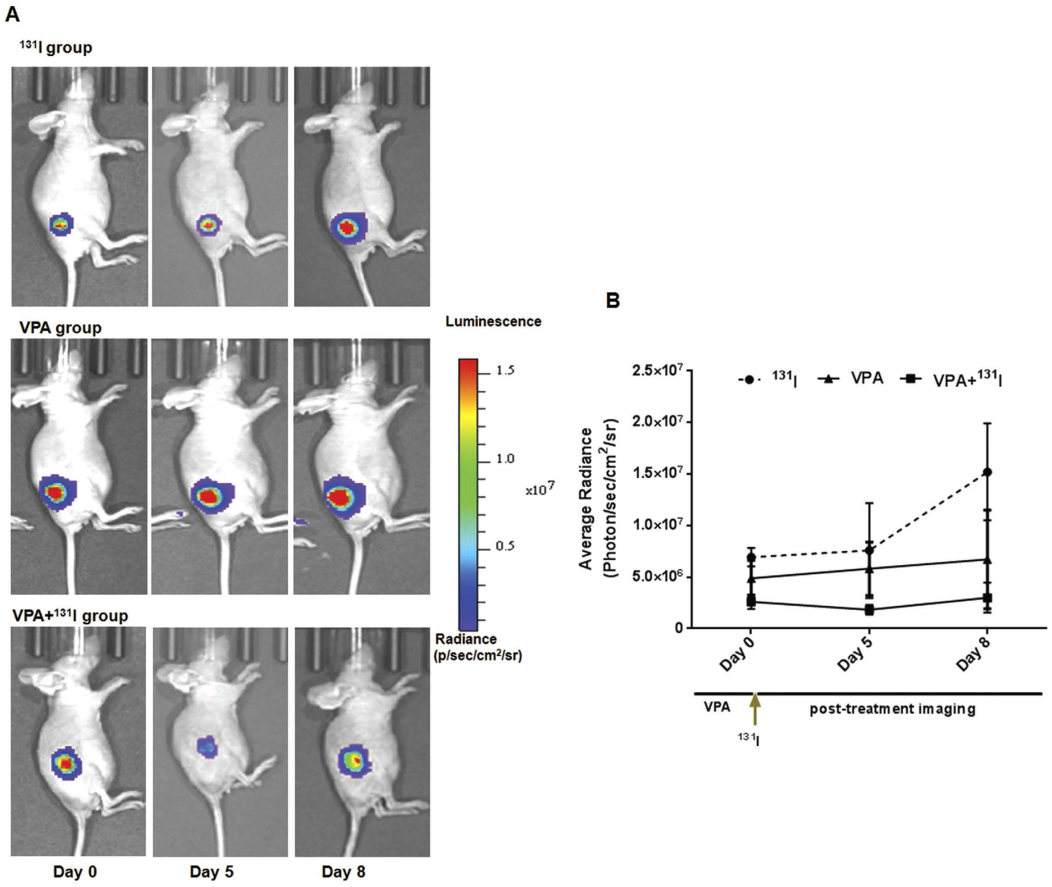

Figure 6. Non-invasive bioluminescence monitoring of Zr-75-1 tumor xenograft bearing mice during the treatment phase. (**A**) Tumor xenografts were established in nude mice using engineered Zr-75-1-CMV-Fluc2.Tdt reporter cells. Mice in ^{131}I group received single intraperitoneal injection of 1mCi of ^{131}I on day 0, and mice in VPA group received 5 doses of 250 mg/kg VPA treatment alone while the experimental group undergone pre-treatment with 250 mg/kg VPA for 5 days before ^{131}I treatment started. (**B**) Graph illustrates mean bioluminescence signal quantities from sets of mice (n = 3) at day 0, day 5 and day 8 when the mice were scanned by injecting D-luciferin.

expression, function and various signaling pathways involved are studied primarily in ER-positive cells[23–25]. Triple negative tumors (ER, PR, HER2 –ve), on the other hand, have worst prognosis and are in high demand of targeted and systemic therapy options. A significant number of TNBC tumor samples showing intense NIS staining[8], can now be modulated further by HDACi, and thus eventually may improve the scope of applying NIS-based targeted radioiodide therapy for this subgroup of patients. NIS mRNA induction is found much more pronounced in estrogen receptor (ER) positive cells than the ER-negative cells. Recent clinical finding reported by us shows that in breast cancer NIS expression has strong association with ER expression among all the BC subtypes[8]. As NIS promoter has several estrogen response elements (revealed by bioinformatics analysis), estrogen is expected to have a direct role in driving NIS transcription. HDACi are also known to act on nuclear receptors including ERα[26]. But surprisingly, in our TF array, ER activation and binding to NIS promoter was not pronounced (i.e. above threshold cutoff margin). Thus, future studies will have to confirm the regulatory mechanism by which HDACi treatment cause enhanced effect in ER positive cells.

Another important aspect of this study is the information elucidated from the TF activation and promoter binding array of 96 major factors. These results show for the first time that candidate TFs which potentially play regulatory role on NIS expression in BC cells. NaB and VPA treatment in MCF-7 cell results in mostly differential activation of TFs except for Stat4 being the only common candidate found in place. Further, *in silico* analysis (using Genomatix and Transfac Software) as well as promoter binding array results provide confirmation on the presence of TF binding sites on NIS promoter (as listed in Table 2) supporting their potential direct role in modulating cellular NIS expression. In thyroid, it is well established that TSH stimulation activates cAMP and CREB resulting in activation of NIS expression[27]. But the role of CREB in regulation of NIS in BC is still unknown. PPAR ligands in combination with other agents were known to induce NIS expression in thyroid tissue[28]. There is no literature available regarding regulation of NIS expression by various TFs like AP1, Stat4 etc. as turned out to be important factors in our results. These observations put forward important mechanistic insights on human NIS promoter induction indicating role of specific TFs in breast tissue which can be explored further in future.

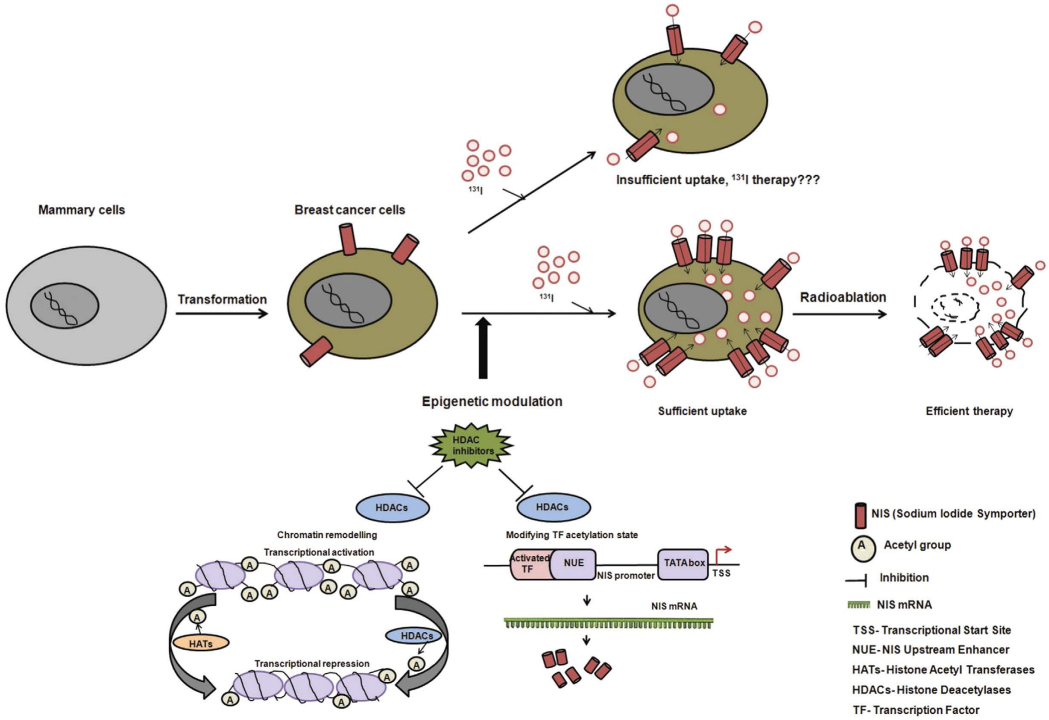

Figure 7. Schematic illustration of potential therapeutic applications of HDACi mediated human NIS modulation in breast cancer. Upregulation of NIS expression during malignant transformation of breast tissue implicated therapeutic application of radioiodine in breast cancer management. To achieve enhanced therapeutic effect, stimulation of functional NIS expression by epigenetic modifiers such as HDACi is a promising strategy.

Further, augmented NIS protein levels after NaB, VPA or CI994 treatment are also found to be sufficient for ^{131}I radioablation in culture. Increased *in vivo* uptake of NIS-mediated ^{99m}Tc-pertechnetate is also confirmed using MDA-MB-231 tumor xenograft and gamma camera imaging. Also, together with the data on ^{131}I therapy in cultured cell, mouse studies using noninvasive bioluminescence imaging has clearly indicated HDACi treatment improved therapeutic benefit *in vivo*. HDACis are expected to show anti-proliferative effect to some extent at the delivered dose in mouse. Therefore, for further significant improvement of NIS-mediated therapeutic efficacy, dose optimization of VPA and ^{131}I can be tried in future. Effective thyroid blocking may also improve therapeutic efficacy as more ^{131}I become available in the body. For successful implementation of endogenous NIS mediated gene therapy approach, the major bottlenecks are insufficient radioiodide accumulation in the tumor bed as well as short tracer retention time, putting a question mark on adequate therapeutic value of this approach. In cultured plate, our results suggest that although HDACi treatment significantly improves NIS-mediated iodide uptake, iodide efflux remains impervious. At this point, there is no proven strategy that shows organification of iodine in BC cells can happen[1], and thus whether or not this process can be tapped to enhance efficacy is a matter of research in future. For effective radioiodide therapy, the membrane localization of NIS protein is a critical factor along with its total expression on the cell. From our study, we have found that treatment of HDACi significantly increases NIS expression but it doesn't alter its localization (Fig. 3D). Even though NIS protein expression has been observed in 70% of the breast cancer patients, its clinical utility has been undermined due the intracellular localization of the protein in majority cases. Therefore for successful therapeutic intervention, finding out potential agents/signalling pathways targeting NIS protein to the cell the membrane should also be explored in future.

In conclusion, to the best of our knowledge, this is the first study that provides important mechanistic insights on HDACi mediated NIS over-expression in breast cancer cell. This study also demonstrates *in vivo* functional improvement as a step forward towards taking this gene therapy strategy to a success. In breast cancer cases, where NIS protein over-expresses upon cancer onset, use of a brief HDACi pre-treatment may turn NIS mediated radioiodide therapy efficacious and thus seems to be a promising strategy for future clinical application. Apart from breast cancer, in thyroid and other non-thyroidal cancer types, where NIS transgene mediated therapy has often been used, may also be impacted further by this transcriptional modulation strategy.

Materials and Methods

Chemicals and Cell lines. HDACi drugs such as TSA [T8852], NaB [B5887], VPA [4543], SAHA [SML0061], TBA [SML0044] and all trans retinoic acid [R2625] were purchased from Sigma, USA. CI994 (1742-10, 50) was purchased from Biovision, CA, USA. Stock solutions (1M) of TSA, SAHA, CI994 and TBA were prepared in DMSO and of NaB and VPA were prepared in sterile MiliQ and stored at −20 °C. Receptor positive MCF-7 and Zr-75-1 BC cells (ATCC) were maintained in RPMI-1640 media (Gibco, Invitrogen, USA).

Receptor negative MDA-MB-231 cells (ATCC) were maintained in Leibovitz's L15 media (Sigma, USA) whereas MDA-MB-468 cells (a gift from Dr. M. Vaidya, ACTREC, India) were maintained in DMEM media (Gibco, Invitrogen, USA) supplemented with 10 mM HEPES. All the media contained 10% fetal bovine serum (FBS) (Gibco, Invitrogen, USA), 1% antibiotic-antimycotic solution (Gibco, Invitrogen, USA). Two thyroid cancer cell lines, NPA and ARO (gifted by Mr. A. Chakraborty, BARC, India), were maintained in IMDM (Gibco, Invitrogen, USA) containing 10% FBS and 0.075% gentamycin solution. All the cells were maintained at 37 °C in a humidified incubator (Thermo Scientific, Rockford, IL, USA) with 5% CO_2 except for MDA-MB-231.

Plasmid Construction. pGL3-NIS-luc+ vector containing 1.34 kb human NIS promoter was a kind gift from Dr. Kenneth Ain, University of Kentucky, USA. Human NIS promoter was PCR amplified using primers (5′-GGCACGCGTATGTGCCACCACG and 3′-GGCGCTAGCGGAGGTCGCCTTG) with 5′-MluI and 3′-NheI enzyme sites and cloned into pcDNA3.1(+) mammalian expression vector containing Fluc2.TurboFP bi-fusion reporter. Positive clones were confirmed by PCR amplification, restriction digestion and sequencing. CMV-TurboFP.Rluc8.6 expression vector was developed as control plasmid using NheI and BamHI restriction sites.

Stable cell lines. The pNIS-Fluc2.TurboFP plasmid DNA was transfected into MCF-7, MDA-MB-231 cells using lipofectamine 2000 (Life Technologies, USA). Clonal selection was achieved using G418 sulphate (500 μg/ml for MCF-7 and MDA-MB-231) (Sigma, USA). Positive clones were confirmed by luciferase reporter activity as well as TurboFP fluorescence expression.

MTT cell cytotoxicity assay. To evaluate cytotoxicity of various HDACi, MCF-7 and MDA-MB-231 (5×10^3) cells were seeded in 96 well plates (Corning, USA). Cells were exposed to different concentrations of HDACi for 48 hours. Cell viability was assessed using the MTT (3-[4,5-dimethylthiazol-2-yl] c-2,5-diphenyltetrazolium bromide) (Sigma, USA) as cell proliferation reagent.

RNA extraction and quantitative real-time PCR. After the cells were treated with HDACi for 48 hours, RNA was extracted using RNeasy kit (QIAGEN, USA). cDNAs were synthesized using the first strand cDNA synthesis kit (Invitrogen, USA). Quantitative real-time PCR was performed using Taqman probe mix on the 7900HT PCR cycler (Applied Biosystems, USA). The Taqman probes for human NIS and GAPDH with assay ids Hs00166567_m1 and Hs02758991_g1 respectively were used (Applied Biosystems, USA). Triplicate samples were run for each sample. The comparative ΔΔCt method was used to calculate relative gene expression.

Immunoblotting and immunofluorescence procedures. Cells were treated with various HDACi for 48 hours and were lysed using cell lysis buffer (Cell Signalling Technology, USA) containing standard protease inhibitors (Santa Cruz Biotechnology, USA). Equal amount of protein from control and treated cells were resolved in 10% SDS-PAGE gel and transferred onto nitrocellulose membrane (Millipore, USA) by semi-dry method. After blocking with 5% BSA (Bovine Serum Albumin), membranes were probed with respective monoclonal antibodies, such as anti-acetyl-histone H3 antibody (06-598, Upstate, USA) and anti-Fluc antibody (G4751, Promega Corporation, USA), or anti-human NIS antibody (FP5A, Abcam, USA), and anti-α-tubulin antibody (T9026, Sigma, USA) followed by washing and secondary HRP-conjugated antibodies. The blot was developed by chemiluminescence (Invitrogen, USA). To determine even transfer and equal loading, membranes were stripped and re-probed with an α-tubulin monoclonal as per standard.

For immunofluorescence study, cells were fixed with 4% paraformaldehyde, washed with PBS and blocked with 2% BSA followed by overnight incubation with primary antibody for human NIS (FP5A, Abcam, USA) and γH2Ax (Pierce Biotechnology, USA) at 4 °C. The cells were then washed with PBS, incubated with anti-mouse (NIS)/ anti rabbit (γH2Ax) Dylight 633 conjugated secondary antibody (Thermo Scientific, Rockford, IL, USA) (1h), washed and counterstained for nucleus using DAPI (Sigma, USA). Fluorescence micrographs were captured using Carl Zeiss LSM 510 Meta confocal microscope.

Luciferase reporter assay. Selected MCF-7 and MDA-MB-231 clonal cell population were seeded and treated with different HDACi for 48 hours. Lysates were collected using passive lysis buffer (Promega Corporation, USA) and luciferase activity was measured using luminescence plate reader (BMG Labtech, Germany).

Transcription factor (TF) activation profiling and NIS promoter binding array. We used a 96 well plate TF activation array (# FA1002, Signosis, USA) as per the manufacturer's guideline. MCF-7 cells were treated with NaB/ VPA for 48 hours and nuclear proteins from both control and treated cells were isolated using standard procedure and used as probe on the array plate. Transcription factor IID (TFIID) was used for normalization of readings. TFs were selected by considering the fold-change method (≤ 1.5 or ≥ 1.5) of treated over untreated cell samples. To characterize binding of various activated TFs to NIS promoter, promoter binding TF profiling array was performed (FA2002, Signosis, USA). Nuclear extracts were prepared from NaB/ VPA treated MCF-7 cells, incubated with oligo-binding mix along with NIS-promoter DNA fragment. Comparing luminescence in presence or absence of competitor human NIS promoter, binding of various TFs were predicted.

Iodide uptake and efflux measurement assays. Iodide uptake and efflux study was performed as described previously[29,30] with minor modifications. After 48 hours of treatment with indicated HDACis, cells were incubated with 10 μM NaI in uptake buffer [Hank's Balanced Salt Solution (HBSS) supplemented with 10 mM HEPES (pH 7.3)]. To determine NIS-specific iodide uptake, cells were incubated with 30 μM KClO4 in uptake buffer for one hour prior to addition of 10 μM NaI. After 30 minutes incubation with NaI at 37 °C, cells were washed with ice-cold uptake buffer. Then 10.5 mM ammonium cerium (IV) sulphate solution and 24 mM sodium

arsenite (III) solution were added. The plate was incubated at room temperature (RT) in dark for 30 minutes and the absorbance at 420nm was recorded. Using logarithmic conversion and standard equation of iodide standards, amount of nanomoles (nmoles) of iodide uptake was calculated from absorbance read-outs.

In iodide efflux measurement study, control or drug treated cells were incubated in uptake buffer with 10 μM NaI at 37 °C for 30 minutes. Cells were washed with ice cold uptake buffer to stop the reaction and fresh uptake buffer without NaI was added. The medium was replaced after every 10 minutes and 10.5 mM ammonium cerium (IV) sulphate solution and 24 mM sodium arsenite (III) solution were added. Following incubation at RT in dark for 30 minutes absorbance at 420nm was recorded.

***In vitro* clonogenic assay.** Control and NaB/ VPA/ CI994 treated MCF-7/ Zr-75-1/ MDA-MB-231 cells were grown in 25 cm^2 flasks and incubated with 50 μCi/ml of ^{131}I in case of MCF-7 or MDA-MB-231 and 100 μCi/ml in case of Zr-75-1 in HBSS supplemented with 10 μM NaI and 10 mM HEPES (pH7.3). The *in vitro* clonogenic assay was performed as described by Mandell *et al.*[29].

***In vivo* preclinical imaging.** The experimental protocol was approved by Institutional Animal Ethics Committee at KNU, Korea and performed in accordance with the guidelines for the Care and Use of the Laboratory Animals. The MDA-MB-231 cells (5×10^6) were implanted along with matrigel (4:1) in 6-week-old BALB/c nude mice subcutaneously. When tumor reached ~300 mm^3 volume, mice were divided into three groups (n = 3): the control (intraperitoneal injection of 100 μL PBS), VPA (250 mg/kg) and VPA (500 mg/kg). Pre- and post-treatment gamma camera imaging using a pinhole collimator (Infinia II, GE Healthcare, USA) was conducted at 20 minutes after ^{99m}Tc-pertechnetate (10.0 MBq) injection. The mice were maintained under isoflurane (Forane®, ChoongWae Co., Seoul, Korea) anesthesia during the entire process. The same procedure was also used for the NaB treatment (500 mg/kg and 1000 mg/kg body weight).

^{125}I autoradiography of tumor xenograft. The experimental protocol was approved by Institutional Animal Ethics Committee at KNU, Korea and performed in accordance with the guidelines for the Care and Use of the Laboratory Animals. Autoradiography of MDA-MB-231 tumor xenograft was performed for NIS mediated radioiodine uptake. Mice with grown tumor were segregated in three groups, i.e. control, VPA treated and NaB treated (n = 4 in each group). After VPA (250 mg/kg) and NaB (500 mg/kg) treatment for 5 days and 24 hours of last drug treatment, all mice were injected with 50–60 μCi ^{125} I via the tail vein. Four hours post injection, mice were sacrificed and tumors were excised and prepared for standard autoradiography procedure. Then frozen sections of 20 μm thickness were cut using cryostat and mounted on glass slides. The glass slides were exposed in the imaging cassette for 24 h; subsequently, the exposed plate was scanned with a film imaging analyzer (Fuji film, FLA-3000) to confirm the uptake. ROI measurements were done from the captured digital images and compared between treatment groups with that of the vehicle treated control.

***In vivo* optical imaging and immunohistochemistry procedures.** The experimental protocol was approved by Institutional Animal Ethics Committee (IAEC) at ACTREC and performed in accordance with the guidelines for the Care and Use of the Laboratory Animals using ACTREC animal house and Molecular Imaging facilities. Female BALB/c nude mice (n = 9) were used for growing subcutaneous tumor using Zr-75-1 cells labeled with Fluc2.Tdt fusion gene. Mice were divided into three groups: the ^{131}I group (intraperitoneal injection of 1mCi Na-^{131}I on day 0) , VPA group (5 doses of 250 mg/kg of VPA alone) and the experimental group (5 doses of 250 mg/Kg of VPA followed by 1mCi Na-^{131}I on day 0). Serial Bioluminescence imaging was performed using IVIS-Spectrum (Caliper Life Sciences) after intraperitoneal injecting 30 mg/ml of D-luciferin (Biosynth International) and viewed in real time on a computer screen using a color scale expressed as total flux (photons per second per square centimeter per steradian [photons/sec/cm^2/sr]). Mice were anesthetized with isofluorane and placed in the imaging chamber with continuous 2% isofluorane administration via nasal cone. Data were analyzed using Living Image version 4.4 software.

For immunohistochemistry (IHC), tumors from drug treated (5 daily doses of 250 mg/kg) and control group were harvested and fixed using standard procedures[8]. For digital scoring of IHC slides, we used the IHCprofiler plugin for ImageJ (software) developed by our group[31].

Statistical Analysis. All data are expressed as mean ± SE and are representative of at least two separate experiments. Statistical significance was analyzed by Student t-test using GraphPad Prism 6 (GraphPad Software, La Jolla, CA). P values of ≤ 0.05 were considered statistically significant.

References

1. Spitzweg, C., Harrington, K. J., Pinke, L. A., Vile, R. G. & Morris, J. C. Clinical review 132: The sodium iodide symporter and its potential role in cancer therapy. *J Clin Endocrinol Metab* **86,** 3327–35 (2001).
2. Kogai, T. *et al.* Differential regulation of sodium/iodide symporter gene expression by nuclear receptor ligands in MCF-7 breast cancer cells. *Endocrinology* **146,** 3059–3069 (2005).
3. Ahn, B. C. Sodium Iodide Symporter for Nuclear Molecular Imaging and Gene Therapy: From Bedside to Bench and Back. *Theranostics* **2,** 392–402 (2012).
4. Ghosh, M. *et al.* Bioluminescent monitoring of NIS-mediated (131)I ablative effects in MCF-7 xenografts. *Mol Imaging* **5,** 76–84 (2006).
5. Tazebay, U. H. *et al.* The mammary gland iodide transporter is expressed during lactation and in breast cancer. *Nat Med* **6,** 871–8 (2000).
6. Moon, D. H. *et al.* Correlation between 99mTc-pertechnetate uptakes and expressions of human sodium iodide symporter gene in breast tumor tissues. *Nucl Med Biol* **28,** 829–34 (2001).
7. Wapnir, I. L. *et al.* The Na+/I- symporter mediates iodide uptake in breast cancer metastases and can be selectively down-regulated in the thyroid. *Clin Cancer Res* **10,** 4294–302 (2004).

8. Chatterjee, S. *et al.* Quantitative immunohistochemical analysis reveals association between sodium iodide symporter and estrogen receptor expression in breast cancer. *PLoS One* **8,** e54055 (2013).
9. Tanosaki, S. *et al.* Effect of ligands of nuclear hormone receptors on sodium/iodide symporter expression and activity in breast cancer cells. *Breast Cancer Res Treat* **79,** 335–45 (2003).
10. Arturi, F. *et al.* Regulation of iodide uptake and sodium/iodide symporter expression in the mcf-7 human breast cancer cell line. *J Clin Endocrinol Metab* **90,** 2321–6 (2005).
11. Micali, S. *et al.* Sodium iodide symporter (NIS) in extrathyroidal malignancies: focus on breast and urological cancer. *BMC Cancer* 14, 303 (2014).
12. Unterholzner, S. *et al.* Dexamethasone stimulation of retinoic Acid-induced sodium iodide symporter expression and cytotoxicity of 131-I in breast cancer cells. *J Clin Endocrinol Metab* **91,** 69–78 (2006).
13. Kogai, T. *et al.* Systemic retinoic acid treatment induces sodium/iodide symporter expression and radioiodide uptake in mouse breast cancer models. *Cancer Res* **64,** 415–22 (2004).
14. Russo, D., Damante, G., Puxeddu, E., Durante, C. & Filetti, S. Epigenetics of thyroid cancer and novel therapeutic targets. *J Mol Endocrinol* **46,** R73–81 (2011).
15. Xu, W. S., Parmigiani, R. B. & Marks, P. A. Histone deacetylase inhibitors: molecular mechanisms of action. *Oncogene* **26,** 5541–52 (2007).
16. Puppin, C. *et al.* Cooperative effects of SAHA and VPA on NIS gene expression and proliferation of thyroid cancer cells. *J Mol Endocrinol* **48,** 217–227 (2012).
17. Kitazono, M. *et al.* Low concentrations of the histone deacetylase inhibitor, depsipeptide (FR901228), increase expression of the Na(+)/I(-) symporter and iodine accumulation in poorly differentiated thyroid carcinoma cells. *J Clin Endocrinol Metab* **86,** 3430–5 (2001).
18. Fortunati, N. *et al.* The pan-DAC inhibitor LBH589 is a multi-functional agent in breast cancer cells: cytotoxic drug and inducer of sodium-iodide symporter (NIS). *Breast Cancer Res Treat* 124, 667–75 (2010).
19. Baldan, F. *et al.* Histone post-translational modifications induced by histone deacetylase inhibition in transcriptional control units of NIS gene. *Mol Biol Rep* **41,** 5257–65 (2014).
20. Haggarty, S. J., Koeller, K. M., Wong, J. C., Grozinger, C. M. & Schreiber, S. L. Domain-selective small-molecule inhibitor of histone deacetylase 6 (HDAC6)-mediated tubulin deacetylation. *Proc Natl Acad Sci USA* **100,** 4389–94 (2003).
21. Chatterjee, S., Thaker, N. & De, A. Combined 2-deoxy glucose and metformin improves therapeutic efficacy of sodium-iodide symporter-mediated targeted radioiodine therapy in breast cancer cells. *Breast Cancer* (*Dove Med Press*) **7,** 251–65 (2015).
22. Dohan, O., Baloch, Z., Banrevi, Z., Livolsi, V. & Carrasco, N. Rapid communication: predominant intracellular overexpression of the Na(+)/I(−) symporter (NIS) in a large sampling of thyroid cancer cases. *J Clin Endocrinol Metab* 86, 2697–700 (2001).
23. Ohashi, E., Kogai, T., Kagechika, H. & Brent, G. A. Activation of the PI3 kinase pathway by retinoic acid mediates sodium/iodide symporter induction and iodide transport in MCF-7 breast cancer cells. *Cancer Res* **69,** 3443–50 (2009).
24. Jung, K. H., Paik, J. Y., Ko, B. H. & Lee, K. H. Mitogen-activated protein kinase signaling enhances sodium iodide symporter function and efficacy of radioiodide therapy in nonthyroidal cancer cells. *J Nucl Med* **49,** 1966–72 (2008).
25. Vadysirisack, D. D., Venkateswaran, A., Zhang, Z. & Jhiang, S. M. MEK signaling modulates sodium iodide symporter at multiple levels and in a paradoxical manner. *Endocr Relat Cancer* **14,** 421–32 (2007).
26. Nebbioso, A. *et al.* HDACs class II-selective inhibition alters nuclear receptor-dependent differentiation. *J Mol Endocrinol* **45,** 219–28 (2010).
27. Kogai, T., Taki, K. & Brent, G. A. Enhancement of sodium/iodide symporter expression in thyroid and breast cancer. *Endocr Relat Cancer* **13,** 797–826 (2006).
28. Park, J. W. *et al.* Troglitazone, the peroxisome proliferator-activated receptor-gamma agonist, induces antiproliferation and redifferentiation in human thyroid cancer cell lines. *Thyroid* **15,** 222–31 (2005).
29. Mandell, R. B., Mandell, L. Z. & Link, C. J., Jr. Radioisotope concentrator gene therapy using the sodium/iodide symporter gene. *Cancer Res* **59,** 661–8 (1999).
30. Waltz, F., Pillette, L. & Ambroise, Y. A nonradioactive iodide uptake assay for sodium iodide symporter function. *Anal Biochem* **396,** 91–5 (2010).
31. Varghese, F., Bukhari, A. B., Malhotra, R. & De, A. IHC Profiler: an open source plugin for the quantitative evaluation and automated scoring of immunohistochemistry images of human tissue samples. *PLoS One* **9,** e96801 (2014).
32. Mann, B. S., Johnson, J. R., Cohen, M. H., Justice, R. & Pazdur, R. FDA approval summary: vorinostat for treatment of advanced primary cutaneous T-cell lymphoma. *Oncologist* **12,** 1247–52 (2007).
33. Sharma, S. *et al.* A Phase II Clinical Trial of Oral Valproic Acid in Patients with Castration-Resistant Prostate Cancers Using an Intensive Biomarker Sampling Strategy. *Transl Oncol* **1,** 141–7 (2008).
34. Yang, J. J. *et al.* A randomized phase II clinical trial of nab-paclitaxel and carboplatin compared with gemcitabine and carboplatin as first-line therapy in locally advanced or metastatic squamous cell carcinoma of lung. *BMC Cancer* **14,** 684 (2014).
35. Richards, D. A. *et al.* Gemcitabine plus CI-994 offers no advantage over gemcitabine alone in the treatment of patients with advanced pancreatic cancer: results of a phase II randomized, double-blind, placebo-controlled, multicenter study. *Ann Oncol* **17,** 1096–102 (2006).

Acknowledgements

We acknowledge Dr. M. Vaidya, ACTREC, India, for providing MDA-MD-468 cells, Mr. Avik Chakraborty, BARC, India, for providing thyroid cancer cell lines, Dr. M. G. R. Rajan and Dr. S. Kulkarni, Radiation Medicine Centre, BARC, India, for providing help to use radioactive culture facility. The authors would like to thank Dr. Shruti Dutta and Mr. Amirali Bukhari in the lab for assistance in the preparation and editing this manuscript. Funding support from TMC-Woman Cancer Initiative funding (#82) to AD is gratefully acknowledged. This work was also supported by National Research Foundation (NRF) grant funded by the Korea government (MSIP) to BCA (No. NRF-2015M2A2A7A01045177).

Author Contributions

A.D. conceptualized and designed the study; M.K., K.S. and S.J. performed the experiments; B.C.A. and K.S. performed and analyzed gamma camera and digital autoradiography imaging experiments; A.D., S.G., B.C.A., K.S. and M.K. analyzed data, wrote the manuscript.

Additional Information

Supplementary information accompanies this paper at http://www.nature.com/srep

Competing financial interests: The authors declare no competing financial interests.

How to cite this article: Kelkar, M. G. *et al.* Enhancement of human sodium iodide symporter gene therapy for breast cancer by HDAC inhibitor mediated transcriptional modulation. *Sci. Rep.* **6**, 19341; doi: 10.1038/srep19341 (2016).